Investigation into the efficiency limitations of InGaN-based light emitters

By

Benjamin George Crutchley

Submitted for the award of the degree of Doctor of Philosophy

Department of Physics
Faculty of Engineering and Physical Sciences, University of Surrey,
Guildford, Surrey, GU2 7XH

October, 2012

ProQuest LLC.
789 East Eisenhower Parkway
P.O. Box 1346
Ann Arbor, MI 48106 – 1346

Abstract

The physical properties of InGaN-based light emitting diodes (LEDs) and laser diodes (LDs) are investigated in this study. A strong focus of the thesis is to investigate the non-radiative recombination process which leads to the relative reduction of the efficiency with increasing current injection in an effect which is known as efficiency droop. The explanation of droop is often inconsistent and contradictory with different experiments or devices produced using different growth conditions. Whilst the literature suggests that Auger recombination, carrier leakage and a defect-related recombination are all separately the cause of droop, the physical cause of such loss mechanisms is often poorly explained.

Results are presented in this thesis which show that there is a poor hole injection efficiency at low temperatures which is particularly problematic in devices which include electron blocking layers. The poor injection is expected to result in the escape of electrons that is exacerbated by an enhancement of the internal polarization fields. The reduction of the LED efficiency with increasing temperature where there are no hole injection issues is shown to be due to an increasing defect-related recombination rate. The temperature and pressure dependence of efficiency droop show that neither Auger recombination nor carrier leakage are required to explain droop. Evidence of carrier localization is presented by the "s-shape" dependence of the emission peak on temperature in an effect which is stronger for green LEDs (depth of 130meV) compared with blue LEDs (58meV). The weak pressure coefficients of the InGaN-based LEDs (green LED 1.20±0.06meV/bar at 5mA and blue LED 2.14±0.06meV/kbar at 5mA) are also partially expected to be due to carrier localization. Based on these findings, droop is expected to be caused by an increase in the defect-related recombination rate at high injection due to the increasing likelihood that carriers will occupy defect sites. A defect-related recombination model for droop is shown to be consistent with the temperature and pressure dependence of efficiency droop. Such processes are also shown to influence InGaN LEDs on silicon substrates and InGaN-based laser diodes.

The findings of this thesis indicate that there is a strong influence of defect-related recombination, in addition to the internal polarization field strength, on the efficiency of InGaN-based emitters. Structural optimization of the device design and an in depth understanding of the types of defects involved are therefore required in order to achieve more efficient InGaN-based emitters.

Acknowledgements

The first and most important acknowledgment to be made has to be to my supervisor, Stephen Sweeney, whose continued support, encouragement and extensive knowledge has been strongly appreciated. This thesis would not have been completed without Stephen's expertise in addition to his enthusiasm for understanding the physics of InGaN-based devices. I consider myself very privileged to have had Stephen as a supervisor.

I am also thankful to Igor Marko for his introduction to experiments, in addition to his discussions, comments and suggestions regarding the research carried out. Shirong Jin, Daren Lock and Andy Prins also deserve a mention for valuable discussions. The study sessions of Solid State and Semiconductor physics carried out with Barnabas Ikyo, Scott Jarvis, Mike Lewis and Graham Read were very useful. Chris Buxey was always a big help in keeping the lab stocked up as well as investigating issues that arose. I also acknowledge Vlad Stolojan for providing TEM images of some of the LEDs investigated in this thesis. I also thank Julie Fletcher for her help in an extensive range of admin-based tasks.

I must also thank Lewis Liu from Cambridge University who provided devices that form part of this thesis. The calculations of the piezoelectric fields as a function of pressure that were carried out by Joydeep Pal and Max Migliorato, from Manchester University, were a big aid in understanding the effects of pressure on the InGaN quantum well devices.

I also acknowledge the financial support of the EPSRC (UK) who continue to support and promote science in the UK.

The encouragement, support, and understanding from Anke Graf were also key factors that led to the competition of this thesis and were very much appreciated. My family and friends, both in Guildford and further beyond, also played a key role in supporting me with all I have achieved. I must also formally state my gratitude to my parents, Patricia and Roy Crutchley, and my aunty, Maria Pasicznyk, for their continued support in my life for which I am very much indebted.

It is the death of the spirit we must fear. To believe only what one is taught and brought up to believe, to repeat what one has been told to say, to do only what one is expected to do, to live like a factory-made doll, to lose confidence in one's independence and the hope of better things - that is the death of the spirit.

Tokutomi Roka (1868-1927), Japanese writer and philosopher

Publications

"Optical properties of InGaN-based LEDs investigated using high hydrostatic pressure dependent techniques"

B.G. Crutchley , I.P. Marko, J. Pal, M.A. Migliorato and S.J. Sweeney

Accepted for publication in physica status solidi, September 2012

"Investigation into the cause of efficiency droop in Blue-Green InGaN LEDs using a high hydrostatic pressure dependent technique"

B.G. Crutchley, I.P. Marko and S.J. Sweeney

Under review in APL

"Investigation into the temperature dependence of the efficiency droop effect in blue-green InGaN LEDs"

B.G.Crutchley, I.P. Marko and S.J. Sweeney

In progress

"Enhancement of efficiency of InGaN-based LEDs through strain and piezoelectric field management"

J. Pal, B.G. Crutchley , I.P. Marko, S.J. Sweeney and M.A. Migliorato

Submitted for review in APL

"LED Junction Temperature Measurement using Generated Photocurrent"

D.A. Lock, S.R.G. Hall, A.D. Prins, B.G. Crutchley, S. Kynaston, and S.J. Sweeney

Submitted for review in IEEE Journal of Display Technology

Presentations

"Efficiency limiting processes in InGaN quantum well LEDs using a pressure dependent analysis"

B.G. Crutchley, I.P. Marko and S.J. Sweeney

UKNC meeting, Cork, Jan 2010, oral presentation

"Efficiency limiting processes in InGaN quantum well LEDs using a temperature and pressure dependent analysis"

B.G. Crutchley, I.P. Marko and S.J. Sweeney

SIOE, Cardiff, March 2010, oral presentation

"Auger Recombination in Blue-Green InGaN emitters"

B.G. Crutchley, I.P. Marko, and **S.J. Sweeney**

ISLC IEEE laser conference, Kyoto, June 2010, oral presentation

"Optical properties of InGaN-based LEDs revealed using temperature and pressure dependence techniques"

B.G. Crutchley, I.P. Marko and S.J. Sweeney

HPSP, Chang Chun, June 2010, oral presentation

"Investigating the cause of droop in InGaN quantum well LEDs using a temperature and pressure dependent analysis"

B.G.Crutchley, I.P. Marko and S.J. Sweeney

Photonics West, San Francisco, Jan 2011, oral presentation

"Investigating the Cause of Efficiency Droop in 465nm InGaN Quantum Well LEDs grown on silicon substrates"

B.G. Crutchley, I.P. Marko, L. Liu, C. Humphreys and S.J. Sweeney

ICNS, Glasgow, June 2011, Poster presentation

"Investigating the cause of green gap in InGaN quantum well LEDs using a temperature and pressure dependent analysis"

B.G. Crutchley, I.P. Marko and S.J. Sweeney

ICNS, Glasgow, June 2011, oral presentation

"An investigation into the cause of efficiency droop using a pressure dependent technique"

B.G. Crutchley, I.P. Marko and S.J. Sweeney

UKNC, Bath, Jan 2012, oral presentation

"An investigation into the cause of efficiency droop in InGaN LEDs using a high hydrostatic pressure and temperature dependent technique"

B.G. Crutchley, I.P. Marko and S.J. Sweeney

SIOE, Cardiff, March 2012, oral presentation

"Optical properties of InGaN-based LEDs investigated using high hydrostatic pressure dependent techniques"

B.G. Crutchley , **I.P. Marko**, J. Pal, M.A. Migliorato and S.J. Sweeney
HPSP, Montpellier, June 2012, oral presentation

List of symbols

$E_{C,V}$	Conduction, valence band edge energy
$\hbar$	(Planck's constant)/(2π)
k	Wavevector
m^*	Electron, hole effective mass
g_{3D}	Density of states in 3D
g_{2D}	Density of states in 2D
f(E)	Fermi function
n,p	Electron, hole concentration
$N_{c,v}$	Effective density of states
k_B	Boltzmann constant
T	Temperature
E_F	Fermi energy
n_q	Quantum number
h	Planck's constant
L	Length
η	Efficiency
P	Power
ν	Frequency
I	Current
e	Charge of an electron
I_{th}	Threshold current
I_r	Radiative current
I_{nr}	Non-radiative current
α_m	Mirror loss
α_i	Internal loss
τ_r	Radiative time constant
τ_{nr}	Non-radiative time constant
A	Monomolecular recombination rate
B	Radiative recombination coefficient
B_0	Unperturbed radiative recombination coefficient
n_0	Carrier concentration where phase space filling becomes important
C	Auger recombination coefficient
N_T	Trap concentration
v_n	Carrier velocity
σ_n	Defect cross sectional area
n	Carrier concentration
τ_{DADR}	Time constant of density activated defect recombination
n_w	Number of quantum wells
n_{DADR}	Carrier concentration required to fill strongest localized states
E_a	Activation energy

E_g	Bandgap energy
E	Electric field
$E^{(SP)}$	Spontaneous electric field strength
$E^{(PZ)}$	Piezoelectric electric field strength
ξ	Piezoelectric tensor
s	Strain field
ε	Dielectric constant
T	Thickness
P^{PZ}	Piezoelectric polarization
P^{SP}	Spontaneous polarization
f	Frequency
n_{leak}	Carrier concentration which is confined to the quantum well
D_{leak}	Carrier leakage rate
S_f	Final state
S_i	Initial state
ρ_f	Density of final states
U	Bloch functions
$\psi_{e,h}$	Electron and hole wavefunctions
J	Current density
A_0	Non-carrier concentration monomolecular rate
D	Rate at which the monomolecular recombination coefficient increases with increasing carrier concentration
n_p	Carrier concentration required to fill potential minima
Bulk	Bulk modulus

CONTENTS PAGE

1 Introduction

There has been a rapid development in the field of nitride semiconductors since the first InGaN based high-brightness blue light-emitting diode (LED) became commercially-available in 1993 [1]. The strong interest in nitride semiconductors is due to the large energy emission range (0.7eV to 6.2eV) that may be achieved from the continuous alloy system as shown in Figure 1-1.

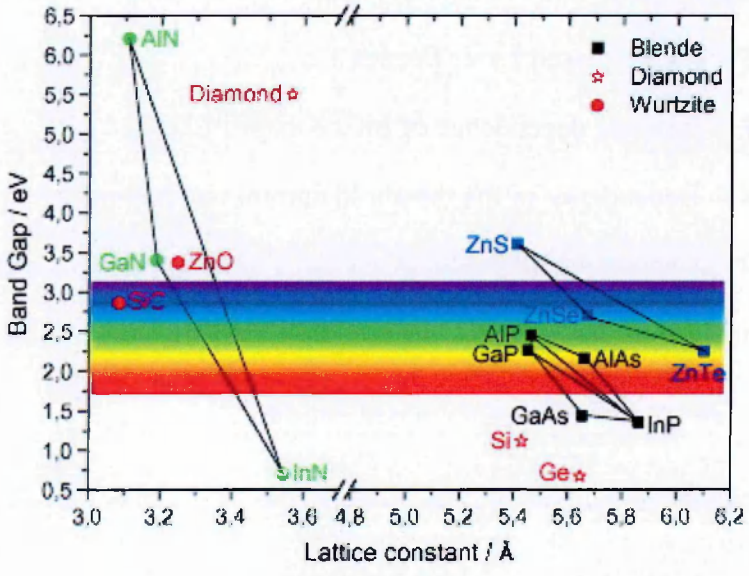

Figure 1-1- Diagram illustrating the band gap of different materials systems and their dependence on lattice constant [2]

Varying the growth temperature and processing times may achieve variations of indium content or quantum well widths that are required to achieve a desired emission wavelength.

The many applications that use InGaN-based emitters are the main driving force behind the technical advancement of nitride semiconductors. These include solid state lighting, televisions and laptops back lighting, displays and communication applications. Whilst the majority of the commercially-available nitride-based applications currently use LEDs, there is also considerable interest in applications which consist of nitride-based laser diodes (LDs). LDs which emit with emission in the violet and blue region have become commercially-available in applications such as high-definition, high-density, blu-ray and DVD players. There is expected to be a similar impact of nitride-based LDs on the optoelectronic industry as that of the nitride-based LEDs over the next decade. Green LDs are currently not commercially-viable but it is expected that the improvement in the efficiency of green laser

diodes and reduced production costs is expected to lead to a large market growth which will reach $500m by 2016 with the green LD expected to be used in 45 million devices [3].

The main driving force in the development of nitride-semiconductors is solid state lighting. Solid state lighting is expected to replace conventional lighting which currently accounts for a fifth of the electrical energy used worldwide [4]. The efficacy rating, a measure of the efficiency and the spectral response of the eye to the wavelength of the emitted light, for conventional lighting technology, such as incandescent and fluorescent bulbs, is unable to show a strong increase due to fundamental conversion limitations. Only 5% of electrical energy is converted into visible light in incandescent light bulbs whilst the remainder of the energy is wasted as heat. The fundamental limitation of fluorescent bulbs is related to the Stoke's loss in converting an emitted UV light wave into one of the visible spectra. The highest efficiency for this type of bulb is 28% [4]. Solid state lighting is expected to become more efficient as there are improvements in the technology used to produce such bulbs.

The efficacy of LEDs is currently increasing at a strong rate with current commercial white LEDs having an efficacy rating of (120 lm/W) [5] and outperforms linear fluorescent lamps (80lm/W) [6]. However, despite the larger efficacy, there is not widespread use of solid state lighting due to the high initial cost of LED bulbs ($22) [7] in comparison with incandescent ($3) [8] and compact fluorescent bulbs ($5.50) [9]. It has been calculated that over a ten year period the LED bulb will be more cost effective in comparison with an incandescent light bulb ($39 for an LED bulb compared to $200 for an incandescent bulb). The currently highly favoured option for lighting is fluorescent bulbs due to their lower initial price and similar long term cost (energy cost over 10 years $43). Therefore reduced initial costs and an efficacy rating of beyond 150lm/W are required in order for solid state lighting to dominate the general lighting markets. Additionally, the bulbs are required to have a high colour rendering rating (the ability for a light source to reproduce various colours of objects). Such an efficacy rating is predicted to be reached for commercial bulbs with good colour rendering in 2015 that would be double the value of fluorescent bulbs and be fifteen times higher than that of incandescent bulbs [10]. Governments have become concerned by the environmental impact of inefficient light bulbs causing many, including an EU-wide directive, to impose a phase-out in the selling of incandescent light bulbs [11]. A similar phase-out of fluorescent bulbs may take place in the future due to the higher energy efficiency of LEDs. Recently, Ikea announced that it would

attempt to set an environmentally friendly example by only selling LED light bulbs by 2016 [12].

Improvements to the production in developing more efficient LEDs is expected to result in solid state lighting replacing conventional light sources over the next decade. The widespread use of solid state lighting will not only benefit users due to the cheaper running costs but there will also be reduced environmental impact due to lower energy consumption of LED bulbs in comparison with conventional light sources. The fluorescent bulbs that are currently used as an energy-saving alternative form of lighting have particularly strong environmental concerns due to the inclusion of mercury.

Long terms predictions show that whilst there is a theoretical limit of 320lm/W for a three colour LED bulb efficacy, with a realistic goal is 213lm/W. The use of bulbs with such an efficacy rating would provide an energy saving of 93% compared with incandescent light sources, 70% compared with compact fluorescent bulbs and 63% compared with linear fluorescent bulbs. This would lead to a total saving in terms of carbon-equivalent emission of 100 megatons a year compared with if incandescent bulbs are used [10].

A major advantage which of solid state lighting is the long lifetime (50000 hours), which is mainly limited by the temperature of the LED and the circuit electronics, compared with incandescent (2000 hours) and fluorescent light bulbs (10000 hours) [13]. LED lighting can also be controlled digitally by the user. This "smart lighting" is also expected to have applications in biology and imaging, display systems, improved lighting in transportation, communications and agriculture [6].

2 Semiconductor Device Theory

2.1 Chapter Introduction

This chapter is an introduction to relevant semiconductor theory that is used to gain an understanding of how semiconductor devices operate. The beginning of the chapter shows that the separation of energy bands (namely, the conduction and valence bands) leads to the emission of photons with a corresponding energy that is approximately equal to this energy separation. The effective mass is then described in order to represent the influence of the ions and core electrons in the material on the electrons in the conduction and valence bands. It is shown that in order to determine the carrier concentration within the conduction and valence bands the density of available states must be considered. The 2D density of states is found to be energy independent and therefore may be exploited in order to achieve a high carrier concentration once states become available. The probability that such energy states are occupied is shown to be determined by multiplying the density of states with the probability that the energy state is occupied.

The next part of the chapter introduces measures that have been used to achieve larger carrier concentrations in the conduction and valence bands by a technique known as doping. Such a technique may provide an n-type material which has a larger number of electrons in the conduction band compared with holes in the valence band or a p-type material which has the opposite effect of a larger number of holes in the valence band compared with the number of electrons in the conduction band. It will be then shown that a pn homojunction is achieved if an n-type material is grown atop p-type material. The homojunction may be modified to include a layer which consists of a smaller band gap to result in improved carrier and light confinement. The quantum well structure is the basis of the semiconductor devices investigated in this study.

It will be shown that light may promote carriers to higher energy levels. In the opposite process the relaxation of carriers to lower energy states may result in the emission of light in a process which may either be stimulated (requiring an incident photon) or spontaneous (involving interaction with a virtual photon).

The properties which impact on the device efficiency are then described where it different aspects of the LED design must be considered in order to achieve the maximum light output power.

The final section of this chapter describes properties of laser diodes.

2.2 Effective mass and energy bands

The separation of energy bands is an important feature in semiconductor materials as the manipulation of this energy separation is used to obtain emitted light wave of a desired wavelength. In such materials, most of the electrons are bound to atoms (valence electrons) and it is only the loosely bound electrons which may be promoted to the conduction band where they are able to conduct. Energy may be supplied to promote electrons from the valence band (bound electrons) to the conduction band (unbound electrons). This process will result in a positive charge occupying a state in the valence band. The positive charge in the valence band is referred to as a hole and the energy gap between the conduction and valence band at zero momentum is known as the bandgap energy as illustrated in Figure 2-1.

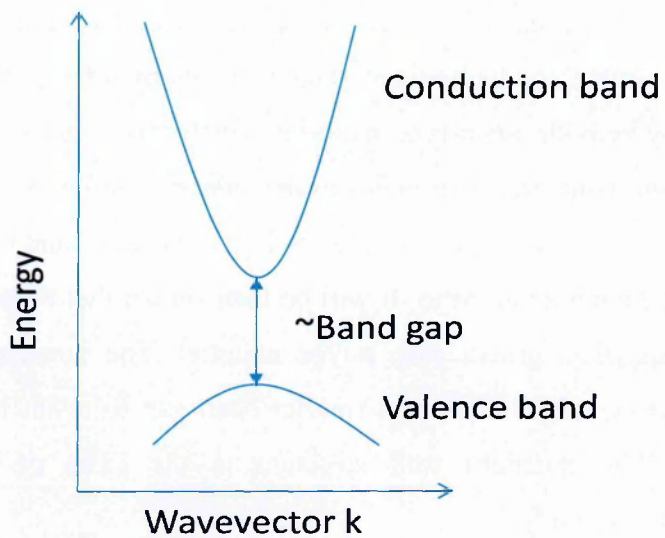

Figure 2-1- The dependence of the energy on wavevector for the conduction and valence bands

Near the band edge the conduction and valence band varies quadratically with momentum, k. The band dispersions, E_{CB} and E_{VB}, may be described by the relationship in Equation 2-1.

$$E_{CB}(k) = E_C + \frac{\hbar^2 k^2}{2m_e^*} \quad \text{2-1a}$$

$$E_{VB}(k) = E_V - \frac{\hbar^2 k^2}{2m_h^*} \quad \text{2-1b}$$

where E_C is the conduction band edge, E_V is the valence band edge, ħ is Plank's constant divided by 2π, k is the wavevector ($\frac{2\pi}{\lambda}$), m_e^* is the electron effective mass and m_h^* is the valence band effective mass.

The release of light from the semiconductor material may take place when electrons in the conduction band recombine with holes in the valence band. The emitted photon will have an energy which corresponds to the difference between the electron and hole energy states.

2.3 Density of States

The available energy states per unit k per unit volume is represented by the density of states. The density of states in k-space in 3D for the conduction and valence bands, $g_{3D,CB}$ and $g_{3D,VB}$, respectively, may be converted into the density of states per unit energy and unit volume to give,

$$g_{3D,CB}(E) = \frac{1}{2\pi^2}\left(\frac{2m_e^*}{\hbar^2}\right)^{\frac{3}{2}}\sqrt{E - E_C} \quad \text{2-2a}$$

$$g_{3D,VB}(E) = \frac{1}{2\pi^2}\left(\frac{2m_h^*}{\hbar^2}\right)^{\frac{3}{2}}\sqrt{E_V - E} \quad \text{2-2b}$$

The confinement of carriers in one direction will result in a modification to the density of states. The density of states in 2D, g_{2D}, is determined as,

$$g_{2D,CB} = \frac{m_e^*}{\pi\hbar^2} \quad \text{2-3a}$$

$$g_{2D,VB} = \frac{m_h^*}{\pi\hbar^2} \quad \text{2-3b}$$

The density of states in 2D is therefore independent of energy. This means that there will be a high number of available energy states once carriers are able to reach the bottom of the

conduction band or the top of the valence band. A comparison of the energy states in 3D and 2D is shown in Figure 2-2.

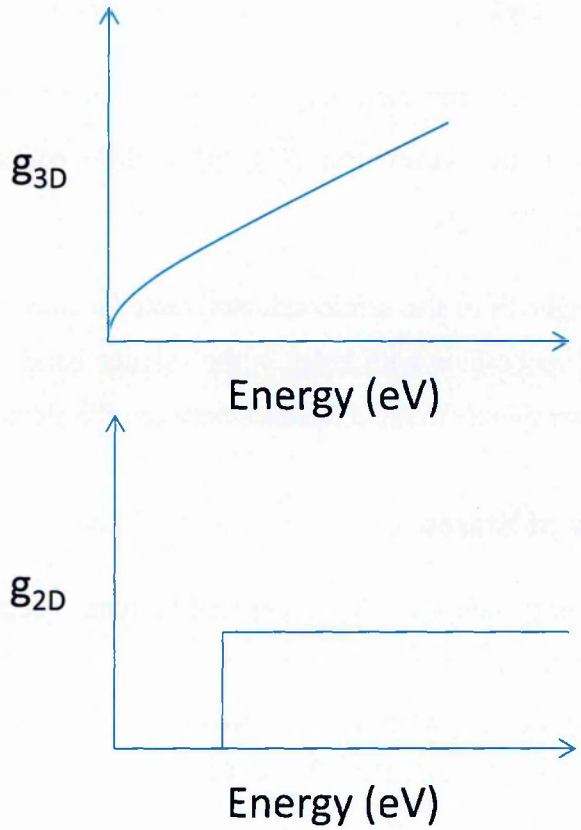

Figure 2-2- The density of states as a function of energy in 3D (upper graph) and in 2D (lower graph).

The density of states must be multiplied by the probability that that energy state will be occupied in order to calculate the carrier concentration within a band. The probability of a particular energy state being occupied may be calculated by considering the Fermi distribution. This distribution uses a Fermi level as a reference energy level where the probability of electron occupation is 0.5. This therefore suggests that most electrons occupy energy states which are below the Fermi level at normal temperatures. The concentration of electrons and holes in the conduction and valence band, respectively, may be determined by using the quasi-Fermi levels. The quasi Fermi levels are Fermi levels for the electrons in the conduction band and holes in the valence band when considered separately. The probability that a particular energy state, E, is occupied in the conduction band, f_{CB}, or the valence band, f_{VB}, given by using the quasi-Fermi distributions, $f_{CB}(E)$ and $f_{VB}(E)$, as given below,

$$f_{CB}(\mathrm{E}) = \frac{1}{\exp\left[\frac{\mathrm{E}-\mathrm{E_{FC}}}{k_B T}\right]+1} \qquad 2\text{-}4a$$

$$f_{VB}(\mathrm{E}) = \frac{1}{\exp\left[\frac{\mathrm{E_{FV}}-\mathrm{E}}{k_B T}\right]+1} \qquad 2\text{-}4b$$

where E_{FC} and E_{FV} are the quasi Fermi levels in the conduction and valence bands, respectively, k_B is the Boltzmann constant, and T is the temperature.

The carrier concentration in the conduction band, n, and the valence band, p, can then be calculated using,

$$\mathrm{n} = \int_{\mathrm{E_C}}^{\infty} g_{CB}(E) f_{CB}(E) dE \qquad 2\text{-}5a$$

$$\mathrm{p} = \int_{-\infty}^{E_V} g_{VB}(E) f_{VB}(E) dE \qquad 2.7b$$

2.4 Doping of Semiconductor Material

Doping is a process whereby impurity atoms are added to the crystal structure to increase the carrier concentration of the conduction and valence bands. The impurity atoms which are introduced to the crystal lattice have energy levels which are slightly below the conduction band (donors) or slightly above the valence band (acceptors). N-type materials are produced as weakly bound electrons from donor atoms are excited to the conduction band whereby they can partake in electrical conduction (see Figure 2-3a). Similarly, p-type materials are achieved as electrons are excited from the valence band to atoms at the acceptor level in a process which results in an increase of holes in the valence band (see Figure 2-3b).

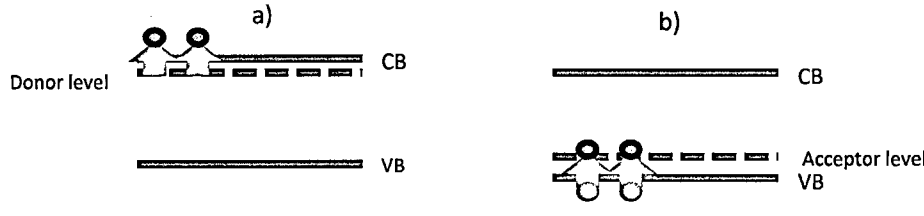

Figure 2-3- Schematically showing the effects of doping for a) n-type material and b) p-type materials

The effect of increasing the electron concentration in the n-type material will cause the Fermi energy to shift towards the conduction band. The increase in the number of holes in the valence band will cause the Fermi energy of the p-type material to be moved towards the valence band. It is the increased probability that electrons in the n-type material will occupy states in the conduction band and holes will occupy states in the valence band that leads to a higher carrier concentration that will increase conductivity.

The Fermi energy may be calculated if it is assumed that at room temperature there is 100% ionization of the dopants. If such is the case, n_D=n, where n_D is the dopant concentration.

Assuming that $n_D=3x10^{18}cm^{-3}$ [14], the energy difference between the conduction band and the Fermi level is determined as,

$$E_C - E_F = -k_B T ln\left(\frac{3x10^{18}}{N_c}\right) \approx 8meV \qquad 2\text{-}6$$

where $N_c = \left(\frac{2\pi m_e k_B T}{\hbar^2}\right)^{\frac{3}{2}}$ where $m_e^* = 0.2m_0$.

The Fermi level in the pGaN can be calculated in a similar manner as ≈ 44meV above the top of the valence band where it is assumed that the acceptor concentration is $1x10^{20}cm^{-3}$ taken from ref.[15] with 100% acceptor ionization.

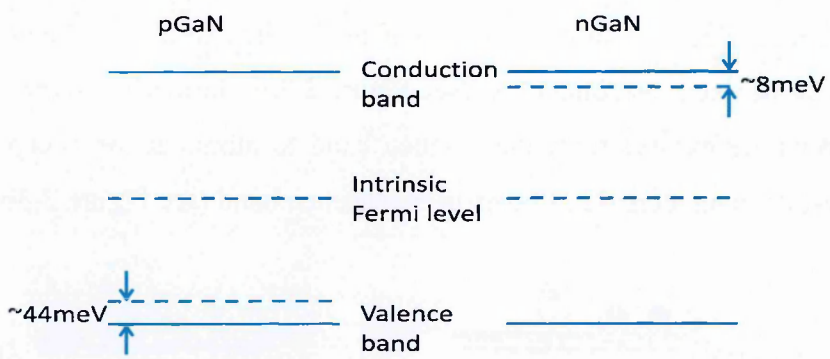

Figure 2-4- The band diagrams of p-GaN and n-GaN where doping changes the intrinsic Fermi level.

2.5 Pn Junction

A pn junction is made if p-type and n-type materials are grown together. The simplest structure of a pn junction is the homojunction which is shown at thermal equilibrium in Figure 2-5.

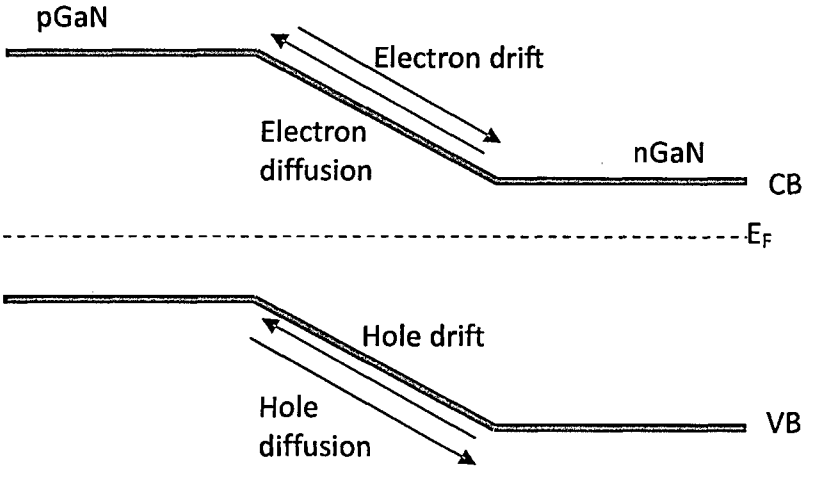

Figure 2-5- Homojunction under zero bias

Electrons in the homojunction will tend to diffuse from the n-type region across the junction into the p-type region. A similar process will result in holes from the p-type region diffusing across the junction into the n-type side. The electrons that have diffused across the junction will be attracted by holes which have diffused into the n-type side of the junction. This will cause the diffused electrons to drift back towards n-type material (see Figure 2-5) and similarly, diffused holes will also be attracted back towards the p-type material. An equilibrium state is reached when the drift and diffusion processes are balanced which will result in a region between the n-type and p-type materials which is known as the depletion region, W_D, as it is depleted of free carriers.

In thermal equilibrium under zero bias the Fermi levels of the p-type and n-type material will align causing a built-in potential which is equal to qV_D, where q is charge and V_D is the potential difference which is formed across the junction (built-in potential). Applying a voltage in the same direction as the built-in potential (reverse bias) will enhance the potential barrier which further restricts the movement of carriers preventing conduction. However, if a strong enough voltage is applied to compensate for the built-in field (forward bias) then there

will be a reduction of the potential barrier and conduction may take place. The effect of forward and reverse bias on the pn junction is shown in Figure 2-6.

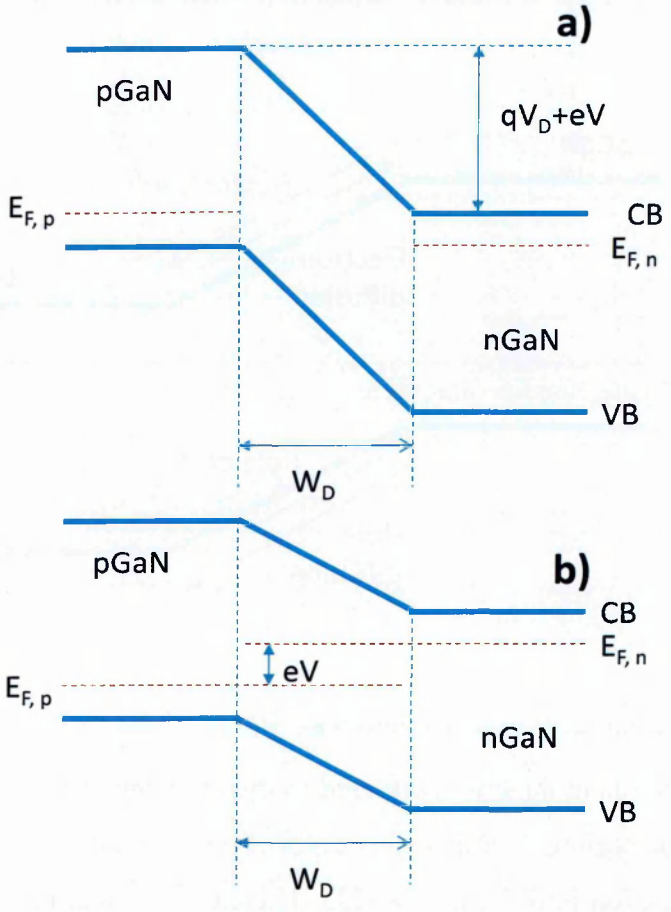

Figure 2-6- Homojunction under a) reverse bias and b) forward bias

The resultant current flow of current in forward (V>0) and reverse (V<0) bias is shown schematically in Figure 2-7.

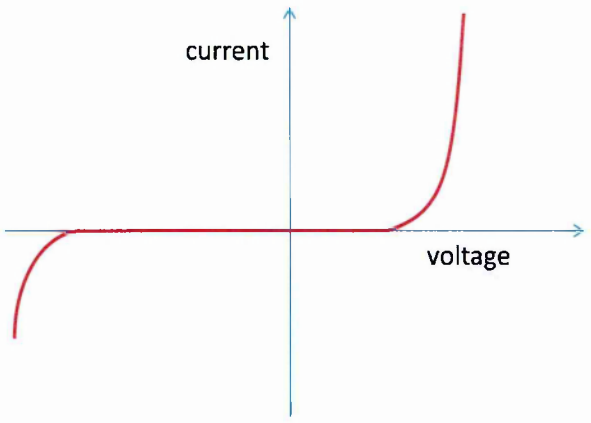

Figure 2-7- The current dependence on voltage for a diode.

One can observe that current will begin to flow once there is a voltage applied which is strong enough to oppose the built-in potential. There is also an exponential increase in current with increasing voltage once there is compensation of the built-in potential.

2.6 Quantum Well Structures

Homojunctions will generally be inefficient light emitters due to high carrier leakage and absorption processes. It is therefore necessary to operate such structures at low temperatures. Most semiconductor-based emitters, however, consist of quantum well structures whereby carriers are confined to an active region of desired energy gap that is surrounded by larger band gap materials as illustrated in Figure 2-8.

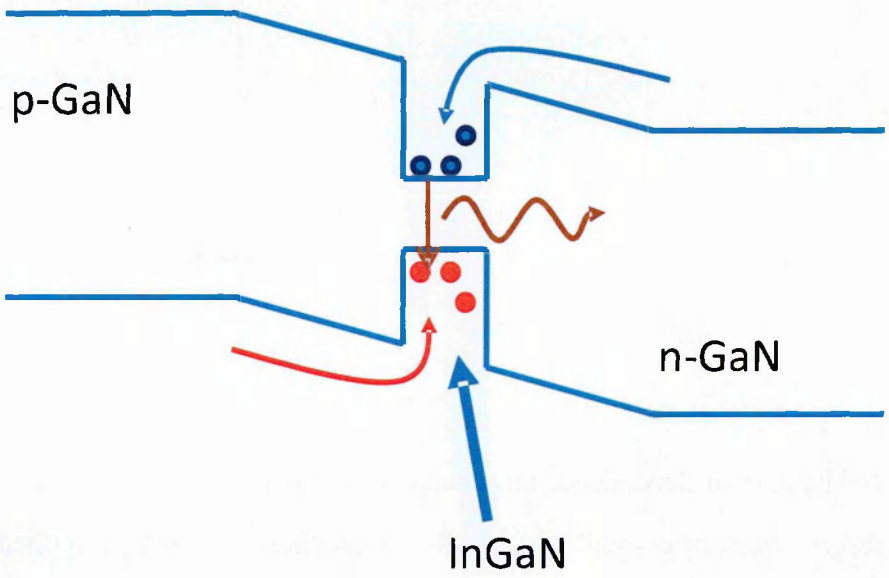

Figure 2-8- A pn junction consisting of a p-GaN, n-GaN and an InGaN active region where electrons are represented by blue dots and holes are represented by red dots.

Electrons and holes will be injected into the active region of the quantum well if a forward bias is applied which is strong enough to overcome the built-in potential. The InGaN active region will have a band gap which is smaller than the band gap of the GaN barriers. Therefore carriers require energy which is larger than this difference in order to escape from the quantum well. The efficiency is therefore improved in comparison with that of the homojunction. The barrier region also has a refractive index (2.54) which is lower than the refractive index of the InGaN active region (3.0) and therefore there will be good light confinement which is important in laser diodes [16].

Another advantage of using a quantum well design is that the energy of the emitting photon can be tuned by varying the quantum well width. This is due to the quantization of carriers where the energy can be determined from,

$$E_{n_q} = \frac{n_q^2 h^2}{8mL^2} \qquad 2\text{-}7$$

where n_q is the quantum number relating to the quantum state. Therefore changes to the quantum well width, L, will cause the energy of the emitted photons to change. The next sections will discuss the different ways in which the devices may emit light.

2.7 Spontaneous emission

The emission of light from LEDs is achieved by the recombination of electrons in the conduction band with holes in the valence band. This process is known as spontaneous emission which is illustrated in Figure 2-9.

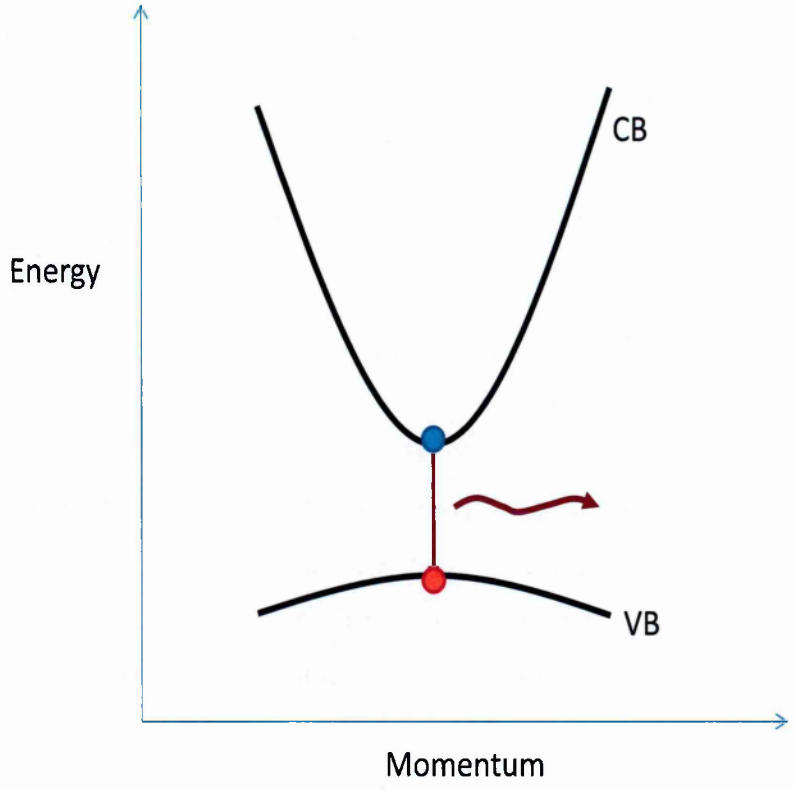

Figure 2-9-Diagram illustrating the spontaneous emission process of an electron in the conduction band recombining with a hole in the valence band.

The emission spectrum from an LED due to spontaneous emission is shown in Figure 2-10.

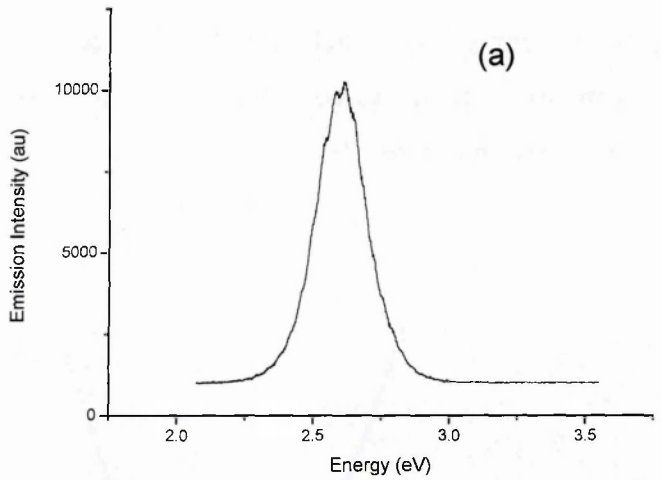

Figure 2-10- Measured emission spectrum due to spontaneous emission of a blue InGaN LED at room temperature.

Figure 2-10 shows that there is a relatively large linewidth of the emission spectra which indicates that the spontaneous emission process involves carriers occupying a range of energies within the conduction and valence bands and that the emitted light will be polychromatic. The larger linewidth of InGaN devices compared with other semiconductor materials such as GaAs is expected to be caused by the localization of carriers at the band edge.

2.8 Stimulated emission

Stimulated emission occurs when electrons in the conduction band are stimulated by photons of a particular energy as illustrated in Figure 2-11.

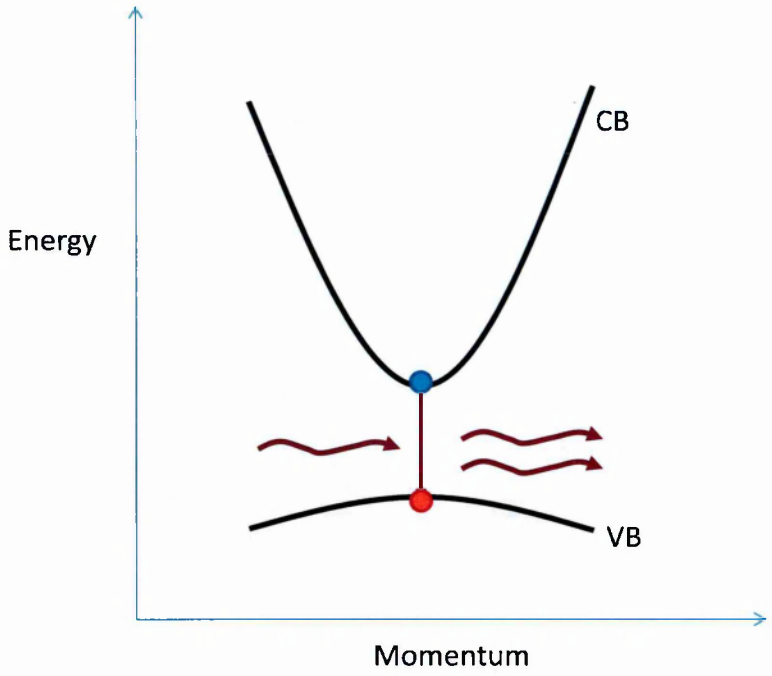

Figure 2-11- Illustration of the stimulate emission process where an incident photon stimulates an electron in the conduction band to recombine with a hole in the valence band to results in two emitted photons.

Laser diodes (LDs) have an optical cavity in order for the stimulated emission process to be sustained and therefore are able to reach high light output powers. The optical cavity consists of two mirrors which reflect emitted photons back and forth through a gain medium that results in lasing being achieved. Incident photons are able to induce additional stimulated emissions that may lead to efficient light emission which is monochromatic, coherent and directional as can be seen by the low linewidth of the emission spectrum as shown in Figure 2-12.

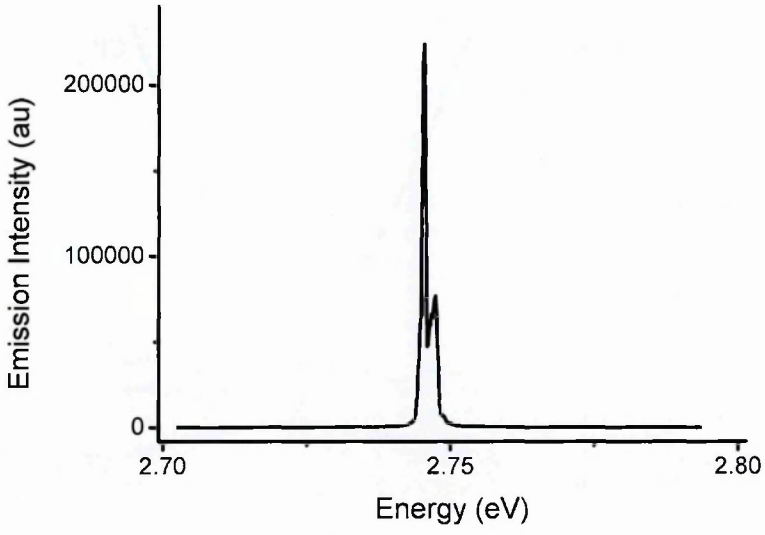

Figure 2-12- Measured emission spectrum due to stimulated emission of an InGaN blue LD at room temperature.

Light emitted from a laser is therefore useful to achieve high irradiance at a single wavelength.

2.9 Internal Quantum Efficiency

The internal quantum efficiency of an LED is the ratio of the amount of light emitted from the active region compared with the amount of charge injected into the active region and is described using the relationship,

$$\eta_{int} = \frac{P_{int}/(h\nu)}{I/e} \qquad 2\text{-}8$$

where P_{int} is the optical output power emitted from the active region, h is Plank's constant, ν is the frequency of the emitted photon, I is the injected current and e is the charge of an electron.

2.10 Extraction Efficiency

The total efficiency of the LED will also be influenced by the extraction efficiency. Photons will either be emitted into free space or will not be emitted from the semiconductor die. Loss processes including absorption of photons by the substrate material or the metal contacts and total internal reflection at the semiconductor die-free space interface reduce the extraction efficiency. The light extraction efficiency is determined by

$$\eta_{extraction} = \frac{P_{int}/(hv)}{P/(hv)} = \frac{\mathrm{P_{int}}}{\mathrm{P}} \quad 2\text{-}9$$

where P is the optical output power emitted into free space.

2.11 External Quantum Efficiency

The external quantum efficiency which accounts for the internal and extraction efficiencies and is described by equation 2-10,

$$\eta_{ext} = \frac{P}{I}\frac{\mathrm{e}}{\mathrm{hv}} = \eta_{int}\eta_{extration} \quad 2\text{-}10$$

where e is the charge of an electron, and I is the injected current.

The efficiency measurements of LEDs may therefore be achieved by taking a ratio of the light output power compared with the injected current,

$$\eta = \frac{P}{I} \quad 2\text{-}11$$

In the remainder of this thesis the external efficiency will be referred to as the efficiency as it is the most useful description of LED performance.

2.11.1 Wall Plug Efficiency

The final measure of efficiency, which is mainly used in the solid state lighting industry, is wall plug efficiency, η_{WP}. This value is a measure of the optical output power compared with electrical input power,

$$\eta_{WP} = \frac{P}{IV} \quad 2\text{-}12$$

where V is the applied voltage.

2.11.2 Light Cone Escape

Only the light emitted at angles close to normal incidence from the active region will be able to be emitted from the semiconductor material. Light that is emitted at an angle which exceeds the critical angle, θ_c, will be totally internally reflected. The critical angle is determined by,

$$sin\theta_c = \frac{n_{air}}{n_s} \quad 2\text{-}13$$

where n_{air} is the refractive index of air and n_s is the refractive index of the semiconductor material.

The angle at which light is internally reflected is described as the light escape cone where photons that are emitted into the cone are emitted from the semiconductor die, whilst light emitted outside of the cone suffers from total internal reflection as shown in Figure 2-13.

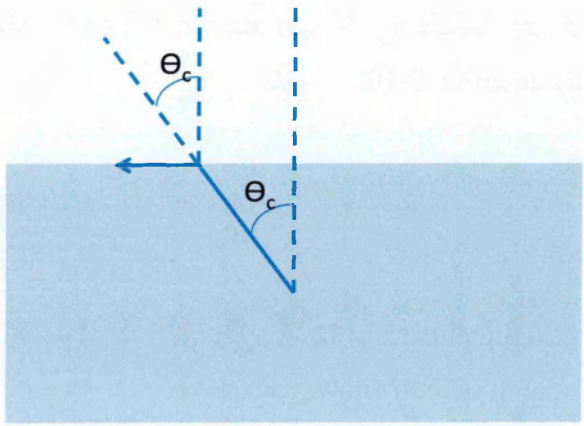

Figure 2-13- Illustration showing total internal reflection will occur in a semiconductor die if the light is emitted at an angle greater than the critical angle, θ_c.

The light intensity, however, will reduce as the angle of incidence is increased from the normal incidence in planar LEDs (see Figure 2-14a). An alternative growth method can be used to obtain a hemispherical design which has isotropic light emission (Figure 2-14b). An enhancement to the light emission at the widest angles can be achieved in parabolic LEDs (Figure 2-14c).

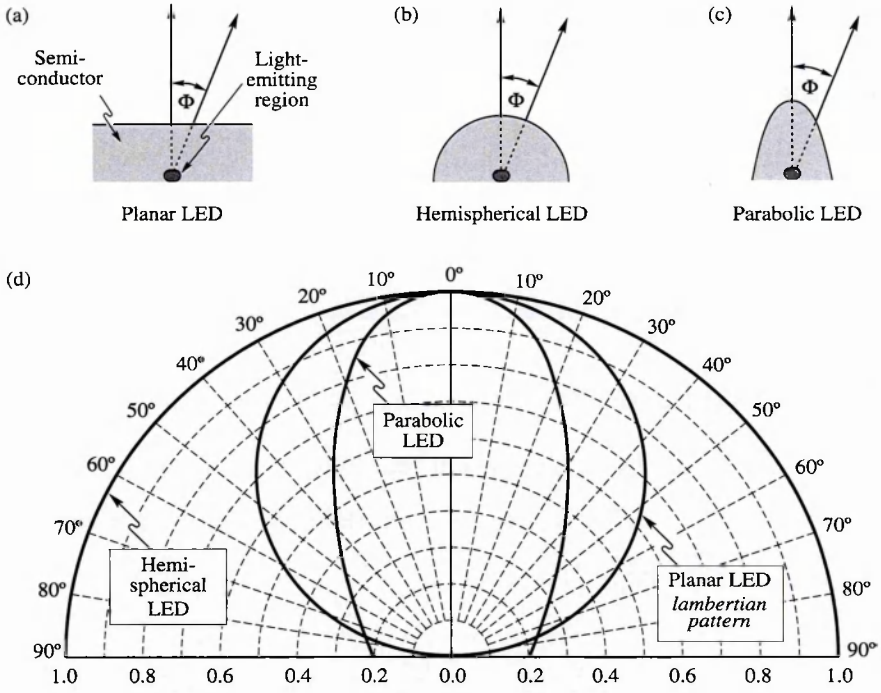

Fig. 5.5. Light-emitting diodes with (a) planar, (b) hemispherical, and (c) parabolic surfaces. (d) Far-field patterns of the different types of LEDs. At an angle of $\Phi = 60°$, the lambertian emission pattern decreases to 50 % of its maximum value occurring at $\Phi = 0°$. The three emission patterns are normalized to unity intensity at $\Phi = 0°$.

Figure 2-14- Schematic illustrating the far field light patterns of planar, hemispherical and parabolic LEDs (diagram from [17])

The light emission properties at different angles are shown in Figure 2-14d for the different LEDs. Despite the advantages of the isotropic emitted light being achieved in the hemispherical LED and a higher intensity of light being emitted at the wider angles in the parabolic LED, most LEDs are grown with planar surfaces due the significantly lower production costs.

2.11.3 Epoxy Domes

Epoxy encapsulates of high refractive index surround the planar LEDs in order to enhance the light extraction efficiency. This process increases the critical angle at which total internal reflection will occur which thereby increases the proportion of light which is emitted from the semiconductor chip. If n_s=3 [18] and n_{air}=1 is considered, then the critical angle is calculated by using Equation 2-17 to be 19.5°. The refractive index of the epoxy dome is approximately 1.5 [19] and therefore if n_{air} is replaced by this value in Equation 2-13, a larger critical angle of 30° is obtained.

The epoxy material may also be altered to obtain desirable properties such as converting the colour of the emitted light with a phosphor. This may have particular benefits in the solid state lighting industry as the colour of the embedded phosphor in the epoxy may be used to provide "warm" or "cold" lighting.

2.12 Semiconductor Laser Properties

2.12.1 Threshold Current

The threshold current, I_{th}, is the current required in order for optical gain to overcome optical losses and consists of radiative, I_r, and non-radiative, I_{nr}, components and is described using the following relationship,

$$I_{th} = I_r + I_{nr} \qquad 2\text{-}14$$

The radiative current is due to spontaneous emission and the non-radiative current consists of contributions from non-radiative recombination such as Shockley-Read-Hall recombination, carrier leakage and Auger recombination. It is therefore important to determine and reduce the loss processes taking place in order to reduce the non-radiative current that will lead to a reduction of the threshold current. This will subsequently improve the output power of the laser diode at a given current.

2.12.2 Gain

The laser gain describes the factor in which the light is amplified per unit length. The lasing threshold is met when the optical gain and losses due to one round trip of a photon are equal. The lasing condition may then be determined by equation 2-19

$$g_{threshold} = \alpha_0 - \frac{1}{2L}\ln(R_1 R_2) \qquad 2\text{-}15$$

where α_0 is the waveguide loss that is due to optical absorption, L is the length of the gain medium, R_1 and R_2 are the reflectivities of the mirrors.

The output power of a laser beyond the threshold has a strong linear dependence on injection current as shown in Figure 2-15.

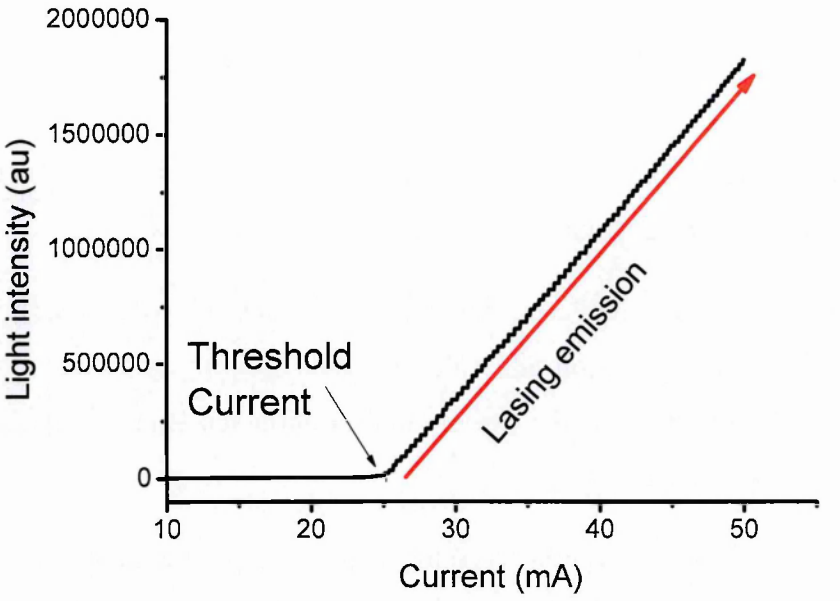

Figure 2-15- Measured light output dependence on injection current for a laser diode showing that there will be a strong increase in the light output power above the threshold current that results from stimulated emission taking place.

2.12.3 External Differential Efficiency

The external quantum efficiency of a laser diode is a measure of the dependence of light output compared with injected current above threshold. The external differential efficiency [20] may be expressed as

$$\eta_0^d = \eta_s^d \eta_i^d \eta_r^d \frac{\alpha_m}{\alpha_i + \alpha_m} \qquad 2\text{-}16$$

where η_s^d is the proportion of the current above threshold that is delivered to the active region, η_i^d is the proportion of the injected carriers that enter the quantum well, η_r^d is the proportion of carriers that enter the quantum well that result in stimulated emission, α_m is the mirror loss and α_i is the internal loss.

Ideally, the quasi Fermi levels splitting pins above threshold [21] causing the spontaneous and non-radiative rates to remain constant. This means that all additional injected carriers above threshold result in an increase in the stimulated emissions rate of photons and therefore above threshold, η_r^d is close to unity.

2.13 Summary of Chapter

This chapter presented relevant information about semiconductor materials which is required to understand how such devices operate. The release of light is achieved when electrons in the conduction band recombine with holes of the valence band where the energy of these bands was described as having a quadratic dependence on momentum.

The density of states and the Fermi function may be considered in order to obtain the carrier concentration in the conduction and valence bands. Doping is a technique which has been found to significantly increase the carrier concentration and lead to significant improvements of the device performance.

Growing a p-type and an n-type material together will cause the Fermi levels to align and thus causing an in-built field which must be compensated for in order for current to flow. The formation of the pn junction is required to obtain a diode.

It was shown that a quantum well structure may be grown in order to achieve efficient carrier confinement. This is due to the larger energy of the GaN barriers resulting in a potential difference which the carriers must overcome in order to escape.

The spontaneous emission was found to provide an energy spectrum which has a range of energies due to the fact that this emission process occurs between carriers that occupy different energy states in the conduction and valence bands. In contrast, a sharp peak of high intensity is shown in the emission spectra of laser diodes. This observation is due to the stimulated emission taking place between electrons and holes of a certain energy difference that will lead to the emission being monochromatic, coherent and in the same direction as the incident photons that cause the transitions.

The final section of this chapter presented information regarding the efficiency of devices. It is shown that the epoxy encapsulate is an important property of LED design which is used to enhance the extraction efficiency.

3 Background and Theory relating to Nitride Emitters

3.1 Chapter Introduction

This chapter is an introduction to the efficiency droop effect which is observed to occur in nitride-based LEDs. The impact of the different recombination mechanisms as a function of current will be described in order to gain insight into efficiency droop. The phase space filling effect will be shown to reduce the radiative recombination rate to an approximately linear dependence on carrier concentration at high currents. The influence of such an effect on the efficiency droop will also be discussed.

The chapter will then describe the dependence of different loss mechanisms on injection current. It will be shown that a loss mechanism which has higher carrier concentration dependence than that of radiative recombination is required to explain efficiency droop. The remainder of this chapter describes the relative likelihood of different processes which have been proposed in the literature to cause efficiency droop such as Auger recombination, carrier leakage and defect-related recombination.

3.2 Efficiency Dependence on Current

The external quantum efficiency that was described in Section 2.11 may be measured by comparing the ratio of radiative recombination to the total recombination. It may be calculated by considering the time constants of radiative, τ_r (which is the inverse of the radiative rate) and non-radiative processes, τ_{nr} (which is the inverse of the non-radiative rate) by using the relationship

$$\eta = \frac{\text{radiative recombination rate}}{\text{non-radiative recombination rate}} = \frac{\tau_r^{-1}}{\tau_r^{-1}+\tau_{nr}^{-1}} = \left(1+\frac{\tau_r}{\tau_{nr}}\right)^{-1} \qquad 3\text{-}1$$

In an experimental measurement, the efficiency is measured by dividing the light output power with the input current (see equation 2-11) and will provide an efficiency dependence on current as shown in Figure 3-1.

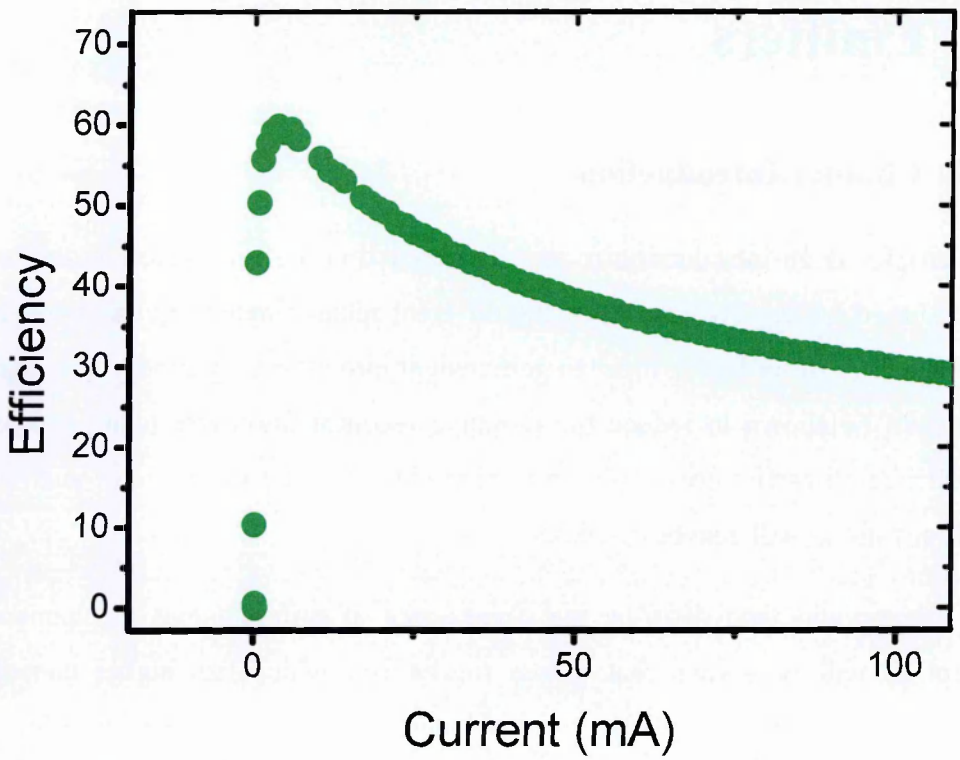

Figure 3-1- Measured efficiency dependence on injection current for a green LED

Figure 3-1 shows that the efficiency of the LED reaches a maximum at a relatively low injection current and reduces upon further current injection in a phenomenon known as efficiency droop. The efficiency droop effect is particularly problematic because most nitride-based applications require large currents where there is higher light output. The recombination mechanisms of InGaN-based emitters are currently under intense scientific investigation to understand the cause of efficiency droop.

3.3 Radiative Recombination

Radiative recombination of electrons in the conduction band with holes in the valence band leads to the generation of photons from semiconductor devices as described in Section 2.7. The rate of radiative recombination is proportional to the concentration of electrons and holes as shown in the relationship,

$$R_{Radiative} = Bnp \qquad 3\text{-}2$$

where B is the radiative recombination coefficient, n is the electron carrier concentration and p is the hole concentration.

The radiative recombination coefficient is a measure of the rate of radiative emission and can be calculated if the band gap energy, absorption coefficient and refraction index of a material are known by using the Roosbroeck-Shockley model [22].

At thermal equilibrium, it is often assumed that the electron concentration will be equal to the hole concentration [22], and hence Equation 3-2 may be re-written as,

$$R_{Radiative} = Bn^2 \qquad 3\text{-}3$$

where n is the carrier concentration assuming n≈p.

3.3.1 Phase space filling

Phase space filling is a process which leads to high energy states being occupied at high injection levels due to the population of low energy states. The relationship in Equation 3-3 shows that the radiative recombination is expected to have quadratic carrier density dependence at low carrier densities. However, previous studies show that phase space filling will reduce the radiative recombination rate at high currents [23, 24]. Figure 3-2 shows an illustration showing a changing momentum value between the electrons and holes at high injection that occurs because of the different effective masses of the conduction and valence bands.

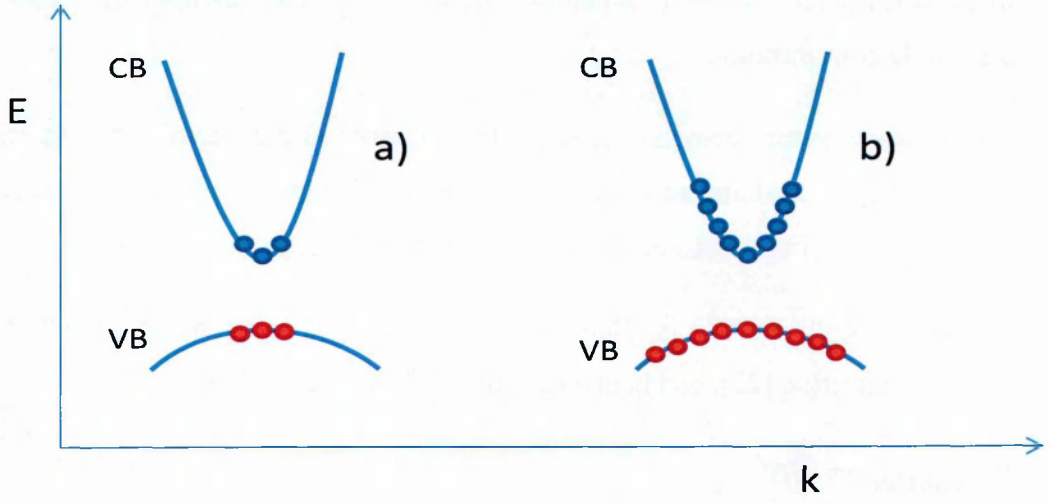

Figure 3-2-The effects of phase space filling whereby at low injection currents (a) there is a similar momentum value at low injection currents (b) an increased momentum mismatch at high injection currents.

The increasing momentum mismatch between the electron and holes will lead to a reduction in the radiative recombination rate at high carrier concentrations, as shown in Figure 3-3 [25].

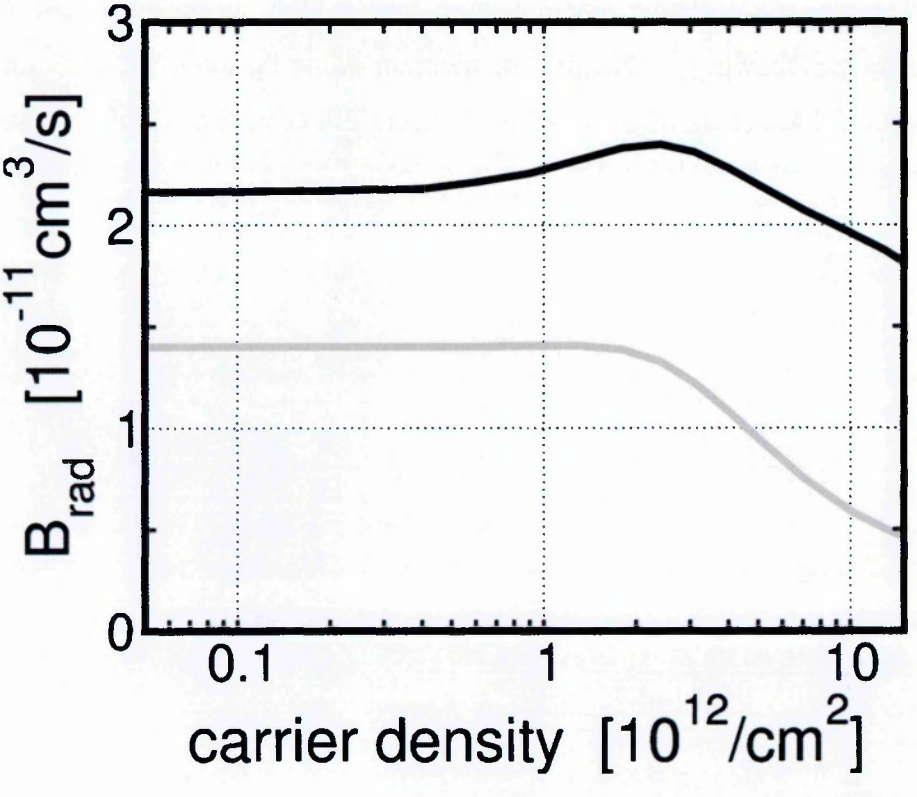

Figure 3-3- Semi-logarithmic scale showing the dependence of radiative recombination on carrier concentration for 410nm device (black line) and a 530nm device (grey line) which takes into account both the increase in the radiative rate due to an increased electron and hole wavefunction overlap and the reduction in the radiative recombination rate due to the increasing momentum mismatch between the electrons and holes at high injection {taken from [26]}.

Figure 3-3 shows the dependence of the radiative recombination coefficient on carrier concentration will be constant at low injection levels and reduce at high injection levels. The dependence of the radiative recombination rate on the carrier injection level will be influenced by the screening of the internal fields with increasing carriers concentration (increasing the radiative rate- mid currents for the 410nm device (black line in figure)) and phase space filling effects (which reduce the radiative rate- at high currents).

The relationship between the radiative coefficient and carrier concentration due to phase space filling effects may be described as [27],

$$B = \frac{B_0}{(1+\frac{n}{n_0})} \qquad 3\text{-}4$$

with B_0 is the radiative coefficient of a material in the absence of phase space filling effects and n_0 is a constant which is caused by phase space filling.

The diagram below shows the influence of the radiative recombination coefficient reducing from $10^{-10}cm^3s^{-1}$ (red line) to $10^{-11}cm^3s^{-1}$ (blue line) on the efficiency. The green line shows the effect of phase space filling where there is a reduction in the current at which the efficiency begins to saturate but the overall trend of an increasing efficiency with increasing current density remains.

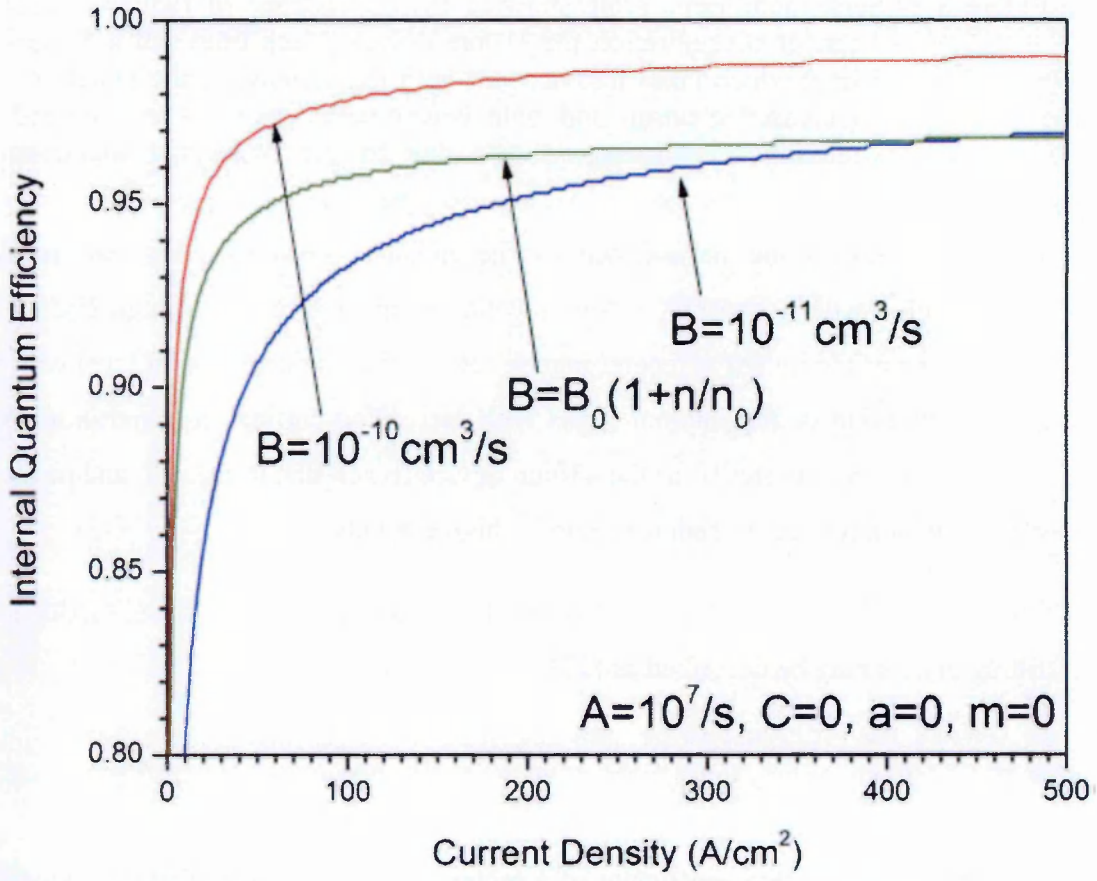

Figure 3-4- Internal quantum efficiency dependence on current density with different radiative parameters. The red line represents $B=10^{-10}cm^3s^{-1}$, the blue line represents a radiative recombination coefficient of $B=10^{-11}cm^3s^{-1}$ and the green line represents the effect of a reducing radiative rate due to phase space filling effects with $B_0=7 \times 10^{11}cm^{-3}s^{-1}$, $n_0 = 5 \times 10^{18}cm^{-3}$ for a 430nm quantum well device {taken from [28]}

It is shown that the influence of phase space filling will not result in efficiency droop but may facilitate an earlier onset of efficiency droop if a droop-causing mechanism is present.

3.4 Non-Radiative Recombination

3.4.1 Defect-related Recombination

The existence of non-radiative recombination in semiconductor devices will reduce the proportion of radiative recombination and limit the device efficiency. One form of non-radiative recombination is Shockley-Read-Hall recombination via defect sites that occurs due to impurity atoms, native defects and dislocations. The existence of defect sites within the forbidden gap is expected to capture electrons from the conduction band and holes from the

valence band and release energy through the emission of a phonon or a photon which has a smaller energy than that of the band gap.

Defect-related recombination is expected to be proportional to the defect density, trap size and carrier concentration providing that the defect density is small compared with the carrier concentration [29, 30]. The non-radiative lifetime, τ_{nr}, due to recombination at defect sites may be described by Equation 3-5.

$$\tau_{nr} = \frac{1}{N_T v_n \sigma_n} \qquad 3\text{-}5$$

Where N_T is the defect trap concentration, v_n is the carrier velocity and σ_n is the cross section of the defect traps.

The monomolecular rate, also known as the Shockley-Read Hall recombination rate, may therefore be determined from,

$$R_{nr} = \frac{n}{\tau_{nr}} = (N_T v_n \sigma_n) n \qquad 3\text{-}6$$

where n is the carrier concentration.

The combined constants (N_T, v_n and σ_n) are usually replaced by the non-radiative recombination coefficient, A, to simplify Equation 3-6 to,

$$R_{nr} = An \qquad 3\text{-}7$$

The efficiency equation (Equation 3-1) can therefore be re-written as the ratio of the radiative recombination rate compared with the total recombination rate which consists of both the radiative and non-radiative monomolecular recombination if all other loss mechanisms are neglected.

$$\eta = \frac{Bn^2}{An + Bn^2} = \left(1 + \frac{\mathrm{An}}{\mathrm{Bn}^2}\right)^{-1} \qquad 3\text{-}8$$

Modelling the efficiency using Equation 3-8 shows that the efficiency is expected to be 100% over the entire carrier density range if monomolecular defect-related recombination is negligible as shown in Figure 3-5 (black line).

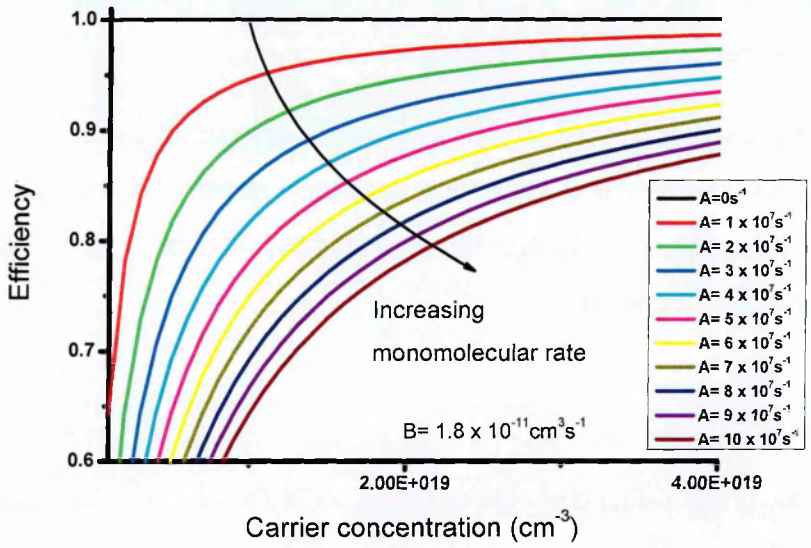

Figure 3-5- Modelled efficiency dependence on carrier density for different monomolecular recombination rates from $0s^{-1}$ to 10^8s^{-1} (radiative recombination rate, B=1.8 x $10^{-11}cm^3s^{-1}$ from Shen *et al.* [31]).

Figure 3-5 also shows that the effects of an increasing monomolecular rate will reduce the efficiency over the entire current range and cause an increase in the carrier concentration at which the efficiency begins to saturate. The modelled increase in defect-related recombination rate is consistent with the experimental observations of Schubert *et al.* where devices of higher dislocation density were found to have a reduced peak efficiency [30]. In the study it is shown that the increased defect-related recombination rate results in a reduction of the efficiency droop. The authors therefore conclude that a defect-related loss mechanism is not the cause of efficiency droop [30]. However, as high efficiency is achieved in InGaN based devices despite a high number of threading dislocations, efficiency droop may be still be caused by a defect-related loss mechanism which will be discussed further in sections 3.4.3 and 3.7.

3.4.2 Auger Recombination

Auger recombination is a non-radiative process where the energy produced by the recombination of an electron with a hole promotes a third carrier to a higher energy state. This process has been suggested to reduce the efficiency of InGaN-based devices at high injection currents [31-33]. To a first approximation the Auger recombination process is expected to have cubic carrier concentration dependence due to the involvement of three carriers. This process is therefore consistent with experimental observations of a cubic carrier concentration

dependence on the injection current in the current regime where efficiency droop occurs as shown in Figure 3-6.

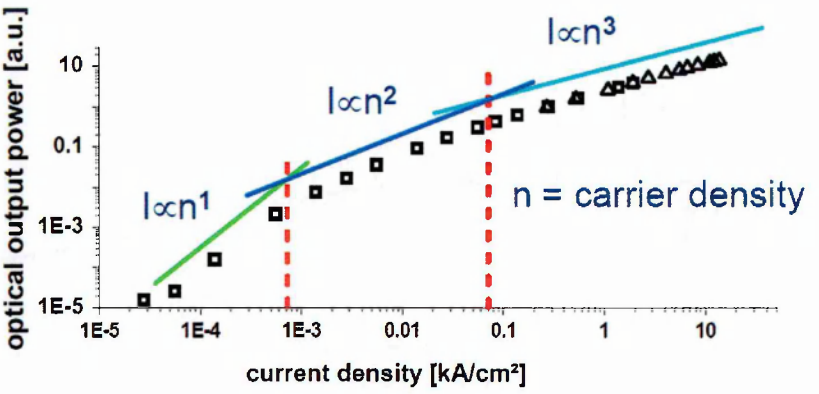

Figure 3-6-Double logarithmic plot of the optic emission power as a function of current density indicating the difference carrier density dependences. This may be the result of different recombination mechanisms occurring in different current regimes [34].

The current density, J, will therefore have contributions from defect-related recombination, radiative recombination and Auger recombination if other loss processes such as carrier leakage are neglected as shown in the relationship,

$$J = \mathrm{eL}(An + Bn^2 + Cn^3) \qquad 3\text{-}9$$

where L is the active layer thickness, e is the electron charge, n is the carrier density and A, B and C are the monomolecular, radiative and Auger recombination coefficients, respectively.

The efficiency is said to be described by using the "ABC" model if defect-related recombination, radiative recombination and Auger recombination are the only recombination mechanisms. The efficiency equation using the ABC model is then,

$$\eta = \frac{Bn^2}{An+Bn^2+Cn^3} \qquad 3\text{-}10$$

Many groups have concluded that Auger recombination is the cause of efficiency droop based on the fact that they can fit their experimentally observed efficiency droop using this model. Figure 3-7 shows that this model will show efficiency droop if Auger recombination is included in the efficiency equation.

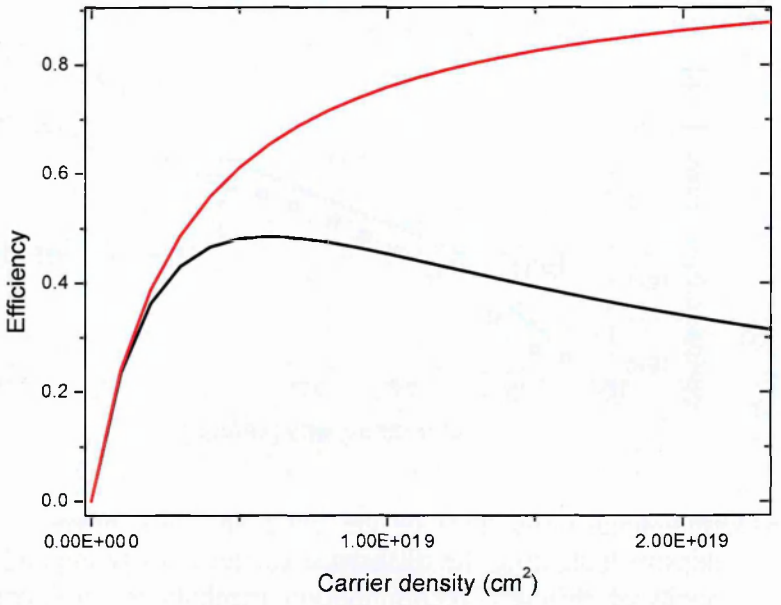

Figure 3-7-Modelled efficiency dependence on carrier density when modelled using an Auger recombination argument using A= 5.7 x $10^{7}s^{-1}$, B=1.8 x $10^{-11}cm^{3}s^{-1}$ and C = 1.6 x $10^{-30}cm^{6}s^{-1}$ (as measured in *Shen et al.*[31]) (black line) compared with the case where there is no Auger recombination (red line).

Despite the good agreement of the model with experimental observations the physical reason for such a high Auger recombination rate in wide bandgap devices is unclear. Theoretical calculations and experimental data predict that the intraband Auger recombination rate reduces as the band gap energy increases as shown in Figure 3-8 and will not be strong enough to cause droop in devices which have band gap energies which are above ~2eV.

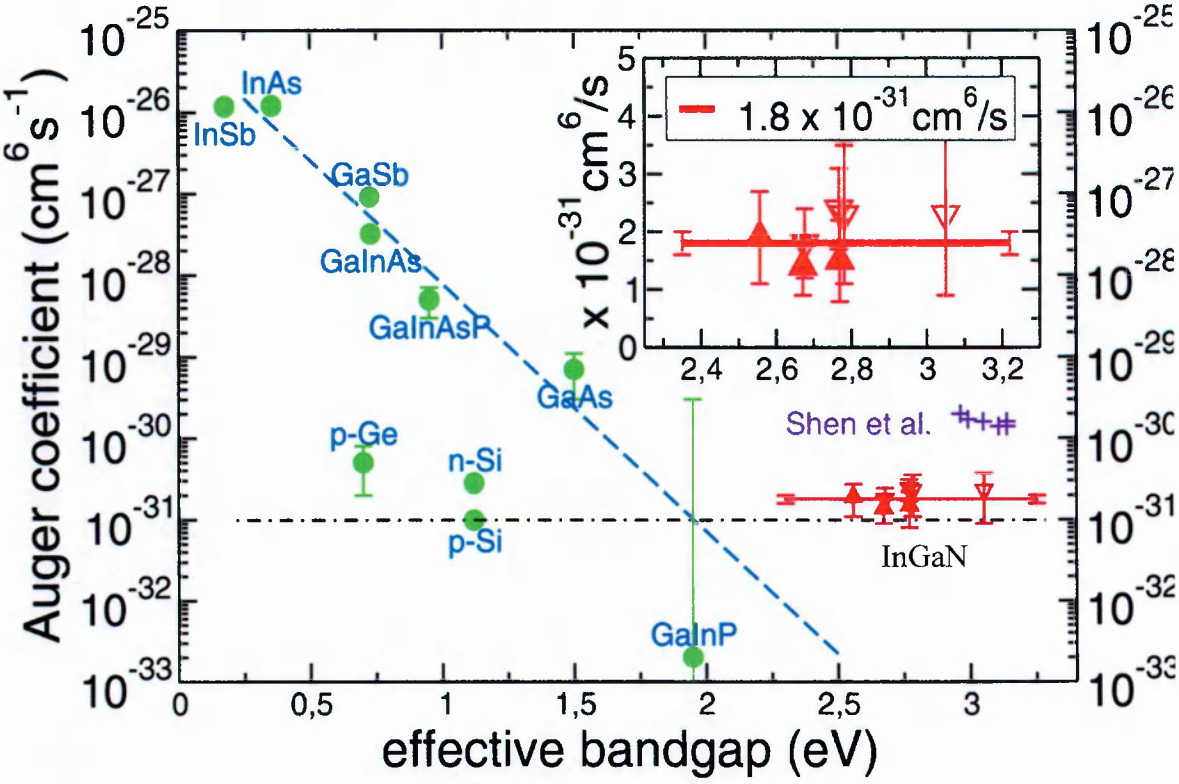

Figure 3-8 Auger recombination coefficient, C, as a function of band gap for different materials determined experimentally and from theoretical calculations. The green dots represent direct Auger recombination, whilst the red dots represents possible indirect Auger recombination (from Brendel *et al.* [35]).

The reduction in the number of states available where the energy and momentum will be conserved following an Auger recombination process reduces with increasing bandgap energy. One would therefore expect a negligible Auger coefficient in nitride-based devices which have bandgap energies of 2-3.5eV. This finding indicates a direct Auger recombination process is unlikely to be the dominant cause of efficiency droop in nitride-based LEDs.

It was suggested by Delaney *et al.* that inter-band Auger recombination may be the cause of efficiency droop [36]. In this process, Auger recombination promotes electrons to higher energy states in a second conduction band as illustrated in Figure 3-9 . Figure 3-9 also shows that there will be a strong increase of the Auger recombination coefficient in the blue-green emission region if this process takes place.

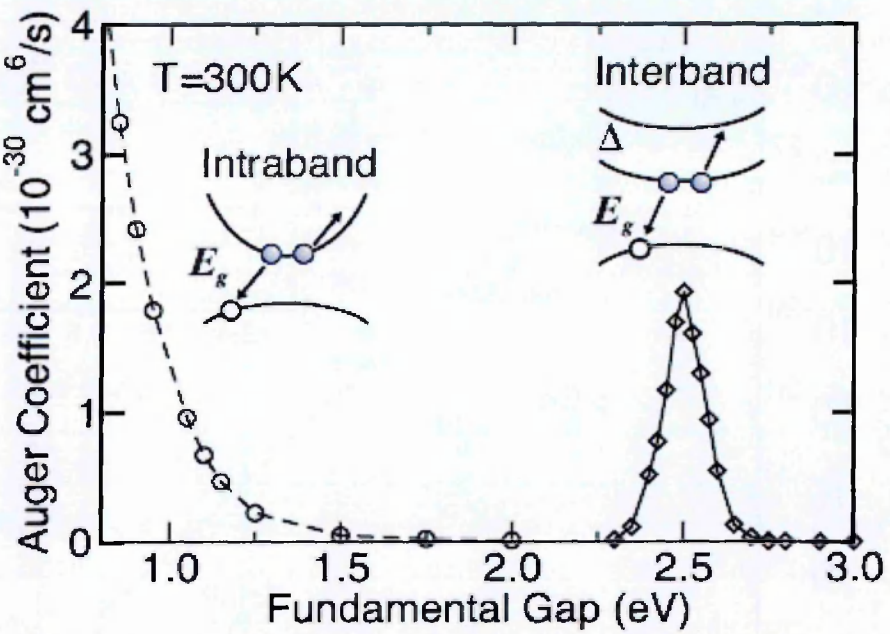

Figure 3-9- The Auger coefficient as a function of band gap energy where there is a sharp resonance in the Auger recombination coefficient due to inter-band Auger recombination that is caused by available states in the second conduction band (from Delaney *et al.* [36])

Inter-conduction band Auger recombination is, however, only predicted to occur in devices of a limited range of energies (2.25eV to 2.75eV) and is unlikely to explain the efficiency droop effects for devices which have emission over the entire violet-blue-green region. Further calculations by Bertazzi *et al.* [37] also indicate that the contribution of Auger recombination due to transitions to the second conduction band will be negligible, hence this theory has not gained traction.

Microscopic many-body calculations [32] were performed to determine whether alternative forms of Auger recombination will also have cubic carrier density dependencies. Pasenow *et al.* [32] show that the carrier density dependence of indirect Auger recombination processes will be similar to that of the direct Auger recombination process and determined that an Auger recombination process which is mediated by a phonon (as illustrated in Figure 3-10) is a more probable cause than a direct Auger process. The release of energy and momentum through the emission of a phonon will satisfy momentum and energy laws leading to an increased likelihood that an indirect Auger process occurs in comparison with the direct Auger recombination process.

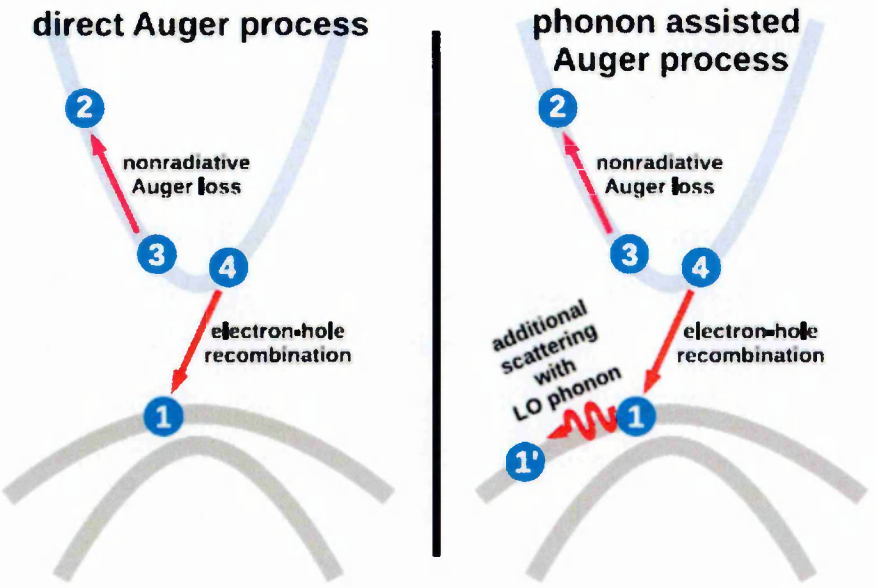

Figure 3-10- Illustration of a direct Auger process (left) and an indirect Auger process which is accompanied by a phonon (right) {taken from [32].

The authors suggest that the phonon-assisted Auger process is expected to be stronger in the nitride-based devices because there is a stronger electron-phonon coupling due to the smaller dielectric constants of the nitrides (GaN, 9.7) compared with longer wavelength devices from other material systems (e.g. GaAs, 12.9). The smaller dielectric constant is expected to cause a stronger coulomb interaction which may enhance the Auger recombination rate. The high effective mass of the holes in the nitride material system and the strong electron-LO phonon Frohlich interaction is also believed to enhance the Auger recombination rate. Carrier localization, which will be discussed in more detail in Section 3.7, is also likely to enhance the Coulombic interaction [38].

Further support that indirect Auger recombination may be significant in nitride based devices is found in the first principle calculations of Kioupakis *et al.* [33]. The calculations indicate that phonon-assisted and alloy scattering processes are the cause of indirect Auger recombination in InGaN. The alloy scattering process is found to be caused by the local break in crystal symmetry that is experienced by introducing indium atoms to the GaN lattice. The cause of the phonon-assisted Auger recombination processes is suggested to be enhanced in the nitride-based material due to their ionic nature which will result in strong carrier-phonon coupling [39]. The calculations find that the Auger coefficient increases, in addition to a reduction of the radiative recombination coefficient [39], with reducing band gap. The authors

therefore attribute indirect Auger recombination as the dominating cause of the "green-gap" problem where devices with emission in the green region have reduced efficiencies compared with devices which emit in the red or blue region.

Photoluminescence measurements taken by Shen *et al.* [31] on quasi-bulk InGaN layers grown on GaN which do not have strong internal polarization fields (these fields will be discussed in more detail in Section 3.6) indicate that droop will occur when carriers are optically excited despite there being no issues relating to the injection of holes (further details of this effect will be discussed in Section 3.5). Droop in the resonant optical excitation experiments was observed to occur at low excitation levels where there is not expected to be the escape of carriers over potential barriers. A fit of the efficiency as a function of excitation density provided Auger coefficients of (1.4-2) x $10^{-30}cm^6s^{-1}$ for different samples. Such an Auger recombination coefficient is four orders of magnitude higher than the value that is extrapolated from the Auger coefficient vs bandgap trend (1x10 $^{-34}cm^6s^{-1}$) (see Figure 3-8).

David *et al.* provide further support that an Auger recombination model will result in efficiency droop by taking radiative and non-radiative differential carrier lifetime measurements [27]. The non-radiative lifetime is measured and extrapolated to obtain a lifetime value for Shockley-Read-Hall recombination. This value is then used with measurements of the efficiency and carrier concentration to calculate the radiative and non-radiative lifetime as a function of carrier concentration. It was found that the non-radiative lifetime is approximately constant at 45ns at low current injection (and hence low carrier concentration). The radiative recombination lifetime was determined to decrease with increasing current due to phase filling effects (see section 3.3.1). This value is shown to be constant at 3ns for high injection levels. A decreasing non-radiative recombination lifetime is measured in this current region that is suggested to be caused by the onset of an additional loss path. The additional loss path at high current injection was found to have a similar carrier density dependence to Auger recombination when phase space filling is considered (i.e. $\propto n^2$).

Zhang *et al.* [40] measured an Auger coefficient of $1.5x10^{-30}cm^6s^{-1}$. In the study, the defect-related recombination coefficient was calculated by determining the trap concentration, N_T, from deep level spectroscopy and the use of the following relationship,

$$A_{nr} = \frac{\sigma N_T v_{th}}{2} \qquad 3\text{-}11$$

where σ is the capture cross-section, N_T is the deep level density and v_{th} is the thermal velocity. The radiative recombination coefficient was determined by simulation and the remaining Auger coefficient and the carrier density at peak efficiency were determined by fitting the efficiency graph using an iterative approach. A similar iterative approach to fit the efficiency curve was carried out by Meneghini *et al.* [41] to produce an Auger coefficient of $1.0x10^{-30}cm^6s^{-1}$. The groups who fit their data to obtain a value for the Auger coefficient neglect carrier leakage and assume that the reduced efficiency with increasing carrier concentration is only due to Auger recombination. Schreibenzuber *et al.*[42], however, used optical gain measurements to separate losses due to carrier leakage and processes taking place within the quantum well to extract an Auger coefficient of $4.5x10^{-31}cm^6s^{-1}$. The literature therefore provides considerable variation of the Auger recombination coefficient that indicates high uncertainty.

Fitting experimental data using an Auger model (also known as the ABC model) are orders of magnitude higher than the trend of Auger coefficient as a function of band gap predict as shown in Figure 3-9. These results clarify that if Auger recombination is the cause of the efficiency droop phenomenon then it must be in the form of indirect phonon-assisted Auger recombination or inter-conduction band Auger recombination. Most groups which suggest that Auger recombination is the cause of efficiency droop reach such a conclusion based on the fact that measured observations can be fitted using the "ABC" model. The fitting using this model may, however, be caused by an alternative non-radiative recombination process which has a similar dependence on carrier concentration.

3.4.3 Defect Recombination at High Injection Currents

The cubic carrier density on injection current at high injection currents where efficiency droop occurs in nitride based LEDs is the central argument that Auger recombination is the cause of the relative reduction in efficiency as currents are increased to high values. However, theoretical calculations carried out in Hader *et al.* [26] find the Auger recombination rate for phonon-assisted transitions is too small to account for efficiency droop. The authors proposed that a defect-related loss mechanism may be the cause of efficiency droop if it has a similar carrier density dependence to the previously assumed Auger recombination at high injection currents. The authors suggest that defect-related recombination will consist of the conventional monomolecular defect-related recombination in addition to a density-activated defect recombination (DADR) process which occurs at high carrier densities.

It is predicted that carriers will be localized away from most defect sites in potential minima at low injection currents (see Figure 3-11a) where only conventional defect-related recombination occurs. However, the carriers will be delocalized due to the saturation of the localized states at the band edge to areas where there is a larger defect-density (Figure 3-11b) causing the onset of density-activated defect recombination.

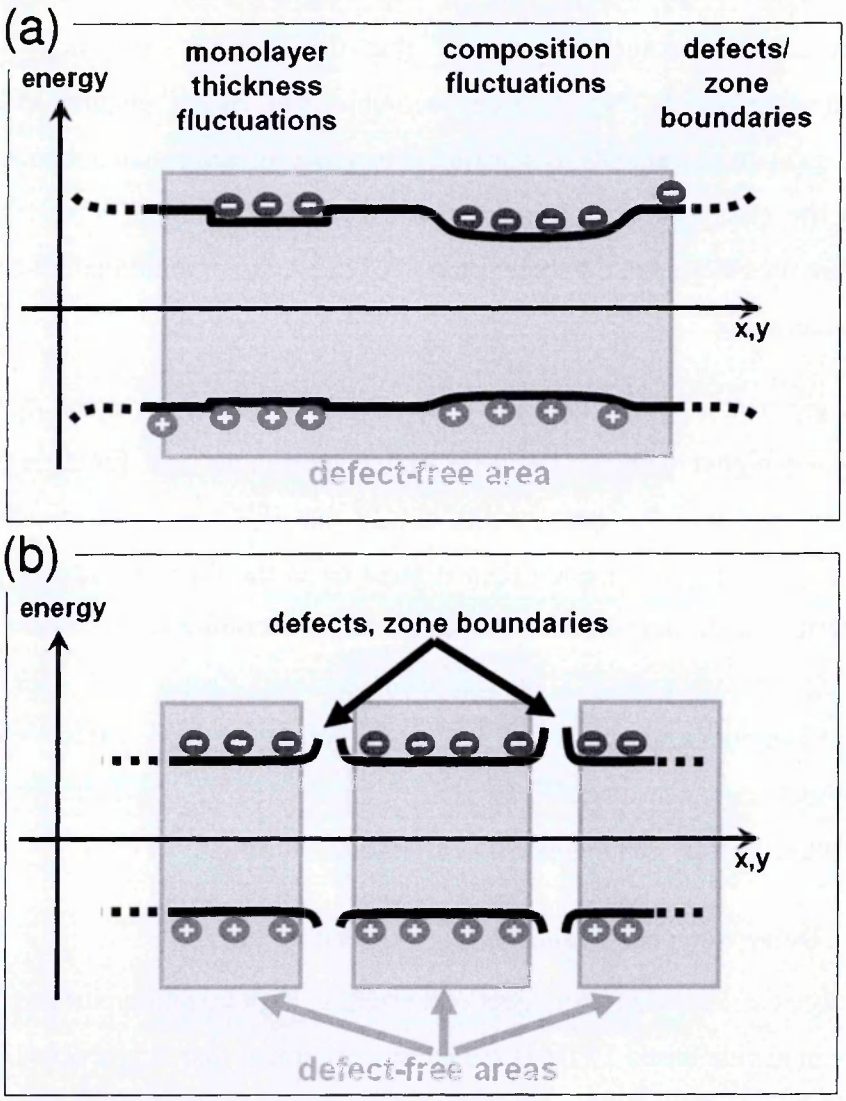

Figure 3-11- Illustration to show (a) the localization of carriers in potential minima due to well-width fluctuations and/or composition fluctuations and (b) areas at higher energies which consist of defects (image from Hader *et al.* [26]).

The loss current density due to defect-related recombination, J_{defect}, is expected to have a similar linear dependence on carrier density in the low current region as described in section 3.4.1 and may therefore be described by,

$$J_{defect} = An \qquad 3\text{-}12$$

The proportion of current which is converted into photons, J_{rad}, is given by,

$$J_{rad} = B(n)n^2 \qquad 3\text{-}13$$

where the influence of phase space filling on the radiative coefficient (section 3.3.1) is also taken into consideration.

In the model it is assumed that at low carrier densities these are the only two recombination paths, conventional monomolecular recombination and radiative recombination. However, at a certain carrier density, n_{DADR}, (related to when carriers are able to escape from potential minima and begin to fill the entire quantum well), there is an additional loss path related to recombination at defect states that become important as carriers become delocalized, J_{DADR}, which can be determined from the relationship,

$$J_{DADR} = \frac{en_w}{\tau_{DADR}} \frac{(n-n_{DADR})^2}{2n_{DADR}} \qquad \text{for } n>n_{DADR} \qquad 3\text{-}14a$$

$$J_{DADR} = 0 \qquad \text{for } n<n_{DADR} \qquad 3\text{-}14b$$

where e is the charge of an electron, n_w is the number of quantum wells, n is the carrier concentration, and τ_{DADR} is the recombination time at high current densities where there is density-activated defect recombination.

The authors suggest that one of the $(n-n_{DADR})$ factor of the density-activated defect recombination accounts for the conventional defect-related recombination and the second factor accounts for an increasing number of defect centres which become available as there is an increase in the carrier concentration. It is therefore assumed that in the simplest form there is a $(n-n_{DADR})^2$ dependence.

It was found that the experimentally observed efficiency droop can be reproduced using the DADR model if this carrier concentration dependence is employed. Therefore unlike conventional defect-related recombination, DADR will have a stronger dependence on the carrier concentration dependence than radiative recombination resulting in efficiency droop as shown in Figure 3-12.

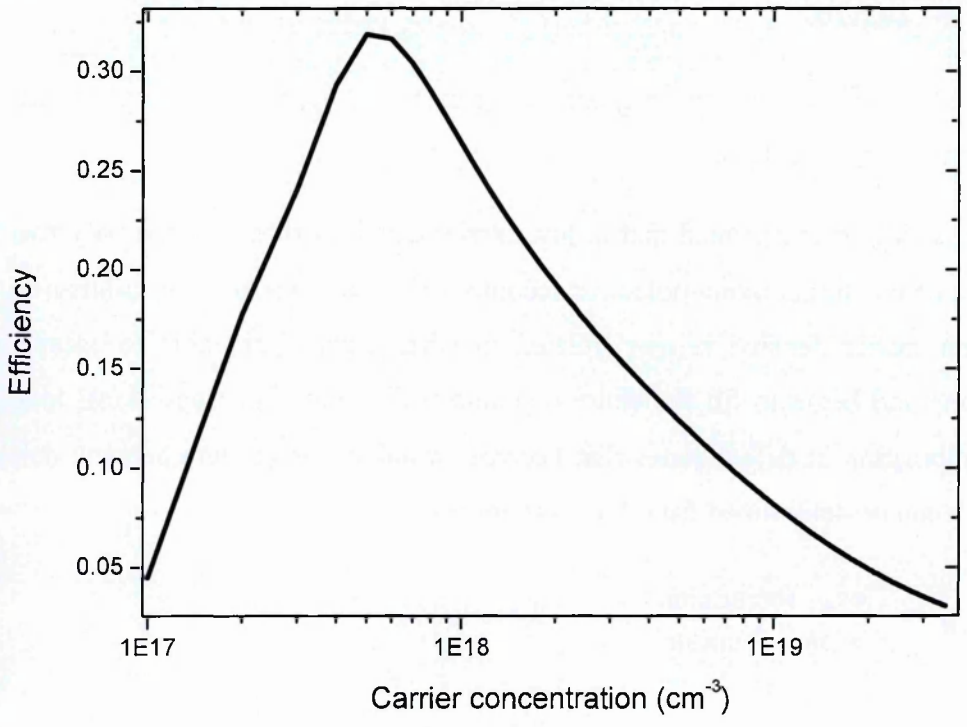

Figure 3-12- The efficiency modelled as a function of carrier concentration with the density-activated defect recombination as a cause of efficiency droop where $A=6.25\times10^{7}s^{-1}$, $B_0=7\times10^{-11}cm^3s^{-1}$, $n_0=5\times10^{18}cm^{-3}$, $\tau_{DADR}=4.5\times10^{-9}s$ and $n_{DADR}=4\times10^{17}cm^{-3}$ {taken from [43]}.

In more recent work by Hader *et al.* [44] it is shown that the efficiency droop curves at different temperatures can be modelled accurately by using the proposed density-activated defect recombination model. The conventional defect-related recombination has a strong temperature dependence related to the temperature activated dependence (proportional to $\exp((-E_a/k_bT))$, where Ea is the activation energy, and the density-activated defect recombination is shown to reduce with increasing temperature. The authors attribute this dependence to a lower occupational probability of the electron and holes with increasing temperature for a given carrier density. Therefore the electron-electron scattering that excites carriers above the potential barriers also decreases with increasing temperature. An increase in the threshold carrier density value, n_{DADR}, is therefore required in order to obtain the necessary scattering required to excite the carriers above the potential barriers of the potential minima.

3.4.4 Carrier Leakage

The final non-radiative loss path which has been proposed by several groups to cause efficiency droop is carrier leakage. The carrier leakage process has previously been shown in GaInNAs materials [45] to be due to the escape of carriers from the conduction band minima which occurs at zero momentum, the Γ valley, to the conduction band minima which exist at different momenta that will cause a strong reduction in the radiative recombination rate. However, the escape of carriers from Γ valley to other conduction band minima to other conduction band minima is not expected in GaN as the energy gap between the A, M and L valleys and the valence band maximum are significantly larger than the separation for the Γ valley as shown in Figure 3-13.

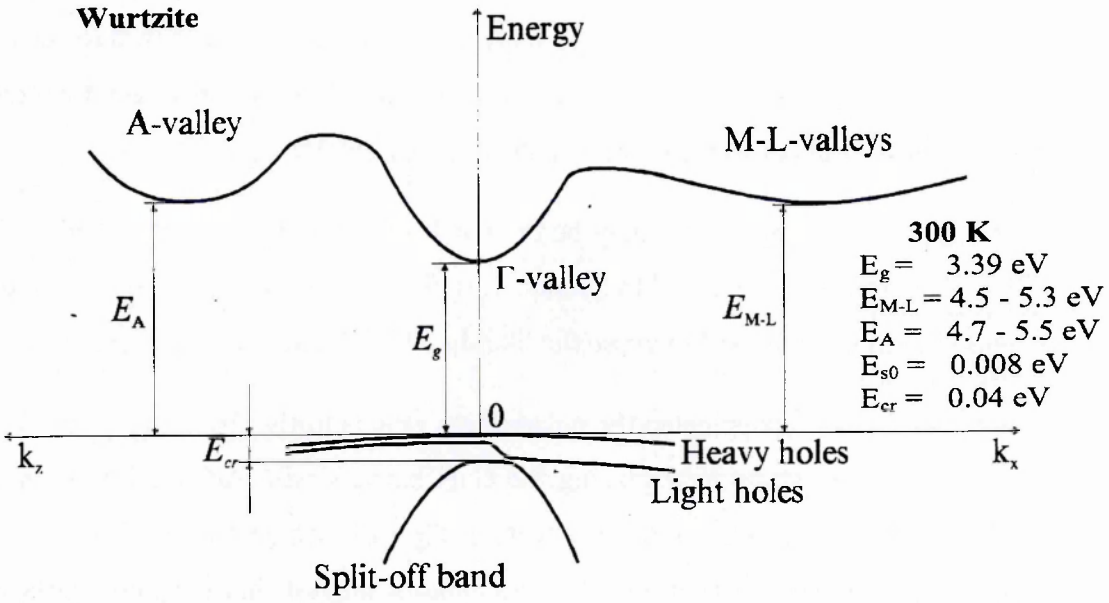

Figure 3-13- The band structure of GaN showing the Γ, A, M and L valleys of the conduction band and the heavy holes, light holes and split of bands of the valence bands (from [46]).

Groups have therefore proposed that the carrier leakage that causes droop is due to the non-capture or escape of carriers in the quantum well as illustrated in Figure 3-14.

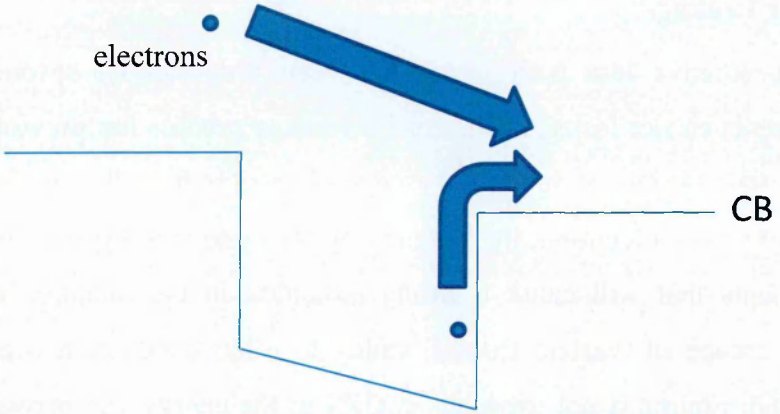

Figure 3-14- Illustration to show the non-capture and escape of electrons from the conduction band of a quantum well.

Direct carrier leakage from the Γ in InGaN to the Γ in GaN is expected to reduce with increasing indium content due to the increasing confinement energy due to a larger band offset. However, this is not consistent with the increasing droop effect for green LEDs in comparison with blue LEDs as will be shown in Section 5.9.

A strong carrier leakage effect may be the result of strong internal polarization fields (which will be discussed in more detail in Section 3.6). Simulations by Kim *et al.* [47] indicate that an increased field strength will increase the likelihood of electron leakage occurring.

Schubert *et al.* [48] investigated the polarization effects further by using quantum wells which consist of reduced strain by replacing the GaN barriers with AlGaInN barriers. Figure 3-15 shows that there is a reduced droop effect for the LED which consisted of AlGaInN barriers along with a reduced peak efficiency. The authors suggest that the lower peak efficiency is caused by poorer growth quality and that the reduced droop effect is a direct consequence of the reduced electron leakage rate. This is due to the reduced internal fields resulting in a larger electron confinement because of a higher effective barrier height.

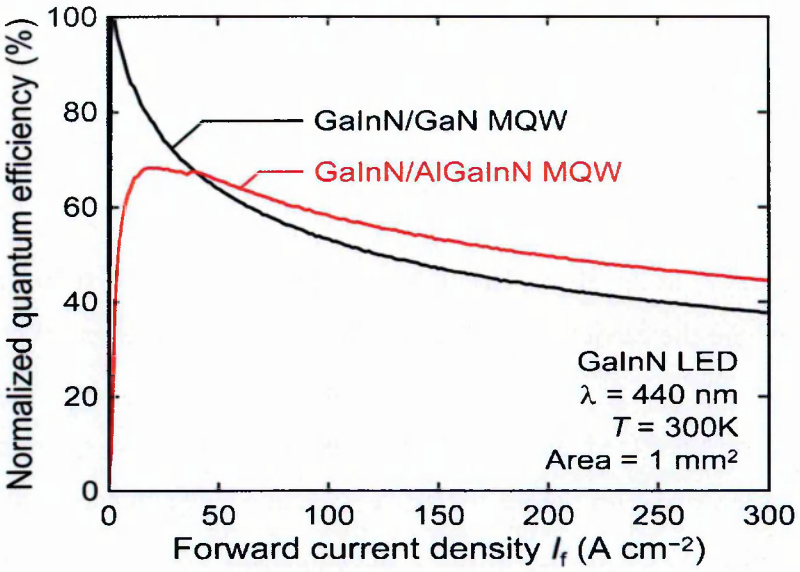

Figure 3-15- Efficiency droop behaviour of GaInN MQW devices with GaN barriers (black) and AlGaInN barriers (red) which has a lower polarization value and reduced droop effect {taken from [48]}

Hole injection issues are expected to result in a low hole concentration within the active region that will subsequently cause electron leakage. Xie *et al.* [49] provide evidence that hole transportation is problematic as it was found that LEDs which consisted of p-doped barriers had a higher current density at which efficiency peaks in addition to a reduced efficiency droop effect. However, it is not clear from the paper whether the overall efficiency is improved or reduced as normalized efficiencies were presented. Similarly, Ni *et al.* [50] observe that reducing the width of the barriers also resulted in a higher current density at which the efficiency peaks. These findings suggest that the efficiency droop phenomenon is a result of poor hole transportation that cause a build-up of electrons that are then able to escape from the quantum well. Despite such findings, the fact that droop is observed in photoluminescence measurements indicates that hole injection is unlikely to be the cause of efficiency droop.

A direct observation of carrier leakage was observed in Vampola *et al.* [51] where an additional larger energy gap quantum well than the active region quantum well was grown between the electron blocking layer and the p-GaN cladding. The authors show that at low injection current the emission results from only the quantum well in the active region. However, an additional peak is observed in the emission spectra as the efficiency begins to show droop behaviour. Although these results show that electron overflow occurs, the cause of this overflow may be due to either direct carrier leakage or an Auger-induced overflow as the

Auger recombination process may also promote electrons to higher energy levels which scatter into the blocking layer.

3.5 Carrier Injection Issues

The efficiency droop effect (see Figure 3-1) indicates that there is a higher efficiency at currents where the carrier concentration is smaller. Optimization of devices has been achieved by reducing the carrier concentration at high currents by growing wider quantum wells. However, the increased well width will also cause a larger quantum confined Stark effect (QCSE) (described in more detail in section 3.6) which will reduce the radiative recombination rate which will be accompanied by an increase in the non-radiative recombination rate. The larger defect density of wider wells is due to an increasing proportion of indium used to grow the quantum well. An alternative method to reduce the carrier concentration and reduce the Fermi level is to increase the number of quantum wells in the active region. However, studies have shown that increasing the number of quantum wells will not reduce the carrier concentration due to the majority of carriers recombining in the quantum well which is closest to the p-GaN side due to the lower hole mobility [50, 52, 53].

The low hole concentration in the active region can be attributed to both the relatively low activation of Mg-dopants (Figure 3-16) and small hole mobility (Figure 3-17) which are issues that are expected to become more prominent at low temperatures.

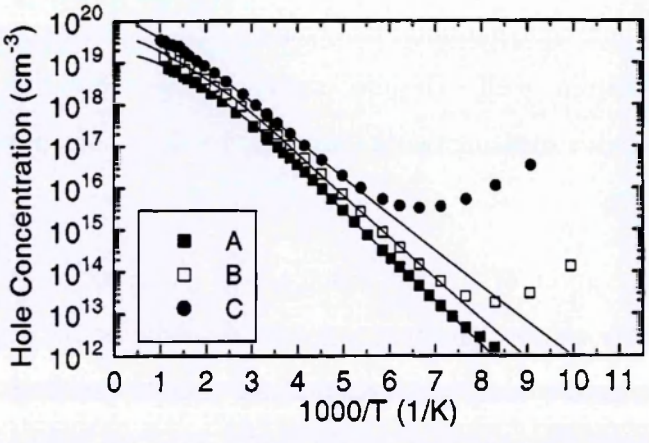

Figure 3-16- Hole concentration as a function of temperature for Mg-doped samples with different concentrations: sample A (1.6 x 10^{19}cm^{-3}), sample B (4 x 10^{19}cm^{-3}) and sample C (8 x 10^{19} cm^{-3}) [54]

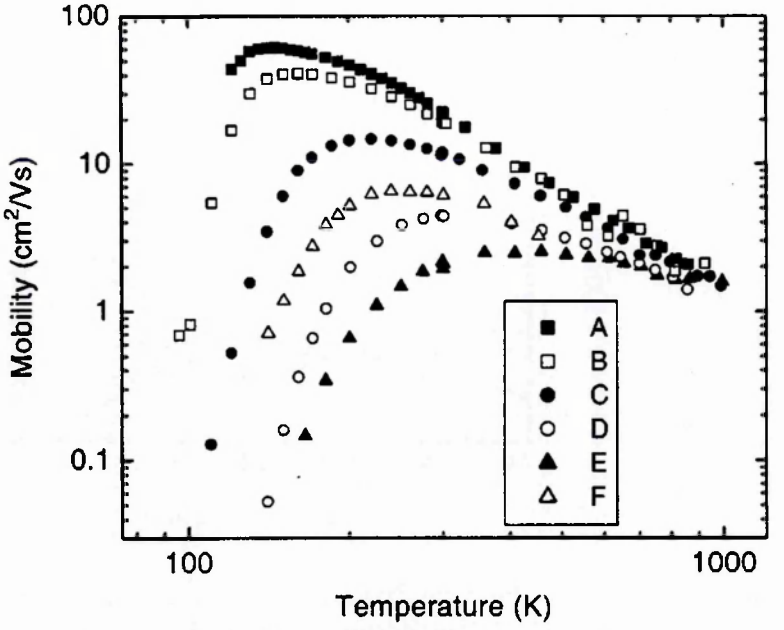

Figure 3-17- Hole mobility as a function of temperature for samples of increasing Mg-doping levels: A (1.6 x 10^{19}cm^{-3}), B (4 x 10^{19}cm^{-3}), C (8 x 10^{19} cm^{-3}), D (2 x 10^{20} cm^{-3}), E (3 x 10^{20} cm^{-3}), F (8 x 10^{20}cm^{-3})[54]

Laubsch *et al.* [34] suggested that a weak temperature dependence of the droop effect is unlikely to be caused by a thermally-activated loss mechanism such as electron leakage. However, the temperature dependence of carrier leakage in InGaN-based devices may be complicated by the improvement of hole injection with increasing temperature. Simulations by Piprek *et al.* [55] show that an increase in the hole transportation will result in an improved electron-hole overlap thereby reducing the carrier leakage effect. *Wang et al.* have shown that there is a reduced droop effect for devices grown with graded barriers (6% droop), as illustrated in Figure 3-18, compared with that of a conventional LED (34%) [56].

Figure 3-18 shows that there is an improved carrier distribution for the device with graded barriers as the Fermi level for holes in the quantum wells which are closest to the n side of the active region is closer to the valence band edge. Simulations in an alternative study also predict that there will be a reduced efficiency droop effect due to improved hole transportation if the conventional GaN barriers are replaced with InGaN barriers in order to aid hole transportation [57].

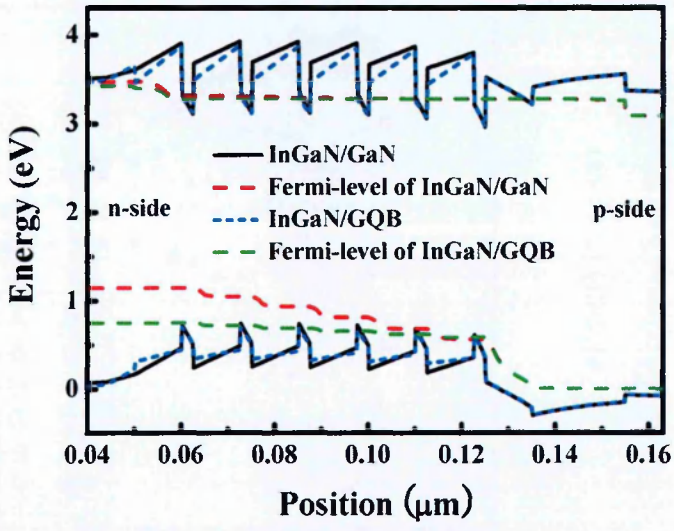

Figure 3-18- Illustration of the band diagram of an LED with graded barriers compared with a conventional LED with the Fermi levels included to show larger distribution of holes in the valence band in the case of the graded barrier case {taken from [56]}.

Another important property of InGaN-based devices is that there is the inclusion of an electron blocking layer (EBL) to reduce electron leakage from the active region [58]. However, the EBL may have a detrimental effect on efficiency due to the hindrance of hole transportation [59, 60]. An increased droop effect was observed by Han *et al.* [60] for an LED which included an EBL. A further increase to the efficiency droop effect was measured for an LED that included an AlGaN EBL of high aluminium content. The authors concluded that hole injection issues due to the inclusion of the EBL enhances the efficiency droop effect. Despite the enhanced droop effect, LEDs which include an EBL are found to have an improved light output performance [59] compared with LEDs that do not consist of an EBL. Figure 3-19 shows the effects of the injection issues on the luminescence properties for LEDs with and without EBLs [59]. Whilst the electroluminescence was found to increase with reducing temperatures for the LED which did not include an EBL (LED1), due to the reducing defect-related recombination rate, the electroluminescence of the LEDs with EBLs (LED2 and LED3) is found to drastically decrease below 200K. These findings are expected to show that there are poor injection issues that are exacerbated by the inclusion of the EBL. Photoluminescence measurements were also taken in order to overcome any issues relating to hole injection and it was found that the LEDs have similar temperature dependences regardless of whether they include an EBL or not.

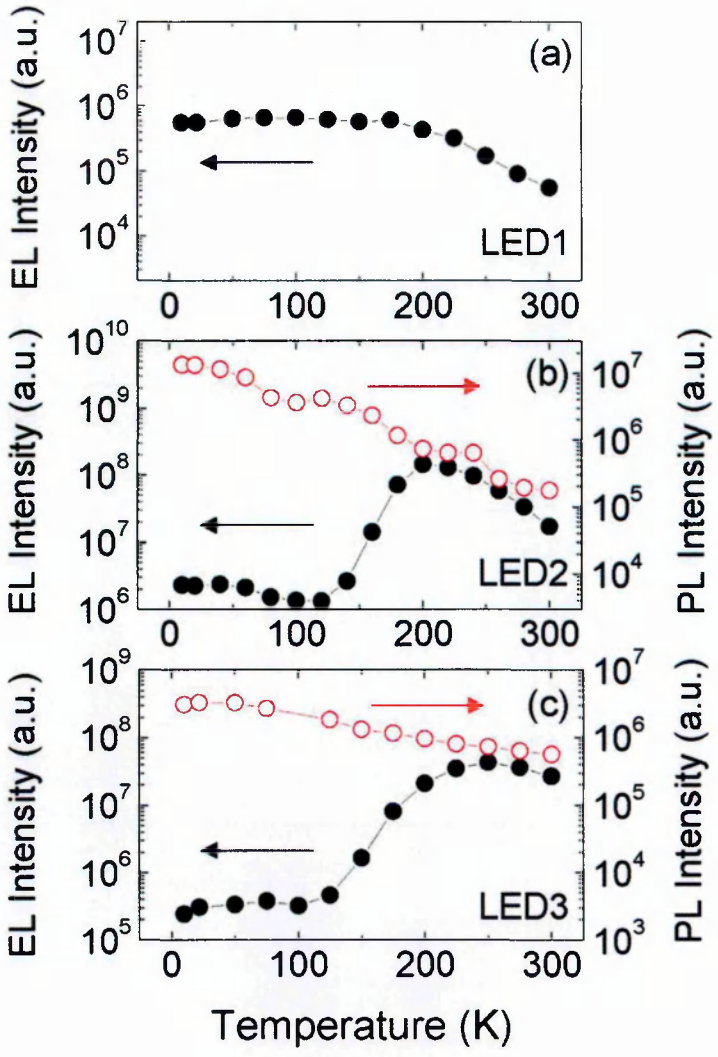

Figure 3-19- Electroluminescence (black dots) and photoluminescence (red dots) dependence on temperature for LED1 (no blocking layer, 3% indium content), LED2 (with EBL, 3% indium content) and LED3 (with EBL, 15% indium content) {taken from [59]}

The inclusion of an EBL is therefore necessary to improve the overall performance of nitride-based LEDs. However, this may come with a trade-off of a strong droop effect. The EBL must therefore be carefully designed to optimize performance by efficiently blocking electrons whilst not impeding the hole injection.

3.6 Piezoelectric and Spontaneous fields

Particular to the nitride-based quantum well devices is the existence of strong internal fields which have been observed to be a magnitude higher than in other III-V materials [61]. Simulations carried out by nextnano software are presented to show the effect of the internal

fields on an InGaN quantum well of 0.16 indium content that is surrounded by GaN barriers and an AlGaN EBL of 0.20 aluminium content. This software uses a k.p model to simulate the performance of quantum structures. Figure 3-20 shows simulations of the band edge and the effect on the electron and hole wavefunctions where there are no internal fields (a) and an internal field strength of 1.1MVcm^{-1}.

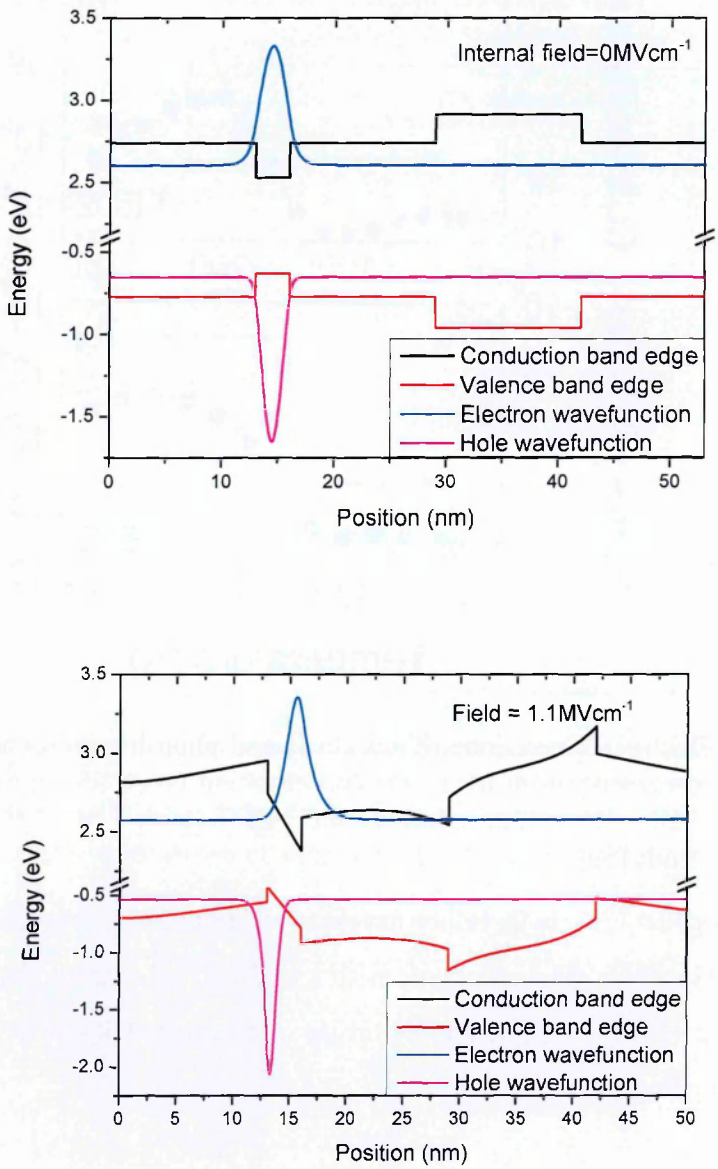

Figure 3-20- Simulations showing show an InGaN quantum well structure with an indium content of 0.16 with a) no internal fields and b) an internal field of strength 1.1MVcm^{-1} and the electron and hole wavefunction overlaps.

The simulations show that the wavefunctions of the electron and hole strongly overlap (93%) in the case where internal field strength is zero. The overlap is found to reduce to (11%) for an internal field strength of 1.1MVcm^{-1}. The influence of the changing wavefunction overlap will have a strong impact on the recombination processes occurring as discussed further in Sections 5.7 and 5.8.

The total electric field in the active (A) or cladding (C) regions results from a contribution of the spontaneous (SP) electric field and the piezoelectric (PZ) electric field as described in Equation 3-15.

$$E_{A,C} = E_{A,C}^{(SP)} + E_{A,C}^{(PZ)} \qquad 3\text{-}15$$

The contribution from the piezoelectric field results from the induced strain which is caused by the difference in lattice constant between materials which are grown on top of one another. The spontaneous field, however, is caused by the material composition and may exist in a system which is unstrained[62].

The strength of the piezoelectric polarization field can be calculated as from Equation 3-16.

$$P^{PZ} = \xi . s \qquad 3\text{-}16$$

where ξ is the piezoelectric tensor and s is the strain field.

The strength of the piezoelectric fields in the active and cladding regions are then

$$E_A^{PZ} = \frac{4\pi t_c (P_c^{pz} - P_A^{PZ})}{t_c \varepsilon_A + t_A \varepsilon_C} \qquad 3\text{-}17$$

$$E_C^{PZ} = \frac{4\pi t_A (P_A^{PZ} - P_C^{PZ})}{t_C \varepsilon_A + t_A \varepsilon_C} \qquad 3\text{-}18$$

where $\varepsilon_{A,C}$ and $t_{A,C}$ are the dielectric constants and thicknesses, respectively, of the active and cladding regions.

The electric field contribution from spontaneous polarization can be calculated as

$$E_A^{SP} = \frac{4\pi t_c (P_c^{SP} - P_A^{SP})}{t_c \varepsilon_A + t_A \varepsilon_C} \qquad 3\text{-}19$$

$$E_C^{SP} = \frac{4\pi t_A (P_A^{SP} - P_C^{SP})}{t_C \varepsilon_A + t_A \varepsilon_C} \qquad 3\text{-}20$$

A similar spontaneous polarization is found for GaN and InN despite a large change in lattice constant as shown in Figure 3-21.

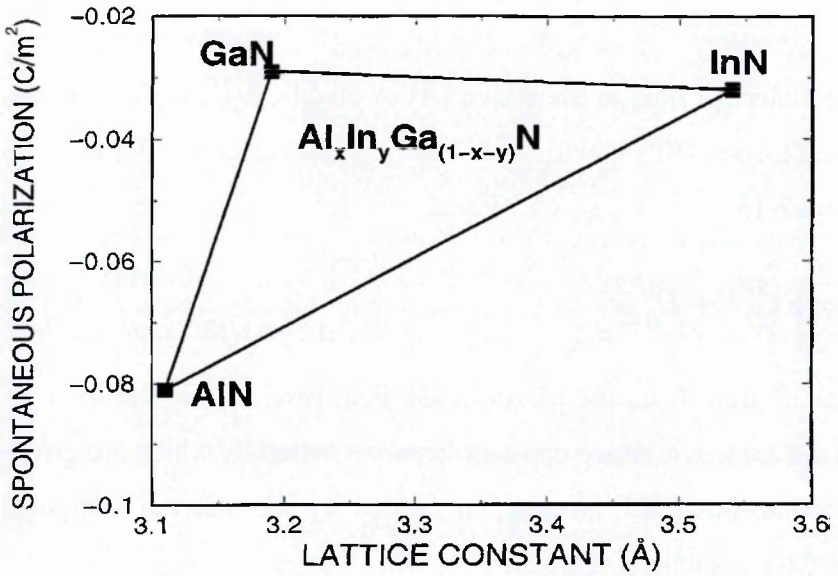

Figure 3-21- Spontaneous polarization for different alloy compositions for the nitride-based material systems as a function of lattice constant {taken from [61]}

Figure 3-22, however, shows there is a stronger change in the piezoelectric polarization between GaN and InN.

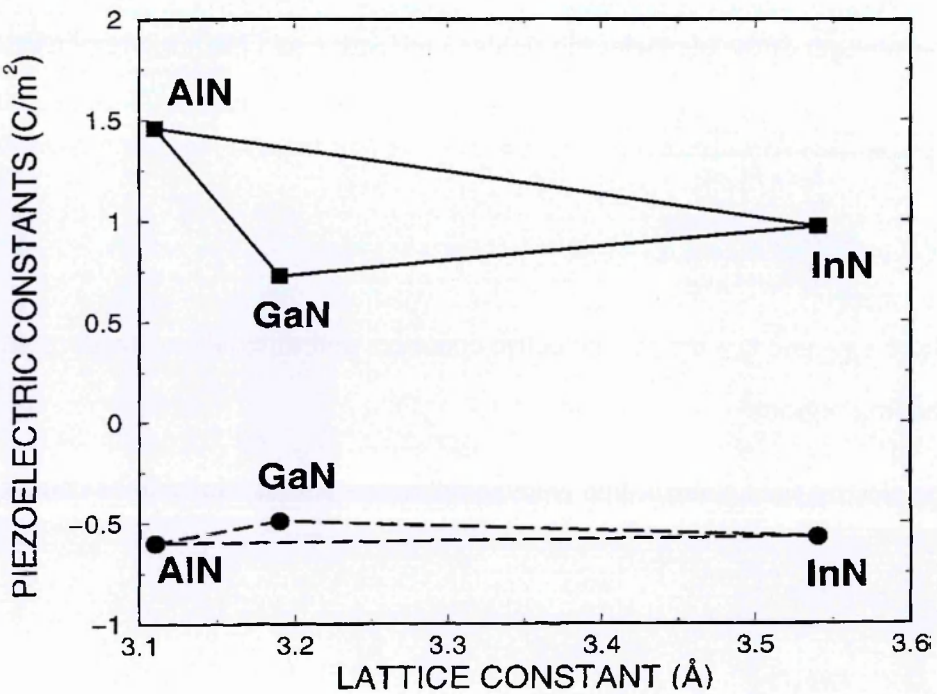

Figure 3-22- Piezoelectric coupling constants e_{33} (squares) and e_{31} (circles) for nitride based materials of varying alloys as a function of lattice constant{taken from [61]}.

The difference in the spontaneous polarization between the active and cladding layers may therefore be neglected in comparison with the changing rate of piezoelectric field with increasing indium content. Therefore the piezoelectric field will be the main contribution to the internal polarization field in InGaN-based devices.

A reduced efficiency droop effect has been observed for devices grown in the non-polar direction where there are no internal fields [63]. However, despite these improvements there remain issues in producing devices which are grown with non-polar orientation due to the difficultly in growth procedures which result in an increased defect density [64, 65]. Whilst a lower efficiency droop effect has been observed in m-plane devices, the light output power remains comparable to devices grown along the c-plane at high injection currents [66] (see Figure 3-23).

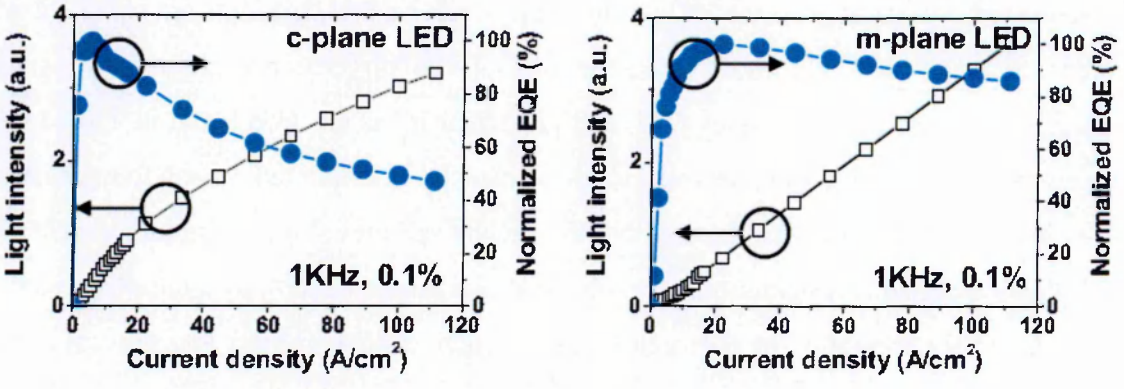

Figure 3-23- Comparison of light output and efficiency droop behaviour of LEDs grown along the c-plane (left) and m-plane (right) {taken from [66]}.

Commercial devices are therefore only expected to be grown along the m-plane if there are significant improvements to the device efficiencies at high injection currents due to the increased difficulty in producing m-plane wafers.

3.7 Localization Effects Caused by Well Width and/or Indium Content Fluctuations

The high internal strain associated with InGaN-based emitters (described in Section 3.6) also causes a large threading dislocation density (10^8-10^9 cm^{-2}) that is expected to result in poor

luminescence. It has been observed in other material systems that devices will have poor performance if the threading dislocation density is above $10^3 cm^{-2}$ [63]. The existence of potential minima due to well width and/or indium content fluctuations have been attributed to be the cause of the high radiative efficiencies of InGaN-based LEDs [67] due to the localization of carriers away from defect sites.

Until relatively recently, the localization of carriers in InGaN-based devices was believed to be caused by strong indium-rich clusters which reduce the band gap energy thereby localizing the carriers away from recombining at non-radiative defect centres [68]. This conclusion was reached due to the observations of dark spots in Transmission Electron Microscopy (TEM) images of InGaN samples which were thought to be areas of large indium content. However, it was shown by Humphreys' GaN group at Cambridge University that the dark spots did not appear in the TEM images if a low beam intensity is used [69]. It was therefore concluded that the dark spots which appeared in the TEM images that use high beam intensity were caused by electron beam damage to the InGaN samples. Much weaker dark dots are observed which may be attributed to slight indium fluctuations. Three dimensional atom probe studies were undertaken on InGaN samples [70] as it is unclear if the electron beam in TEM imagery also causes damage to the samples even if a low intensity is employed. It was found that there is no evidence of indium clustering and that the InGaN samples show an indium distribution which follows a random distribution. The observations suggest there an alternative process which results in the formation of potential minima which localize carriers and prevent defect-related recombination in the InGaN material system.

Quantum well fluctuations have been observed in the more established AlGaAs material system which were able to localize carriers at low temperatures [71]. This localization effect was found to be only important at low temperatures. However, due to the high strain and piezoelectric effect found in the InGaN material system, the fluctuations in InGaN could lead to a stronger localization of carriers at higher temperatures. Quantum well thickness fluctuations of 1-2nm are shown in TEM imagery would result in a localization energy of 60meV which is sufficient to localize carriers at RT (k_bT= 25meV) [72]. Therefore the localization effect may have an influence on the efficiency droop phenomenon (see Sections 3.4.3 and 5.10).

3.8 Chapter summary

The efficiency droop phenomenon, a process whereby there is a relative reduction of efficiency following a low current peak, was introduced in this chapter. The cause of efficiency droop has been widely debated in the literature with the main arguments including Auger recombination, carrier leakage and density-activated defect recombination.

It has been shown that phase-space filling effects are likely to reduce the current at which the efficiency will peak but will not cause the efficiency droop effect itself. It was therefore concluded that the efficiency droop phenomenon results from an onset of an additional non-radiative recombination process at higher currents.

The observation that the light output power has cubic carrier density dependence at high currents where efficiency droop occurs is the main argument supporting the view that an Auger recombination processes is the cause of efficiency droop. The direct Auger recombination process was determined to be negligible in the wide band gap region and therefore a phonon-assisted Auger recombination is proposed by several groups to be responsible for efficiency droop. Different groups have found that an Auger coefficient that is significantly higher than expected is required to model the experimentally observed efficiency dependence on current using a simple ABC model. The Auger recombination was therefore attributed to phonon-assisted Auger recombination where energy and momentum are conserved by the emission or absorption of a phonon which accompanies the Auger recombination process.

However, calculations performed by other groups find that the Auger recombination rate, including that of phonon-assisted Auger recombination, is too small to explain efficiency droop. Another argument was therefore proposed as the cause of efficiency droop in the form of density-activated defect recombination whereby there in an additional defect-related recombination path at high currents. This model attributes the high peak efficiencies achieved at low injection levels to be due to carriers being localized in potential minima which form due to well-width and/or indium composition fluctuations. It was suggested that the additional defect-related loss path is the result of carrier delocalization leading to carriers occupying areas of higher defect density.

Carrier leakage is the third candidate loss mechanism that is often attributed as the cause of efficiency droop. In this process, carriers either escape from, or overshoot, the quantum well to recombine elsewhere. Simulations show that the existence of internal piezoelectric fields (which result from high strain effects that are caused by the lattice constant mismatch between the active and cladding regions) will enhance the droop effect. Observations also found that there is a stronger droop effect with reducing hole injection efficiency. This is expected to be due to an enhancement of the electron leakage rate.

The final section of this chapter described the effects of an inhomogeneous energy band edge which may be the cause of the high peak efficiencies in nitride-based devices. This is due to a reduction of defect-related recombination as carriers are localized in potential minima. The existence of the potential minima may also play a role in the efficiency droop process.

Investigating the validity of the different models forms a significant part of this thesis.

4 Experimental Techniques

4.1 Chapter Aim

This chapter describes the experimental techniques used in this study to investigate the recombination processes occurring in InGaN-based devices. The first part of this chapter shows images of commercial blue and green InGaN-based LEDs which were produced using transmission electron microscopy (TEM). The TEM images reveal important structural properties which are useful for the analysis.

Spectroscopy measurements are then described which may be used to achieve information on the radiative recombination that takes place in InGaN blue-green LEDs. Another technique used in this study to investigate the device structure is photo-current spectroscopy which involves the absorption of light at different wavelengths. The final method to investigate the light output performance of the devices is by the use of silicon diode integrating spheres which are connected to light power meters.

The temperature and pressure dependence of the light output performance in InGaN-based devices are the main techniques used in this thesis. Two cryogenic systems are described, a closed cycle helium gas cryostat and a liquid nitrogen cryostat, which are used to achieve temperatures between 20K and 400K. The final section of this chapter describes the technique of applying pressure to semiconductor devices. Pressure techniques result in a change in the bandgap energy of the devices and therefore provide a valuable tool to investigate different recombination mechanisms.

4.2 TEM characterization of commercially-available devices

The devices used in most of this study are commercial LEDs manufactured by Nichia Corporation. The device details are therefore not supplied due to commercial secrecy. However, structural characterization of the devices may be achieved by the use of transmission electron microscope (TEM) images as shown in Figure 4-1 for a blue and a green LED.

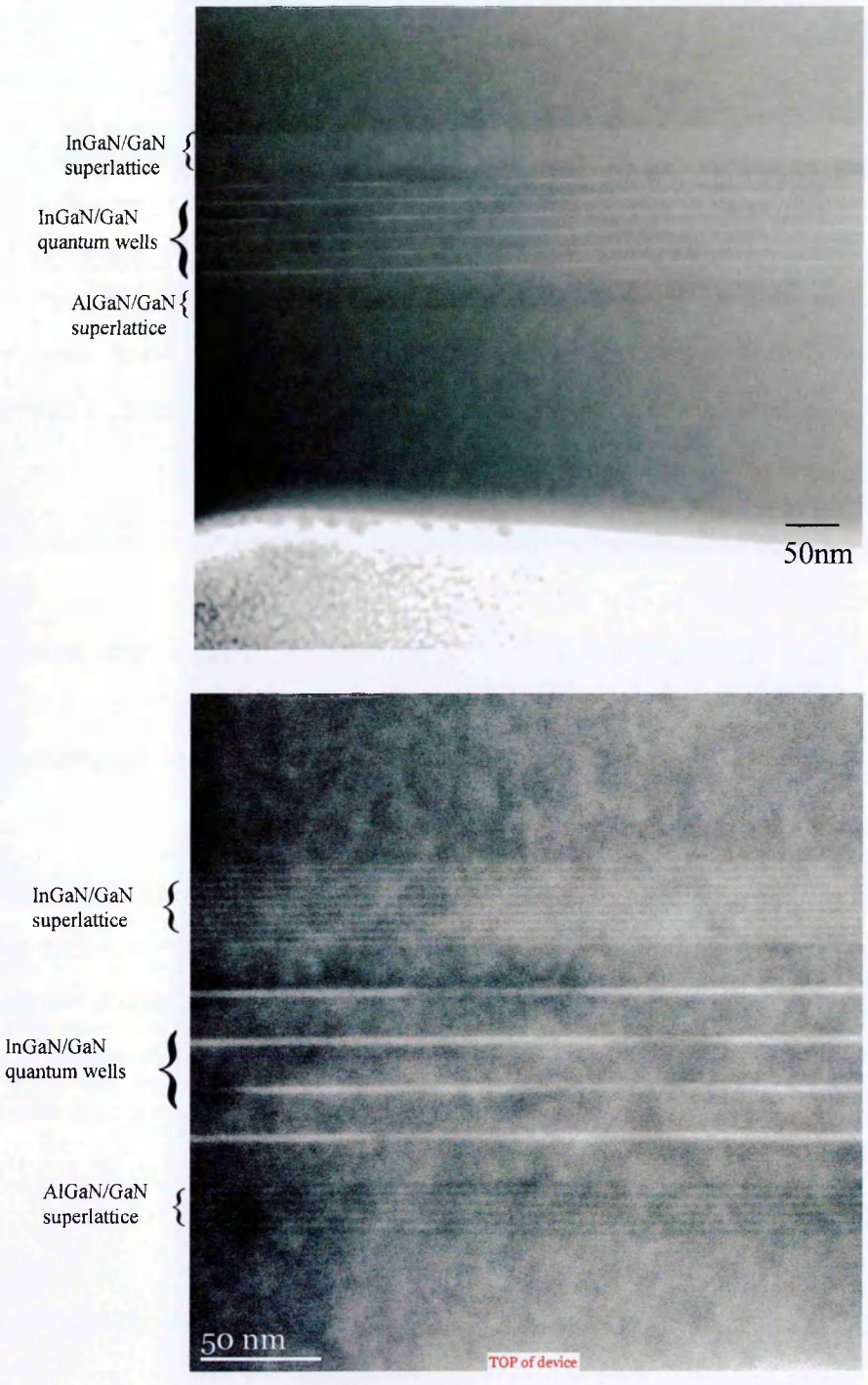

Figure 4-1- Transmission electron microscope images of a blue LED (upper image) and a green LED (lower image)

The images show that at the top of the devices (p side) there is a six layer superlattice followed by the active region. There is another superlattice which consists of ten layers that is included after the active region at the n-side of the device. The areas of different brightness in the images show elemental contrast. Bright areas are higher atomic numbers and darker areas are lower atomic numbers. It can then be concluded that the six layer superlattice at the top of

the device is likely to consist of AlGaN ("dark" lines indicating a low atomic number) layers separated by GaN. The active region of the blue LED is made up of 6 InGaN ("light" lines indicating a high atomic number) quantum wells which are separated by GaN barriers. The green LED shows four "light" lines which indicate that there are four quantum wells in its active region. On the bottom of the devices there are further "light" lines which are less bright compared with those of the active region which are expected to be lower indium content InGaN layers separated by GaN layers. This superlattice is expected to be included to reduce the threading dislocations from reaching the active region where they will reduce the radiative efficiency [73]. These dislocations arise because of the large lattice mismatch and thermal incompatibility of the GaN layer and the substrate material which is usually sapphire. The addition of the superlattice at the bottom of the device is expected to be included to reduce dislocation density within the quantum well [74]. The AlGaN/GaN superlattice on the top may be attributed as an electron blocking layer [59] which is included in order to prevent electrons from leaking out from the active region to the pGaN side where they may recombine with holes.

The analysis of the contrasting lines is achieved through the use of imaging software imageJ to produce intensity profiles, an example of which is shown for the blue LED in Figure 4-2.

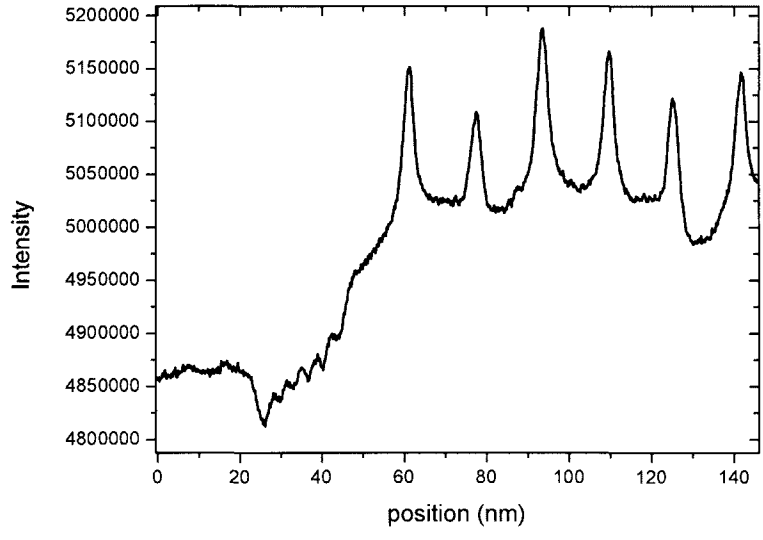

Figure 4-2- The intensity profile of a blue LED taken by TEM imagery using the computing software imageJ.

The information obtained from the TEM images may be used to construct schematics of the blue and green LEDs as shown in Figure 4-3.

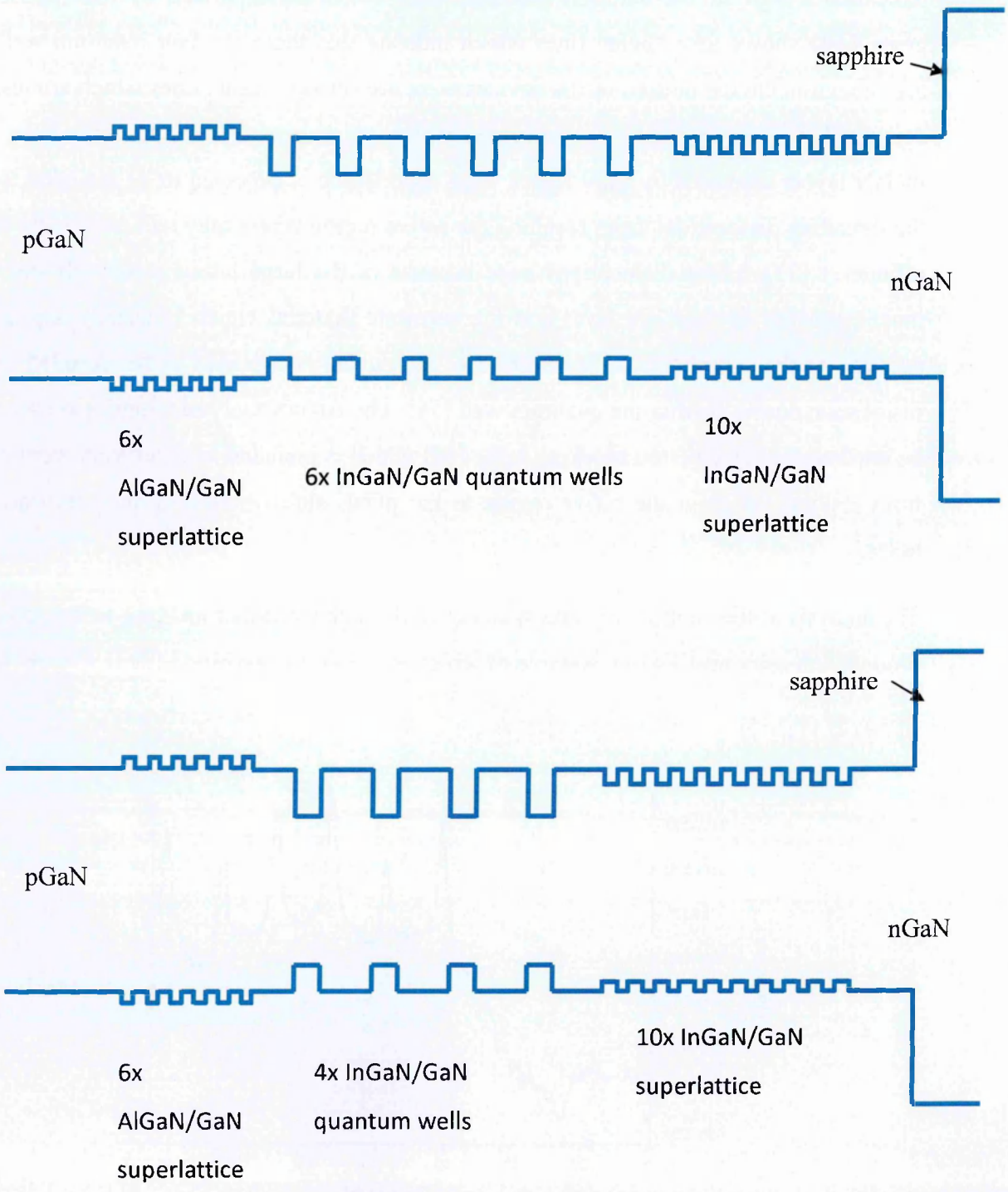

Figure 4-3- Schematic of the LED structure for the blue LED (top illustration) and the green LED (lower illustration) showing an active region of 6 MQWs and 4 MQWs, respectively.

Dimensional information can also be obtained from the TEM images whereby it is observed that 1.8nm AlGaN layers are separated by 1.8nm GaN layers. The InGaN quantum wells are determined to be 2.9±0.4nm with GaN barriers of 13.2±0.6nm (blue LED) and 16nm (green LED), and the InGaN/GaN superlattice next to the nGaN side consisted of 1.8nm layers with barriers of 1.8nm.

A further schematic of the LEDs can be used to show the different layers used to construct the LEDs.

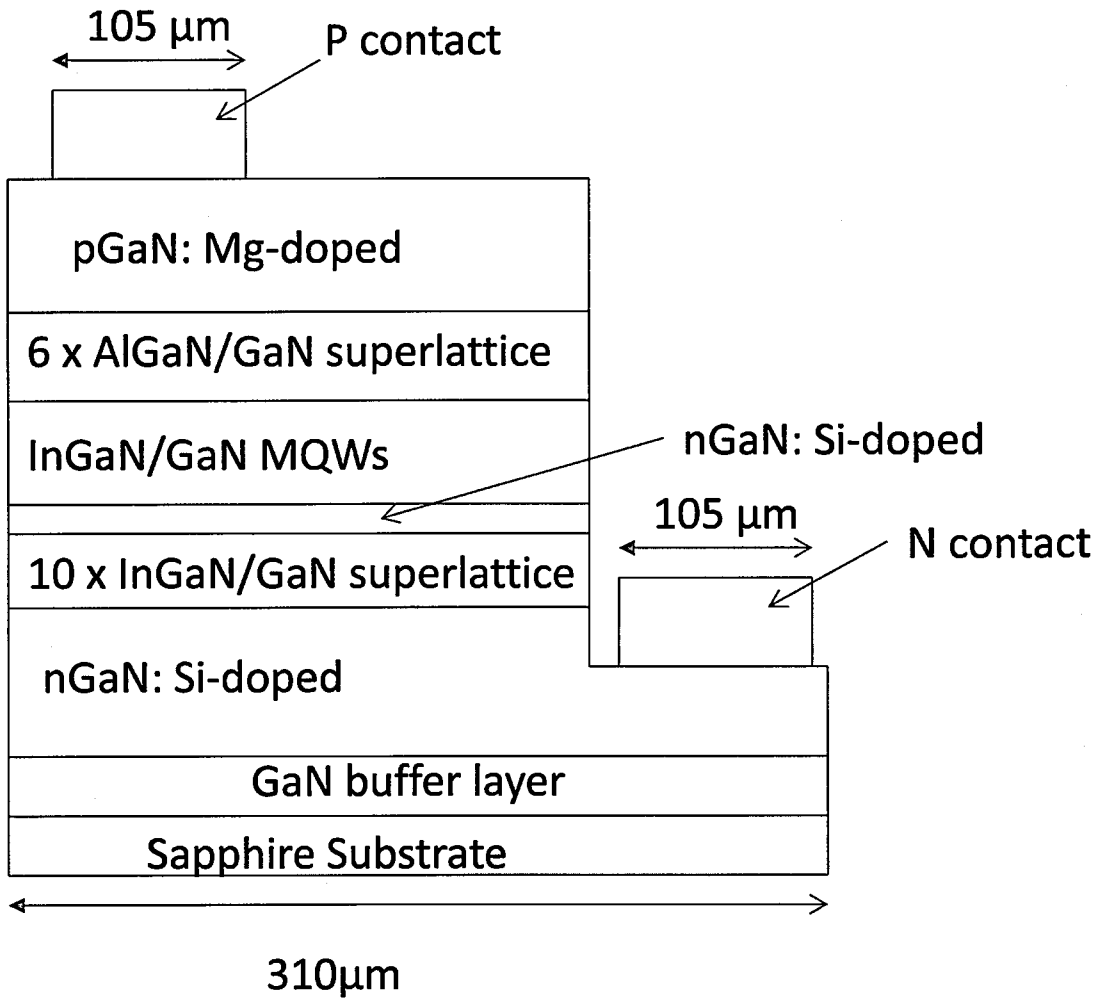

Figure 4-4- Schematic showing the different layers of the LED structure for a blue LED and the dimensions

The dimensions of the top surface of the LED, shown in Figure 4-5, were measured using a microscope.

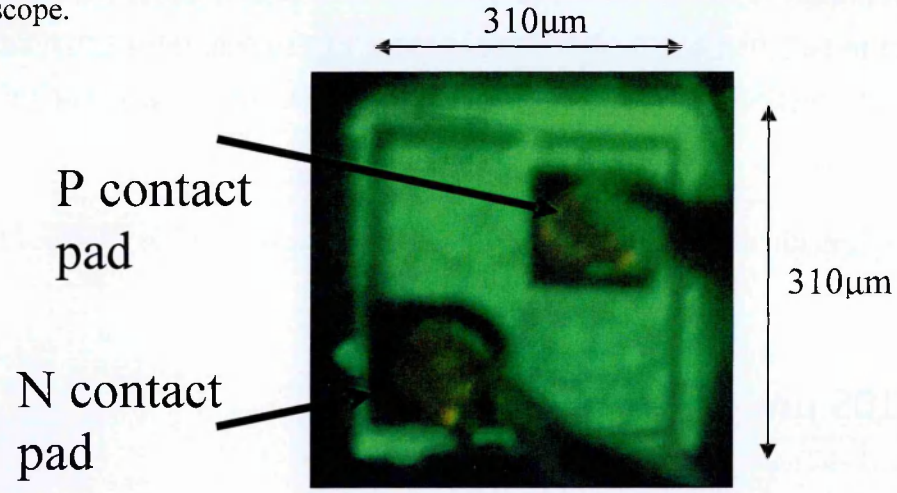

Figure 4-5- A schematic indicating the dimensions of the top surface of the LEDs with the contact pads shown

4.3 Preparation of commercial devices

The epoxy encapsulates of the LEDs (see Section 2.11.3) will influence the performance of devices under changing temperature and pressure conditions. It is therefore required that the epoxy encapsulate is removed before undertaking the experiments. The packaged LED must be placed in dichloromethane at room temperature for 24 hours to dissolve the epoxy resin in order to obtain the bare chip semiconductor device. The bare die is then mounted onto transistor outline (TO) headers using thermally conductive paint which is baked at 175°C for two hours. Finally the contact pads of the semiconductor chip are bonded to the legs of the transistor outline header using a gold wire bonder. The device characteristics were found to be similar before and after the deencapsulating and bonding process as shown in Figure 4-6 and Figure 4-7.

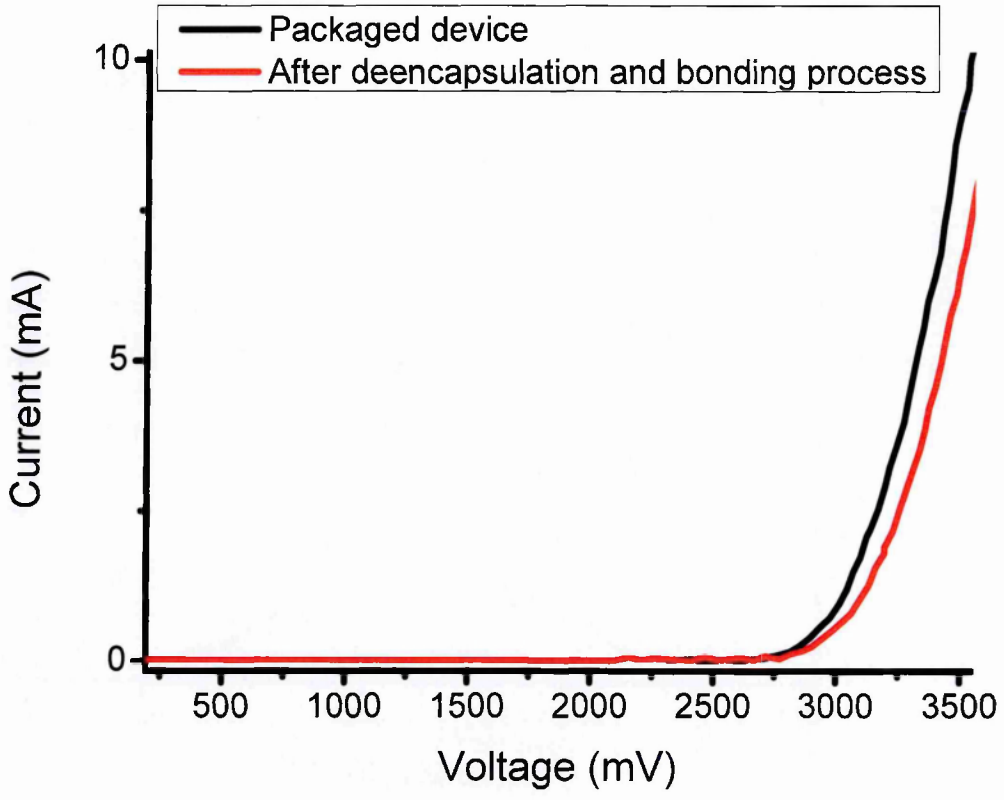

Figure 4-6-The current dependence on voltage for a packaged device before and after deencapsulating and bonding processes

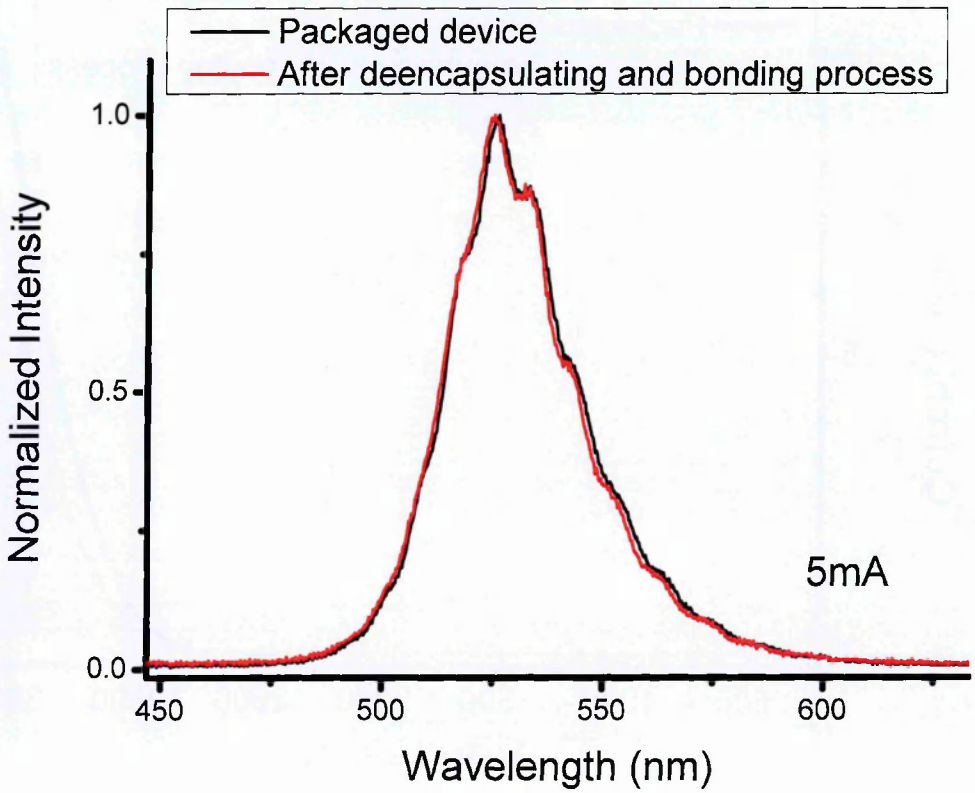

Figure 4-7- Spectra of a device before and after deencapsulating and bonding processes at 5mA.

Figure 4-6 shows the turn-on voltage remains at a similar value for the device in the packaged condition compared with the turn-on voltage of the LED following the deencapsulating process. The slight change in voltage for a fixed current is likely to be due to a small increase in the series resistance. The process is also shown to have negligible impact on the optical properties of the device as shown in the spectral measurements at 5mA (Figure 4-7).

4.4 Pulsed and Continuous Wave Measurements

Joule heating is an effect whereby the flow of electrical current may generate heat in a resistive material. Current may be provided in pulsed mode where the signal is periodically turned on and off in short pulses in order to minimize the influence of Joule heating. An illustration of the signal is shown in Figure 4-8.

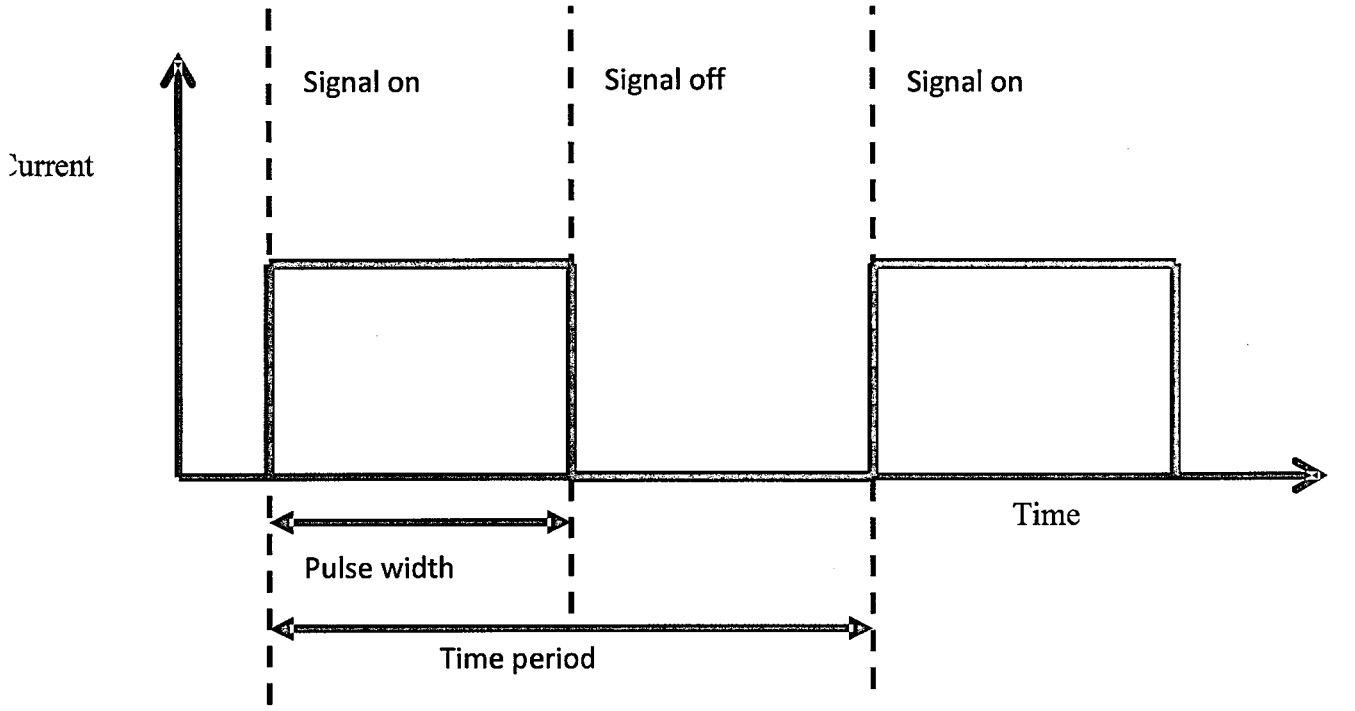

Figure 4-8- Schematic illustrating the pulse mode of current flow where the signal is periodically turned on and off.

The frequency and period of the pulses are used to determine the duty cycle of the pulse as shown below.

$$Duty\ cycle = \frac{pulse\ width}{time\ period} \qquad 4\text{-}1$$

In the experiment the frequency, f, is set and hence the time period can be calculated from

$$Time\ period = \frac{1}{f} \qquad 4\text{-}2$$

The duty cycle can also be calculated from

$$Duty\ cycle = pulse\ width\ x\ f \qquad 4\text{-}3$$

The efficiency was measured at different pulse widths in order to determine which pulse width would provide the maximum light output power whilst minimizing the effects of Joule heating as shown in Figure 4-9.

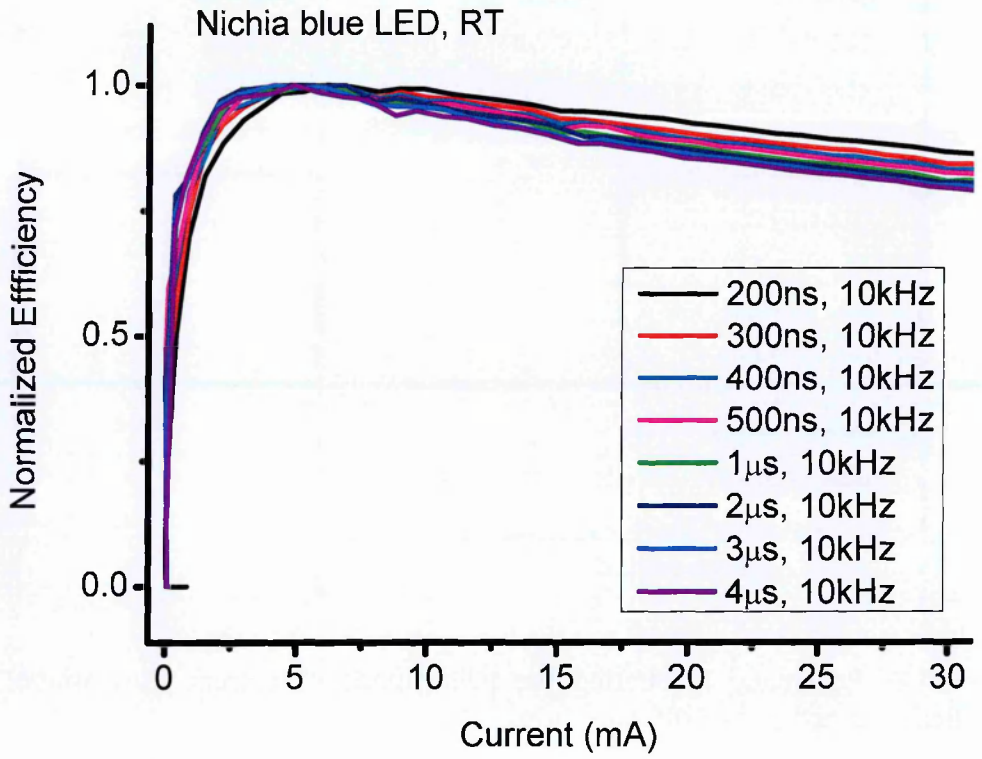

Figure 4-9 Electroluminescence efficiency as a function of current for different pulsed widths at a frequency of 10kHz.

A pulse width of 2μs with duty cycle of 2%, which is typical for investigations into InGaN devices [48, 50, 75], was chosen as there is high light output whilst the effects of Joule heating are acceptable.

Accurate measurements of the current and voltage are gained in the experiments by the use of oscilloscopes (Tektronix TDS 3012) and a current probe as schematically shown in Figure 4-10.

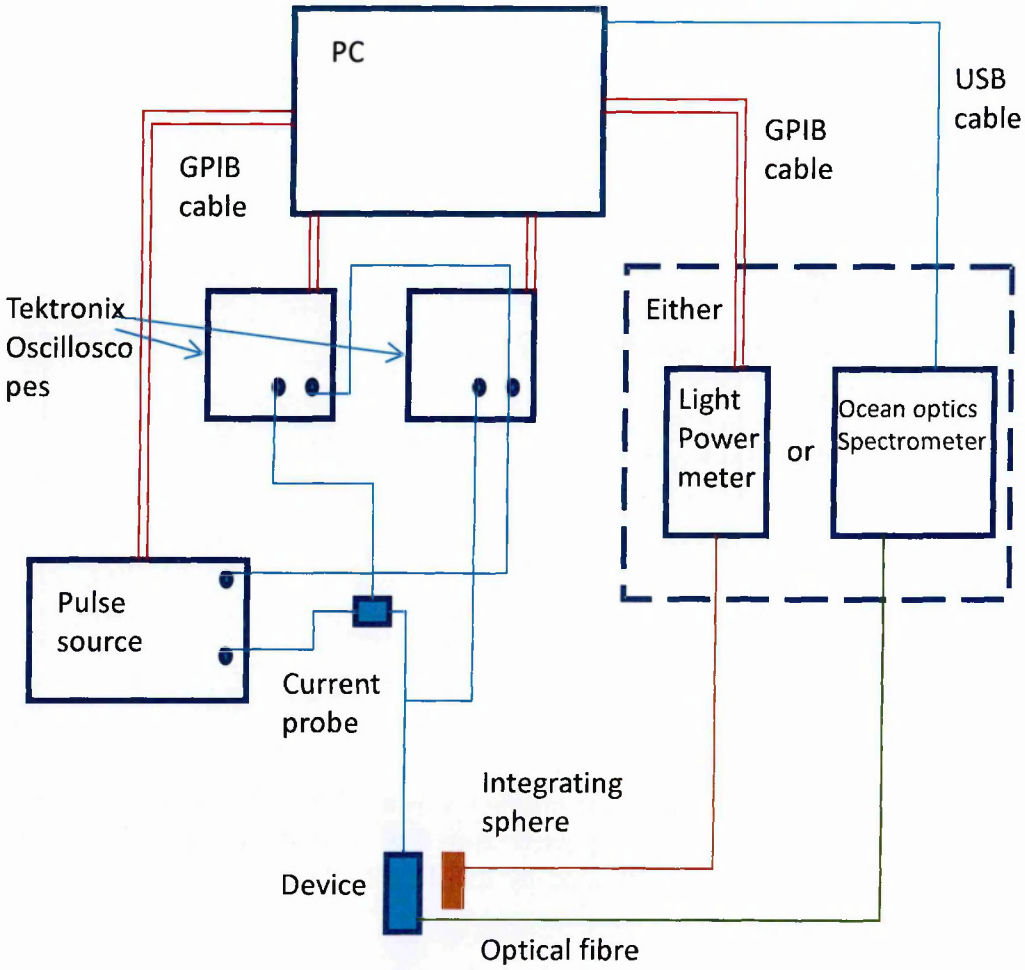

Figure 4-10- Experimental set up when pulsed mode is used to power the device where the light output is measured by either an Ocean optics spectrometer or an integrating sphere

The study into efficiency droop may also be investigated by using the CW mode as efficiency droop has been observed in both CW and pulsed mode as shown in Figure 4-11. Since the devices are driven in CW mode in applications it is useful to be able to compare the behaviour under CW and pulse conditions.

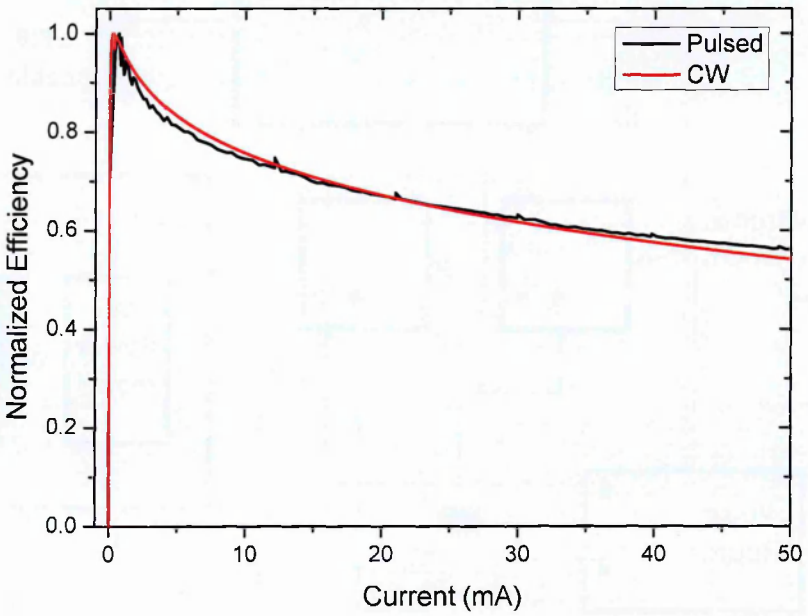

Figure 4-11- Electroluminescence efficiency as a function of current showing efficiency droop occurs in both pulsed and CW conditions. The efficiency in the pulsed conditions is divided by the duty cycle in order to be compared with the CW mode.

The advantages of using CW mode include an enhanced time-averaged light output power due to a continuous current flow and easier control of either the input current or voltage of the LED. This is particularly useful at low temperatures where the peak efficiency was found to occur at very small currents (less than 0.1mA) which are difficult to accurately measure in the pulsed measurements.

The set up to take measurements in CW mode is shown in Figure 4-12.

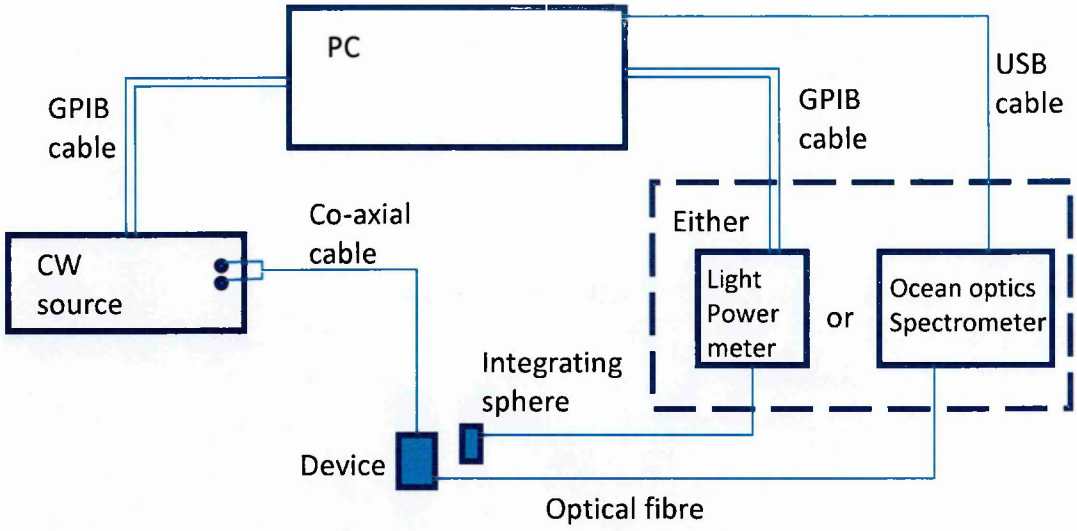

Figure 4-12- Experimental set up in supplying a CW current to the device where the light output is measured by either using a light power meter or an Ocean optics spectrometer

4.5 Spectroscopy Studies

4.5.1 Ocean Optics Spectrometer

The spectral response of the light being emitted from the LEDs is a useful feature which can be used to investigate the processes which influence the radiative emission. In this study the spectral studies were carried out with an Ocean Optics spectrometer. The schematic in Figure 4-13 shows how such spectrometers operate.

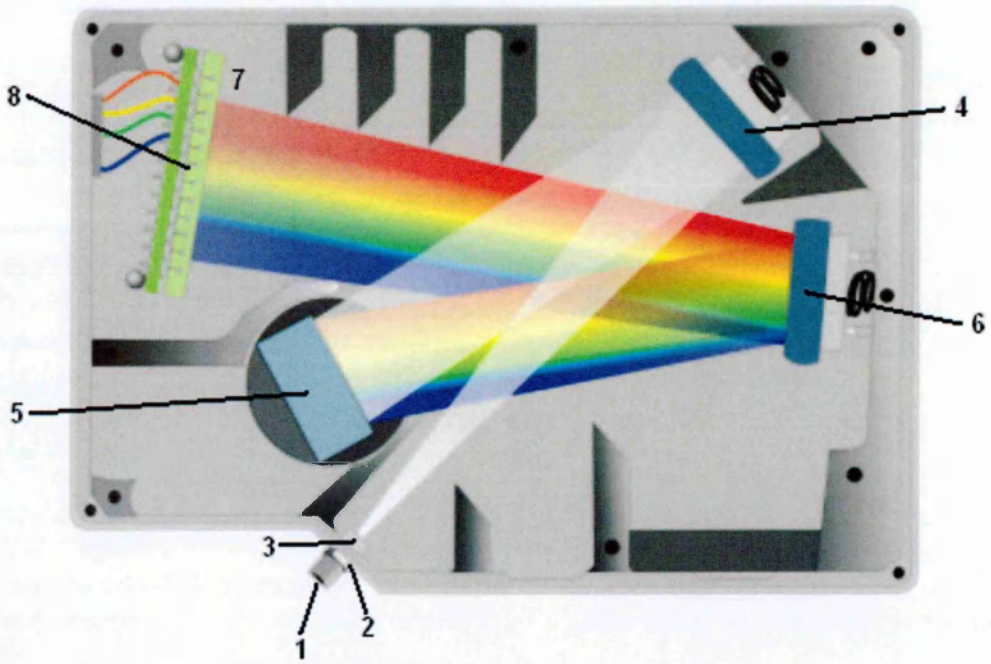

Figure 4-13- Diagram of the Ocean optics spectrometers used in the study {taken from [76]} where 1- SMA connector, 2- slit, 3- filter, 4- collimating mirror, 5-grating, 6-focussing mirror, 7- detector collection lens, and 8- CCD detector showing how light of different wavelengths can be detected.

The Ocean Optics spectrometers are set up to collect light which is transmitted through an optical fibre that is coupled to the spectrometer through a fibre connector. The light beam is then focussed onto a grating by the use of a collimating mirror. The grating directs the diffracted light onto the focussing mirror which then focuses the light through a lens onto a charge-coupled device array (CCD) detector. The CCD detector converts optical signals into electrical signals which can then be transmitted to the computer.

4.5.2 Photocurrent Spectroscopy

Important information about semiconductor materials can be obtained by the use of photocurrent spectroscopy. This technique relies on the photoelectric effect where the illumination of the semiconductor material will result in the promotion of electrons from the valence band to the conduction band that subsequently forms a current. The set-up of the experiment can be seen Figure 4-14.

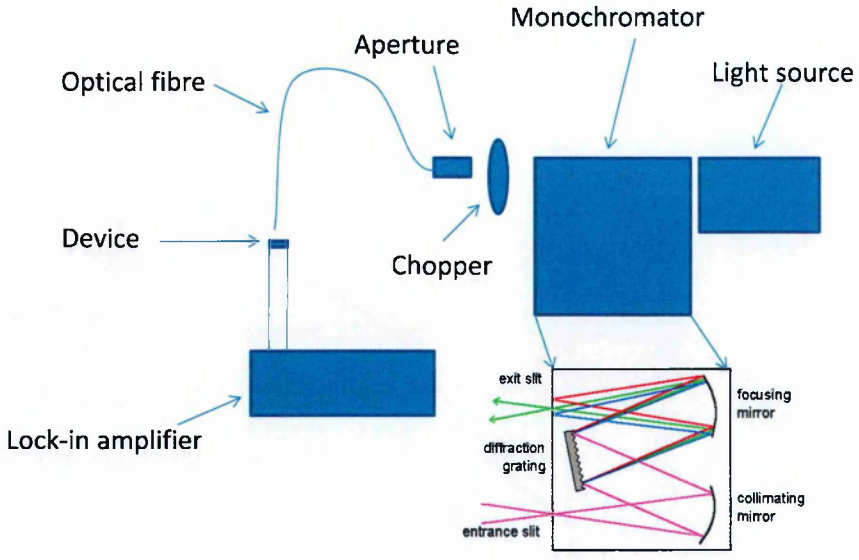

Figure 4-14- Schematic of the photocurrent set-up where light of a desired wavelength may be emitted onto the device and the induced current may be measured using a lock-in amplifier{image of monochromator from [77]}

The light emitted from a tungsten carbide light bulb is focussed into a monochromator which only allows light transmission of a desired wavelength. Light from the tungsten carbide light bulb enters the monochromator where a collimating mirror focuses the light onto a diffraction grating. The diffraction grating will diffract wavelengths of light at different angles. The positioning of the diffraction grating will therefore only allow the desired wavelength of light to be emitted through the exit slit. This technique is very useful as it provides a means of measuring the absorption spectrum of a device.

4.6 Light Output Power Measurements

To measure the light output power that is emitted from a device an integrating sphere which is connected to a power meter is used. The collection efficiency is higher in the silicon-based integrating sphere compared with optical fibres due to a larger aperture which also makes it easier to achieve constant collection efficiency. The integrating sphere has a spherical shape and is coated with a white reflective coating in order for any light which is incident on the integrating sphere to be collected by scattering reflections. The light collection was taken by either an Anritsu Optical power sensor MA9802A, which is connected to an Anritsu Optical multimeter or an ILX integrating sphere which is connected to an ILX OMM-6810B optical multimeter.

The responsitivity must be considered when taking measurements as shown for a typical silicon based detector in Figure 4-15.

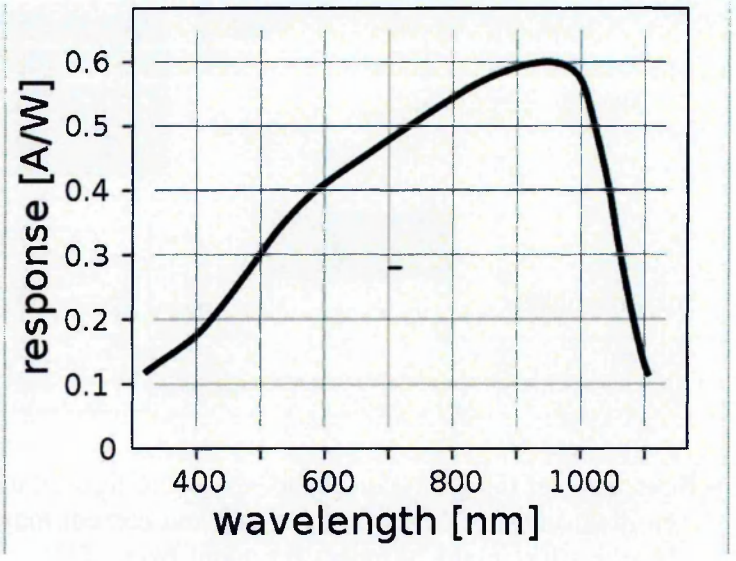

Figure 4-15- Responsitivity of silicon-based detectors as a function of wavelength [78]

4.7 Temperature dependence experiments

The temperature of the devices was altered by the use of cryostat systems. In this study two different cryostats are used in order to investigate different temperature regions. Low temperatures, from 20K, were achieved by the use of a Leybold closed cycle helium RDK cryostat which has a maximum temperature of 300K. The closed cycle helium cryostat uses the Joule-Thomson effect to cool the cold finger whereby the expansion of the helium gas results in a drop in temperature. The varying pressure of the helium gas in each of the gas lines is achieved by a compressor system which causes different flow rates of the helium gas (see Figure 4-16). The desired temperature is set by a temperature controller. Electrical heaters are then able to increase the temperature to the desired stable temperature. Rotary and turbo pumps are used to generate a vacuum around the cold finger to reduce the conduction and convection of heat onto the cold finger and to remove water vapour which would otherwise condensate on the sample at low temperature.

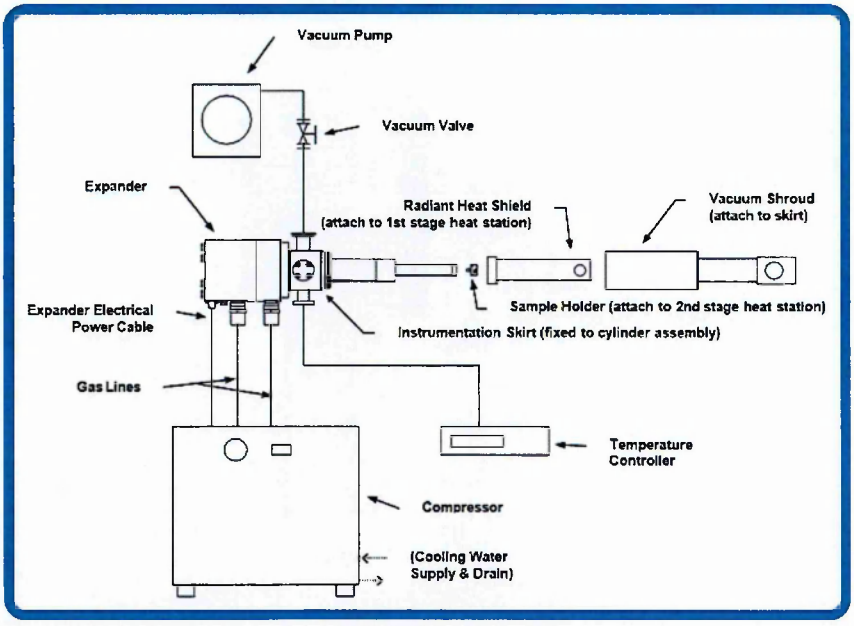

Figure 4-16- Schematic indicating the operation of the helium closed-cycle cryostat where a compressor changes the rate at which the helium flows through gas lines and causes the sample to cool {taken from [79]}.

An electrical feed-through is used to provide current to the device. The device was attached to a copper plate which was made "in-house" in order to provide a good thermal contact. There were additional measures taken to ensure a good thermal contact in the form of applying thermal compound paste to the bottom of the transistor outline header and silver dag on the edge of the transistor outline header. Thermal compound paste was also used between the copper plate and the cold finger.

A liquid nitrogen cryostat, as shown in a diagram Figure 4-17, was used to investigate the temperature range between 80K up to 400K.

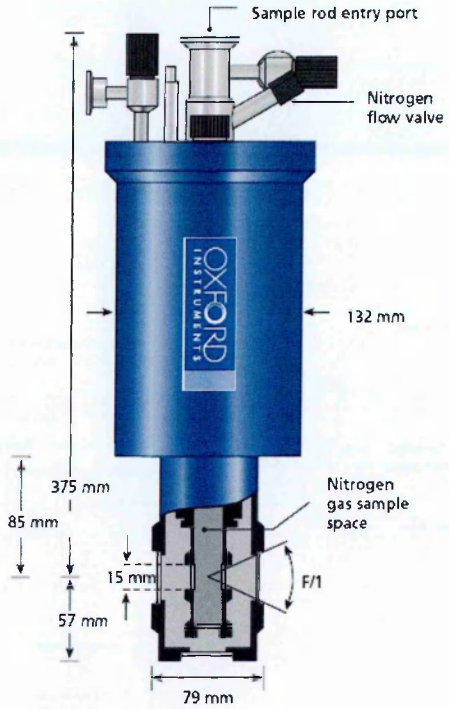

Figure 4-17- Diagram of the liquid nitrogen cryostat {taken from [80]}.

The device was mounted onto a sample rod which is inserted through the sample rod entry point (see Figure 4-17) into the sample space. The sample space is then required to be filled with nitrogen gas that provides the thermal transport to the device. The cryostat has optical windows in order for the emitted light to be collected from outside the cryostat.

The reduction of temperature can be achieved in this cryostat by inserting liquid nitrogen into reservoirs which are required to be kept under a high vacuum. The temperature of the sample space can then be adjusted by three electrical heaters which are regulated by a temperature controller as shown in Figure 4-18.

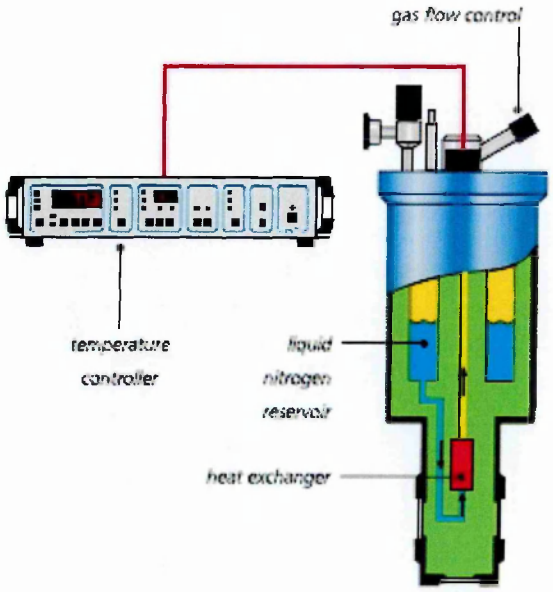

Figure 4-18-Schematic showing a desired temperature may reach in the liquid nitrogen cryostat by the use of a temperature controller which controls the electrical power to a heat exchanger {taken from [80]}.

4.8 High Pressure experimental set up

The application of high pressure is a very powerful technique that has been used to investigate the carrier dynamics of semiconductor devices. The application of high pressure will cause the compression of the semiconductor crystal reducing the lattice constant. This will lead to an increase in the bandgap energy and has the advantage that there are no significant changes to the carrier distribution that will occur in temperature-dependent measurements. The recombination mechanisms may then be investigated using this technique on a single device which is tuned to emit at different wavelengths. The bandgap-dependent properties may therefore be investigated without the need to grow a set of different wavelength emitting devices which would require different growth runs which may also influence the material characteristics.

A gas compressor system was used in this study to apply high pressure to the InGaN-based devices. A schematic of the system is shown in Figure 4-19 where there are three stages which provide the application of pressure.

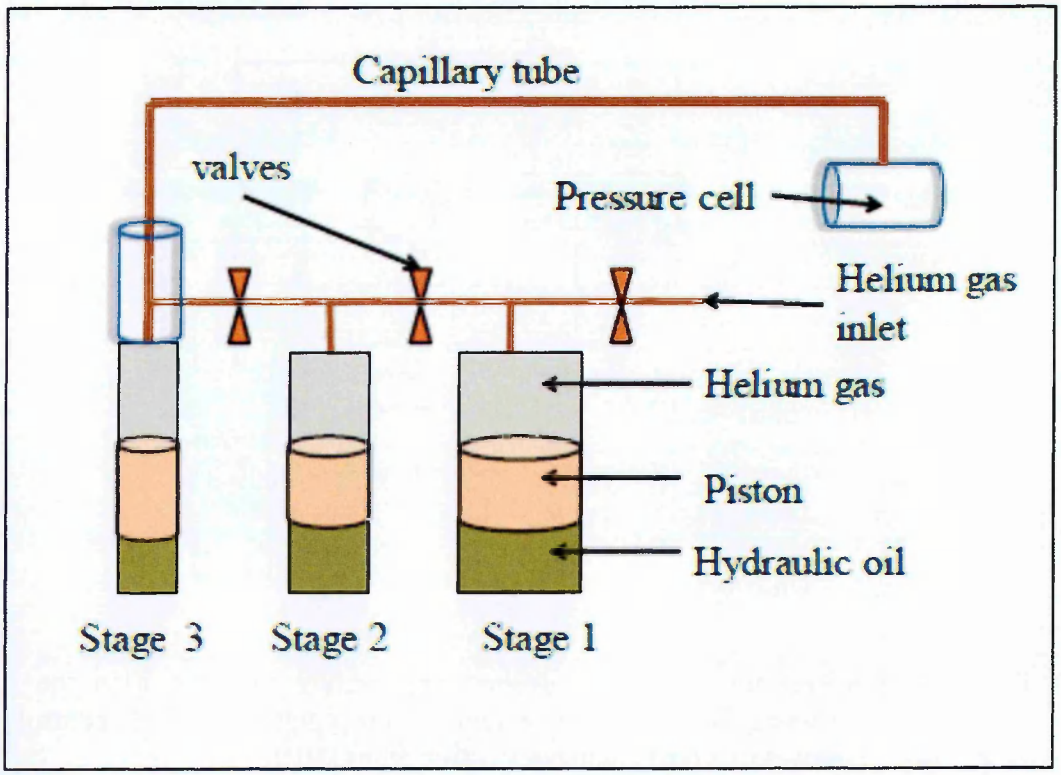

Figure 4-19- Schematic showing the three stages in which pressure can be applied to a pressure cell up to 10kbar by the compression of oil [81]

The capillary tube and the pressure cell are made from a high strength beryllium-copper alloy in order to withstand the high pressures that are applied by this system. A diagram of the pressure cell,

Figure 4-20 , shows that the side of the cell has electrical feed-throughs and has a sapphire window from which the emitted light from the device can be collected.

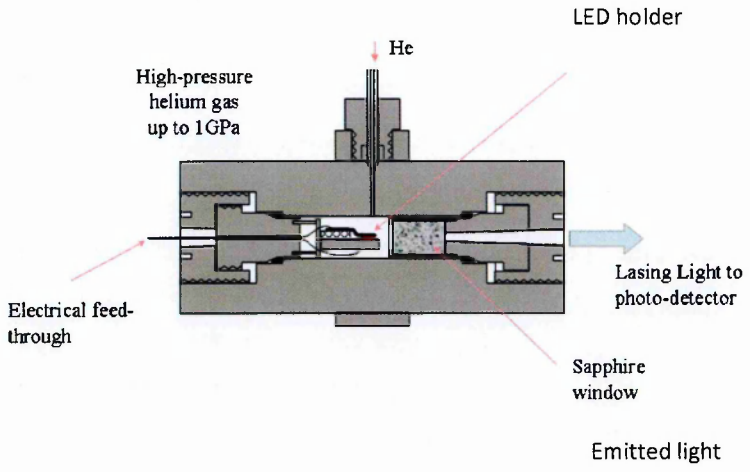

Figure 4-20- Diagram of the pressure cell showing helium gas being inserted into the cell, electrical feed-throughs which supplies electrical connection to the device and a sapphire window where the light may be collected.

Helium gas is pumped into the pressure cell and the capillary tube in order to provide a pressure medium which may be compressed. Pressure is generated by a compressor system in three stages. These stages use the compression of oil to apply pressure to the piston. Valves are closed between each stage in order to maintain the current pressure which is up to 1kbar after the first stage and 3kbar after the second stage. The piston is moved up in the third and final stage in order to provide further compress of the helium gas that applies pressures of up to 10kbar. Careful preparation of the system is required in the form of cleaning non-reusable seals on both the piston and the pressure cell in order to achieve high pressures. This can be achieved by inserting the seals with washing liquid detergent into a beaker which is then inserted into an ultrasonic bath. Thorough cleaning of the piston and pressure cell is also achieved by the use of methanol.

4.9 Chapter Summary

This chapter focussed on describing the techniques employed to study the recombination mechanisms of InGaN based devices.

It was then shown that pulsed measurements of 2μs at 10kHz may achieve the highest light output with acceptable Joule heating. It was shown that efficiency droop occur in both pulsed and CW conditions and therefore CW measurements at small injection levels (where there is

expected to be a low influence of Joule heating) may also be used to investigate the cause of such an effect.

The methods used to investigate the emission spectra of the devices were then presented. Photocurrent is also found to be a valuable technique to investigate the absorption properties of the devices. The optical output power of the devices is also measured using silicon-based integrating spheres which are connected to light power meters.

One of the main techniques used to study the recombination mechanisms of InGaN-based devices in this study is by changing the temperature at which the devices operate. This is shown to be achieved by the use of either a closed cycle helium cryostat or a liquid nitrogen cryostat.

The use of high pressure to investigate semiconductors was presented in the final section of this chapter. It was shown that a gas compressor system which uses three separate stages may generate pressures of up to 10kbar. The pressure system is shown to consist of a piston-in-cylinder which builds up pressure by compressing helium gas in a compressor system which is delivered to the cell with a capillary tube. The devices may be inserted into this pressure cell with electrical and optical connections.

5 Efficiency Droop Models in GaN-based Emitters

5.1 Chapter Aim:

The aim of this chapter is to extend the information on the efficiency droop phenomenon that was introduced in Chapter 3 by discussing relevant droop models to investigate the likelihood of the different candidate loss processes as the cause of efficiency droop. The efficiency droop phenomenon has attracted a lot of attention in recent years and despite extensive studies to date, the cause of this effect remains controversial. In this chapter the mechanisms that have been suggested as the cause of efficiency droop are discussed. The influence of different recombination mechanisms and their current dependence is investigated to understand which processes are most likely to be the dominant cause of efficiency droop. Near identical results may be obtained when modelling the efficiency using the different proposed loss mechanisms which are expected to have a higher dependence on carrier concentration compared with that of radiative recombination.

It is shown that the efficiency droop effect is stronger in green LEDs compared with blue LEDs. Measurements also reveal that the internal polarization field strength is stronger for the green LED. The influence of the internal field on the efficiency and its impact on efficiency droop is therefore investigated. The existence of the internal fields is shown to result in an earlier onset of efficiency droop. It is expected that there is a reduced recombination rate for devices with increasing internal polarization field strength. This is because there is a stronger quantum confined Stark effect (QCSE) that will cause a reduction in the electron-hole wavefunction overlap. The impact of the internal fields on candidate droop causing mechanisms is also described. It is shown that the Auger coefficient is expected to reduce for increasing field strength which is the result of a reduction in the electron and hole wavefunction overlap. This effect, however, is expected to cause an increase in the carrier concentration and may lead to a larger Auger recombination rate (Cn^3). If such is the case, it is expected that there will be an increase in the current at which efficiency peaks when the field is increased. An increasing internal polarization field is found to cause a stronger efficiency droop if carrier leakage is the dominant loss process due to the reduced influence of the

electron blocking layer. It is shown that whilst there is expected to be a small influence of the internal fields on defect-related recombination, there will be a proportional increase of this loss mechanisms with increasing field strength due to the reduced radiative recombination rate. A defect-related recombination cause of efficiency droop is proposed in the final section of this chapter whereby the defect-related recombination coefficient increases, in addition to a reducing radiative recombination rate, with increasing current. This is due to the fact that carriers will increasingly occupy defect states with increasing injection. A defect-related recombination model is accurately fitted to the measured efficiency vs current behaviour of both blue and green LEDs.

5.2 Phenomenon of Efficiency Droop in InGaN-based LEDs

The efficiency droop phenomenon was introduced in Section 3.2 where it was found that there is a relative reduction of efficiency as current is increased following a peak at low current density. The efficiency droop problem is observed for nitride-based devices which emit over the entire visible emitting range. It is also important to note that the efficiency droop phenomenon will also take place in other material systems [82] where there is a loss mechanism which has a higher dependence on carrier concentration than radiative recombination. The efficiency droop effect limits wider exploitation of InGaN-based LEDs as the relative reduced efficiency at high currents will cause a higher required electrical input power in order to achieve the desired light output power. Figure 5-1 shows that there is an increase of the light output power as the current density is increased despite the relative reduction of efficiency at high current densities.

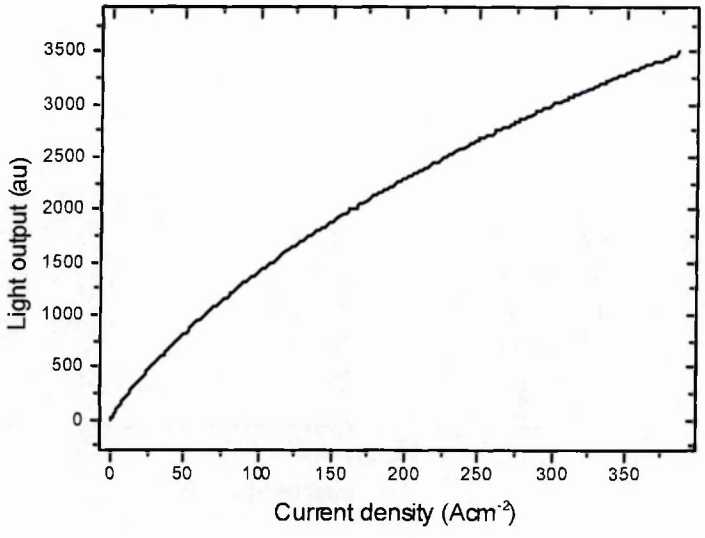

Figure 5-1- The electroluminescence light output power of a blue LED increasing as a function of current density in pulsed mode

At high injection the sublinear dependence of the light output power as a function of current density is consistent with a non-radiative loss process becoming increasingly dominant.

5.3 Effect of efficiency droop on laser diode applications

The radiative efficiency of InGaN LDs is closely connected to efficiency in LEDs and studies on both LEDs and LDs are beneficial to each other. The effect of droop in InGaN LEDs is particularly problematic for LDs as the lasing threshold current density (~2kA/cm^2 for blue-green emitters) is substantially higher than the current density at which the effect of droop in blue-green LEDs begins (~10A/cm^2). The reduced radiative efficiency of the LDs at high current will cause an increase in the threshold current. Thus a larger input power is required to obtain threshold due to the droop-causing process enhancing the losses experience by the laser. The effect of efficiency droop is observed in the efficiency measurements of LDs below the threshold current where the dominant contribution to the light output power will be spontaneous emission as shown in Figure 5-2.

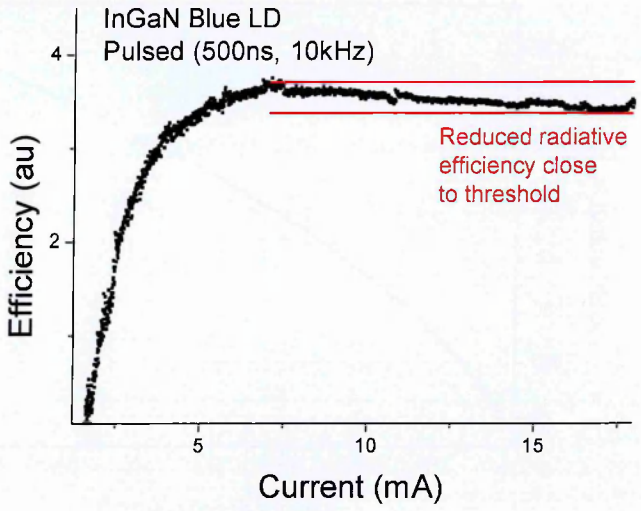

Figure 5-2- The electroluminescence efficiency as a function of current for a blue LD in pulsed mode with 500ns, 10kHz pulses showing the droop effect also takes place in laser diodes and will therefore increase the threshold current

The relative reduction of efficiency as current is increased from ~6mA to ~20mA will therefore lead to a higher required current in order for lasing to occur that will subsequently cause a relative reduction of lasing power at a given current.

5.4 Efficiency scenarios

The influence of different recombination processes on the efficiency is described in Section 3.3 and 3.4. In this section the influence of different recombination processes on the efficiency will be modelled as a function of carrier density. The modelled efficiency as a function of carrier concentration may be used to provide a valuable insight into the effects which cause efficiency droop due to the different dependencies of the recombination processes. Equation 3-1 showed that the efficiency represents the ratio of the radiative recombination rate to the total recombination rate. Considering the ideal case where there is only radiative recombination taking place the efficiency, η, will be determined by,

$$\eta = \frac{Bn^2}{Bn^2} = 1 \qquad 5\text{-}1$$

where B is the radiative recombination coefficient and n is the carrier concentration.

In this ideal case the efficiency would obviously remain at 100% for all carrier concentrations (see Figure 5-3). However, experimental observations show that there is an increase of the efficiency with injection in the low current regime and therefore there is expected to be an additional contribution from defect-related recombination. The effects of the defect-related recombination may be taken into account in the efficiency equation to give,

$$\eta = \frac{Bn^2}{An+Bn^2} \qquad 5\text{-}2$$

where A is the monomolecular defect-related recombination coefficient.

Figure 5-3 shows that if only defect-related and radiative recombination take place then the efficiency will gradually increase with increasing carrier concentration and will theoretically approach 100% for sufficiently large carrier concentration. This efficiency dependence on carrier concentration is caused by the radiative recombination having a stronger dependence on the carrier concentration ($\propto n^2$) compared with that of defect-related recombination ($\propto n$). Therefore the proportion of radiative recombination will increase as the carrier concentration is increased as shown in Figure 5-3. The modelling uses the radiative recombination and monomolecular recombination coefficients determined by Shen *et al.* [31] which are described in more detail in Section 3.4.2.

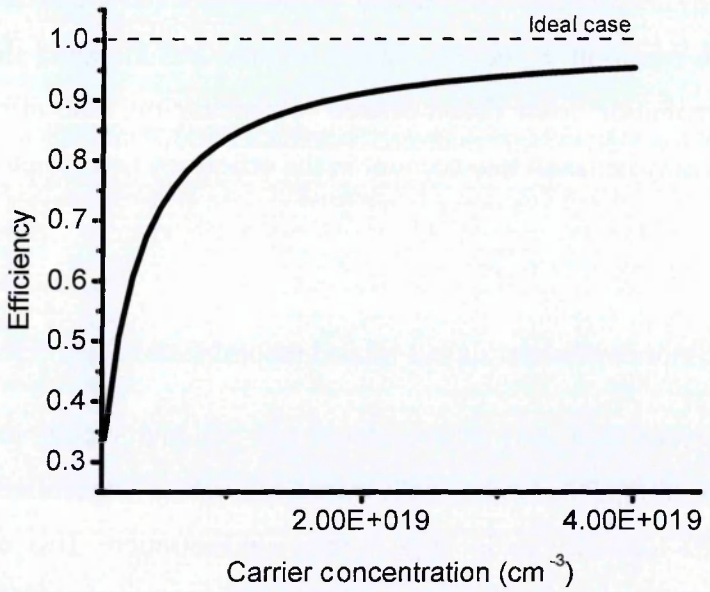

Figure 5-3- Modelled efficiency as a function of carrier density where only radiative recombination and recombination at defect states within the active region take place (with $A=5.7x10^{7}s^{-1}$ and $B=1.8x10^{-11}cm^{3}s^{-1}$)

As can be seen in Figure 5-3, the inclusion of defect-related recombination ($\propto n$) in the efficiency equation cannot result in efficiency droop. Efficiency droop is also not expected to occur for a larger defect-related recombination rate. Figure 5-4 shows that for both $A= 5.7 \times 10^{7}s^{-1}$ (from Shen *et al.* [31]) and $1.4 \times 10^{8}s^{-1}$ will result in an efficiency which increases with increasing carrier concentration due to the increasing dominance of radiative recombination compared with defect-related recombination.

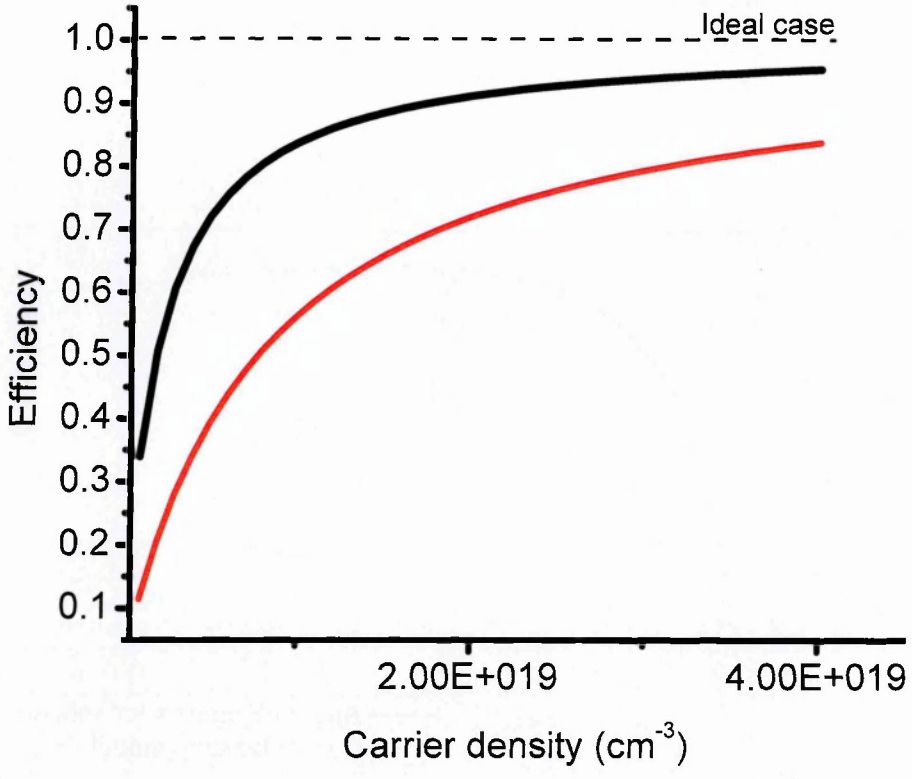

Figure 5-4- Modelled efficiency as a function of carrier density for processes which involve radiative recombination and recombination via defect states for monomolecular coefficients of A= 7 x $10^7 s^{-1}$ (black line) and A=14 x 10^7 s^{-1} (red line)

The lack of efficiency droop if only defect-related and radiative recombination processes take place suggests that a non-radiative process which has a higher dependence on the carrier concentration than radiative recombination is required in order to cause efficiency droop. Figure 5-5 shows the efficiency dependence on carrier concentration if the effects of Auger recombination (black symbols), which is assumed to have a cubic carrier concentration dependence [32], or carrier leakage (red symbols), which is assumed to have an exponential dependence on the carrier concentration due to the increasing likelihood that carriers will escape at high injection [83], as determined by using the efficiency equations,

$$\eta = \frac{Bn^2}{An+Bn^2+Cn^3} \text{ (Auger recombination model)} \quad 5\text{-}3$$

$$\eta = \frac{Bn^2}{An+Bn^2+D_{leak}exp(\frac{n}{n_{leak}})} \text{ (Carrier leakage model)} \quad 5\text{-}4$$

Where D_{leak} is the rate at which carriers will escape from the quantum well and n_0 is the carrier concentration which is confined to the quantum well.

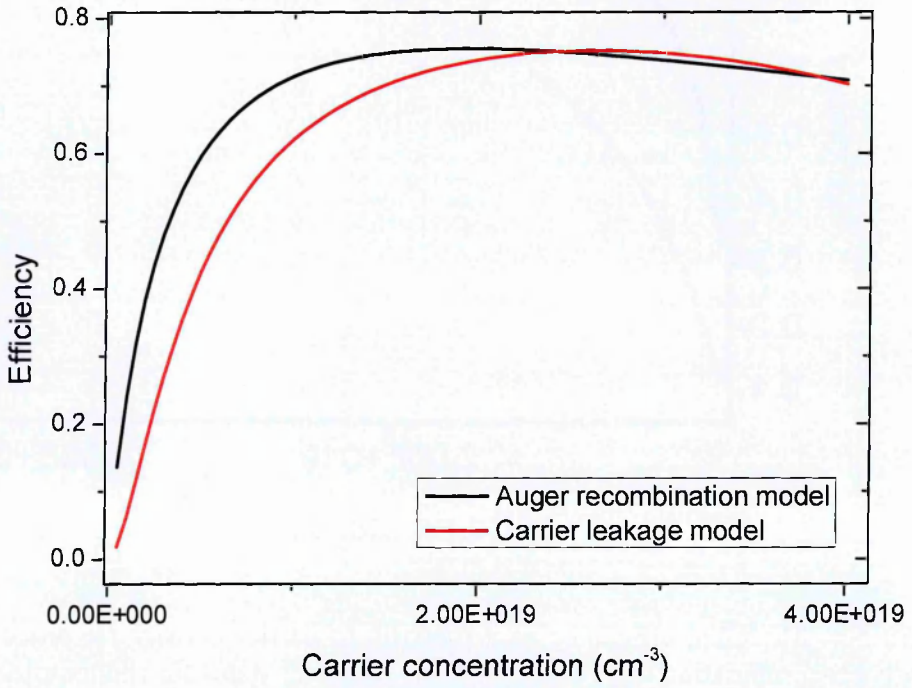

Figure 5-5-The modelled efficiency dependence on carrier concentration if the recombination paths consist of defect-related recombination, radiative recombination and the addition of Auger recombination (black line) or carrier leakage processes (red line). The models use A= $5.7\text{x}10^{7}\text{s}^{-1}$, B=$1.8\text{x}10^{-11}\text{cm}^{3}\text{s}^{-1}$, C=$1.5\text{x}10^{-31}\text{cm}^{6}\text{s}^{-1}$, D_{leak}=$2\text{x}10^{26}\text{cm}^{6}\text{s}^{-1}$ and n_0=$1\text{x}10^{19}\text{cm}^{-3}$.

Figure 5-5 shows that the effects of including a non-radiative recombination process with a higher dependence on the carrier concentration than that of the radiative recombination will result in efficiency droop.

The final efficiency droop model that is discussed in the literature was proposed by Hader *et al.* [26] where there is an additional density-activated defect recombination which becomes important at high injection as described further in Section 3.4.3. A theoretical study by Piprek *et al.* [43] finds that this loss mechanism may also be modelled to provide similar results as the model of Auger recombination and carrier leakage as shown in Figure 5-6.

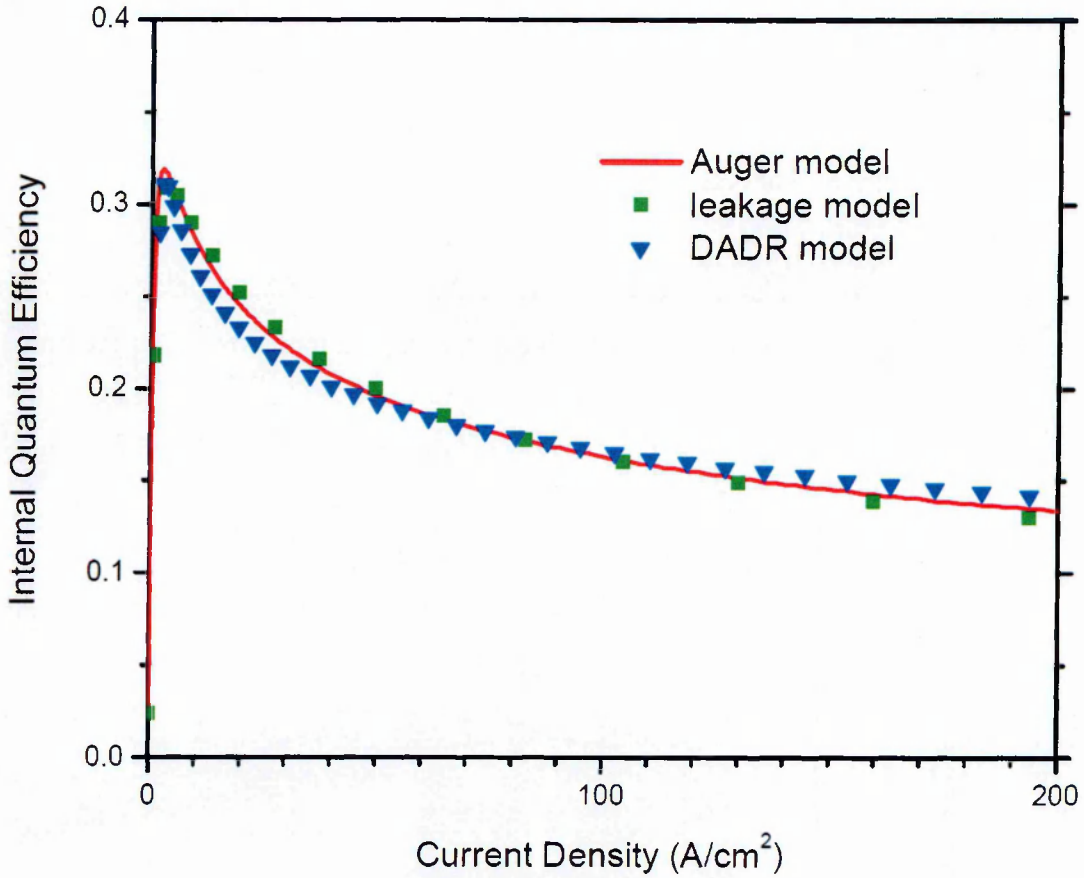

Figure 5-6- Graph to show that models which employ either Auger recombination, carrier leakage or density activated defect recombination may be able to reproduce near-identical results of efficiency droop {taken from [43]}

This observation shows that there is a strong need for experiments or device growth which may be used to differentiate between the candidate loss mechanisms in order to unambiguously determine the dominant cause of efficiency droop.

5.5 Influence of changing monomolecular rate on the efficiency droop phenomenon

The strong lattice constant mismatch between the InGaN well and GaN barrier has been shown to cause a high dislocation density as described in Section 3.7 which is expected to cause a high defect density in the devices. It is therefore important to consider the influence of the monomolecular recombination rate on efficiency droop. Figure 5-7 shows the effect of a changing monomolecular defect-related recombination coefficient, A, from $1x10^7s^{-1}$ to $9x10^7s^{-}$

[1] on the efficiency droop. This range is consistent with the monomolecular defect-related recombination coefficient value of $5.7x10^7s^{-1}$ determined by Shen *et al.* [31]. An Auger recombination model is used in the analysis as this model has accurately been shown to model efficiency droop. The values of the Auger recombination and the radiative recombination coefficient used in this modelling were the obtained from Shen *et al.* [31]. It is important to note that a carrier leakage or density-activated defect recombination also could have been used in the analysis to determine the influence of a changing monomolecular recombination rate.

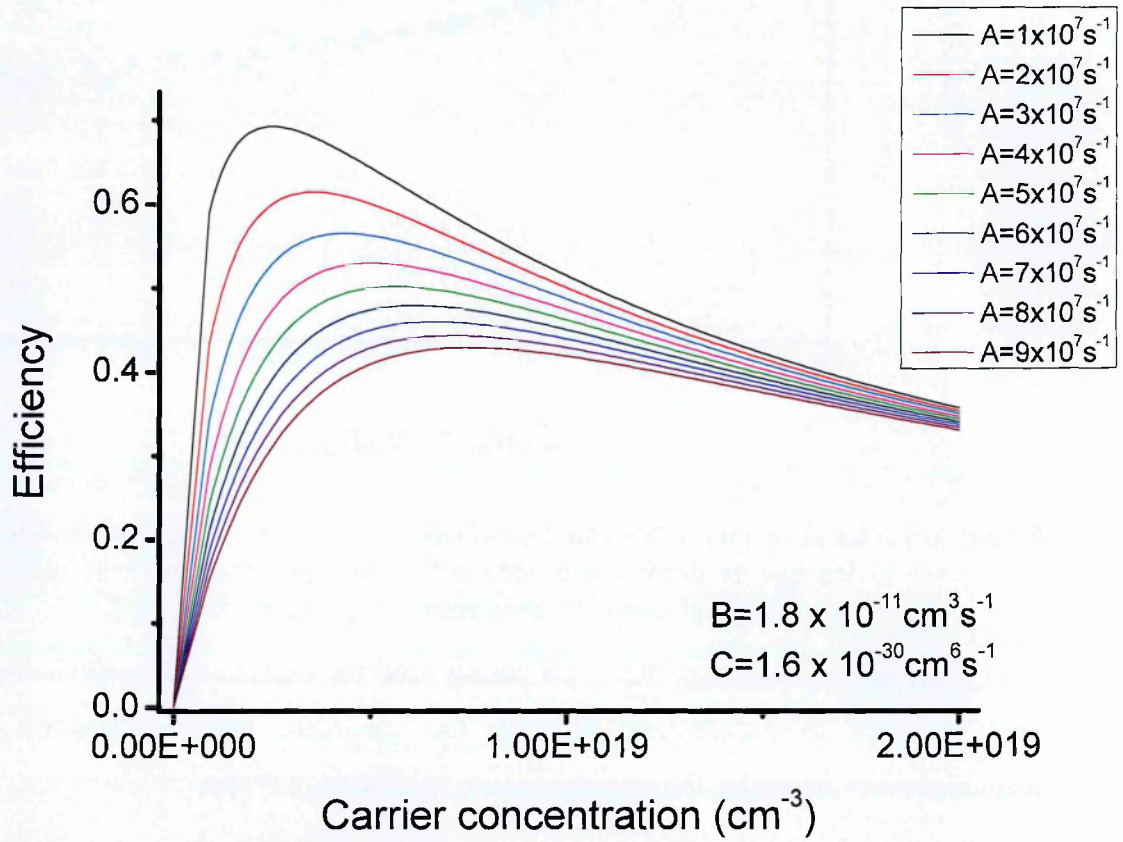

Figure 5-7- The modelled efficiency droop behaviour for different defect-related recombination rates if an Auger recombination model is used

The peak efficiency is found to reduce and occur at a higher carrier concentration with increasing defect-related recombination rate. The droop effect is expected to be reduced with increasing defect-related recombination due to a reduction in the proportion of radiative recombination at lower carrier densities that results in the reduced peak efficiency. These findings suggest that the efficiency at high current densities, as required for most applications,

has a relative small dependence on the monomolecular recombination rate compared to that of the peak efficiency.

5.6 Influence of the internal fields on the efficiency droop phenomenon

The existence of the strong internal fields in nitride-based devices (as described in more detail in Section 3.6) is expected to have an impact on the recombination processes as will be discussed in the following sections of this chapter. Experimental evidence of the internal field is observed in the photocurrent experiments as there is a strong Stokes shift for both blue and green LEDs as shown in

Figure 5-8 and Figure 5-9, respectively.

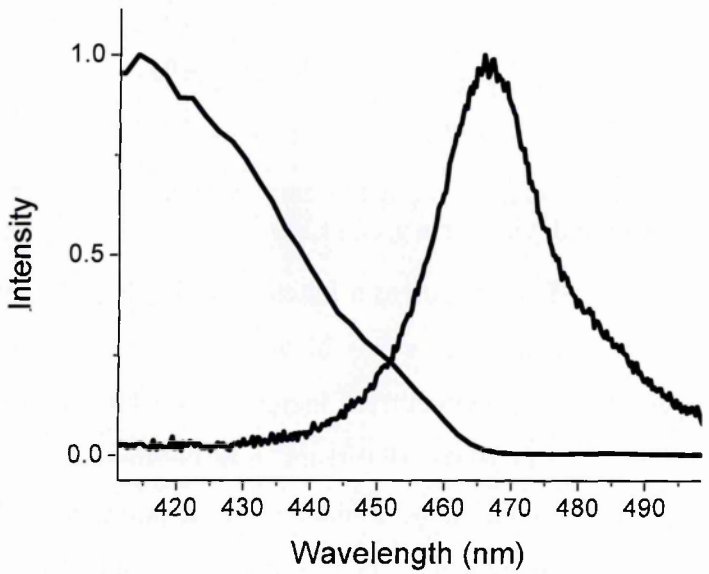

Figure 5-8- Photocurrent intensity as a function of incident light beam wavelength and the emission spectrum of the device for a blue LED

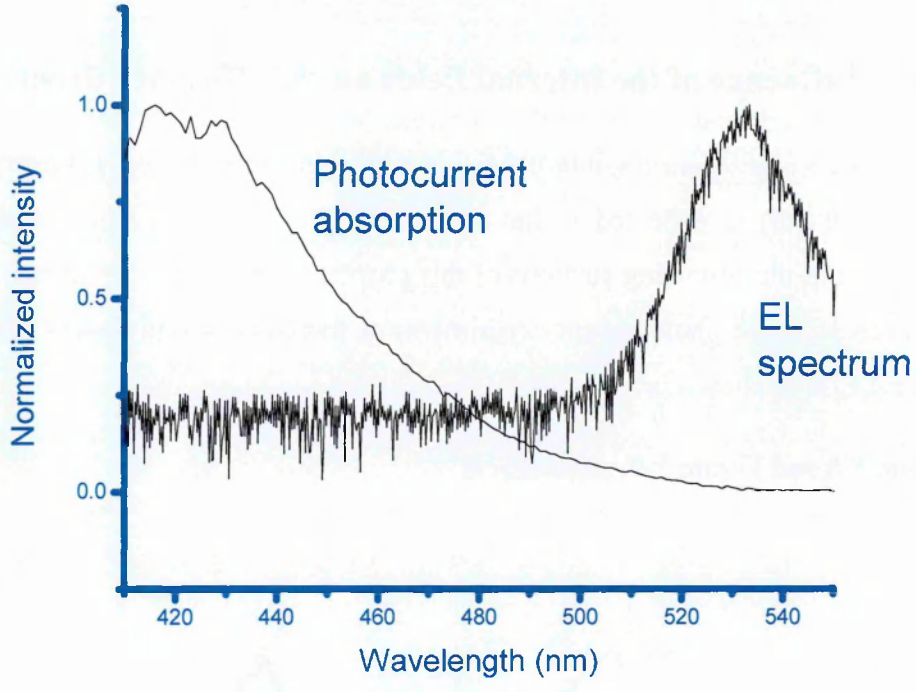

Figure 5-9- Photocurrent intensity as a function of incident light beam wavelength and the emission spectrum of the device for a green LED

The relatively weak rate of absorption as a function of incident light wavelength in both LEDs compared with most flat band devices may be attributed to the existence of the internal fields. The smaller rate at which the photocurrent increases as a function of emission wavelength in the case of the green LED ($0.012\pm0.001 nm^{-1}$) is compared with that of the blue LED ($0.021\pm0.001 nm^{-1}$) is expected to be explained by a stronger internal field strength. The saturation of the absorption rate with decreasing wavelength (increasing energy) is due to saturation of available states. Further evidence that these LEDs have strong internal fields is observed by the blue shift of the peak emission energy as a function of injection current as shown in Figure 5-10 [84].

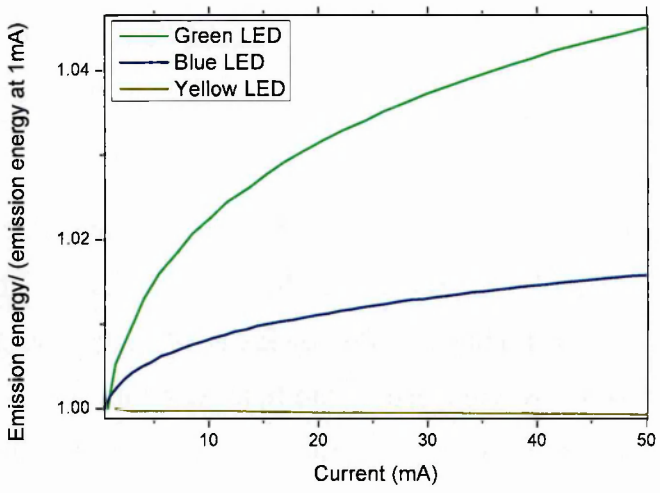

Figure 5-10- The electroluminescence peak emission energy normalized to the peak emission energy at 5mA as a function of current for a green LED (green line), blue LED (blue line) and a yellow AlGaInP LED (yellow line)

This blueshift is expected to be the result of carrier screening of the internal field with increasing current in an effect which is stronger for the green LED. Figure 5-10 also shows that the peak emission energy is relatively constant as a function of current for an AlGaInP yellow LED which is free of the strong internal fields.

5.7 The influence of the internal polarization field strength on the radiative recombination rate

The spontaneous emission rate, R_{se}, is given by Fermi's golden rule [85],

$$R_{se} = \frac{2\pi}{\hbar}\left|\langle S_f|H'|S_i\rangle\right|^2 \rho_f \qquad 5\text{-}5$$

where S_f is the final state, S_i is the initial state, H' is the operator for the physical interaction and ρ_f is the density of final states.

The perturbation Hamiltonian can be expressed as a function of the transmission matrix element $|M'_T|^2 = |\langle u_c|e.p|u_v\rangle|^2$, where $u_{c,v}$ are the conduction band and valence band Bloch functions, $|e.p|$ is the transition matrix and the envelope function overlap $|\Gamma_{e-hh}|^2 = \langle\psi_e|\psi_h\rangle^2$, where $\psi_{e,h}$ are the electron and hole wavefunctions [86].

The overlap of the electron and hole wavefunctions therefore has a strong impact on the radiative recombination rate [87, 88]. An increased QCSE will cause a larger separation of the electron and hole wavefunction overlap leading to a reduction of the radiative recombination rate as described in Section 3.6.

The reduced radiative recombination rate with increasing internal polarization field strength at a fixed current will be accompanied by an increasing non-radiative defect-related recombination rate. The findings of Berkowicz *et al.* [88] show that there will be a strong reduction in the overlap of the electron and hole wavefunctions (inverse of the left y-axis of Figure 5-11) with increasing quantum well width due to an enhanced QCSE. The authors also measured an increasing radiative recombination lifetime with increasing well width (see right axis of Figure 5-11).

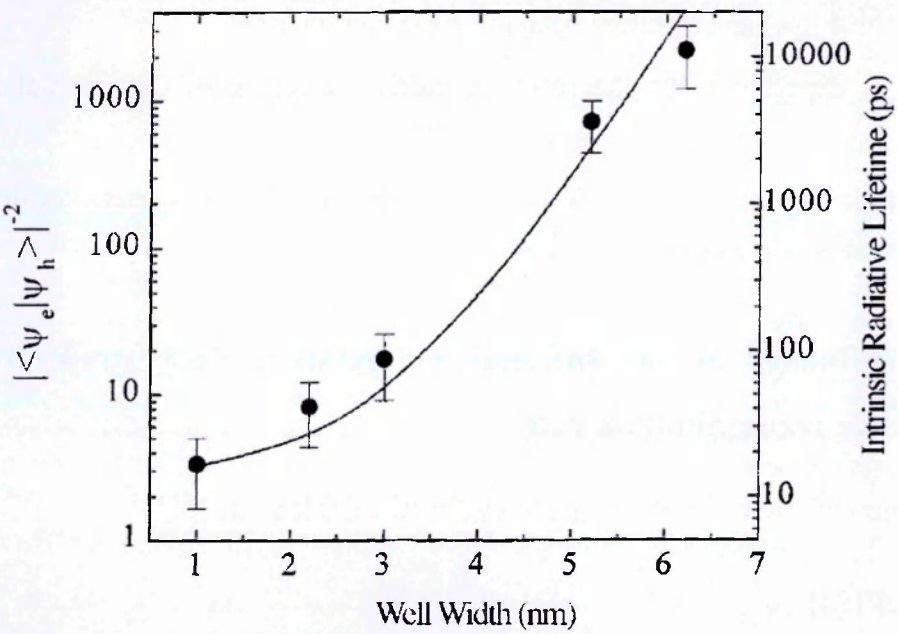

Figure 5-11- The squared overlap of the electron and hole wavefunctions (left y axis) as a function of well width. The y axis (right side) also shows the increase of the radiative lifetime as a function of well width [88].

Similar observations were also found in Bai *et al.* [89] and Li *et al.* [90] where a reduced radiative recombination rate was measured for LEDs which consist of wider width wells.

Figure 5-12 shows theoretical calculations performed in this study for a blue LED consisting of a 3nm quantum well with an indium content of 0.16, 13nm barriers and an AlGaN electron blocking layer with 0.2 Al content at 300K by the use of the simulation software nextnano. It

is shown that a reduction in the electron and hole wavefunction overlap will cause a strong reduction to the overlap of the electron and hole wavefunctions with increasing internal polarization field strength.

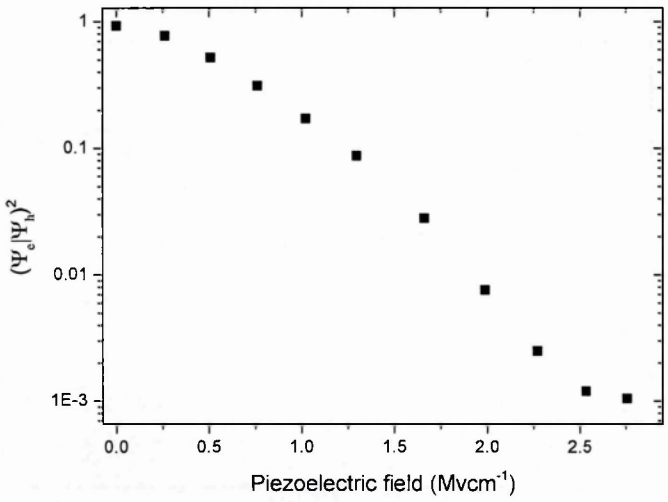

Figure 5-12- The modelled overlap of the electron and hole wavefunctions as a function of internal polarization field strength for a blue LED with 16% indium content using Nextnano software.

The strong reduction of the electron and hole wavefunction overlap is the cause of the reduced radiative recombination rate as internal polarization field strength is increased as shown in Equation 5-5.

The effect of the radiative recombination rate on efficiency droop is now considered. A reduced radiative recombination rate is shown to cause a strong reduction in the peak efficiency but a similar droop effect is expected as shown in Figure 5-13 for different radiative recombination coefficients.

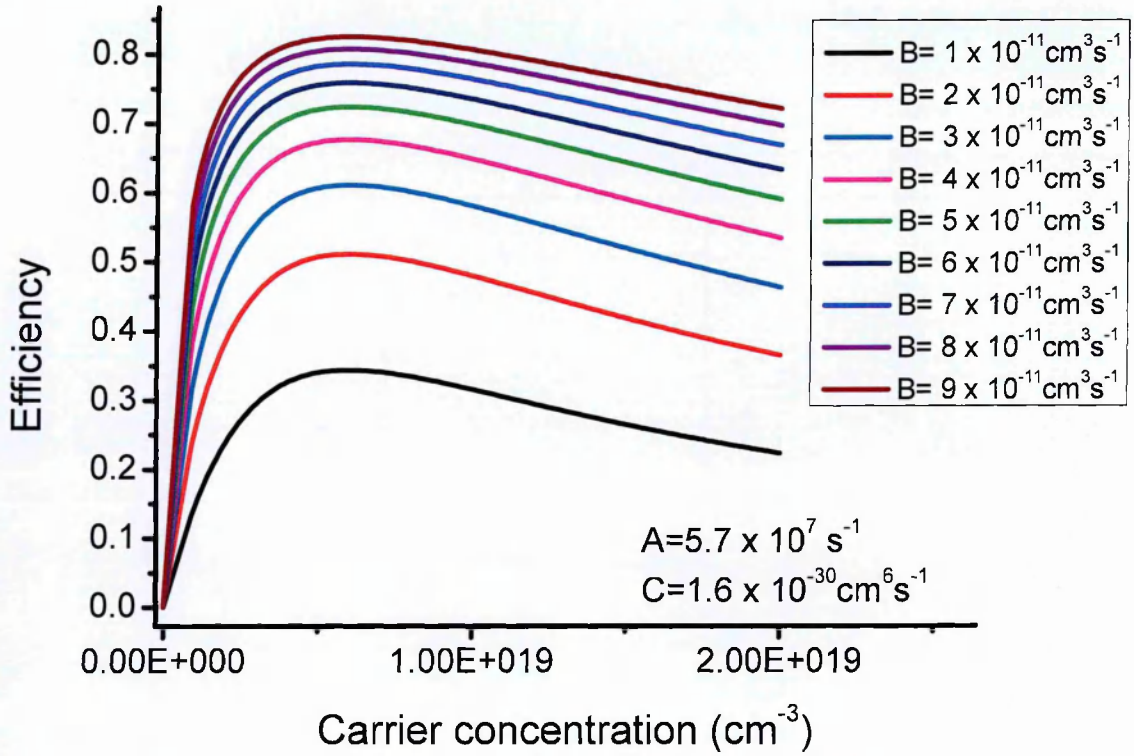

Figure 5-13- The modelled efficiency dependence on carrier injection for different radiative recombination coefficients if an Auger recombination model is employed

The efficiency over the entire current range is found to be considerably higher if there is an increase to the radiative coefficient. This therefore shows that design optimization is required to enhance the radiative recombination rate in order to achieve more efficient devices. The influence of the internal fields on candidate non-radiative loss mechanisms which have been suggested to cause efficiency droop will now be discussed.

5.8 The influence of the internal fields on candidate loss causing mechanisms

5.8.1 Carrier leakage

Carrier leakage has previously been shown to increase with increasing internal polarization field strength [47, 48, 91]. This is due to the increasing separation of the electron and hole wavefunction overlap increasing the likelihood of electron leakage. The effectiveness of the electron blocking layer will also be reduced with increasing internal polarization field strengths as the conduction band edge on the p-side of the quantum well will be at a relatively

lower energy compared with if there was no internal polarization field as can be seen in Figure 3-20.

Section 3.6 showed that whilst there is a reduced droop effect in devices grown along the m-plane [66], the light output remains similar to that of devices which are grown along the c-plane. An alternative technique is therefore required to determine whether a reduction in the internal polarization field strength does indeed reduce the efficiency droop effect due to a reduction of the carrier leakage rate.

5.8.2 Auger recombination

Auger recombination is another loss mechanism which has widely been speculated as the dominant cause of efficiency droop. The Auger recombination coefficient, which is proportional to the probability that Auger recombination will take place, is expected to reduce with increasing strength of the internal fields [92] due to the increased separation of the electron and hole wavefunction overlap. However, the increased strength of the internal fields within InGaN-based devices may enhance the Auger recombination rate (Cn^3) [27, 40] due to the carrier concentration increasing for a given current.

If Auger recombination is present then it will be the dominant recombination process at high currents. At lower currents the dominant recombination will be radiative. Therefore the dominant recombination process will change from being radiative to an Auger process with increasing current density. The dominant recombination process will influence the factor in which the carrier concentration increases due to an increase in the internal field strength.

There will be an increase of the carrier concentration by a factor of $\sqrt{2}$ if the internal field strength is increased by a factor of 2 in the current regime where radiative recombination is the dominant recombination process. However, the carrier concentration will increase by a factor of $\sqrt[3]{2}$ for an internal field strength which increases by a factor of 2 at higher currents where Auger recombination is the dominant recombination process.

The proportional increase in carrier concentration may be calculated as a function of current density by considering equation 3-9 ($J=eL(An+Bn^2+Cn^3)$). Figure 5-14 shows there is a strong reduction in the factor at which the carrier concentration will increase due to the internal field strength increasing by a factor of 2. This is due to Auger recombination becomes increasingly dominant over radiative recombination as there is an increase in the current density.

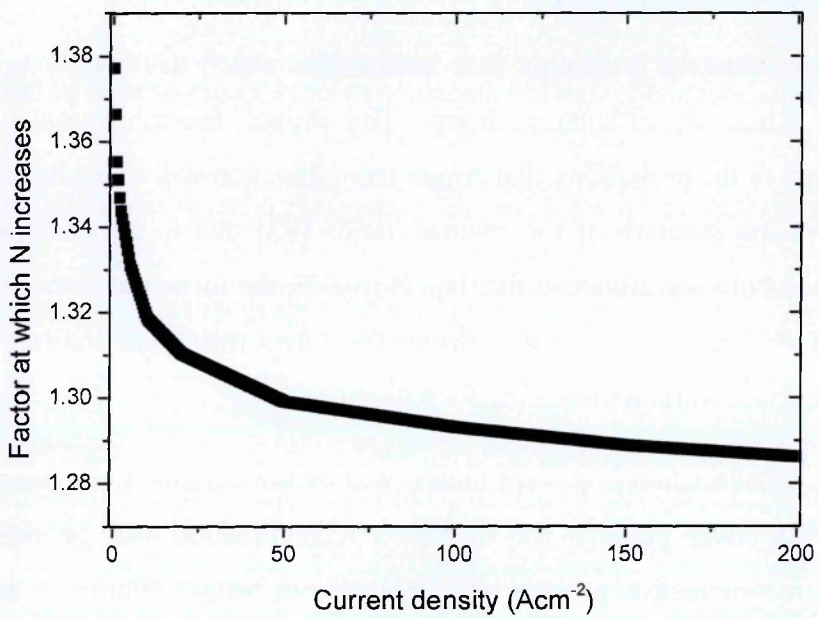

Figure 5-14- The proportional increase of the carrier concentration as a function of current density if the radiative and Auger coefficients are reduced by a factor of 2.

The increase in the carrier concentration as a function of current density may then be used to determine the effect of reducing radiative and Auger recombination rates on efficiency droop as shown in Figure 5-15.

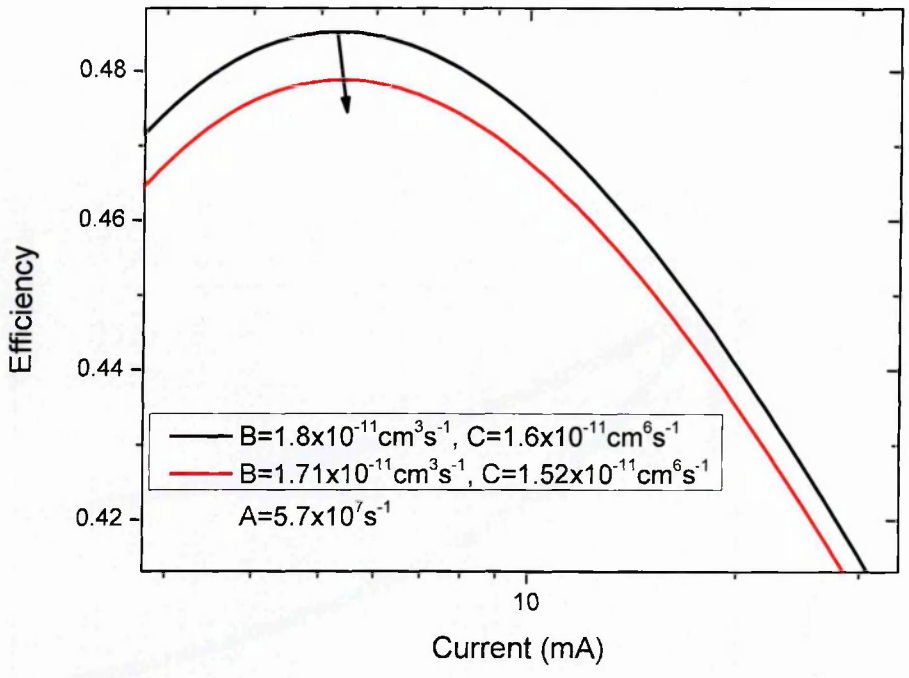

Figure 5-15- The modelled fit of the efficiency as a function of current where the red line represents the behaviour if there is an equal reduction of the radiative and Auger recombination coefficients.

The onset of efficiency droop will occur at a slightly larger current density if the increase in the internal field strength results in a reduction of the radiative and Auger recombination coefficients by a factor of 2. The droop effect however, will remain similar and the efficiency will reduce due to the proportional reduction of radiative recombination.

5.8.3 Defect-related recombination

The increase of the internal fields is expected to have a lower influence on defect-related recombination compared with the radiative recombination rate. Previous studies find that the reduction of the quantum well width will cause a strong enhancement of the peak efficiency due to the enhanced radiative recombination rate as there is a larger overlap of the electron and holes wavefunctions as shown in Figure 5-11. This finding suggests that the defect-related recombination has a weaker dependence on the internal polarization field strength compared with the radiative recombination rate. Whilst the defect-related recombination coefficient may not significantly change with increasing internal polarization field strength, it is expected that there will be a relative increase in the defect-related recombination due to the reduced radiative recombination rate at a fixed current (see section 5.7).

5.9 Efficiency droop in blue and green LEDs

In agreement with previous studies [26, 33], the results of this study show that the efficiency droop phenomenon is stronger for green LEDs compared with blue LEDs as shown in Figure 5-16.

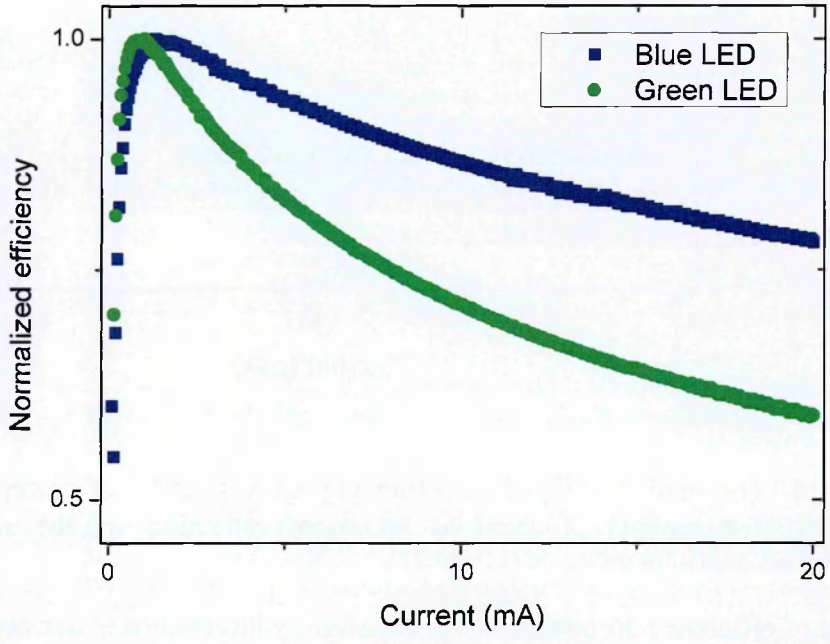

Figure 5-16- The measured efficiency normalized to the peak efficiency showing the droop effects in a blue LED (blue squares) and a green LED (green circles)

The cause of the stronger droop effect in the green LED may be due to its stronger internal polarization field strength. Whilst the carrier leakage rate is expected to be increased for larger internal field strengths (see section 3.4.4) the relatively larger band offset in the green LED compared with the blue LED will reduce the likelihood of carrier escape. Therefore the increased droop rate in green LEDs may only be explained using a carrier leakage argument if the carrier leakage rate due to the stronger fields dominates over the reduced carrier leakage rate due to the increased band offset.

The difference in the Auger recombination rates for the blue and green LEDs is unclear. Whilst the Auger coefficient is expected to be reduced in the green LED due to a reduced wavefunction overlap, the overall Auger recombination rate may be increased due to a higher carrier concentration as described in the previous section and due to lower band gap energy.

The density-activated defect recombination (for more details see section 3.4.3) model may also explain the stronger droop effect for the green LED in comparison with the blue LED. LEDs of higher indium content will generally have a larger dislocation density due to larger strain effects which result from a larger lattice mismatch. The increased droop effect in the green LED may therefore be explained using this model if there is a lower carrier concentration at which the density-activated defect recombination occurs and a lower density-activated defect recombination lifetime for the green LED as shown in Figure 5-17.

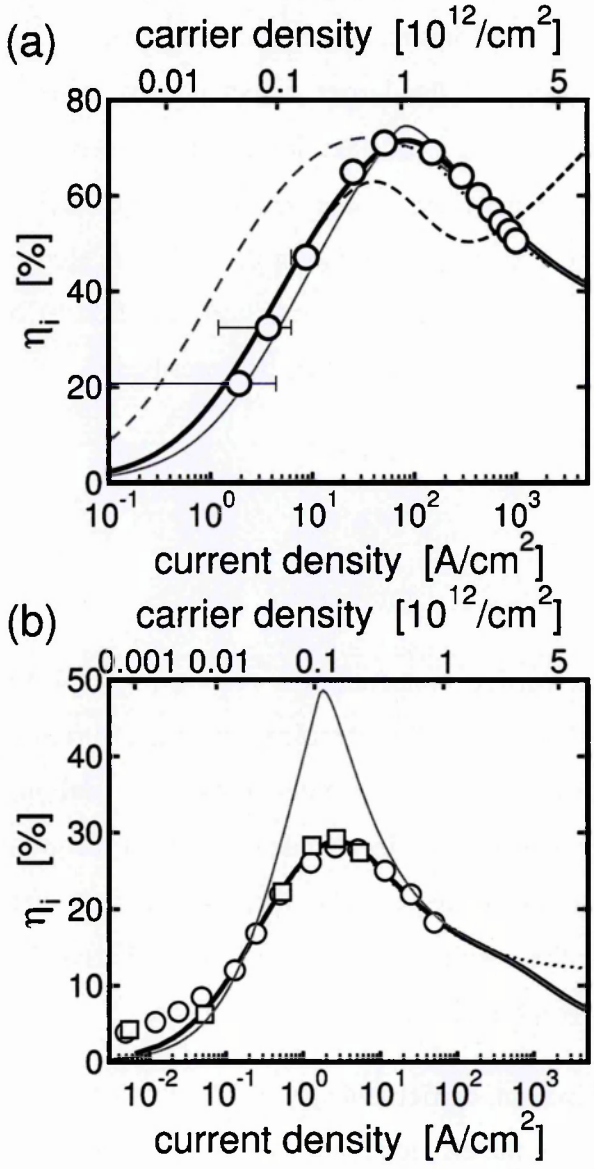

Figure 5-17- The fitting of experimental data whereby a density-activated defect recombination model is applied for a blue LED (top) and a green LED (bottom)

5.10 Injection dependent monomolecular coefficient as a cause of efficiency droop

The defect-related recombination coefficient, A, is considered a constant as a function of current in all the models previously described. However, the existence of potential minima due to well width and/or indium content fluctuations, observed in TEM studies [72], is expected to localize carriers away from defect sites to cause a reduced defect-related recombination coefficient at low currents. A model is proposed in which efficiency droop may be explained by a defect-related recombination coefficient which increases with increasing carrier concentration because of the larger defect density where carriers have delocalized. It is assumed that there will be a constant defect-related recombination coefficient at low injection due to only sites within the active region bandgap being involved in the defect-related recombination. To a first approximation the defect-related recombination can be assumed to increase linearly with increasing carrier concentration at high currents. The defect-related recombination coefficient may therefore be described as,

$$A = A_0\,, \qquad \text{for } n<n_p \qquad \text{5-6a}$$

$$A = A_0(1 + D(n - n_P))\,, \qquad \text{for } n>n_p \qquad \text{5-10b}$$

where n_p is the carrier concentration required to fill the potential minima. A_0 is the monomolecular defect-related recombination in the current regime where there is no carrier concentration dependence as per the conventional model applied in most III-V systems. D is the rate at which the monomolecular defect-related recombination increases with increasing carrier concentration above n_p. The increased defect-related coefficient at higher carrier concentration is the result of a reducing non-radiative lifetime that causes a subsequent increase in the recombination rate via defect states.

If Auger recombination, carrier leakage and density activated defect recombination is assumed to be negligible then the efficiency may be determined using Equation 3-8. Figure 5-18 shows that efficiency will show droop behaviour if this model is employed. The A_0 coefficient is considered to be $5.7\text{x}10^{7}\text{s}^{-1}$ which is consistent with the measurements of Shen *et al.* [31]. B_0 $=7\text{x}10^{-11}\text{cm}^3\text{s}^{-1}$ is comparable with the values determined in previous experiments [27, 31]. $n_p=8\text{x}10^{17}\text{cm}^{-3}$ is in line with the carrier concentration used for modelling the onset of density-

activated defect recombination of Piprik *et al.* [43]. It is assumed that $D=7.52x10^{-19}s^{-1}cm^{-3}$ which will result in a similar non-radiative lifetime to that determined experimentally by David and Grundmann at high injection currents ($\sim10^{-9}s^{-1}$).

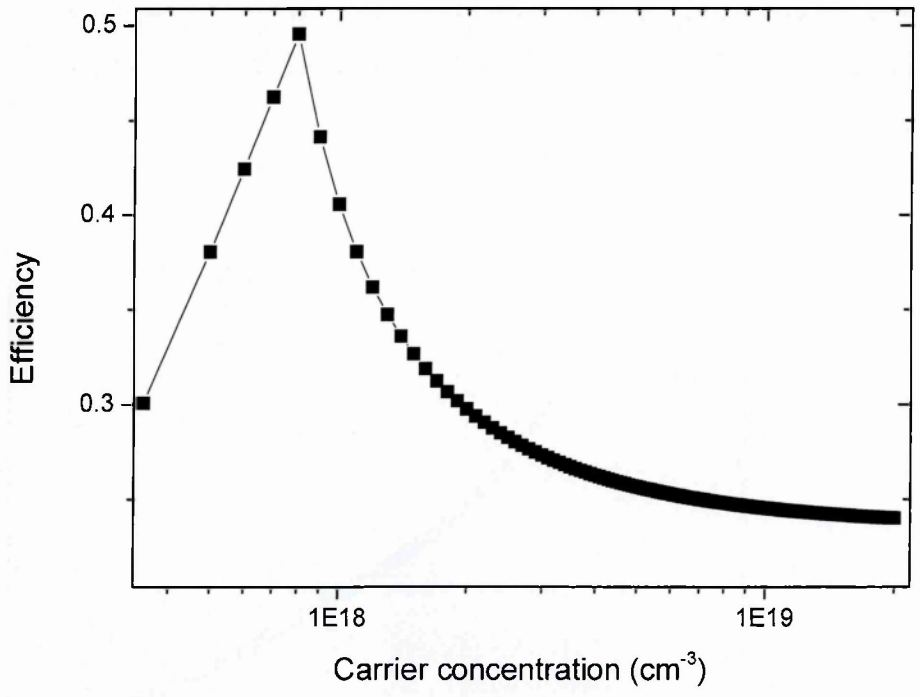

Figure 5-18- The modelled efficiency as a function of carrier concentration whereby there is an increase of the monomolecular defect-related coefficient. $A=5.7x10^{7}s^{-1}$, $B_0=7x10^{-11}cm^{3}s^{-1}$, $D=7.52x10^{-19}s^{-1}cm^{-3}$ and $n_p=8x10^{17}cm^{-3}$.

It can be seen that using this model with an increased monomolecular coefficient with increasing carrier concentration will indeed provide efficiency droop. Previous studies have shown that the radiative recombination rate is also expected to have a carrier density dependence which changes from having a quadratic to an approximately linear dependence due to phase-space filling effects [93]. David and Grundmann [27] have determined that the radiative recombination coefficient will have a dependence on the carrier concentration as follows,

$$B = \frac{B_0}{(1+n/n_0)} \qquad 5\text{-}7$$

where B_0 is the unperturbed radiative recombination rate and n_0 is the characteristic carrier density which leads to a saturation of the radiative recombination rate as there is an increase of

carrier concentration. The cause of the saturated radiative recombination rate is due to the reduced optical matrix element at high injection [23, 25] as shown in Section 3.3.1.

Figure 5-19 shows that efficiency droop will occur if there is an increase of the monomolecular defect-related recombination coefficient and a reduction of the radiative recombination coefficient at high currents. The values used are the same as those in the modelling of Figure 5-18 with n_0= $5x10^{18}cm^{-3}$ which has been determined by Eliseev *et al.* [23] and Piprek *et al.* [43].

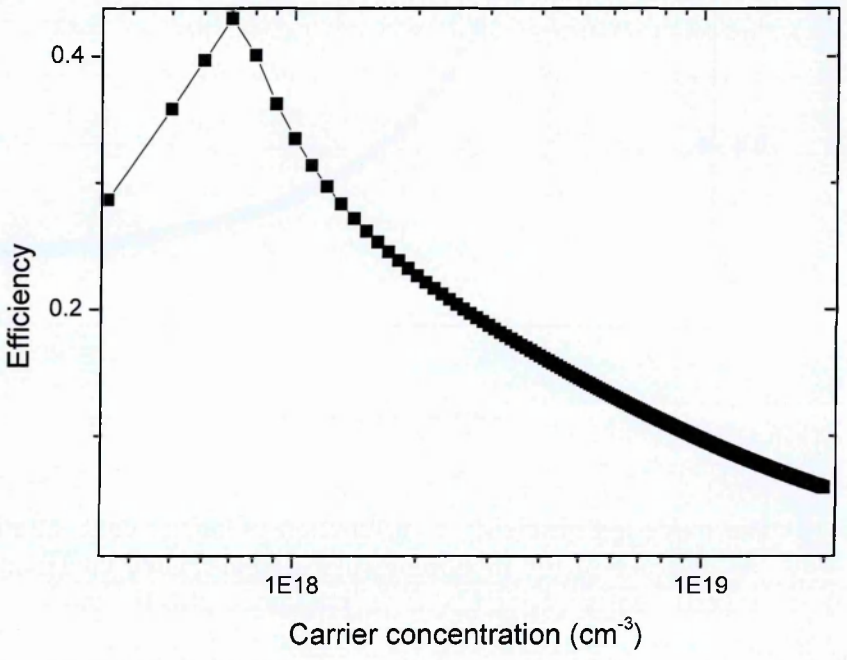

Figure 5-19- The modelled efficiency dependence on carrier concentration where the monomolecular and radiative recombination coefficients have dependences on the carrier concentration where A=$5.7x10^{7}s^{-1}$, B_0 =$7x10^{-11}cm^{3}s^{-1}$, n_0= $5x10^{18}cm^{-3}$, D=$7.52x10^{-19}s^{-1}cm^{-3}$ and n_p=$8x10^{17}cm^{-3}$

Figure 5-19 shows the model is more consistent with the observed droop behaviour measured in experiments if the effect of the reduction of the radiative recombination coefficient is also taken into account. This is because there is not a saturation of the droop rate as shown in Figure 5-17 if phase space filling is not considered in the model.

Figure 5-20 shows the dependence of the defect recombination coefficient on the carrier concentration as determined from Equation 5-10.

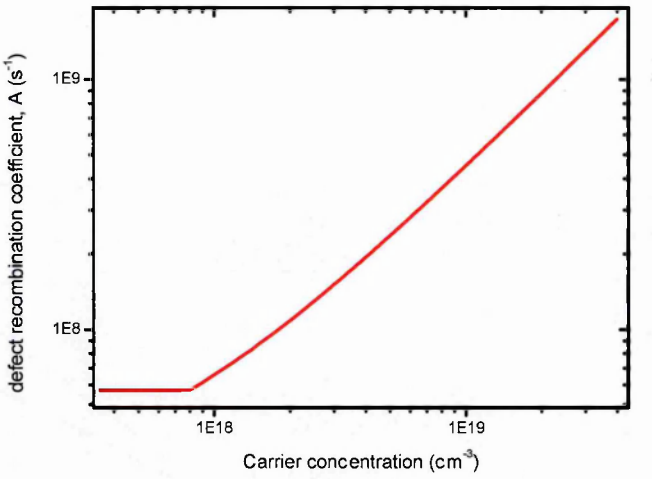

Figure 5-20-The modelled defect recombination coefficient as a function of carrier concentration as determined by eq.1 with $A_0=5.7x10^7s^{-1}$, $D=7.52x10^{-19}s^{-1}cm^{-3}$, $n_p=8x10^{17}cm^{-3}$

Similarly, the radiative coefficient as a function of carrier concentration that is determined by using Equation 5-11 is shown in Figure 5-21.

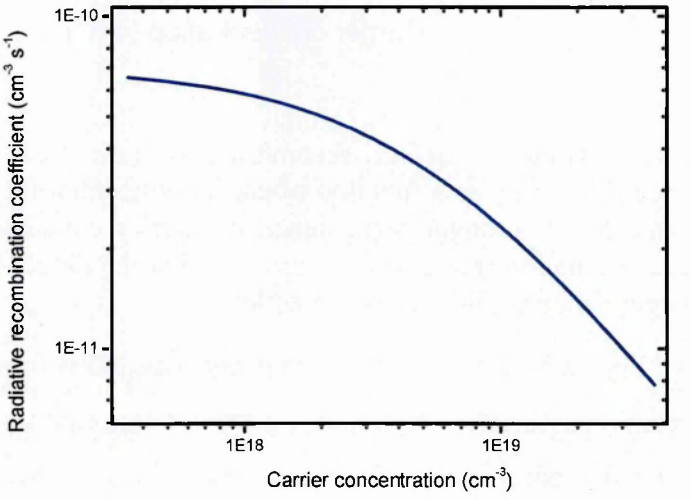

Figure 5-21- The modelled radiative recombination coefficient as a function of carrier concentration that reduces due to phase-space filling effects determined from eq.3 with $B_0=7x10^{-11}cm^3s^{-1}$ and $n_0=5x10^{18}cm^{-3}$

The recombination rate of monomolecular recombination is calculated by multiplying the monomolecular recombination coefficient by the carrier concentration, n, and the radiative recombination rate is calculated by multiplying the radiative recombination coefficient by the

cubic dependence, n^2. The recombination rates as a function of carrier concentration is shown in Figure 5-22.

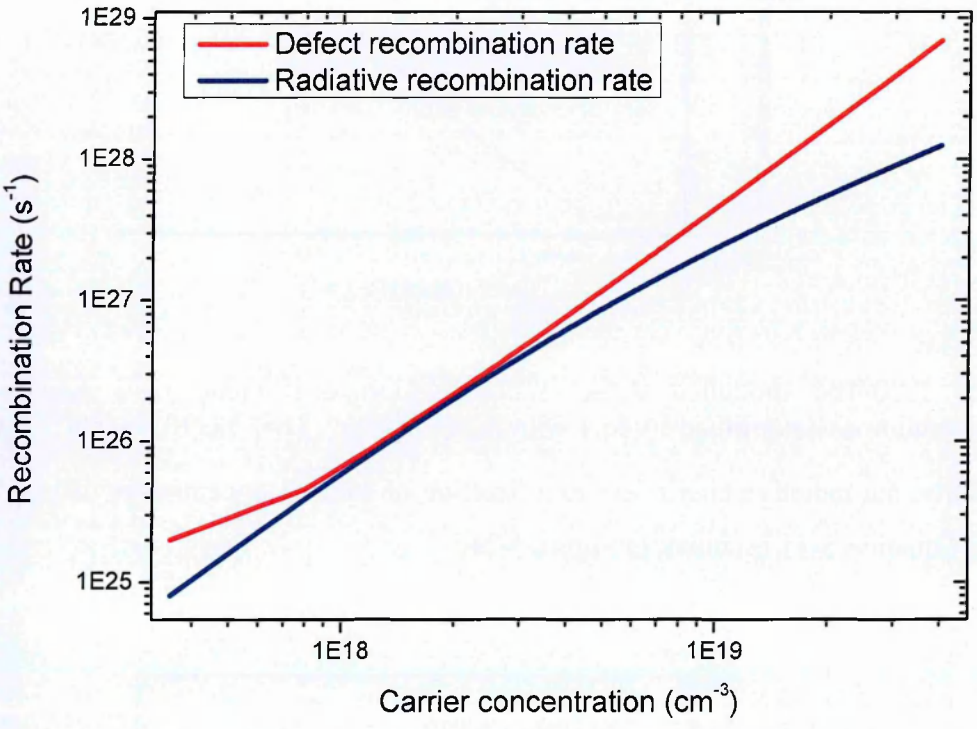

Figure 5-22- The modelled defect recombination rate (red line) and the radiative recombination rate (blue line) as a function of carrier concentration showing that the radiative recombination rate has a stronger dependence on carrier concentration compared with the defect-related recombination rate at low currents, whilst the defect-related recombination rate has a stronger dependence at high current injection.

It can be seen in Figure 5-22 that at low carrier concentrations there is a stronger increase in the radiative recombination rate with increasing carrier concentration than compared with that of the defect-related recombination. This will result in an increase of the efficiency as a function of carrier concentration. However, as the carrier concentrations is increased above ~ $10^{18}cm^{-3}$, the rate at which the monomolecular recombination rate increases with increasing carrier concentration will be larger than that of the radiative recombination rate. This will cause the efficiency to show droop behaviour. The dependence of the recombination rates on carrier concentration is the result of phase space filling effects reducing the radiative recombination rate and the increase of the defect-related recombination leading to an increase of the monomolecular recombination coefficient at high carrier concentrations.

The efficiency of both a blue and a green LED may be modelled using this argument where there is stronger defect-related recombination at high currents. A scaling factor has been included in the efficiency measurements to take into account the collection efficiency for the experimental data. The carrier density is calculated by using the area of the chip as determined in 4.2. The model uses $A_0=5.7x10^7s^{-1}$ and $5x10^7s^{-1}$ for the blue and green LEDs, respectively, which are in line with previous studies [26, 31]. The slightly smaller value for the green LED is attributed to stronger carrier localization effects which are the result of higher indium content [94]. It is assumed that $n_p = 8x10^{17}cm^{-3}$ and $6x10^{17}cm^{-3}$ for the blue and green LED, respectively. The rate at which the monomolecular recombination coefficient increases with carrier density, D, is $7.8x10^{19}s^{-1}cm^{-3}$ and $6x10^{19}s^{-1}cm^{-3}$ for the blue and green LED, respectively.

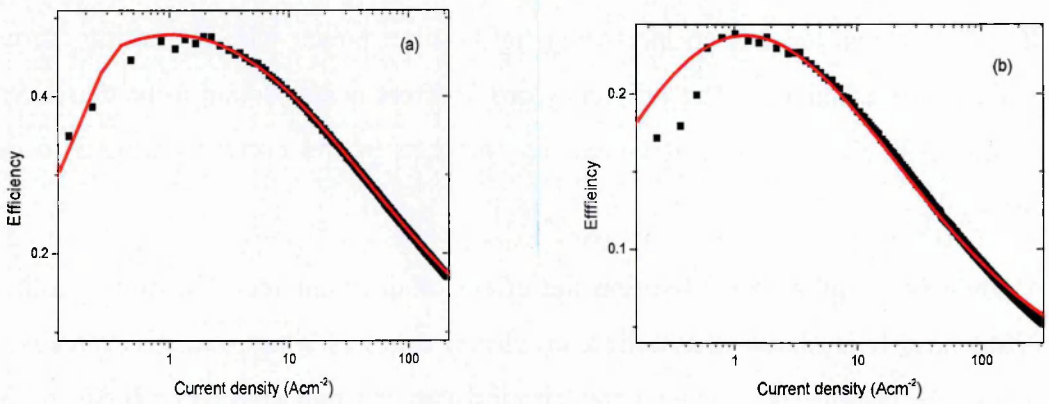

Figure 5-23-The measured efficiency dependence on current density fitted using a model of efficiency droop that uses an increasing defect-related recombination coefficient as a function of carrier concentration for (a) a blue LED where $A_0=5.7x10^7s^{-1}$, $B=7x10^{-11}cm_3s^{-1}$, $n_p=8x10^{17}cm^{-3}$, $D=7.8x10\text{-}19s^{-1}cm^{-3}$ and $n_0=5x10^{18}cm^3$ and (b) a green LED with $A_0=5x10^7s^{-1}$, $B=2x10^{-11}cm_3s^{-1}$, $n_p=6x10^{17}cm^{-3}$ and $n_0=5x10^{18}cm^3$.

The experimentally measured efficiency droop has been shown to be fitted by employing a model whereby there is an increase of the defect-related recombination coefficient as a function of current density. The parameters A_0, B_0, n_0 were taken by the literature and the D and n_p values were obtained from the fit. The efficiency equation will therefore only require defect-related and radiative recombination in order for droop behaviour to occur. The additional impact of phase space filling effects in the model will lead to efficiency droop which is more consistent with experimental observations. The proposed model of an

increasing defect-related recombination rate is a simple model where to a first approximation it has been assumed that there is a linear increase of defect-related recombination with increasing carrier concentration. A more realistic model would include consideration of the rate at which there is a reduced carrier localization with increasing injection. Another basic assumption of the model is that there is a defect-related recombination coefficient is independent on carrier concentration at low injection levels due to only the active region bandgap defect sites being involved. In reality, there may also be a dependence on carrier concentration at low injection levels which is likely to have a lower dependence on injection than that at high injection due to the stronger carrier localization effects.

5.11 Chapter Summary

The efficiency droop effect that occurs in nitride-based emitters is the main topic of this chapter. Different models are presented which have been suggested to result in such an effect. It is shown that there is an increasing light output power with increasing current despite the reduction in efficiency. The efficiency droop effect is also found to be detrimental in InGaN-based laser diodes where it causes an increase to the current required to achieve lasing threshold.

Models are employed to describe the effect of different recombination mechanisms on the efficiency. It is shown that efficiency droop requires a non-radiative process which has a higher dependence on carrier concentration that the radiative recombination. Models which include Auger recombination or carrier leakage may provide near identical results. It is also shown that droop will occur if the efficiency is modelled using the DADR argument for efficiency droop.

A larger defect-related recombination coefficient with increasing carrier density is shown to have a strong effect on reducing the peak efficiency but there will be little influence at the high injections that are required for normal operation in most devices.

Photocurrent results indicate that internal polarization fields exist in the LEDs in an effect which is stronger in the green LED. Consistent with these results is the stronger blueshift with increasing current of the green LED compared with that of the blue LED which may be attributed to a larger carrier screening effect of the internal field. The existence of the high internal field strength is found to have a strong effect on the radiative recombination rate. This

is due to the reduction of the electron and hole wavefunction overlap with increasing internal field strength. A reduction of the radiative recombination coefficient is shown in a model to cause a strong reduction to the efficiency over the entire current range, but should only have a small effect on the efficiency droop.

The effect of the internal field strength on the candidate droop-causing mechanisms is then discussed. It was shown that carrier leakage is expected to be enhanced with increasing field strength due to the reduced effectiveness of the EBL. The influence on the Auger recombination rate is less clear. Whilst a reduction to the Auger recombination coefficient is expected to occur due to the separation of the electron and hole wavefunction overlap, there will also be an increase to the carrier concentration at a fixed current because of the reduced recombination rates. If such is the case then the efficiency will reduce and the onset of efficiency droop will occur at a larger current.

The stronger efficiency droop in the green LED compared with the blue LED may be explained by an increase in the internal fields which enhances the droop-causing mechanism. The increased dislocation density of the green LED due to larger strain effects may also be the cause of the increased droop effect.

In the final section of this chapter a defect-related recombination model is presented as the cause of efficiency droop. Carriers are suggested to be localized in potential minima at low currents causing a reduced defect-related recombination rate. The delocalization of carriers with increasing carrier concentration leads to an increased likelihood that carriers will recombine at higher energy defect sites. An increasing defect-related recombination coefficient with increasing injection, along with a reduction in the radiative recombination rate due to phase space filling, was shown to fit the experimentally measured efficiency droop in blue and green LEDs.

6 Temperature Dependence of the optoelectronic properties of blue-green InGaN LEDs

6.1 Chapter aim

The temperature dependence of InGaN-based blue-green LEDs is presented in this chapter. The results show that the devices have the poorest performance at the lowest temperatures. An increasing light output power at a fixed current of 20mA is observed with increasing temperature from 80K up to 150K and 280K for the blue and green LED, respectively. A reducing light output power is observed with further increases of temperature in both LEDs. Such observations are likely to be caused by two different loss mechanisms, with opposite dependencies on temperature, dominating in different temperature regimes. The sublinear dependence of the light output on current injection at low temperatures suggests that defect-related recombination with states in the band gap is suppressed with decreasing temperature. Therefore an alternative loss mechanism which has a higher dependence on current than that of the radiative recombination is expected to cause the poor performance of the LEDs at low temperatures. It is also observed that the LEDs have a low peak efficiency and strong droop effect at low temperatures. This is consistent with a loss mechanism becoming increasingly dominant with reducing temperature. The increasing effect of the loss mechanism that is responsible for the strong droop behaviour is expected to be due to issues relating to the hole injection efficiency. Evidence of hole injection issues is presented in the form of an increasing turn-on voltage with decreasing temperature. The reduction of the hole injection efficiency as temperature is decreased is expected to cause an increase to the effective internal polarization field strength which will increase the likelihood that electron leakage occurs.

For comparison, the temperature dependence of a blue LED which did not include an EBL is investigated. It was shown that the turn-on voltage of this devices increases at a weaker rate with decreasing temperature than that of the LEDs which included an EBL. This may be attributed to improved hole injection efficiency in this device as it does not include an EBL which hinders hole injection into the quantum well. For this device, the efficiency droop effect

is still found to become stronger with reducing temperature. This shows that the carrier leakage becomes larger with decreasing temperature and is related to hole injection issues.

Evidence that a carrier leakage process occurs is observed at low temperatures by the existence of a second emission peak in the spectra of the green LED.

The temperature dependence of the peak emission energy shows that carrier localization is expected to take place in InGaN devices. A characteristic "s-shaped" dependence of the peak emission energy on temperature is observed for both the blue and green LEDs. Further evidence of carrier localization effects occurring is shown by the increasing FWHM with decreasing temperature below 100K.

The final section of this chapter shows efficiency droop at temperatures where hole injection is not expected to be problematic. The temperature dependence of efficiency droop is shown to be fitted using a defect-related recombination model as the cause of efficiency droop.

6.2 Temperature dependence of the light output power in blue-green InGaN LEDs

Temperature-dependence techniques have been used in previous studies to gain information about the dominant recombination mechanism that limits the efficiency in semiconductor devices. This is due to different loss mechanisms having specific dependencies on temperature [29]. In this study, the effect of temperature is found to have a similar influence on the optoelectronic properties in both blue and green LEDs as shown in Figure 6-1.

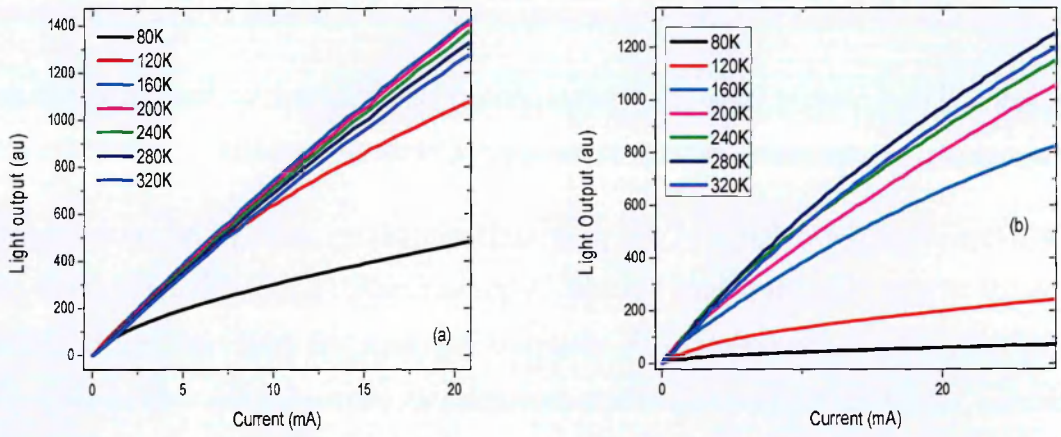

Figure 6-1- The electroluminescence light output power as a function of current for (a) a blue LED and (b) a green LED in pulsed mode at different temperatures.

It can be observed that the light output power is lowest at the lowest temperature (80K) for both the LEDs. Figure 6-2 shows this dependence more clearly where the light output at a fixed current of 20mA increases with increasing temperature up to ~150K and ~280K for the blue and green LEDs, respectively. There is a reduction of the light output power as temperature is further increased beyond these temperatures.

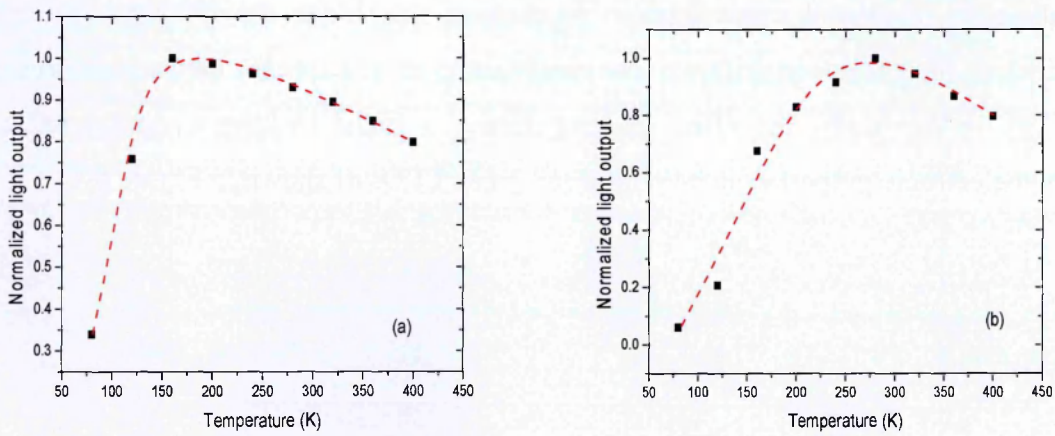

Figure 6-2- The electroluminescence light output normalized to the highest light output value as a function of temperature at 20mA in pulsed mode with a pulse width of 2μs and a frequency of 10kHz for (a) a blue LED and (b) a green LED.

The highest light intensity occurs at a higher temperature for the green LED in comparison with that of the blue LED. This is expected to be the result of stronger localization effects for the green LED [94] that has a stronger effect at reducing defect-related recombination. This

will result in a higher temperature required in order for defect-related recombination to become the dominant loss mechanism for the green LED. Figure 6-2 suggests that there are competing non-radiative recombination processes which have different temperature dependencies. The increase of the light output power with increasing temperature up to 160K and 280K for the blue and green LEDs, respectively, indicates that there is a reduction of the dominant loss mechanism. In contrast, increasing the temperature above these temperatures is expected to increase the impact of the dominant loss mechanism that results in the reduction of light output power.

Figure 6-3 shows that there is a sublinear dependence of the light output power as a function of current. This observation is expected to show that the dominant loss mechanism at low temperatures is not due to defect-related recombination with sites in the active region bandgap. This is because devices consisting of a high density of defect sites within the active region bandgap will have a superlinear dependence on current owing to the fact that there is a stronger dependence of radiative recombination on the injection current compared with that of the active region bandgap defect-related recombination. The sublinear measurements at low temperature therefore show that there is a strong reduction in the defect-related recombination with defect sites in the active region bandgap with decreasing temperature as previously predicted [29].

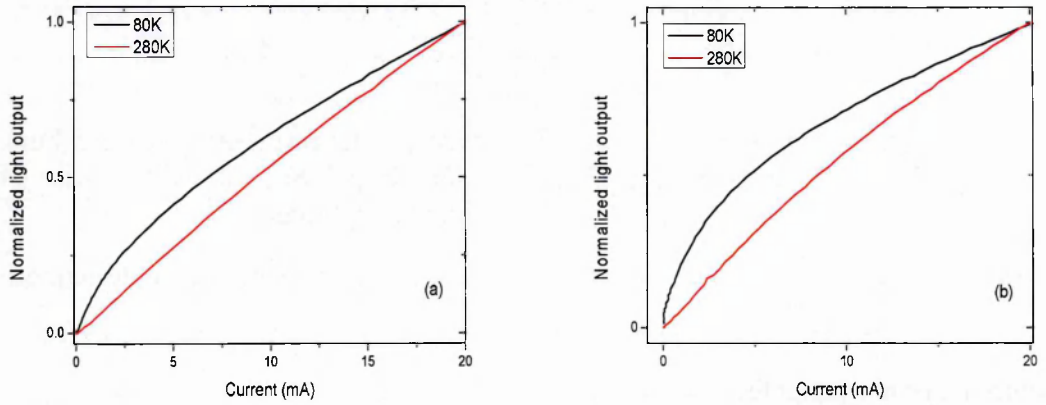

Figure 6-3- The electroluminescence light output normalized to the value at 20mA as a function of current at 80K and 280K for (a) a blue LED and (b) a green LED in pulsed mode with a pulse width of 2μs and a frequency of 10kHz showing the sublinear behaviour at low temperature in both cases.

The reduction of the active region bandgap defect-related recombination rate with decreasing temperature therefore suggests that there is another loss process which causes the poor performance of the LEDs at low temperature. Such a loss process reduces with increasing temperature causing the light output dependence on current to become increasingly linear.

6.3 Temperature dependence of efficiency droop in blue-green InGaN LEDs

Figure 6-4 shows the efficiency droop effect at different temperatures for a blue and a green LED. The efficiency droop effect is observed to be strongest at 80K with a reduced peak efficiency which indicates that there is a loss mechanism which is strongest at low temperatures.

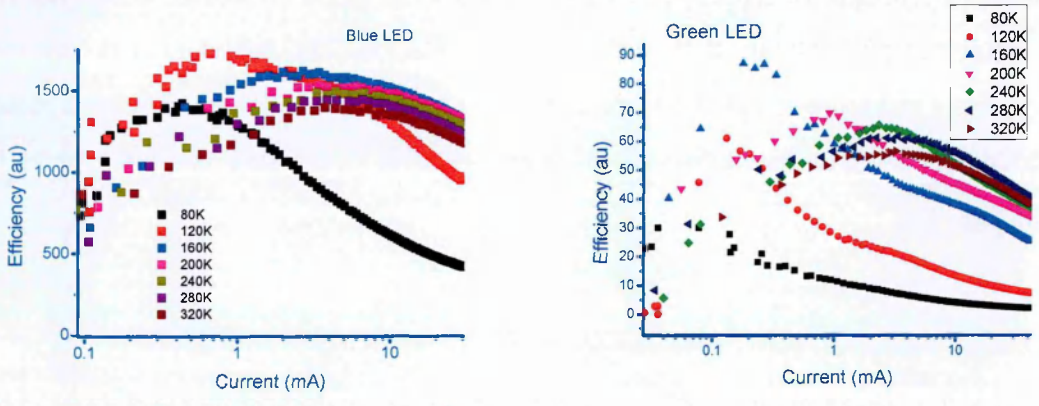

Figure 6-4- The electroluminescence efficiency dependence on current for a blue LED (left graph) and a green LED (right graph) in pulsed mode with a pulse width of 2μs and a frequency of 10kHz at different temperatures

As previously described, the active region bandgap defect-related recombination is expected to reduce with decreasing temperature due to a "freeze out" of defect sites [29]. Recombination with defects sites at relatively high energy is also expected to reduce at low temperature due to increased carrier localization. Auger recombination and carrier leakage rates have also been shown to reduce with decreasing temperature [95-97] and therefore one would not expect these non-radiative mechanisms to cause of the low peak efficiency and strong efficiency droop at low temperatures. The poor performance of the LEDs at low temperature is therefore expected to be caused by an alternative process occurring at low temperatures which leads to an increase a non-radiative process.

6.4 Hole injection issues at low temperature

The reduction of temperature is expected to reduce the mobility of carriers (see section 3.5). Figure 6-5 shows that poor hole injection causes an increase in the turn-on voltage with reducing temperature in both LEDs.

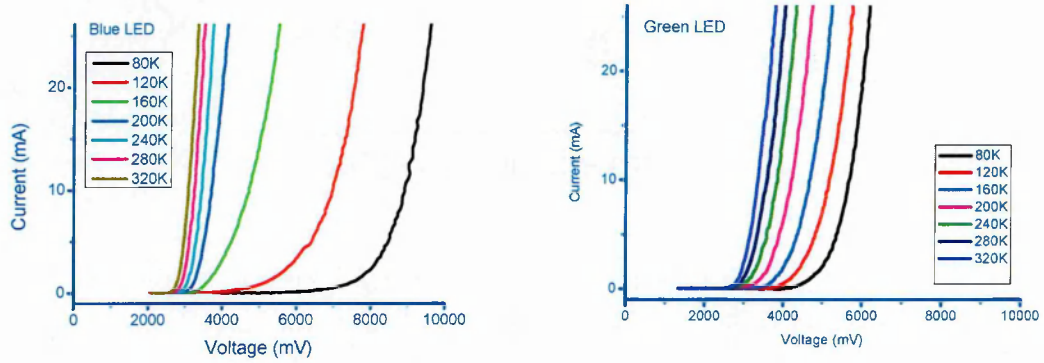

Figure 6-5- The current dependence on applied voltage at different temperatures for the blue LED (left graph) and a green LED (right graph) in pulsed mode with a pulse width of 2μs and a frequency of 10kHz

The increase in turn-on voltage with decreasing temperature is observed to be stronger for the blue LED compared with that of the green LED. This observation can be explained by stronger hole injection issues in the blue LED which results from a larger number of quantum wells (see Chapter 4).

A further reduction in concentration of holes will result from the low activation of Mg-dopants with reducing temperature.

The increase in the applied voltage is expected to cause an enhancement in the effective internal field strength [98, 99] as the field due to the applied voltage is in the same direction as the internal polarization fields. The effect of applying voltage to the internal polarization field is illustrated in Figure 6-6.

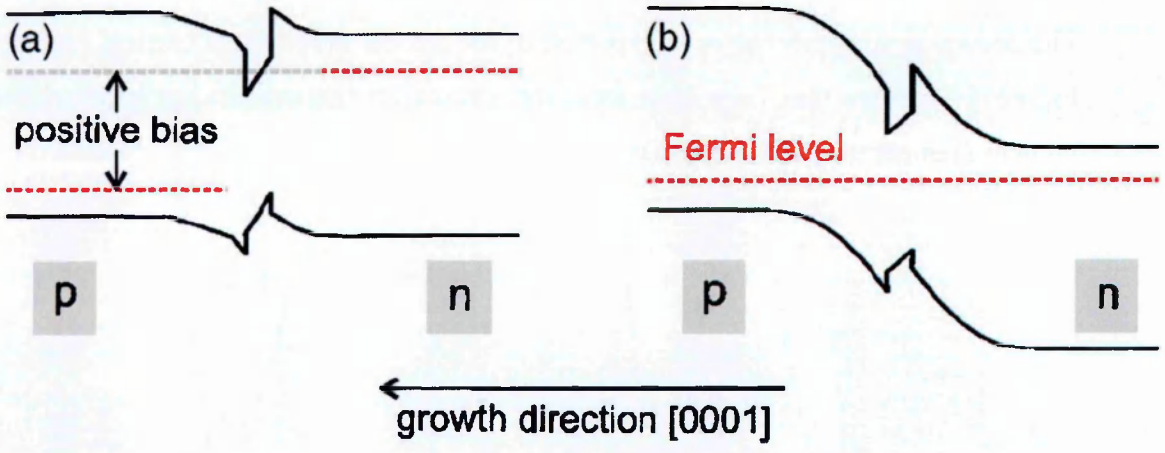

Figure 6-6- Schematic indicating the effect of applying a bias to the pn junction causing an increase to the internal field strength [98]

Previous studies have shown that an indication of the internal field strength may be achieved by measuring the blueshift as a function of current [48]. Figure 6-7 shows that the blueshift as a function of current is weakest at the lowest temperatures and is found to increase with increasing temperature in both LEDs.

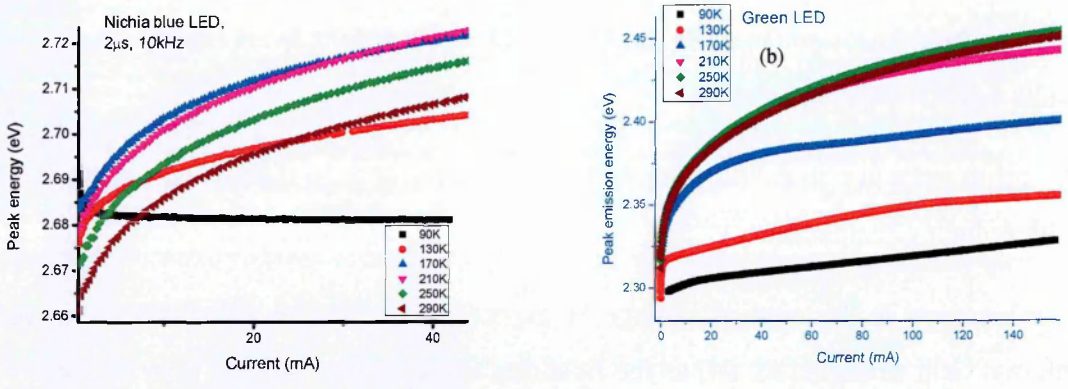

Figure 6-7- The blueshift of the peak emission energy as a function of current at different temperatures for (a) a blue LED and (b) a green LED in pulsed mode with a pulse width of 2μs and a frequency of 10kHz.

The reduced blueshift at low temperatures may be the result of the emission spectra being highly influenced on the non-radiative recombination mechanism which causes the strong droop. For example, there will be fewer carriers available to screen the internal field if there is a strong carrier leakage rate and thus a reduction in the blueshift as a function of current will be observed. The peak emission energy shift is therefore measured over a fixed current range

which is below the peak efficiency. CW measurements are required to accurately obtain low currents (below 10μA) where it is assumed that Joule heating will be negligible. The blueshift in the peak emission over a fixed current range (from 0.5μA to 10 μA) was observed to be the largest at low temperatures and found to reduce with increasing temperature as shown in Figure 6-8 and Figure 6-9.

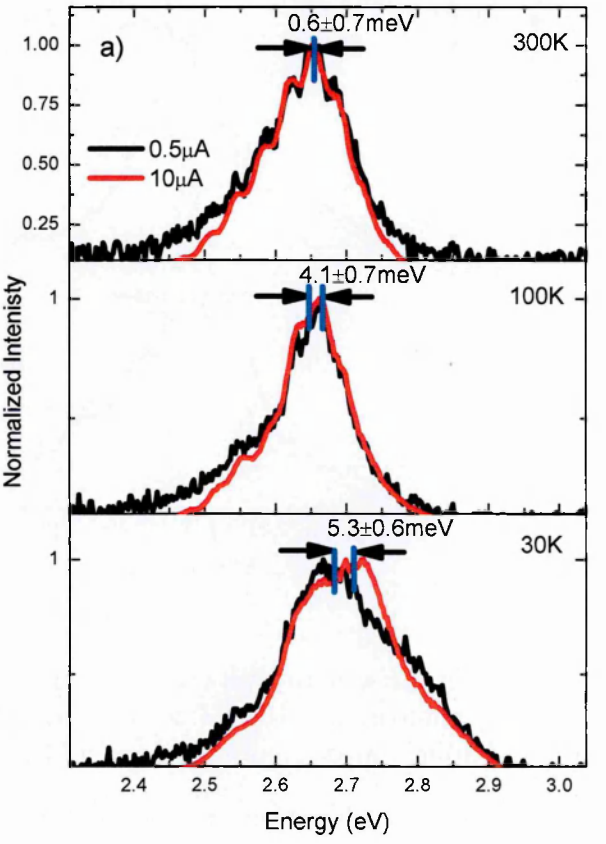

Figure 6-8- The blueshift in the electroluminescence emission peak for a current of 0.5μA (black line) compared to 10μA (red line) at 30K (lower graph), 100K (middle graph) and 300K (upper graph) for a blue LED in CW mode.

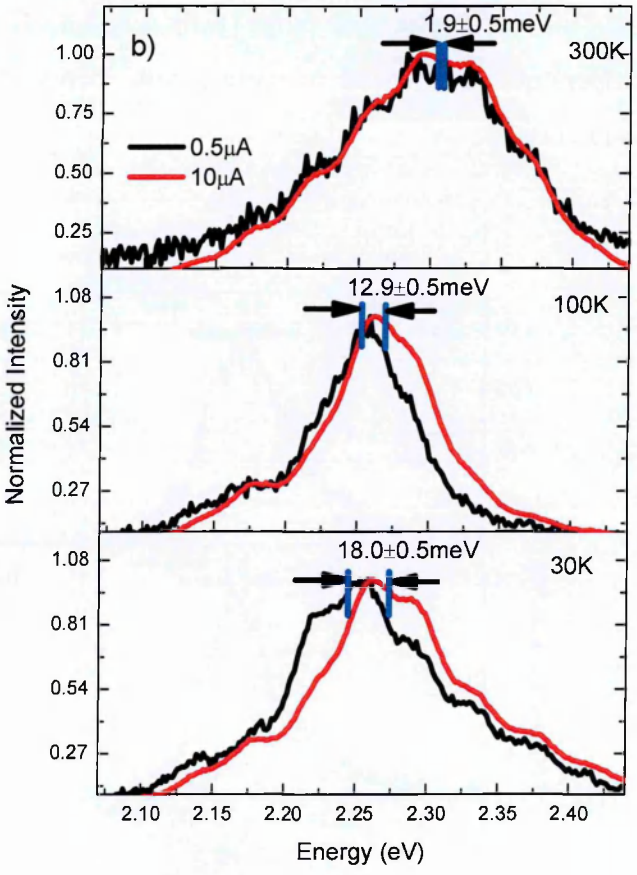

Figure 6-9- The blueshift in the electroluminescence emission peak for a current of 0.5μA (black line) compared to 10μA (red line) at 30K (lower graph), 100K (middle graph) and 300K (upper graph) for a green LED in CW mode.

It is noteworthy to comment on the stronger blueshift in the peak emission as current is increased from 0.5μA to 10μA at all temperatures for the green LED compared with the blue LED. This is expected to be caused by the stronger internal fields within the green LED due to its higher indium content (see section 5.9).

The increased internal field strength at the lowest temperatures is likely to increase the dominant non-radiative recombination process that causes the poor performance of the LEDs at the lowest temperatures. Previous studies have found that the carrier leakage rate will be larger for devices which have a higher internal field strength [48]. Such observations can be explained by the stronger field causing the conduction band n-side of quantum well to be at a higher energy than the conduction band at the p-side of the well. The reduced effectiveness of the electron blocking layer will therefore increase the probability of electron leakage as

described in Section 3.4.4. The increased peak efficiency and reduced efficiency droop effect with increasing temperature up to ~120K and ~160K for the blue and green LEDs, respectively, (see Figure 6-4) is therefore expected to be the result of a reduced carrier leakage rate with increasing temperature. These observations are in agreement with the theoretical calculations of Piprek *et al.* [55] where the improvement of the hole injection efficiency with increasing temperature was found to reduce the electron leakage rate.

6.5 Temperature dependence of the blue LED without an electron blocking layer

The inclusion of the electron blocking layer (EBL) has been shown to reduce the rate at which electrons escape from the active region to recombine elsewhere. However, previous studies have also shown that the EBL may also hinder hole transportation (see Section 3.5). The reduction of hole injection efficiency at low temperatures is expected to increase the turn-on voltage (Figure 6-5). A blue InGaN-based LED (with emission at ~465nm) which did not include an EBL was observed to have a turn-on voltage which increases at a reduced rate with decreasing temperature compared with a blue LED (with emission at 460nm) which included an EBL as shown in Figure 6-10.

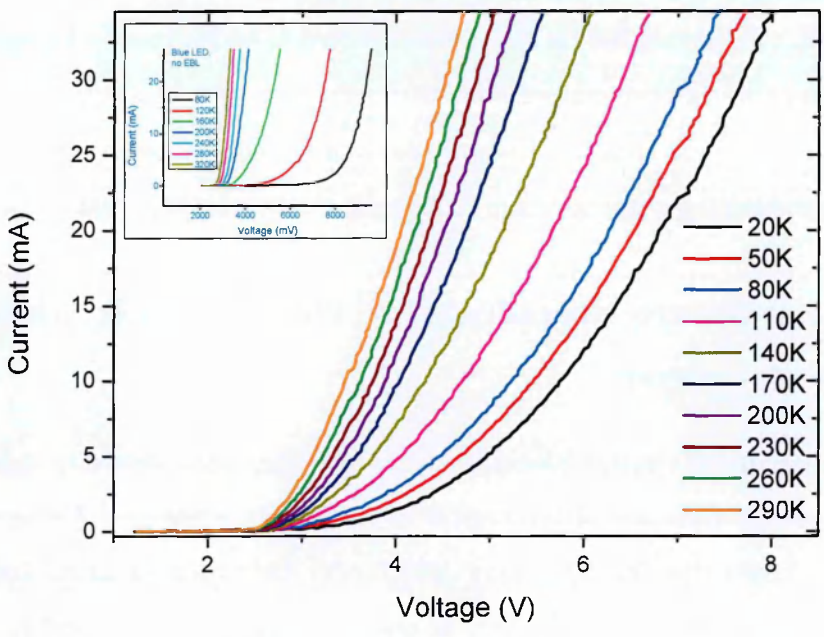

Figure 6-10- The current dependence on applied voltage for a blue LED which does not include an EBL in pulsed mode with a pulse width of 2μs and a frequency of 10kHz (inset- comparison of the dependence of current on voltage for a blue LED that includes an EBL).

The increase in the turn-on voltage with reducing temperature is expected to also occur in this device despite the fact that an EBL is not included. This is due to the low activation of the Mg-dopants at low temperatures and a poor distribution of the holes among the quantum wells as holes struggle to overcome potential barriers [52]. Figure 6-11 shows a comparison of the voltage at a fixed current for the blue LEDs with and without an EBL.

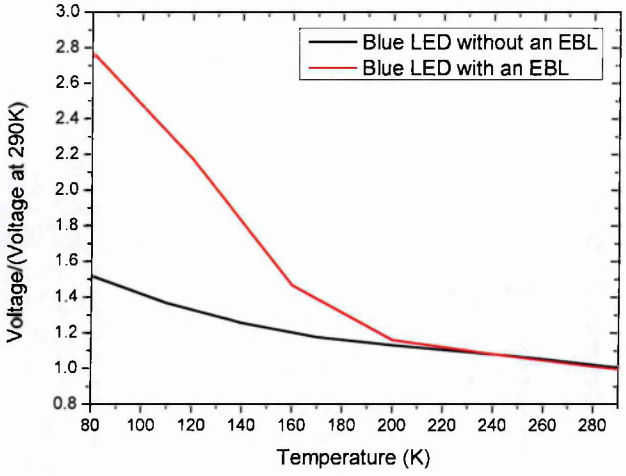

Figure 6-11- The voltage divided by the voltage value at 290K as a function of temperature for a blue LED without an EBL (black line) and a blue LED that includes an EBL (red line) that is taken at a fixed current of 10mA.

The LED which includes an EBL is observed to have a relatively voltage which is a factor of 2 higher for a fixed current of 10mA compared with that of the LED without an EBL at 80K. These results show the EBL has a strong impact on reducing the hole injection efficiency at low temperature.

The larger turn-on voltage in comparison with at room temperature for the blue LED without an EBL is expected to enhance the effective internal polarization field. Figure 6-12 show the temperature dependence of the efficiency droop for the blue LED without an EBL.

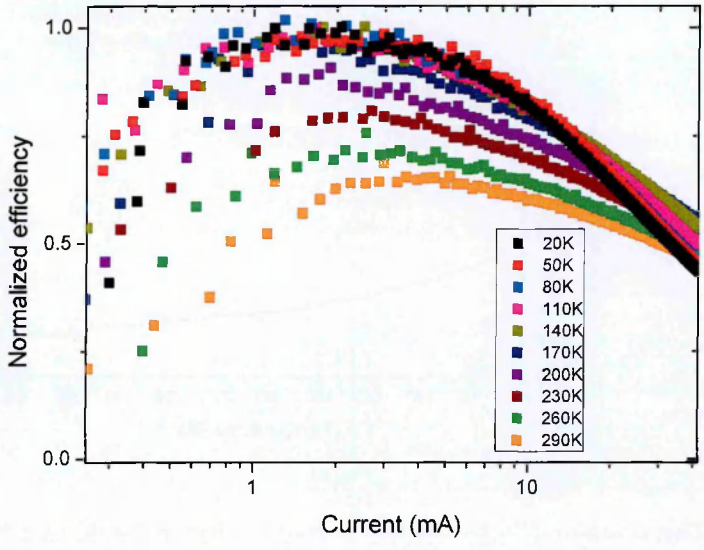

Figure 6-12- Electroluminescence efficiency normalized to the peak efficiency value at 20K as a function of current at different temperatures for a blue LED with no EBL in pulsed mode with a pulse width of 2μs and a frequency of 10kHz.

It can be seen that whilst the highest peak efficiency occurs at the lowest temperature, there is also a stronger efficiency droop effect. Figure 6-13 shows that the dependence of the peak efficiency on temperature.

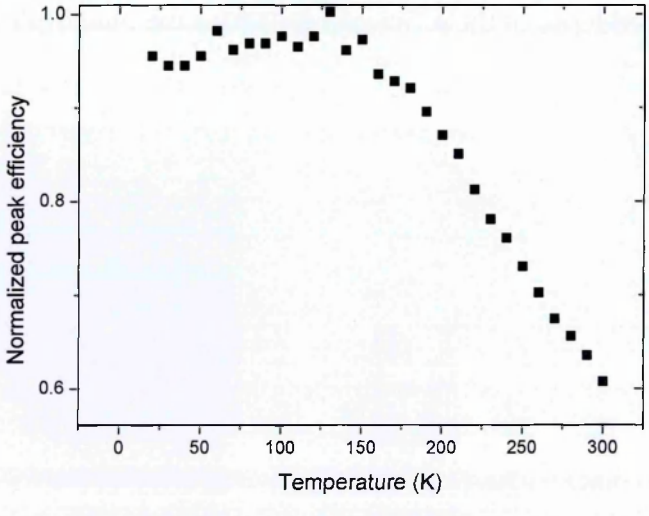

Figure 6-13- Peak electroluminescence efficiency values normalized to the peak efficiency value at 20K as a function of temperature in pulsed mode with a pulse width of 2μs and a frequency of 10kHz.

The peak efficiency is observed to be approximately constant for temperatures below 150K before showing a strong reduction with further increases of temperature. Interestingly, the efficiency at high injection currents is found to increase with increasing temperature from the lowest temperatures up to 150K but then reduce with further increases in temperature as shown in Figure 6-14.

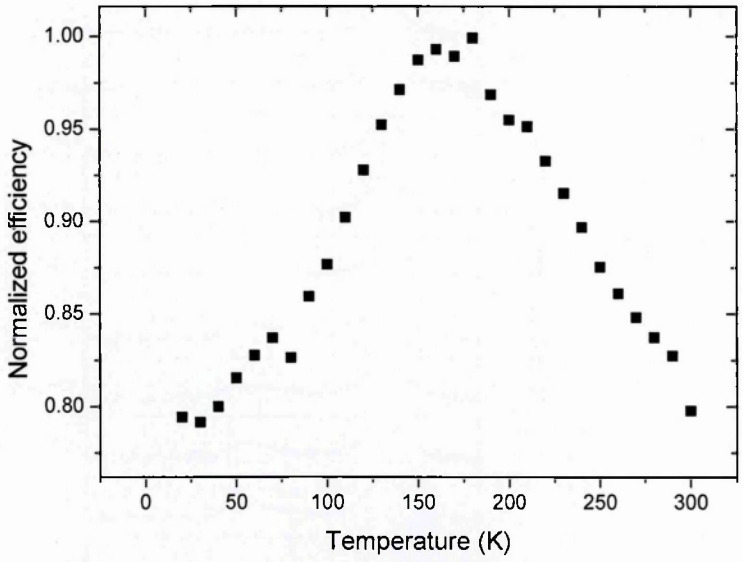

Figure 6-14- The efficiency normalized to the highest efficiency value (which occurs at 180K) as a function of temperature at 40mA in pulsed mode with a pulse width of 2μs and a frequency of 10kHz.

The reduction of efficiency with increasing temperature above 130K is likely to be due to an increasing proportion of active region band gap defect-related recombination in the low current regime. The insensitivity of the peak efficiency on temperature below 130K may be explained by the reduction of the active region bandgap defect-related recombination rate being countered by an increase in the carrier leakage rate that is caused by the poor hole injection with decreasing temperature. The stronger influence of carrier leakage at high currents is expected to be reason that there is a reducing efficiency with decreasing temperature below 150K as shown in Figure 6-14.

6.6 Evidence for carrier leakage

Evidence that a carrier leakage process takes place at low temperatures is found by the existence of a second emission peak in the spectra of the green LED at different temperatures shown in Figure 6-15.

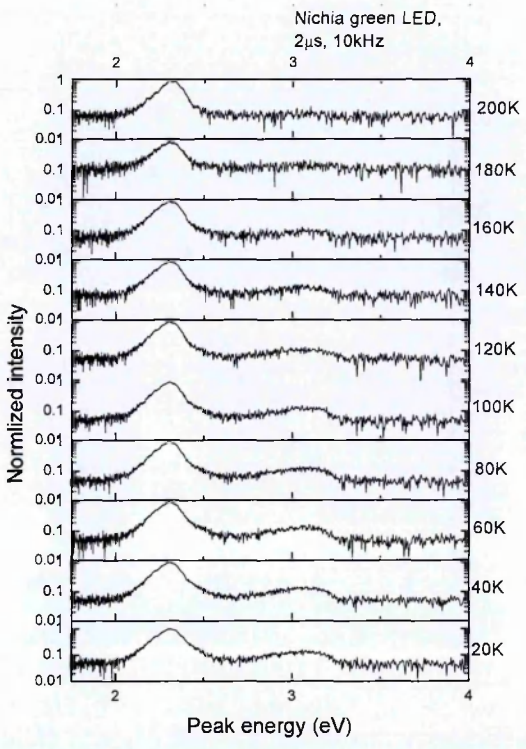

Figure 6-15- The electroluminescence emission spectra at a fixed current of 10mA at different temperatures for a green LED in pulsed mode with a pulse width of 2μs and a frequency of 10kHz.

The weak temperature dependence of the peak emission energy of the second peak suggests that the transition involves carrier recombination at a defect-level. This peak is found to occur at an energy of ~3.07eV. This energy corresponds to the energy difference between the conduction band and the Mg-dopant acceptor level within the p-GaN layer [100] as shown schematically in Figure 6-16.

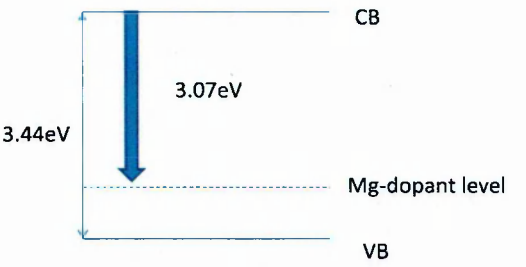

Figure 6-16- Schematic showing the transition between the conduction band to the Mg-acceptor level in GaN.

The weakening intensity of the second peak with increasing temperature may be explained by a reducing carrier leakage rate. The second peak did not appear at any temperature in the emission spectra of the blue LED as can be seen in Figure 6-15.

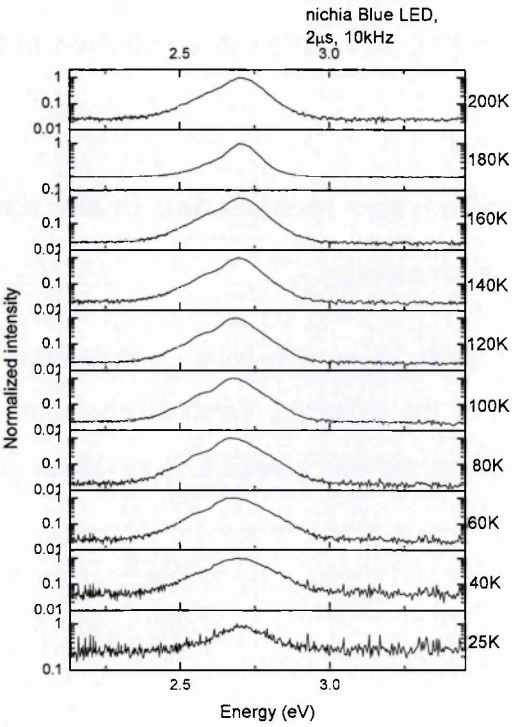

Figure 6-17- The electroluminescence emission spectra at a fixed current of 10mA at different temperatures for a blue LED in pulsed mode with a pulse width of 2μs and a frequency of 10kHz.

These observations suggest that there is a stronger carrier leakage rate in the green LED compared with the blue LED. This may be explained by the stronger internal polarization fields for the higher indium content green LED. These findings are in agreement with those of Shin *et al.* [101] where the second emission peak was also only observed at low temperatures

in the case of a green LED which was also attributed to recombination at the Mg-acceptor level.

6.7 Temperature dependence of Auger recombination

Auger recombination is unlikely to explain the temperature dependence of the LEDs. Whilst the Auger recombination rate has been shown to be reduced as temperature is reduced [44, 95], the analysis does not include the effect of a possible increase to the internal field strength. Whilst the increase in the carrier concentration (Section 5.8.2) with reducing recombination rates for stronger fields may cause an increase to the Auger recombination rate it is unlikely to cause the strong efficiency droop effect that occurs at low temperatures. This is due to the fact that there will also be a reduction in the Auger coefficient with reducing electron hole wavefunction overlap [92] in addition to a reduction in the Auger recombination rate with reducing temperature.

6.8 Evidence of carrier localization in the temperature dependence of the peak emission energy

It is observed that there is an "S-shape" dependence of the peak emission energy on temperature, instead of the expected Varshni behaviour, that provides evidence that carrier localization occurs in the blue and green LEDs as shown in Figure 6-18.

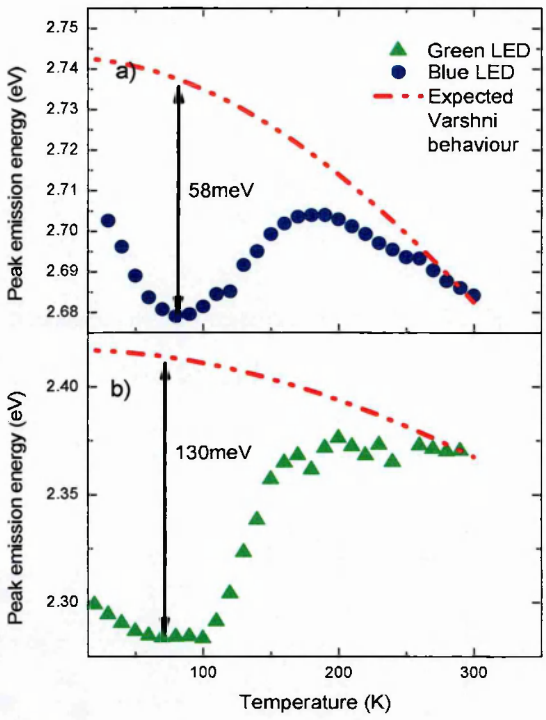

Figure 6-18-The electroluminescence peak energy emission as a function of temperature for a blue LED (a) and a green LED (b) with the expected Varshni behaviour of the LEDs where the bandgap at 0K is extrapolated to 2.74ev and 2.42eV, Varshni thermal coefficients for α =1 x 10^{-3}eVK^{-1} and 1.06 x 10^{-3}eVK^{-1}, and β =1196K and 1620K, for the blue and the green LED, respectively. The Varshni fitting coefficients for the blue LED were taken from *Shan et al.* [102] and extrapolated for the green LED. The measurements are taken in pulsed mode with a pulse width of 2μs and a frequency of 10kHz.

The "S-shape" dependence of the peak emission on temperature may be explained by the existence of potential minima that localize carriers as discussed further in Section 3.7. The reduction of the peak emission energy as temperature is increased from the lowest temperature to ~100K may be attributed to the redistribution of carriers from weakly localized states to relatively stronger localized states. At ~100K the strongly localized states are occupied and therefore the effect of increasing temperature up to ~190K will cause the carriers to fill higher energies within the localized states. A further increase of temperature above ~190K will result in a redshift of the peak emission energy due to the band gap shrinkage with increasing temperature that is commonly observed in most other semiconductor materials. The larger depth of the "s-shape" for the green LED (130meV) compared with the blue LED (58meV) may be attributed to stronger carrier localization effects which are caused by a larger indium content. Similar findings were also observed in Lee *et al.* [103] where the depth of the

"s-shape" was found to reduce at high currents which was attributed to reduced carrier localization with increasing injection. This observation shows the importance of carrier localization in InGaN-based materials and suggests that an efficiency droop model which involves an increase in defect-related recombination with increasing current may take place due to reduced carrier localization and subsequent recombination at defect sites at higher energies (see section 5.10).

Further evidence of carrier localization is seen by the increase of the FWHM as temperature is reduced below ~100K for both LEDs (see Figure 6-19).

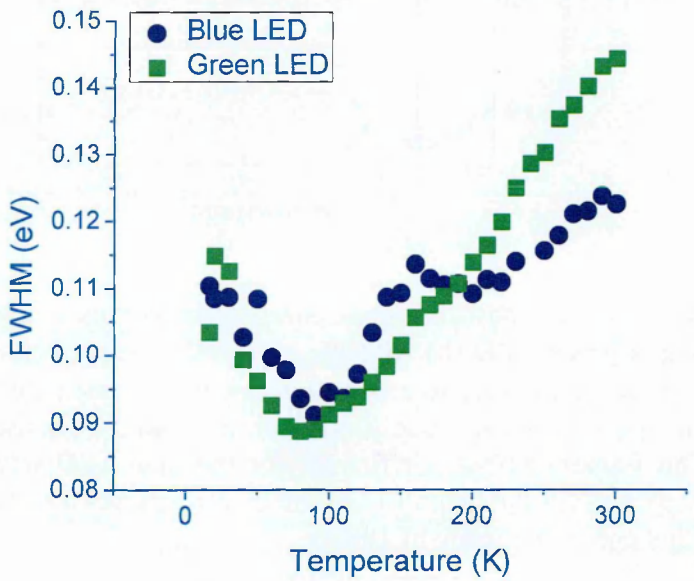

Figure 6-19-The electroluminescence FWHM (full-width half maximum) for the blue (blue circles) and green (green squares) LEDs in pulsed mode with a pulse width of 2μs and a frequency of 10kHz as a function of temperature

The increased FWHM with reducing temperature below 100K may be attributed to carriers being confined in weakly localized energy states that result in a larger spread of photon energies at low temperatures. There will be a reduction of the FWHM as carriers are redistributed into stronger localized states with increasing temperature up to 100K. The increase in FWHM with increasing temperature above 100K is due to the thermal broadening of the carrier distribution which results in carriers reaching higher energy states.

6.9 Efficiency droop above room temperature

The reduction of carrier localization with increasing temperature is expected to cause an increase in defect-related recombination in InGaN-based devices. The light output power reduces with increasing temperature at temperatures where hole injection is not problematic as was shown in Figure 6-2. Figure 6-20 shows that the efficiency over the entire current range reduces with increasing temperature above room temperature for both blue and green LEDs.

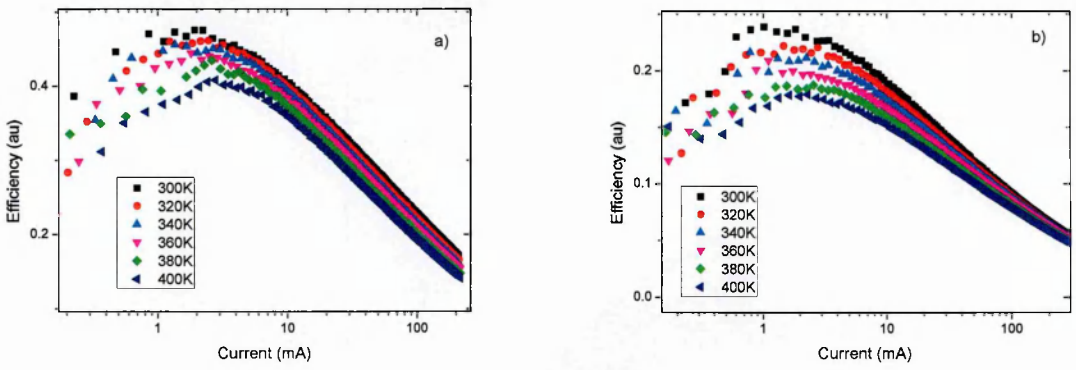

Figure 6-20- The electroluminescence efficiency dependence on current at different temperatures for a) a blue LED and b) a green LED in pulsed mode with a pulse width of 2μs and a frequency of 10kHz above room temperature

Interestingly, the efficiency droop effect is found to reduce with increasing temperature above room temperature. The stronger reduction of the peak efficiency compared with the reduction of efficiency at high currents can be attributed to the active region bandgap defect-related recombination having a larger influence at low injection currents [30]. The reduced droop effect with increasing temperature is unlikely to be caused by carrier leakage or Auger recombination as both of these processes have been shown to become increasingly problematic at high temperatures [44, 95-97] as described earlier.

6.10 Modelling of the temperature dependence of the efficiency droop

Figure 6-21 shows that the efficiency dependence on current density above room temperature may be fitted using the model whereby the cause of efficiency droop is due to a defect-related process as described in Section 5.10.

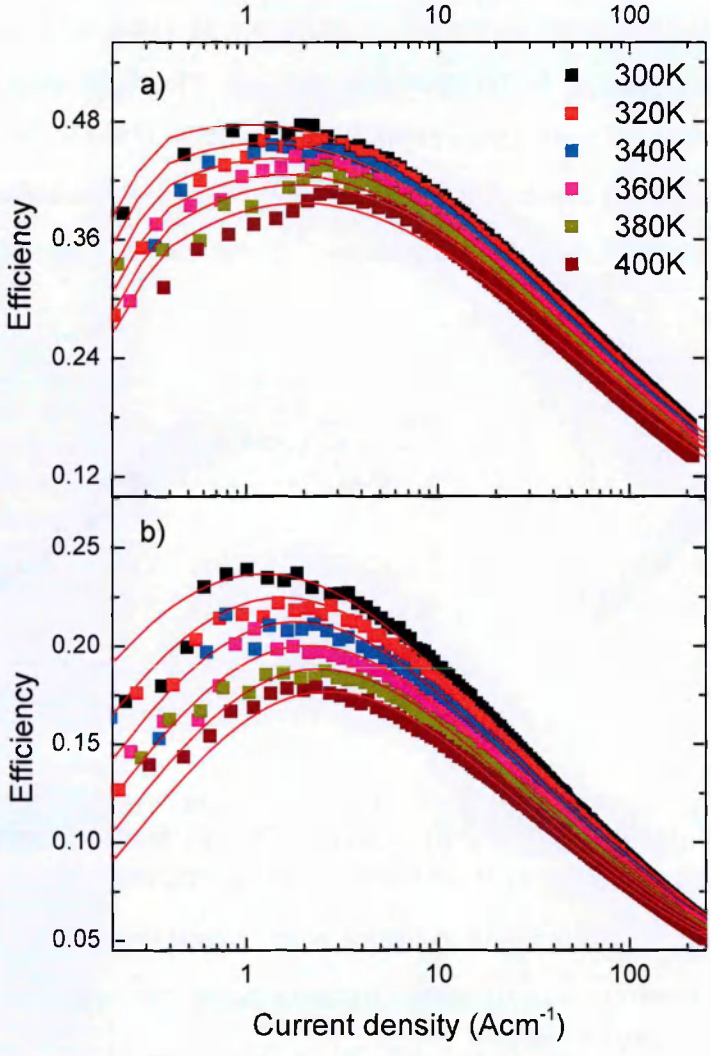

Figure 6-21- The efficiency dependence on current at different temperatures for a blue LED (upper graph) and a green LED (lower graph) which have been fitted using a defect-related model as the cause of efficiency droop where A $\propto T$, B $\propto T^{-\frac{7}{4}}$, D$\propto \exp(\frac{E_A}{k_B T})$.

A scaling factor has been included with the experimental data in order to account for the system efficiency. A good agreement between the model and the experimental data is found. The model uses an A_0 coefficient which has a linear dependence on temperature as shown in Figure 6-22.

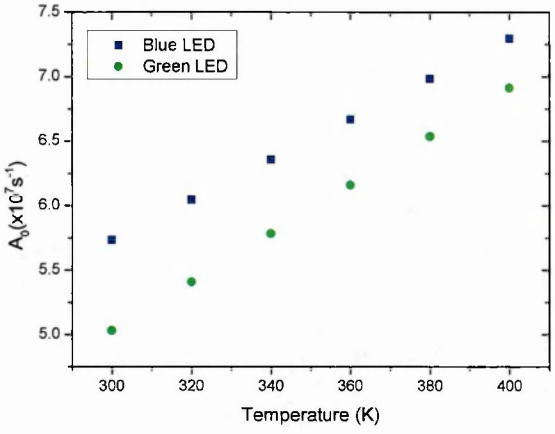

Figure 6-22- The modelled temperature dependence of the A_0 parameter for the blue LED (blue squares) and the green LED (green circles) where a linear relationship is used.

The increase of the A_0 coefficient as temperature is due to carriers obtaining higher energy and therefore being more likely to recombine with defect sites within the bandgap and at high energy. The carrier concentration required to fill the potential minima, n_p, is assumed to be temperature insensitive as the thermal broadening of the carrier distribution will be countered by the reduction of the occupational probabilities of low energy states with increasing temperature [44]. Temperature insensitive values of $n_p = 8x10^{17}cm^{-3}$ and $n_p=6x10^{17}cm^{-3}$ for the blue and green LED, respectively, are therefore assumed.

The rate at which there is an increase in the monomolecular recombination coefficient as there is an increase of the carrier concentration at high injection, D, has a $\exp(E_a/k_BT)$ with values activation energies of 38meV and 95meV for the blue and the green LED as shown in Figure 6-23.

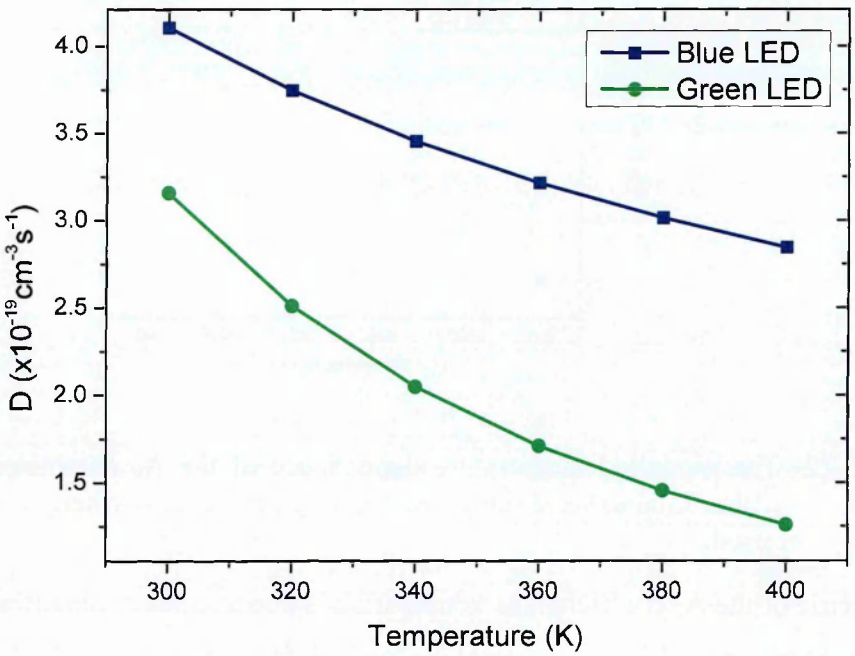

Figure 6-23- The modelled temperature dependence of the D parameter for the blue LED (blue square) and the green LED (green circles) where an $\propto \exp(\frac{E_A}{k_B T})$ is used.

The temperature dependence of D may be explained by the strong reduction in the influence of the potential minima with increasing temperature in an effect which is larger for the green LED. This is due to larger carrier localization and a higher defect density.

The model uses the $T^{-7/4}$ dependence for B_0 that was determined by Hader *et al.* [44] as shown in Figure 6-24. Hader *et al.* obtained this temperature dependence by fitting experimental data and therefore the physical cause of such dependence is unknown. The dependence of the radiative recombination coefficient with temperature is complex and will be influenced by the reducing bandgap and an increasing radiative lifetime due to the thermal broadening of the carrier distribution causing a lower proportion of carriers recombining at zero momentum with increasing temperature.

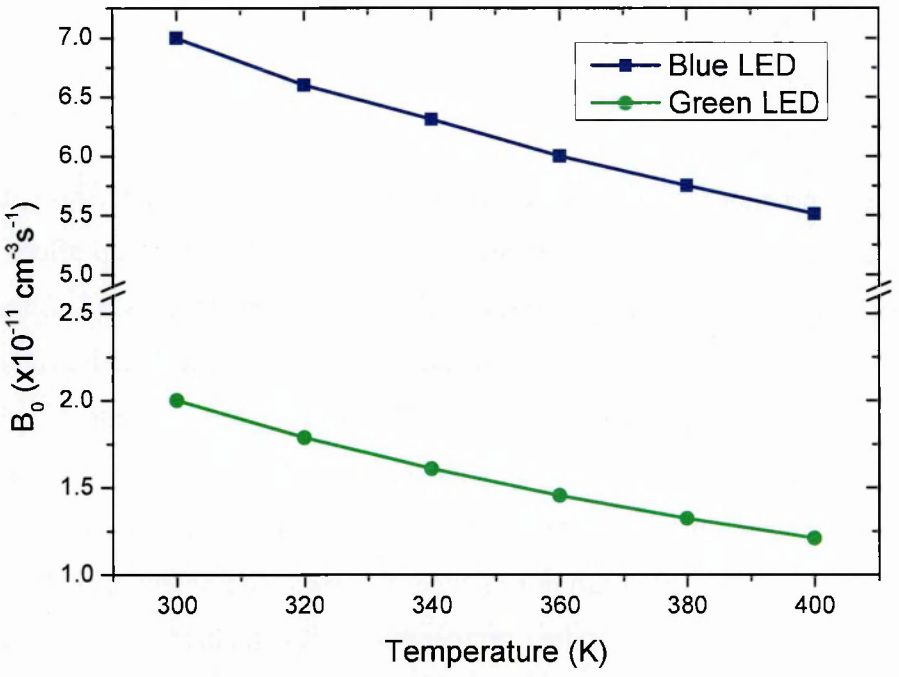

Figure 6-24- The modelled temperature dependence of the B_0 parameter for the blue LED (blue squares) and the green LED (green circles) where a $\propto T^{-\frac{7}{4}}$.

The higher B_0 value for the blue LED is due to a reduced internal field strength [26] and an enhancement to the radiative rate due to the larger bandgap [33] in comparison with the green LED. The parameters A_0, B_0, and n_0 were obtain from the literature values and the n_p and D values were determined by fitting the data.

The strong temperature dependence of the peak efficiency compared to the efficiency at high currents is expected to be due to the stronger influence of carrier localization at low injection levels. In contrast, at high injection levels there is a relatively low influence of the carrier localization due to carriers filling the potential minima resulting in a similar proportion of defect-related recombination at all temperatures.

6.11 Chapter summary

The aim of this chapter was to determine the recombination processes which dominate the emission of blue-green InGaN-based LEDs. The use of temperature-dependent studies is a valuable technique to identify the dominant loss mechanism due to loss processes having different temperature dependencies. The findings of this study show that there is poor performance of the LEDs at low temperatures. The efficiency droop effect was also observed to be more severe at low temperatures. This indicates that there is a loss mechanism which is stronger at low temperatures. Poor injection of holes into the active region is expected to increase the rate of the dominant loss mechanism. Evidence of poor injection is found in the form of a higher required voltage to obtain a fixed current with reducing temperature. The rate at which there is an increase in the applied voltage with decreasing temperature is found to be reduced for a device which did not include an EBL. This observation indicates that the EBL hinders hole transportation at low temperatures. The highest peak efficiency was found to occur at the lowest temperatures in this device. This is expected to be due to reduced active region bandgap defect-related recombination with decreasing temperature. Interestingly, the efficiency at high current injection was found to increase with increasing temperature up to 160K before reducing with further increases of temperature. The behaviour suggests that hole injection issues are present even in devices without an EBL. Such findings show that poor hole mobility and weak activation of Mg-dopants cause poor hole distribution and an enhanced carrier leakage rate at low temperatures. The poor injection of holes was shown to cause an increase to the effective internal polarization field strength. A stronger blueshift for a given current range below where the peak efficiency occurs at low temperatures provides evidence of a stronger internal field strength.

Evidence that a leakage process occurs at low temperatures is observed in the form of an additional emission peak, which has an energy that corresponds to the energy difference between the conduction band and the Mg-dopant level in the p-GaN layer, in the spectra of the green LED at low temperatures. Interestingly, this peak did not feature in the spectra of the blue LEDs. Such observations suggest that carrier leakage is stronger in the green LEDs due to the stronger internal field strength.

Another loss process which has previously been shown to have a strong influence on the output power of InGaN-based devices is defect-related recombination at sites within the band

gap. It is shown that there is a reduction of this loss mechanism with reducing temperature as the light output dependence on increasing current becomes increasingly sublinear. The increasing influence of bandgap defect-related recombination is expected to result in the reduction of the peak efficiency with increasing temperature above 120K and 160K for the blue and green LEDs, respectively. The high proportion of bandgap defect-related recombination is likely to result from the high threading dislocation density in InGaN-based LEDs. An "s-shape" dependence of the emission peak on temperature is observed for both blue and green LEDs suggesting that carrier localization takes place. The larger depth of the "s-shape" in the case of the green LED indicates that the random indium fluctuations are expected to be larger in devices of higher indium content. Additionally, an increase in the FWHM with reducing temperature below 100K is observed which is also expected to be the result of carriers occupying weakly localized states with a range of energies. The reduced effect of carrier localization at high temperature will lead to an increased proportion of defect-related recombination that will reduce the efficiency with increasing temperature.

Such findings support the idea that there is a reduction of carrier localization with increasing current resulting in an increase in the defect-related recombination rate. It is shown that the efficiency droop effect at different temperatures may be modelled using a defect-related recombination process as the cause of efficiency droop for temperatures where hole injection efficiency is not expected to be problematic. The results indicate that the luminescence of InGaN-based LEDs above room temperature is strongly influenced by defect-related recombination and therefore efforts should be made to reduce both the defect density and develop an in-depth understanding of the defects involved.

7 Pressure Dependence of InGaN

7.1 Chapter Aim:

This chapter focuses on the technique of applying high hydrostatic pressure to semiconductor materials that have revealed important properties of nitride-based materials as well as those in other material systems. High pressure is a valuable technique to investigate and understand the impact of properties which have dependencies on the bandgap. In this study, the pressure coefficient of blue-green LEDs, which represents the rate at which the bandgap changes with increasing pressure, is investigated. It is shown that the pressure coefficients of blue-green InGaN-based devices are much weaker that those which have previously been determined for GaN and InN binary materials. The results also show that the pressure coefficient increases as a function of injection current. The different mechanisms that influence the peak emission energy and their expected dependencies on current are described in this chapter in order to determine the cause of the increasing pressure coefficient with increasing current. The results are consistent with an increasing piezoelectric field strength with increasing pressure. Such fields become screened at high injection currents causing the pressure coefficient to increase from 2.14±0.06me/kbar at 5mA to 2.32±0.01meV/kbar at 300mA for the blue LED and from 1.20±0.06meV/kbar at 5mA to 1.49±0.03meV/kbar at 300mA for the green LED.

The increase of the piezoelectric field strength with increasing pressure is the result of a changing internal strain that is caused by the different compressibilities of the InGaN quantum well and the GaN barrier. Such changes in strain are expected to increase the piezoelectric constants resulting in larger polarization field strengths of the wells and barriers. The difference in the rate at which the polarization strength increases with applied pressure between the wells and barriers is found to be the reason why there is an increasing field strength. Calculations indicate that the field increases from 2.47MVcm^{-1} to 2.56MVcm^{-1} and 4.54MVcm^{-1} to 4.70MVcm^{-1} for the blue and green LEDs, respectively.

The final section of this chapter describes the influence of indium inhomogeneities on the pressure coefficient in InGaN-based structures. It is shown that indium inhomogeneities will cause a reduction in the pressure coefficient at a similar rate to that at which is due to the increased piezoelectric field. The reduction in pressure coefficient is expected to be the result

of an increasing energy at the top of the valence band which counters the increasing band gap energy with increasing pressure.

7.2 The influence of pressure on III-N semiconductors

Pressure has proved to be a valuable tool in determining the fundamental properties of a number of semiconductors. Extensive studies of semiconductor materials have revealed important electro-optical properties which have led to the optimization of device performance. Pressure may also be applied to lasers to provide tunability of wavelength which has a number of potential applications.

The change in the emission energy of the semiconductor material is the result of a reduced lattice constant with increasing pressure. This causes the conduction band minima to shift upwards causing an increase to the energy difference between conduction band minimum and the valence band maximum as illustrated in Figure 7-1.

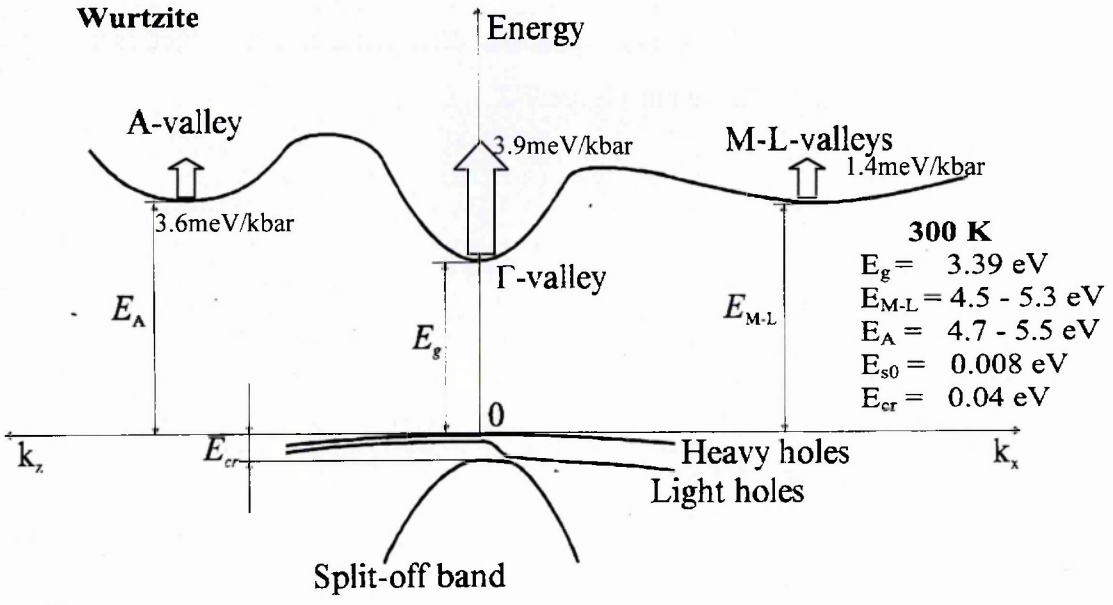

Figure 7-1- The band structure diagram showing the pressure coefficients of the of the Γ, A, M and L conduction band minima in GaN taken from [46].

Figure 7-1 shows that the conduction band of wurtzite GaN has different minima which include the Γ, A, M and L valleys. Direct recombination is expected to occur between electrons from the Γ conduction band minimum with holes from the valence band maximum as described in further detail in Section 3.4.4. This is due to the large energy difference between the A (1.3eV), M and L (both 0.9eV) conduction band minima with the Γ conduction

band minimum which makes electron occupation of the Γ conduction band minimum more energetically favourable. Despite the Γ conduction band minimum having a stronger dependence on pressure (3.9meV/kbar) than the A (3.6meV/kbar), M and L (both 1.4meV/kbar) conduction band minima [104], the pressure range used in this study (10kbar) is too small to cause the Γ conduction band minima to move above the other indirect valleys.

7.3 Pressure coefficients

The pressure coefficient, which represents the rate at which the peak emission energy increases as a function of pressure at a fixed current, provides important information about different materials. Previous studies have shown that GaN, InN and InGaN materials have lower pressure coefficients than those of most other III-V material systems. One of the reasons for this observation is due to the small compressibility of nitride-based materials. For example, the bulk modulus, which is inversely proportional to the compressibility, for GaN (210GPa) [105] and InN (140GPa) [106] is larger than that of GaAs (78.4GPa) [107].

An example of the emission energy spectra at different pressures which is used to calculate the pressure coefficient is showed in Figure 7-2.

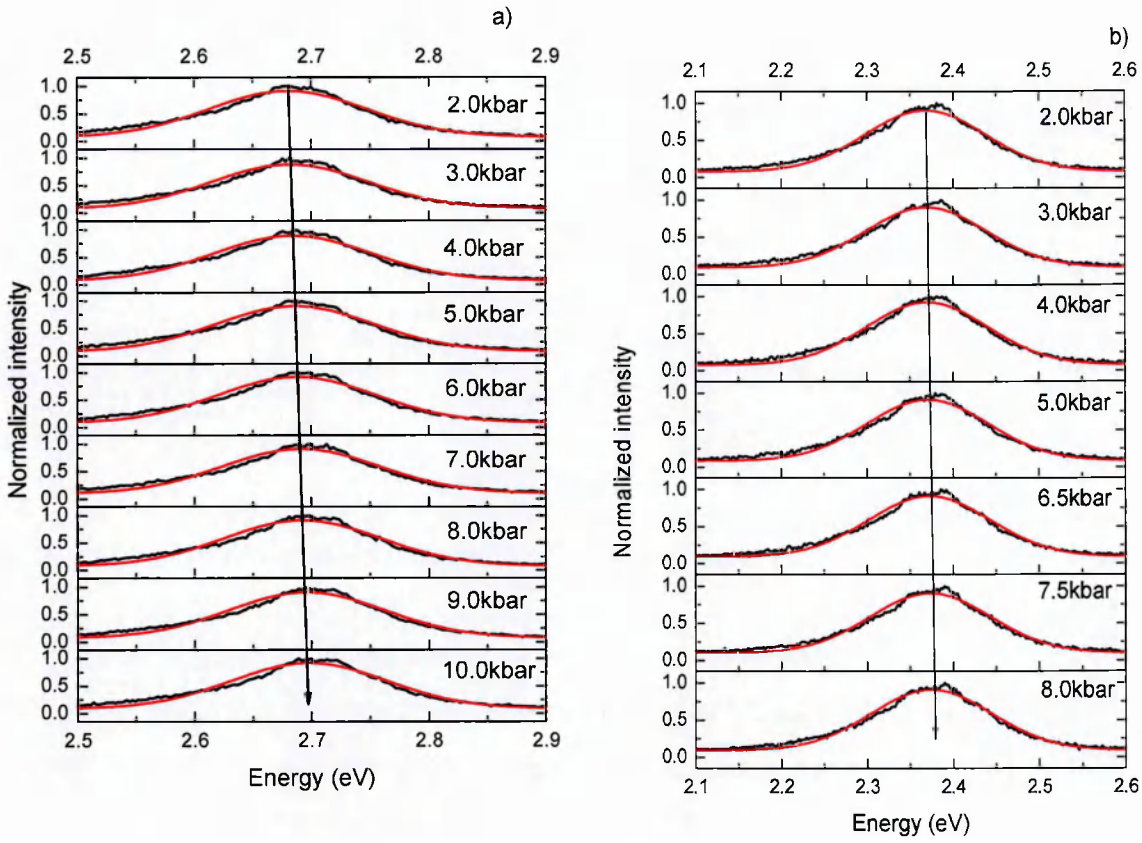

Figure 7-2- The electroluminescence emission spectra for a fixed current of 5mA at different pressure for (a) a blue LED and (b) a green LED in pulsed mode with a pulse width of 2μs and a frequency of 10kHz with a Gaussian fit used to determine the peak energy value

A Gaussian fit was applied to the data to determine the peak photon emission energy at different pressures for a fixed current. The determination of the pressure coefficients of this study rely on measuring the electroluminescence peak emission. The carrier distribution will therefore have an influence on the pressure coefficient causing the dE_{peak}/dP value to be different from the dE_g/dP value as will be discussed. The peak electroluminescence energy is used to calculate the pressure coefficients of the blue and green LEDs as shown in Figure 7-3.

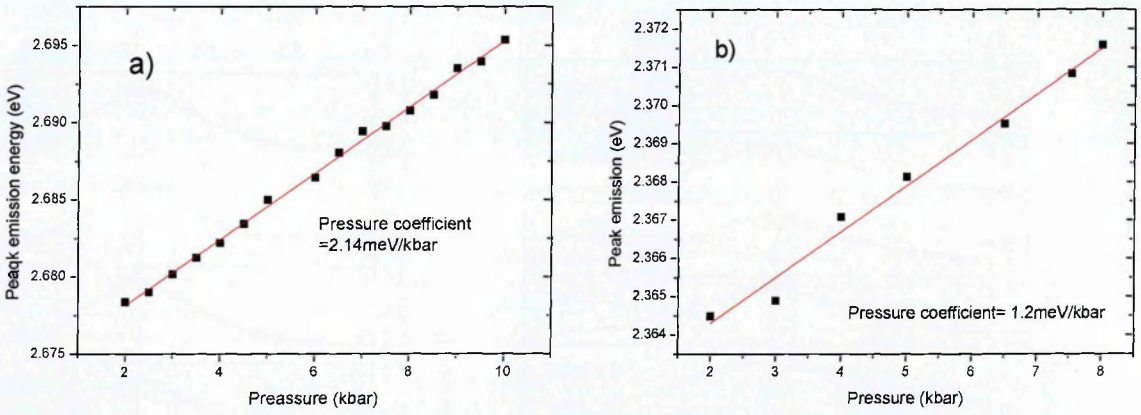

Figure 7-3- The electroluminescence peak emission energy as a function of pressure for a) a blue LED and b) a green LED in pulsed mode with a pulse width of 2μs and a frequency of 10kHz at a current of 5mA

The pressure coefficient of the blue and green InGaN LEDs are found to be smaller than those of the binary GaN (3.9meV/kbar) and InN (2.7meV/kbar) structures [108, 109]. This indicates that there are mechanisms taking place that cause a reduction of the peak emission energy dependence on pressure in InGaN quantum well devices. The following sections will describe different effects on InGaN as pressure is applied.

7.4 Pressure induced strain

Nitride based materials have strong internal polarization fields [61] which are the result of strain and the relatively high piezoelectric constants compared with other material systems as previously discussed in section 3.6. For example, the piezoelectric constants are e_{33}= 0.73Cm^{-2} and e_{31}=-0.49Cm^{-2} for GaN, compared with e_{33}= -0.12Cm^{-2} and e_{31}=0.06Cm^{-2} for GaAs. The induced strain due to the application of pressure is expected to oppose the biaxial compressive strain [110-112]. This is because the reduction of the lattice constant in the GaN barrier occurs at a weaker rate than that of the InGaN well. The reduced strain as a function of pressure is assumed to be mainly caused by changes between the InGaN quantum well and the GaN barrier rather than being influenced by the sapphire substrate. This is due to GaN on sapphire epilayers having previously been shown to have similar behaviour as a function of pressure with that of bulk GaN [108, 113].

In order to calculate the pressure induced strain the relationship of the changing lattice constant as a function of pressure [111], a(P), is used,

$$a(P) = a_0(1 - \left(\frac{P}{Bulk}\right)) \qquad 7\text{-}1$$

where a_0 is the lattice is the strain at zero pressure, P is pressure (in GPa) and Bulk is the bulk modulus.

The changing lattice constants are then used in the strain equation, equation 7-2, to determine the relative change in the amount of strain as a function of pressure.

$$strain(P) = \frac{a_{InGaN}(P) - a_{GaN}(P)}{a_{GaN}(P)} \qquad 7\text{-}2$$

where a_{InGaN} is the lattice constant of InGaN and a_{GaN} is the lattice constant of GaN.

Figure 7-4 shows the relative change in strain compared with the strain at ambient pressure as a function of hydrostatic pressure for the blue and green LEDs.

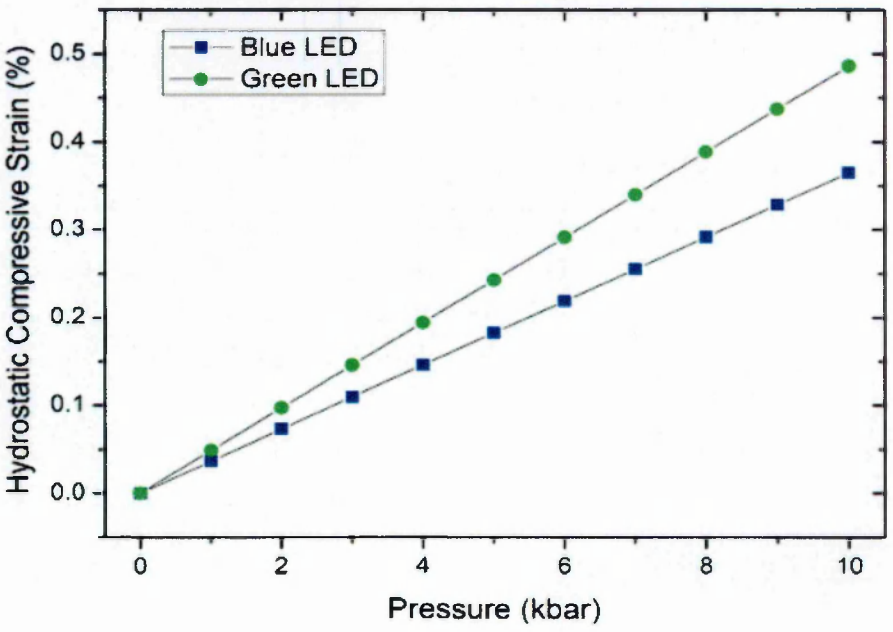

Figure 7-4- The calculated percentage change in the hydrostatic compressive strain as a function of pressure for a green and blue LED

The change in the strain will have an impact on the piezoelectric polarization of the barriers and wells and will cause an increase to the internal field strength as described in more detail in the next section.

7.5 Piezoelectric fields as a function of pressure

One would intuitively expect that the polarization, which is calculated by Equation 7-2, will reduce as a function of pressure due to a reduction in the biaxial strain of the quantum well.

$$P_{PZ} = 2strain_{zz}e_{33} - strain_{xx}e_{31} \qquad 7\text{-}3$$

where $strain_{zz}$ is the total strain in the growth direction, $strain_{xx}$ is the total in-plane strain and e_{33} and e_{31} are the piezoelectric constants.

However, calculations in Shimada *et al.* [114] show that the piezoelectric constants will increase as the internal strain is reduced for GaN as shown in Figure 7-5.

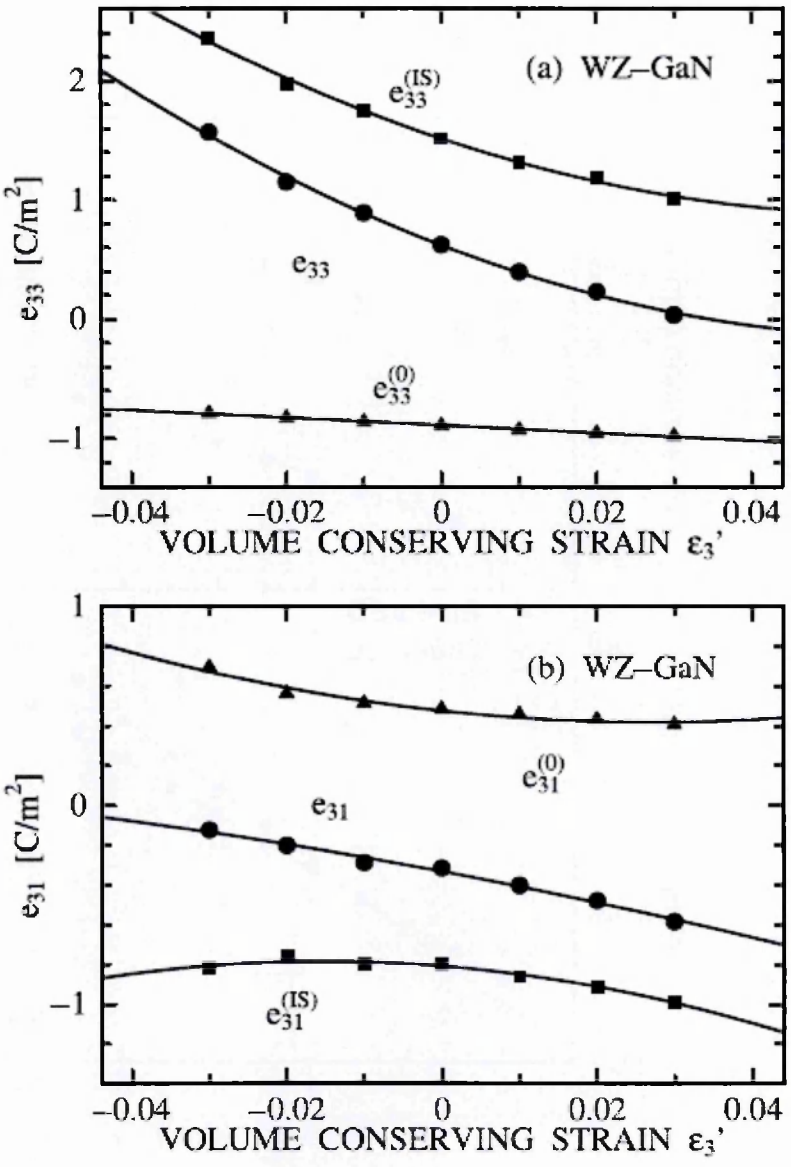

Figure 7-5- The dependence of the piezoelectric constants, e_{33} (upper graph) and e_{31} (lower graph) on the volume conserving strain for GaN {taken from [114]}.

The changes of the polarization in the barrier and well due to the reduction of strain and the subsequent increase of piezoelectric constants can therefore be calculated as shown in Figure 7-6 for a blue LED and a green LED.

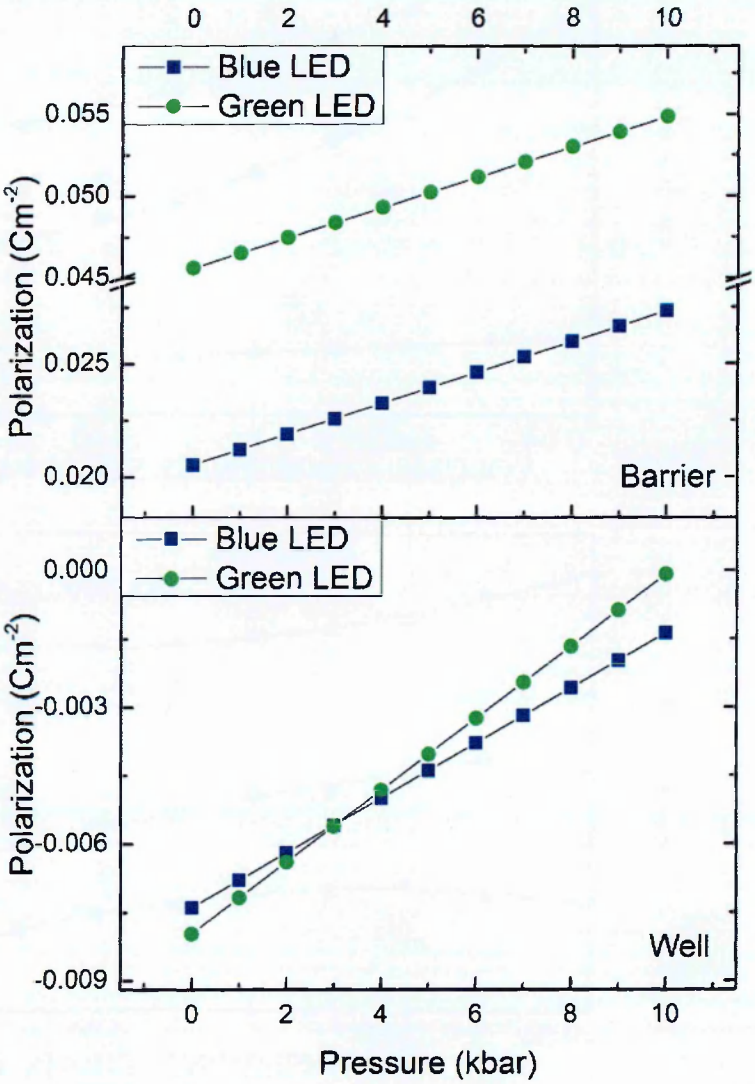

Figure 7-6- The calculated change in the polarization strength in the barrier (upper graph) and well (lower graph) for the blue LED (blue squares) and green LED (green circles)

The polarization strengths are calculated by using non-linear piezoelectric coefficients from Pal *et al.* [115]. The changing polarization of the barrier and well can be used to calculated the internal field strength as a function of pressure by using the relationship,

$$F_{PZ} = \frac{L_b(P_b - P_w)}{L_b\varepsilon_w - L_w\varepsilon_b} \qquad 7\text{-}4$$

where $L_{b,w}$ is the width of the barrier and well, respectively. $P_{b,w}$ is the polarization of the barrier and well, respectively and $\varepsilon_{b,w}$ is the dielectric constant of the barrier and well, respectively.

As determined by the TEM images in Chapter 4, L_b is 13nm and 16nm for the blue and green LEDs, respectively, and L_w is 3nm in both LEDs. The dielectric constants were considered to be 10, 10.5 and 11.4 for the GaN barrier, blue quantum well and green quantum well, respectively where the values for the blue and green LEDs were obtained from a linear interpolation [115] as shown in Figure 7-7.

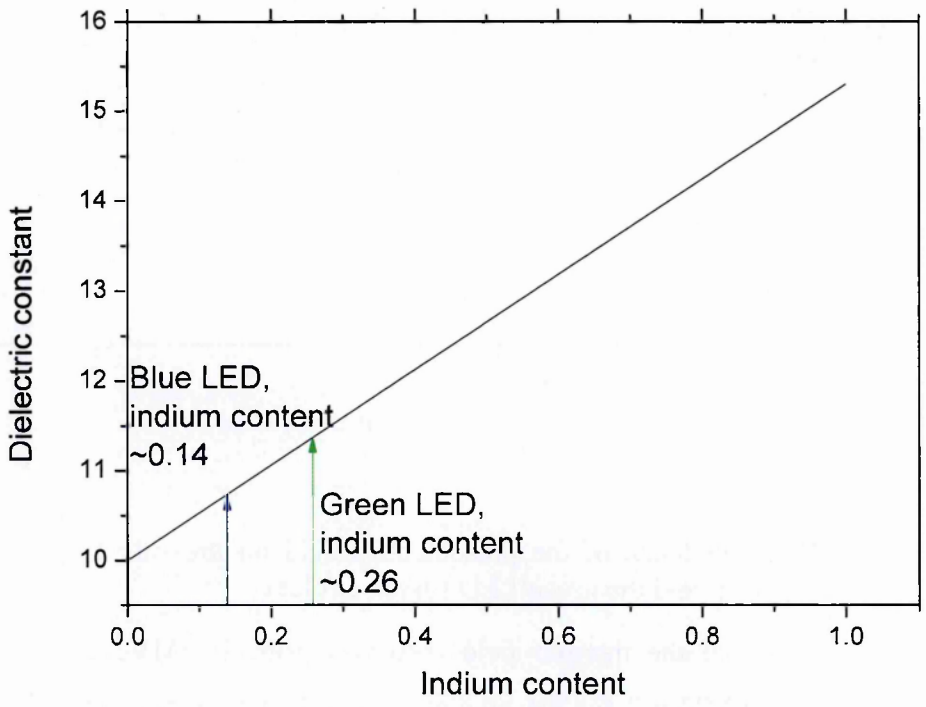

Figure 7-7- The dielectric constant as a function of indium content where Vergard's law has been assumed with the dielectric constants of GaN and InN taken to be 10 and 15.4 that were obtained from ref. [115]

The increase of the electric field as a function of pressure can then be calculated as shown in Figure 7-8.

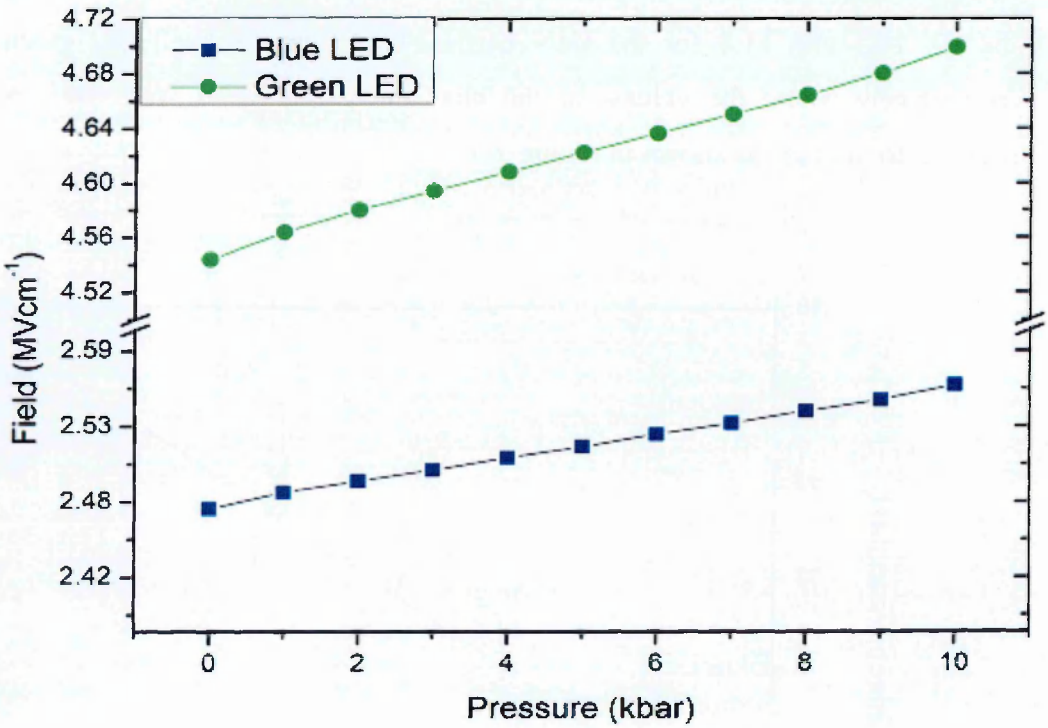

Figure 7-8- The dependence of the piezoelectric field on pressure for the blue LED (blue squares) and the green LED (green circles).

Figure 7-8 shows that the internal field increases from 2.47MVcm^{-1} to 2.56MVcm^{-1} and 4.54MVcm^{-1} to 4.70MVcm^{-1} for the blue and green LEDs, respectively. These results show that the rate at which the internal field strength increases as a function of pressure is similar for both the blue and green LED at approximately 4% over a pressure range of 10kbar.

7.6 Effect of the increasing piezoelectric field strength on the pressure coefficient in InGaN quantum well devices

The increase of the internal polarization field strength will cause strong band-bending of the quantum well as pressure is applied. Subsequently, there will be an increase of the quantum confined Stark effect causing the peak emission energy to red-shift. The calculated increase in the internal field strength as a function of pressure that was determined in the previous section is used in the nextnano software to determine the effects of the increasing piezoelectric field strength on the pressure coefficient. The simulation which uses k.p theory to calculate a

redshift of the peak emission energy with increasing piezoelectric field strength for a blue LED as shown in Figure 7-9.

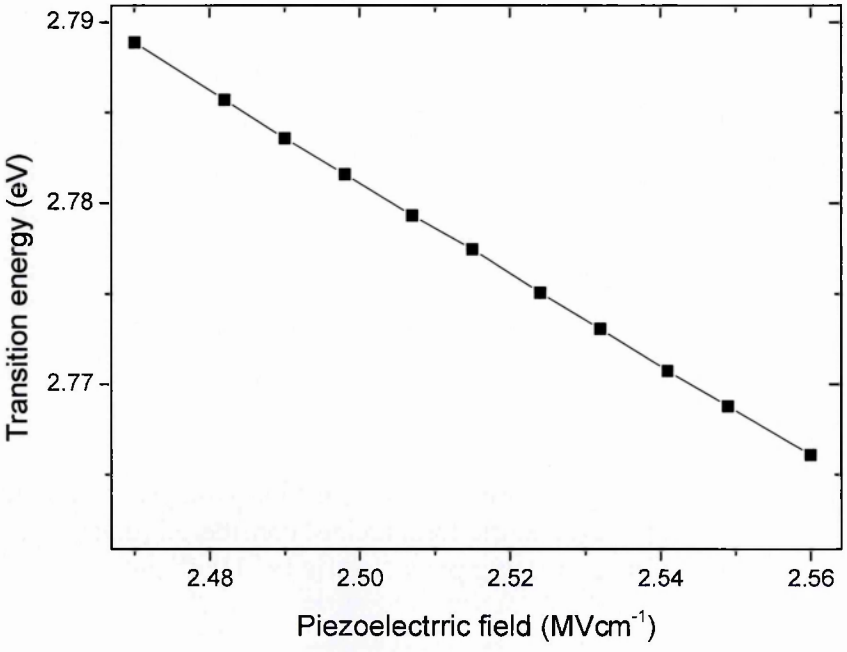

Figure 7-9- The calculated peak emission dependence on piezoelectric field strength for a blue LED with an indium content of 0.16.

The redshift of the peak emission due to the increasing piezoelectric field as pressure is applied will counter the blueshift of the peak emission energy that results from the upwards movement of the conduction band with increasing pressure (see Section 7.2). Figure 7-8 compares these two effects with increasing pressure where it is assumed that the pressure coefficient of InGaN in the absence of piezoelectric fields will be 3.75mev/kbar taken from a linear interpolation of the pressure coefficient between GaN and InN.

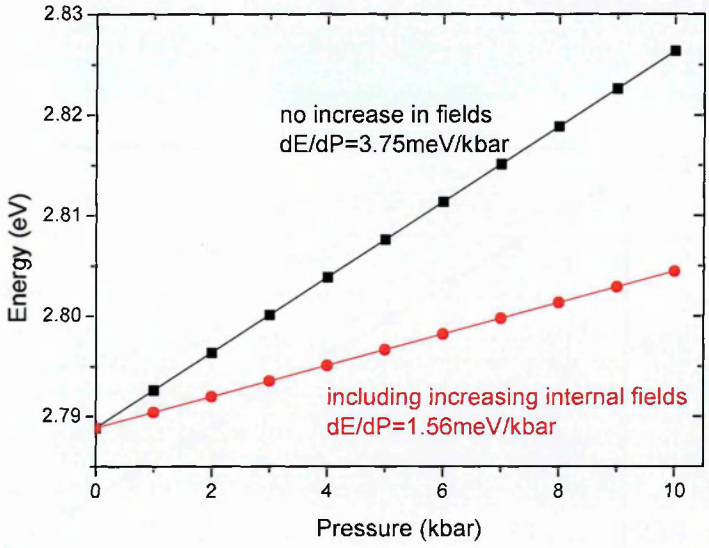

Figure 7-10- The calculated transition energy dependence on pressure if the effects of an increasing piezoelectric field are not considered (black line) and including the effects of an increasing piezoelectric field with pressure (red line) for a blue LED.

The calculations show that the increasing internal polarization field strength with increasing pressure will cause a reduction of the transition energy at a rate of -2.19meV/kbar. The calculations show that this effect will reduce the InGaN pressure coefficient for a blue LED with an indium content of 0.16 from 3.75meV/kbar (in the absence of internal fields) to 1.56meV/kbar. The experimentally determined pressure coefficient of 2.14meV/kbar for a blue LED as shown in Figure 7-3 is within experimental error of this calculated value. The larger pressure coefficient in the measurements is expected to be due to carrier screening of the internal field, as discussed further in the next section of this chapter, which are not considered in the calculations.

7.7 Emission dependence on current at different pressures

It is important to consider how the peak emission energy will be influenced by different mechanisms with increasing current when calculating the pressure coefficient as a function of currents. Joule heating will be an effect which increases the temperature of the device due to the conduction taking place in a resistive material as previously described in Section 4. The Joule heating effect will cause the emission peak to show a redshift with increasing current due to the reducing bandgap with increasing temperature (see section 6.8). It is important to

reiterate here that the emission peak in the measurements of this study is not expected to be significantly influenced by Joule heating as pulsed current is applied (see section 4.4).

Band filling effects are expected to result in a blueshift of the emission peak with increasing current. This is due to carriers occupying higher energy states with increasing current due to the filling of lower energy states filled. The existence of potential minima is expected to enhance the band filling effect [94]. The carrier screening of the internal polarization fields will also result in the blueshift of the emission peak and is expected to be the dominant cause of the strong blue shift observed in InGaN-based LEDs as shown for a blue LED in Figure 7-11.

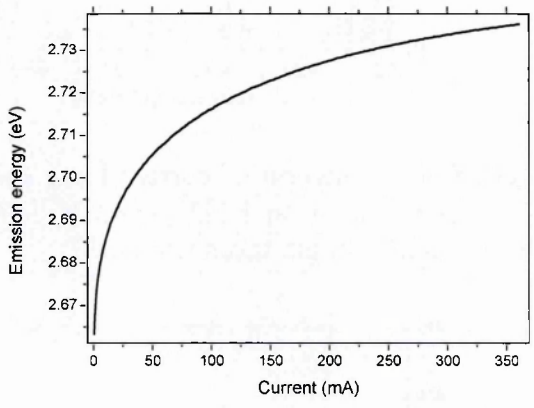

Figure 7-11-The electroluminescence emission peak energy as a function of current for a blue LED in pulsed mode with a pulse width of 2μs and a frequency of 10kHz at room temperature and ambient pressure.

The existence of internal polarization fields is expected to provide a larger contribution to the blueshift with increasing current compared with the contribution from band filling effects. Figure 7-12 provides evidence of this as a device with AlGaInN barriers (consisting of a reduced polarization field strength) has a weaker blueshift. Figure 7-13 shows that there is a red-shift of the emission energy for a device grown along the m-plane that is expected to be caused by heating effects. Section 5.6 also shows that for a yellow AlGaInP LED there is not a significant effect on the shift in peak emission due to band filling effects for a device which does not have a strong internal field.

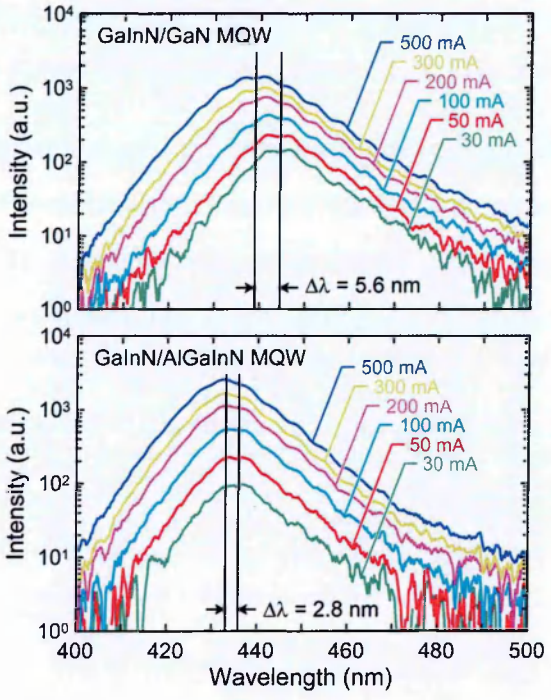

Figure 7-12- The blueshift as a function of current for a conventional c-plane InGaN LED compared with that of an LED grown with AlInGaN barriers to reduce the polarization field strength taken from [48]

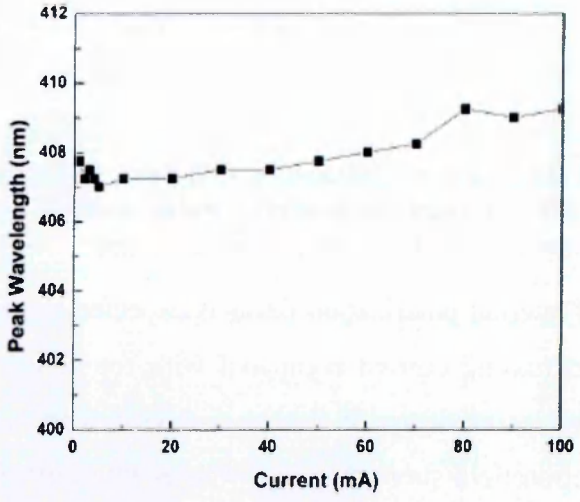

Figure 7-13- The emission wavelength dependence on current showing a slight redshift for an m-plane LED taken from [116]

The emission dependence on current at different pressures may therefore be used to gain an understanding of the recombination processes occurring in InGaN structures.

Measurements reveal that there is a large blueshift with increasing current which becomes stronger as pressure is applied in both LEDs as shown in Figure 7-14 and Figure 7-15.

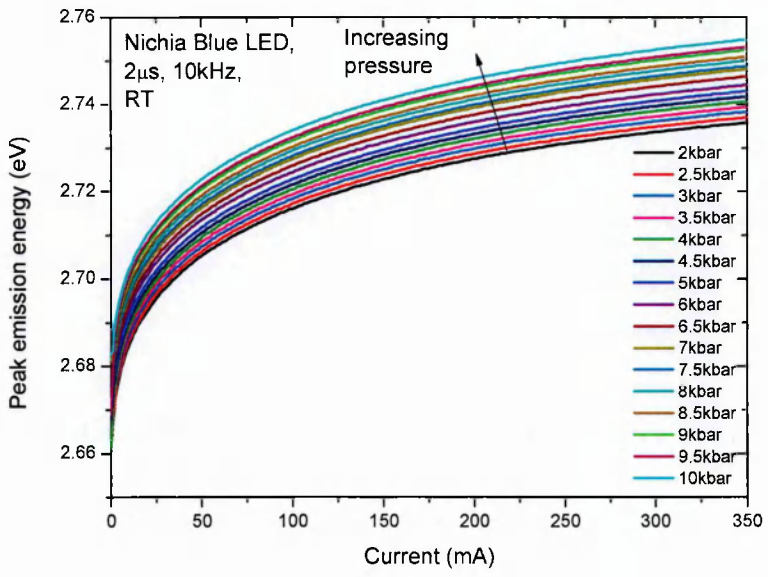

Figure 7-14- Electroluminescence peak emission wavelength as a function of current for a blue LED in pulsed mode with a pulse width of 2μs and a frequency of 10kHz at different applied pressures.

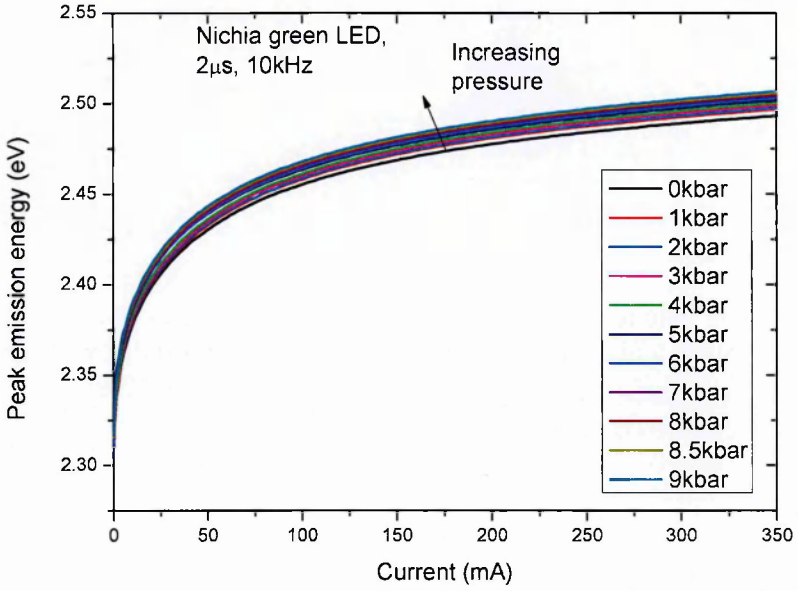

Figure 7-15- Electroluminescence blueshift as a function of current for a green LED in pulsed mode with a pulse width of 2μs and a frequency of 10kHz under different applied pressures.

A larger blueshift as a function of current was observed for the green LED and is expected to be caused by the stronger strength of the internal field in the green LED that is the result of a larger internal strain that occurs with increasing indium content.

The increasing blueshift with increasing pressure shows that the increasing piezoelectric field will cause a greater blueshift of the emission energy as a function of current with increasing pressure. This is expected to show that there is a larger QCSE with increasing pressure causing a larger current to screen the fields.

7.8 Pressure coefficients of blue-green InGaN LEDs at different currents

Figure 7-16 and Figure 7-17 show that the pressure coefficient is larger at a high current of 300mA in both the blue and green LEDs compared with the pressure coefficient at a low current of 5mA.

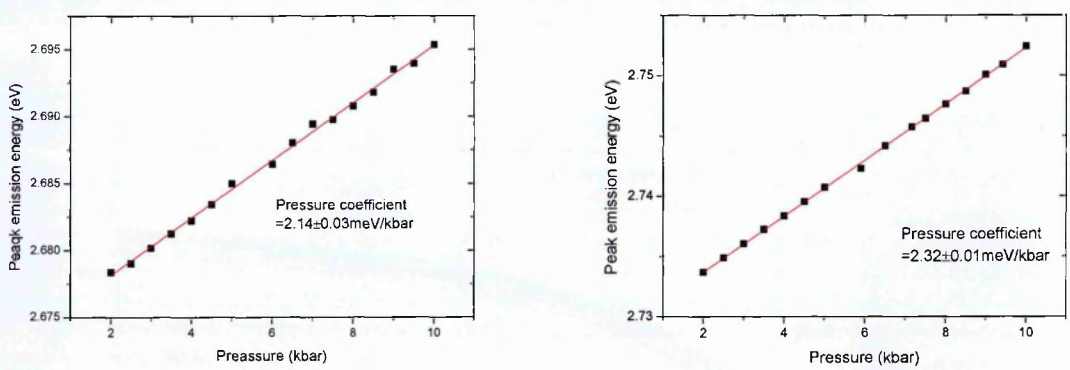

Figure 7-16- The electroluminescence peak emission energy vs pressure for a blue LED at a) 5mA and b) 300mA in pulsed mode with a pulse width of 2μs and a frequency of 10kHz resulting in a pressure coefficient of 2.14±0.03meV/kbar at 5mA and 2.32±0.01meV.

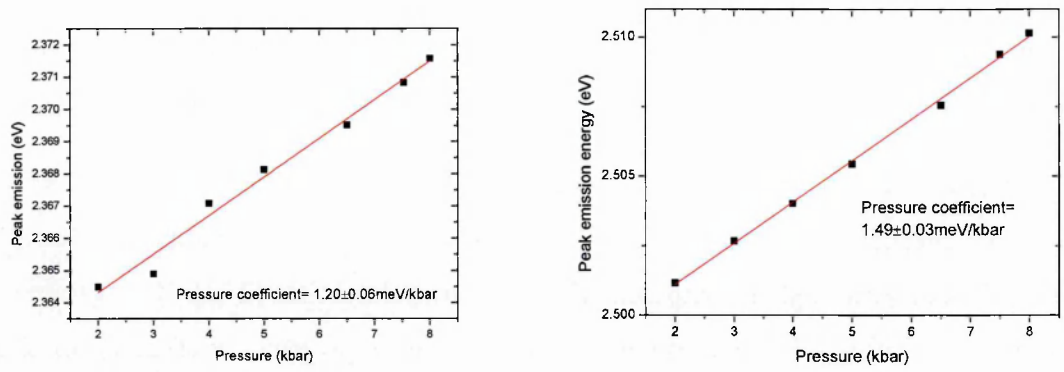

Figure 7-17- The electroluminescence peak emission energy vs pressure for a green LED at a) 5mA and b) 300mA in pulsed mode with a pulse width of 2μs and a frequency of 10kHz where the pressure coefficient of 1.20±0.06meV/kbar and 1.49±0.03meV/kbar is measured at 5mA and 300mA, respectively.

The weaker pressure coefficient at low currents may be explained by an increased influence of the internal field due to low carrier screening. Figure 7-18 shows that there is an increasing carrier screening effect with increasing current as there is observed to be an increase in the pressure coefficient.

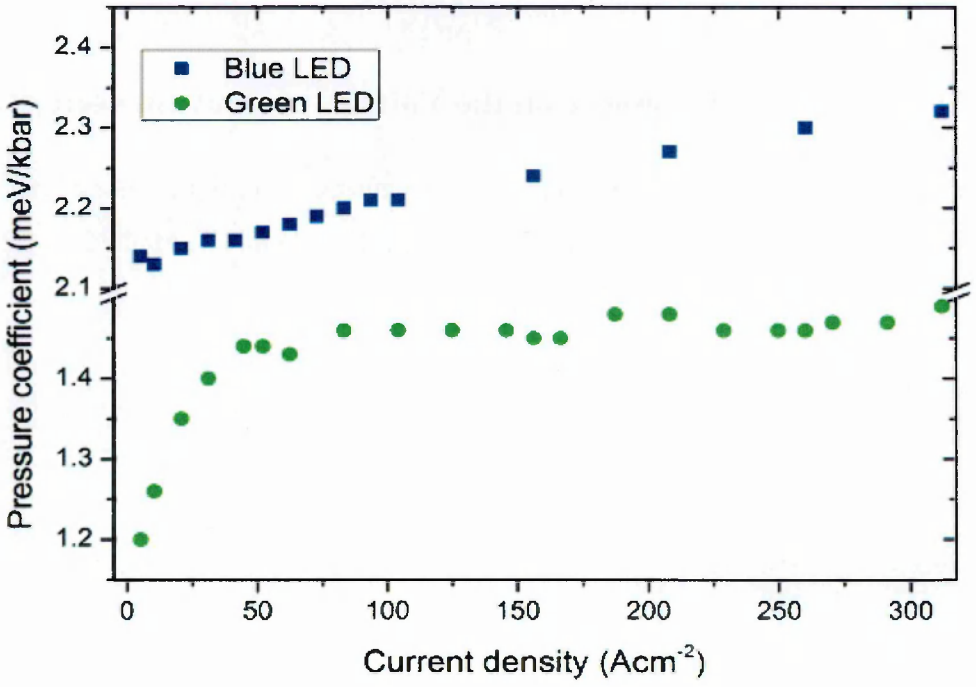

Figure 7-18- Pressure coefficient as a function of current density for the blue LED (blue squares) and the green LED (green circles) in pulsed mode with a pulse width of 2μs and a frequency of 10kHz.

The sharp rise in the pressure coefficient of the green LED in comparison with the blue LED is expected to be due to the stronger internal field strength and the effects indium inhomogeneities as will be discussed in more detail in 7.10.

Consistent with our findings, it has been shown in previous photoluminescence studies that the pressure coefficients of semi-polar LEDs (which have a significantly smaller effect of the internal fields) are higher compared with those of polar LEDs [117]. It was found that a blue LED grown along the semi-polar orientation has a pressure coefficient of 2.9meV/kbar compared with that of the blue polar LED, 1.6meV/kbar. The study also showed that a green LED grown along the semi-polar direction also has a larger pressure coefficient (1.9meV/kbar) compared with the green LED grown along the polar direction (1.0meV/kbar). The previous studies used photoluminescence techniques where there is a small carrier density. The reduced pressure coefficient of the green LED compared with the blue LED is also consistent with the findings of our study. This is expected to show that there is expected to be an additional cause of the weak pressure coefficient as will be discussed further in Section 7.10.

7.9 Influence of pressure on the Voltage-current characteristics

Further evidence that the piezoelectric field is enhanced at high pressures can also be observed with the increase of voltage for a given current as pressure is applied as shown for the blue and the green LEDs in Figure 7-19.

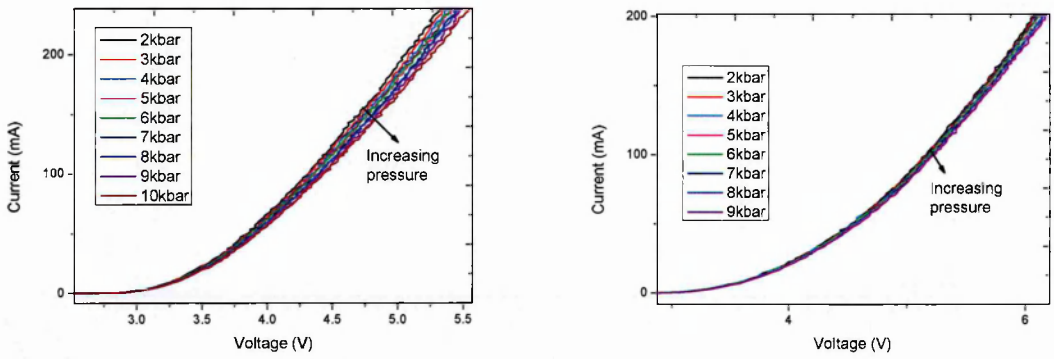

Figure 7-19- The current dependence on voltage at different pressures for (a) a blue LED and (b) a green LED in pulsed mode with a pulse width of 2μs and a frequency of 10kHz.

The larger voltage for a fixed current with increasing pressure is expected to be the result of a reduced injection efficiency with increasing internal field strength. The increase in voltage for a fixed current of 100mA as pressure is applied to the LEDs is shown in Figure 7-20.

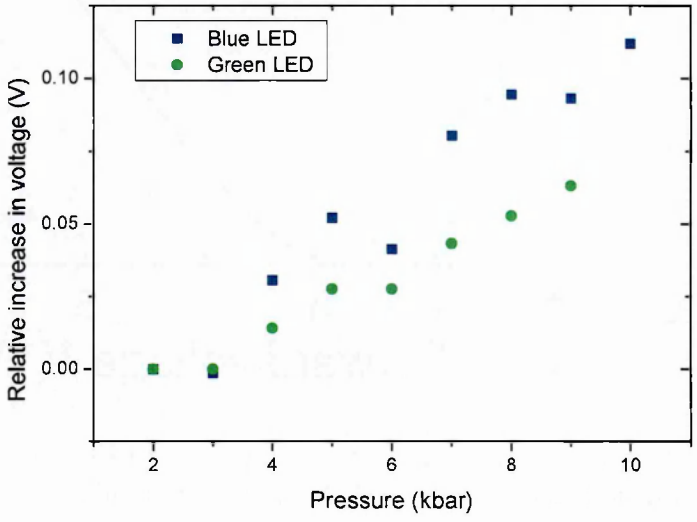

Figure 7-20- The relative increase in voltage (Voltage-Voltage at 2kbar) as a function of pressure for a blue LED (blue squares) and a green LED (green circles).

A stronger relative increase of the voltage with increasing pressure for the blue LED compared with the green LED is observed. This is expected to be due to enhanced injection issues with increasing field strength due to the larger number of quantum wells for the blue LED (see chapter 4) which hinder hole transport.

These observations are in agreement with the findings of Schubert *et al.* [48] where it was shown that an InGaN-based LED which consists of AlInGaN barriers, instead of conventionally used GaN barriers to reduce the polarization mismatch between the quantum well and the barrier also results in a reduced voltage at a fixed current compared with conventional InGaN-based LEDs as shown in Figure 7-21.

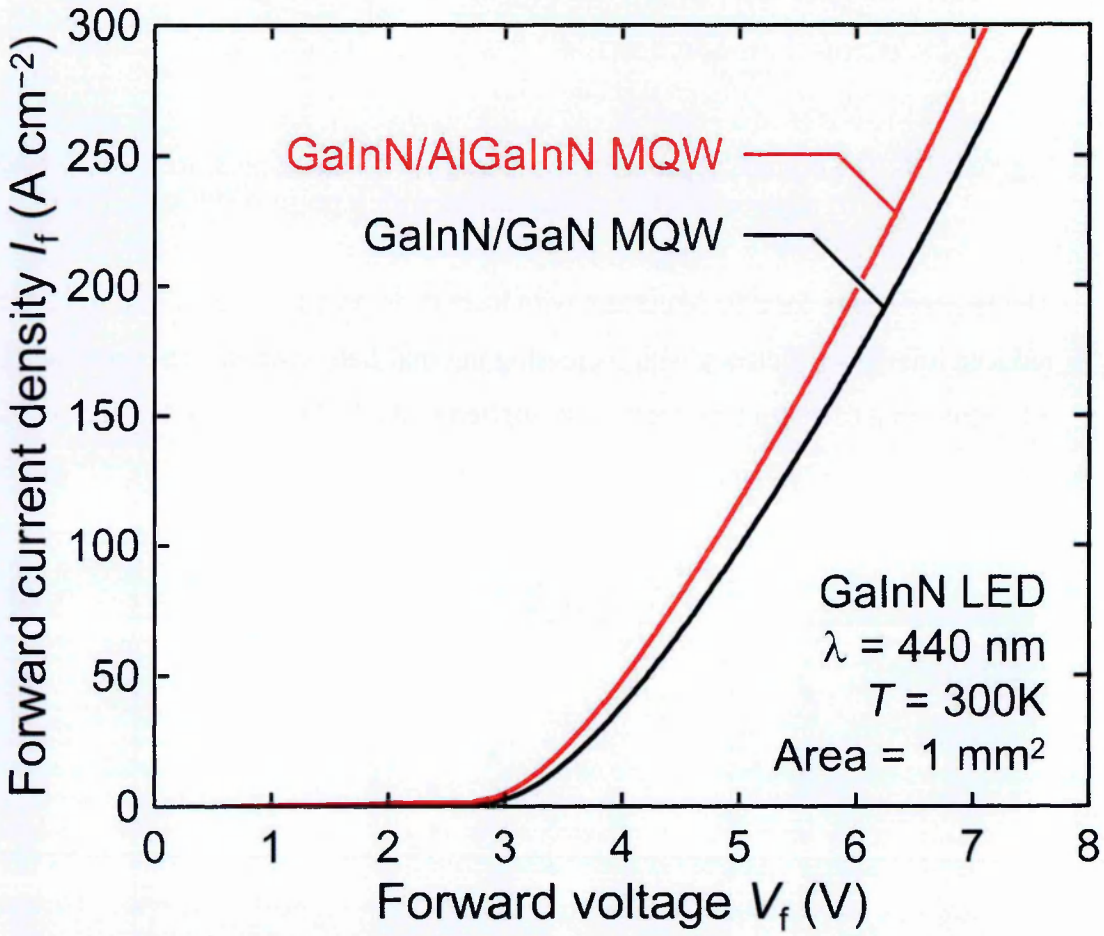

Figure 7-21- The current dependence on voltage for an LED with GaN barriers (black line) and an LED with AlGaInN LED (red line) [48].

The reduced injection efficiency for stronger internal fields is a consequence of the triangular barriers impeding the flow of carriers into the quantum well as shown in the simulation of a blue 6QW InGaN/GaN LED (Figure 7-22).

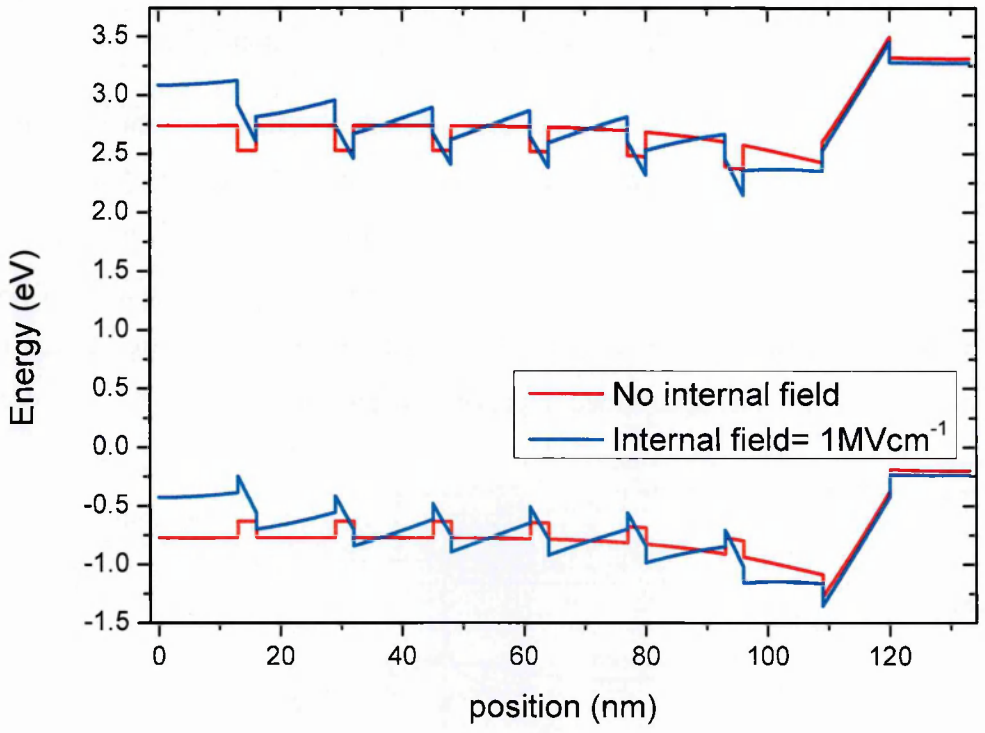

Figure 7-22- Simulation of the band structures of an InGaN/GaN LED with no internal polarization fields (shown in red) and with an internal field strength of 1MVcm^{-1} (shown in blue).

The reduced injection efficiency with stronger internal field results in a larger required applied voltage in order for carriers to be injected into the quantum wells. Consequently, the increased voltage will cause the n-side to be of higher energy than the p-side of the device. This will cause a reduced effectiveness of the electron blocking layer leading to a larger probability of electron leakage.

7.10 The influence of indium inhomogeneities on the pressure coefficient in InGaN structures

The calculated increase of the internal field strength as a function of pressure was found to be similar for the blue and green LEDs as shown in Figure 7-8. Therefore the reduced pressure coefficient of the green LED (1.20±0.06meV/kbar at 5mA) in comparison with that of the blue LED (2.14±0.03meV/kbar at 5mA) is unlikely to be the result of the increasing internal polarization field strength with increasing pressure (see Section 7.5).

A weaker pressure coefficient for structures of higher indium content was also observed in high-pressure photoluminescence measurements on InGaN epilayers [118]. These structures do not have of internal fields and therefore confirm that the weak pressure coefficient for InGaN structures compared with GaN and InN is caused by an additional process. Figure 7-23 shows the pressure coefficient is expected to reduce with increasing indium content up to indium contents of 0.5 as determined in previous measurements.

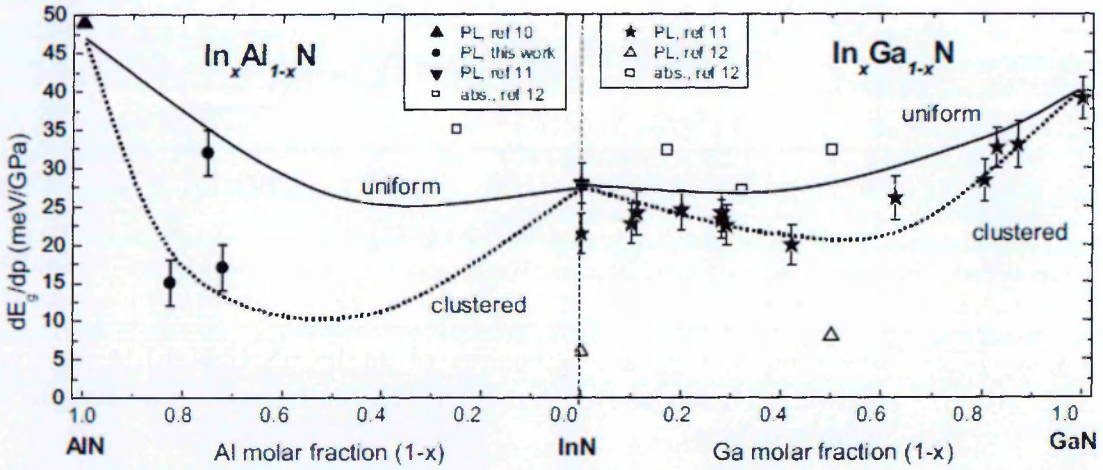

Figure 7-23- The pressure coefficient as a function of Aluminium and indium fraction in the case where the aluminium and indium distributions are uniform and clustered [118].

The strong bowing of the pressure coefficient as a function of indium content is expected to be caused by the existence of indium inhomogeneities. This is due to the reducing bond lengths between the In, N and Ga atoms in the case of a clustered distribution compared with a uniformed distribution as schematically illustrated in Figure 7-24.

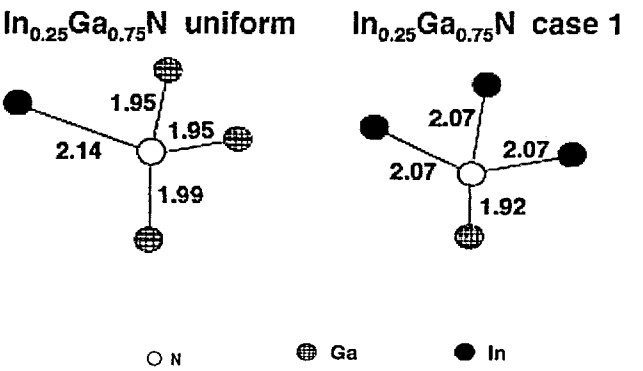

Figure 7-24- Schematic showing the arrangement of the Ga, In, and N atoms with bond lengths (in Å) for the case where the indium distribution is uniform and clustered (case 1) for a structure with an indium content of 0.25 {image taken from Gorczya *et al.* [119].

Figure 7-24 shows that there is a relative shortening of the bond length if the indium distribution is clustered (2.07 Å) compared with the case where there is a uniform indium distribution (2.14 Å). The shortened bond length will lead to hybridization of the indium p and s states with those of the N atoms in the case where there is indium clustering. This will cause the top of the valence band to be at a relatively higher energy compared with the case where there is a uniform indium distribution. Density of states calculations for a structure with an indium content of 0.25 in Gorczyca *et al.* [119] predict that the energy at the top of the valence band will increase by ~0.45eV if the indium distribution is clustered (Figure 7-25-Lower) compared with if there is a uniform indium distribution (Figure 7-25-Upper). This increase represents the case where there is 100% indium clustering and therefore in real devices the indium clustering effect is expected to be smaller. The authors use the bottom of the valence band (N-2s band) as an energy reference level.

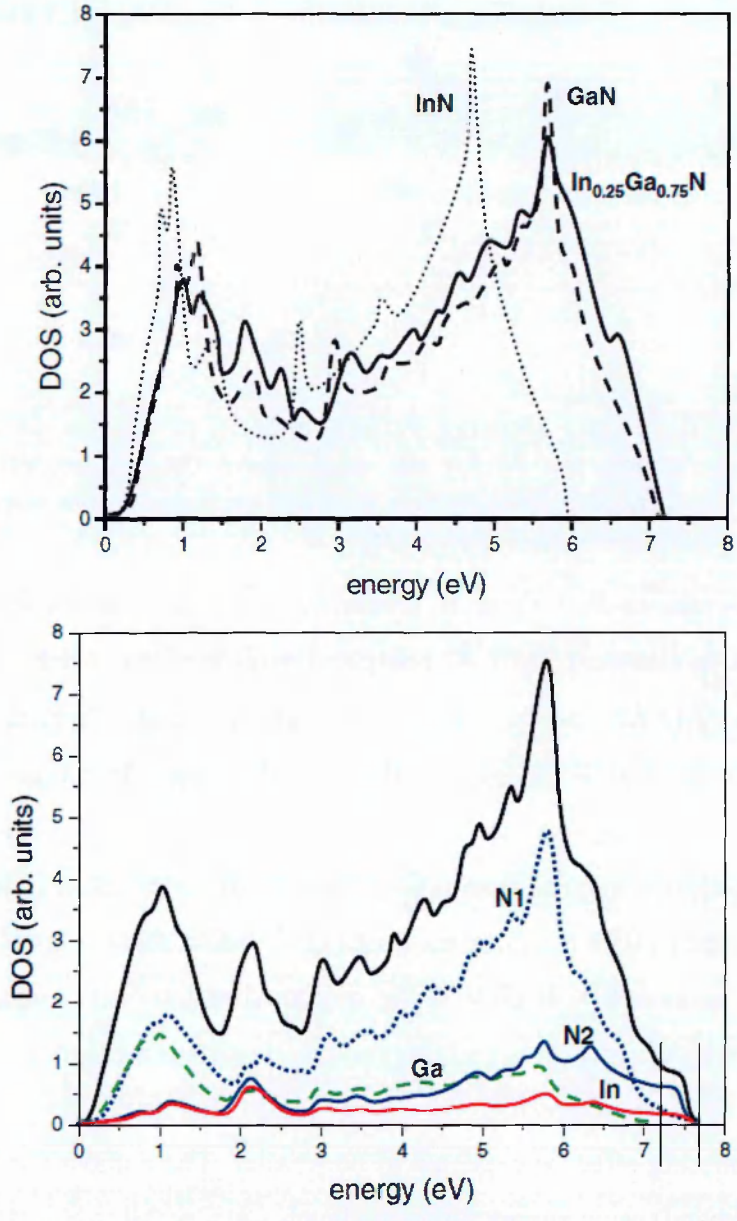

Figure 7-25- The density of states for the valence band if the indium distribution is uniform (upper graph) and if the indium distribution is clustered (lower graph). The lower graph shows an increased energy of ~0.45eV at the top of the valence band. The bottom of the valence band is taken as a reference point.

The effect of indium clustering is illustrated in Figure 7-26.

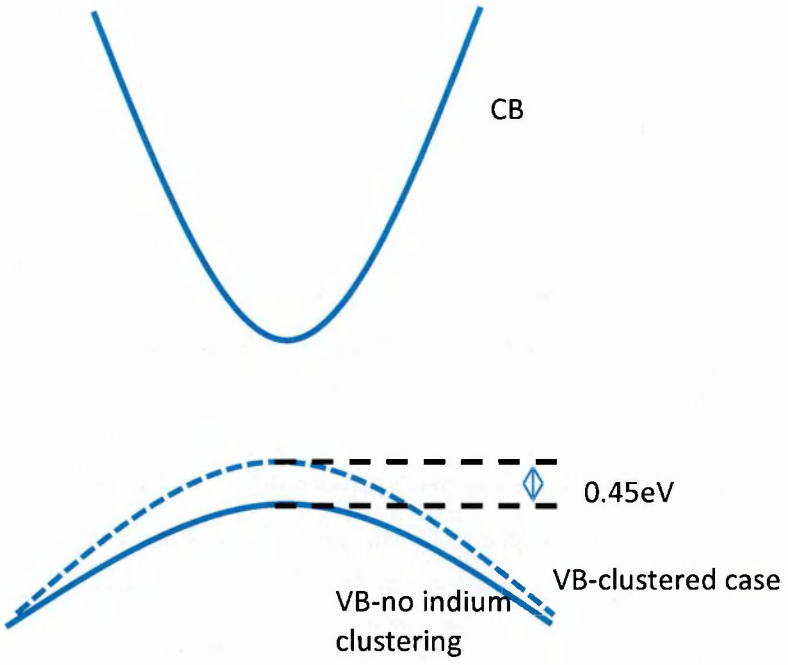

Figure 7-26- An illustration of the conduction band (CB) and valence band (VB) where the valence band if indium clustering takes place (dashed line) is found to be at an energy which is ~0.45eV higher than the case where there is no indium clustering (straight line).

The increased energy at the top of the valence band will cause a reduction of the band gap energy and consequently leads to a bowing of the bandgap energy with increasing indium content [119, 120]. Applying pressure causes a further shortening of the bond length leading to a stronger effect of hybridization. This will result in a further increase of the energy at the top of the valence band with increasing pressure. The increased energy at the top of the valence band will therefore counter the increase of band gap that takes place with increasing pressure leading to a reduced pressure coefficient. The reduced pressure coefficients of the blue LED (2.14±0.03meV/kbar) and a larger reduction for the green LED (1.20±0.06meV/kbar) compared with GaN and InN is therefore consistent with indium clustering taking place within the quantum wells of the LEDs in an effect which is stronger for the higher indium content green LED. The inhomogeneous indium distribution is expected to be due to InGaN being a random alloy rather than gross indium clustering.

7.11 Chapter summary

The pressure dependence of InGaN blue-green LEDs is presented in this chapter. It is shown that the pressure coefficient of InGaN-based emitters is much weaker compared with other III-V material systems. Whilst this effect may partially be explained by relatively low compressibility of InGaN, there are further effects which reduce the pressure coefficient as lower pressure coefficients of blue and green InGaN-based LEDs are observed compared with those of GaN and InN.

It was shown that the blueshift with increasing current becomes larger with increasing pressure in both the blue and green LEDs. This observation is expected to be explained by an increase in the internal piezoelectric field strength with increasing pressure. The pressure coefficient was found to increase with increasing current for both LEDs and is expected to be due to the carrier screening of the internal polarization fields. The influence of the internal fields is found to be strong even at high injection due to the lower pressure coefficients compared with those of GaN and InN.

The cause of the increased piezoelectric field with increasing pressure is due to the pressure-induced strain causing an increase to the polarization of the well and barriers with increasing pressure. The difference in the rate at which the polarization of the well and barriers changes as a function of pressure is shown to cause an increase to the piezoelectric field strength. It was found that there will be an increase of approximately 4% of the internal polarization field strength as pressure is applied up to 10kbar.

The final section of the chapter showed that the existence of indium inhomogeneities will also lead to a reduced pressure coefficient. This is due to the hybridization of the indium and nitrogen states at the top of the valence band that will reduce the bandgap energy. The effect of pressure will enhance such an effect as the nitrogen-indium bonds become smaller. This will result in a further increase of the energy at the top of the valence band which will consequently reduce the rate at which the bandgap increases with increasing pressure. The lower pressure coefficient of the green LED compared with the blue LED is found to be in agreement with its higher indium content causing larger indium clustering effects.

8 Pressure Dependence of the optoelectronic properties of InGaN blue-green LEDs

8.1 Chapter Aim:

This chapter aims to extend the findings of the previous chapter in investigating the performance of blue-green InGaN-based LEDs as a function of applied pressure. The previous chapter showed that the application of pressure causes an increase of the piezoelectric field strength. High pressure is therefore an important tool that can be used to investigate the influence of the piezoelectric field strength on the recombination processes of InGaN-based devices.

A reducing light output power in both the blue and green LEDs with increasing pressure is observed. This reduction is shown to be consistent with a reducing radiative recombination rate that is caused by an increasing quantum confined Stark effect (QCSE) with increasing piezoelectric field strength. The proportional reduction of the light output power with increasing pressure is shown to be similar at low and high currents. This suggests that the reduced radiative recombination rate causes a similar reduction in the performance of the LEDs over the entire current range. The results further show that pressure will cause a reduction to the efficiency over the entire current range, but the efficiency droop effect will be approximately pressure insensitive. This result is consistent with defect-related recombination being the cause of efficiency droop since pressure is expected to changes the carrier leakage and Auger recombination rates.

The final section of this chapter shows that a model which uses a defect-related recombination argument as the cause of efficiency droop may be used to fit the efficiency measurements at low and high pressure. The fitting of the efficiency dependence on current at high pressure is found to be consistent with a comparatively reduced radiative recombination rate, which leads to an increased carrier concentration, and a pressure insensitive defect-related recombination coefficient.

8.2 Light output characteristics as a function of pressure

The internal fields that exist within InGaN-based LEDs (see Section 3.6) are expected to be enhanced with hydrostatic pressure as described in the previous chapter. The benefit of using high-hydrostatic pressure to investigate the influence of the internal fields is that a single device may be used which therefore eliminates the influence of different growth conditions such as the threading dislocation density, the density of other defects and issues associated with device processing. This is an important property because m-plane LEDs (see Section 3.6), which have been shown to exhibit a larger defect density, have previously been shown to have a reduced efficiency droop but with a lower peak efficiency [66]. Consequently, the light output power remains comparable in m-plane with c-plane devices at high injection currents (see Figure 3-23).

In this study, the light output power is found to reduce with increasing pressure as shown in Figure 8-1 for the blue and green LEDs.

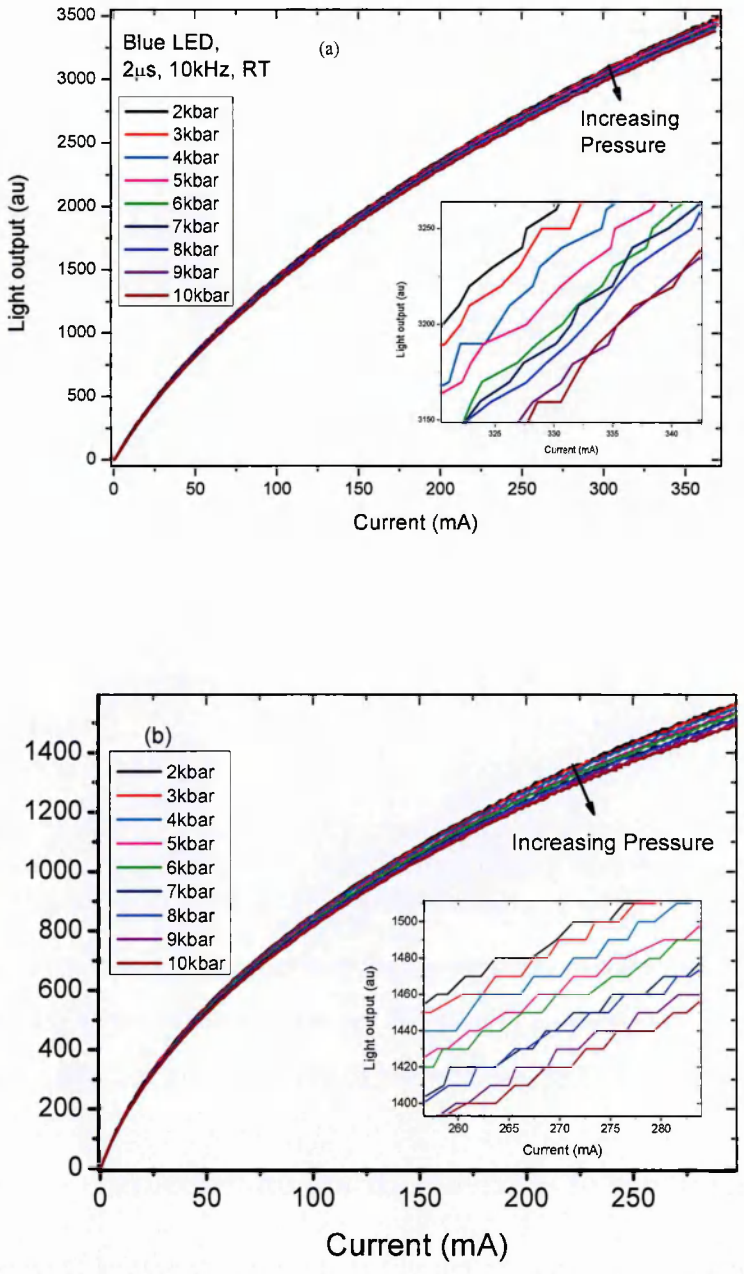

Figure 8-1-The electroluminescence light output power as a function of current at different pressures for (a) blue LEDs and (b) green LED in pulsed mode with a pulse width of 2μs and a frequency of 10kHz. Insets show the light output power dependence on pressure at high current.

Interestingly, the proportional reduction of light output power as a function of pressure for a fixed low current value of 10mA is found to be similar to the reduction of the light output power at a fixed high current of 250mA as shown in Figure 8-2.

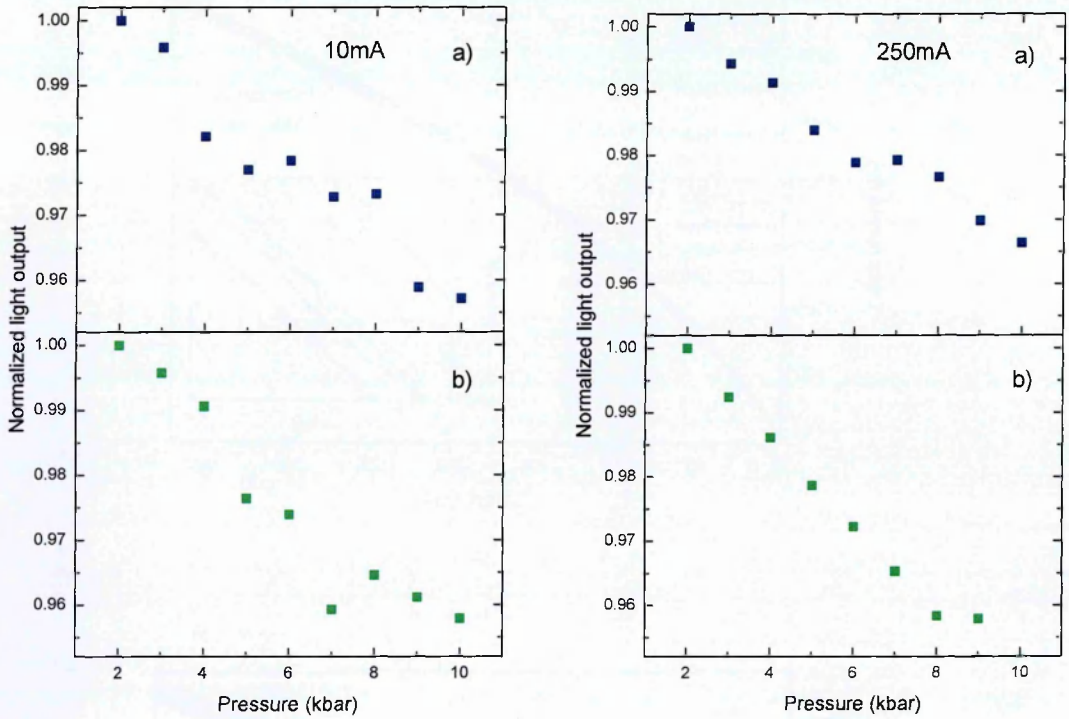

Figure 8-2- The normalized electroluminescence light output as a function of pressure at 10mA (left graph) and 250mA (right graph) for (a) a blue LED and (b) a green LED in pulsed mode with a pulse width of 2μs and a frequency of 10kHz

The similar dependence of the light output power on pressure at low and high currents suggests that the influence of pressure is the same over the entire current range. The cause of this dependence will be discussed further in the following sections.

8.3 Dependence of efficiency droop on pressure

The light output dependence on current at different pressures (Figure 8-1) can be converted into efficiency in order to show the effect of pressure on the efficiency droop phenomenon as shown in Figure 8-3.

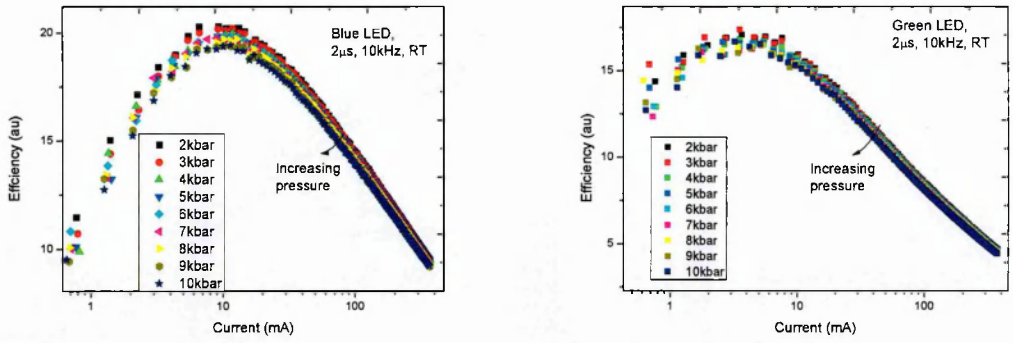

Figure 8-3- The electroluminescence efficiency as a function of current for (a) a blue LED and b) a green LED in pulsed mode with a pulse width of 2μs and a frequency of 10kHz

A reduction of the efficiency over the entire current range for both LEDs is observed. Measurements of the efficiency droop effect at different pressures were also performed in CW mode at low currents (<20mA) where there is expected to be a minimal influence of Joule heating [28]. The benefit of using CW measurements is that there a significant increase in the light output power which reduces noise in addition to easier control of the injection current. Applications will also use CW mode so it is beneficial to investigate the LEDs using CW mode. The efficiency as a function of current at different pressures for the blue and green LEDs is shown in Figure 8-4.

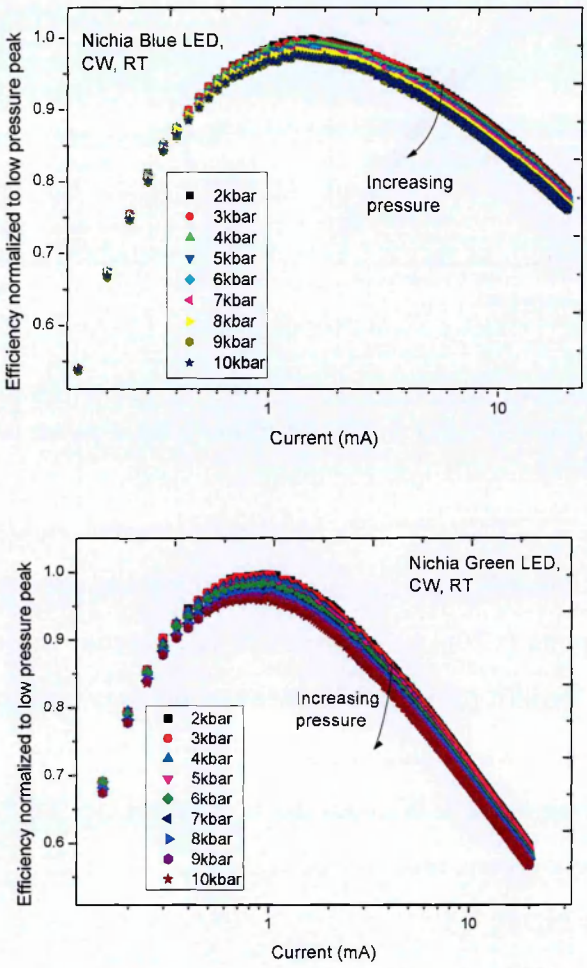

Figure 8-4-The electroluminescence efficiency as a function of current at different pressures for a blue LED (upper graph) and a green LED (lower graph) in CW mode

The application of pressure was found to reduce the peak efficiency in both LEDs. It is also found that the current at which the efficiency peaks is reduced with increasing pressure as shown in Figure 8-5.

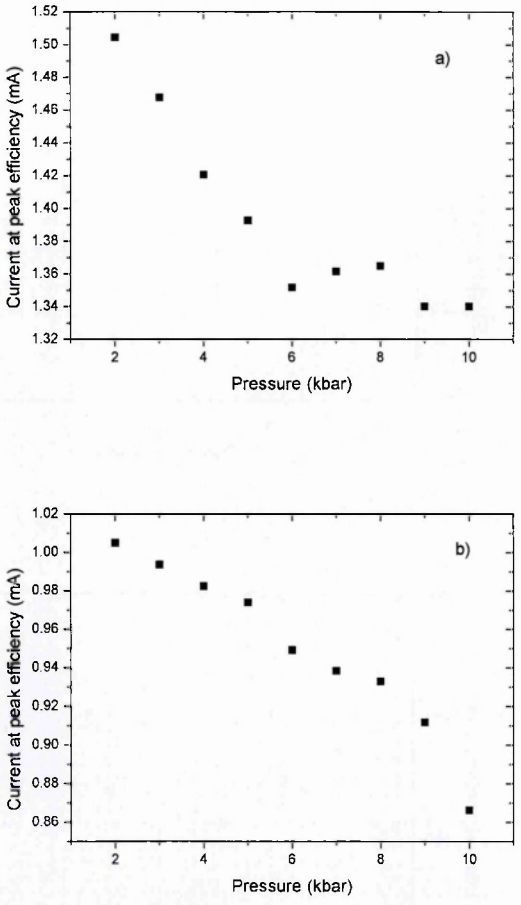

Figure 8-5- The electroluminescence peak efficiency current as a function of pressure for a) a blue LED and b) a green LED in CW mode.

The reduction in the current at which the peak efficiency occurs shows that there is an earlier onset of efficiency droop. This therefore suggests the non-radiative recombination process which causes droop occurs at a lower current with increasing pressure.

Figure 8-6 shows the rate at which the efficiency reduces from the peak efficiency to the efficiency at 20mA as a function of pressure. The efficiency reduction is an indication of the droop rate at different pressures.

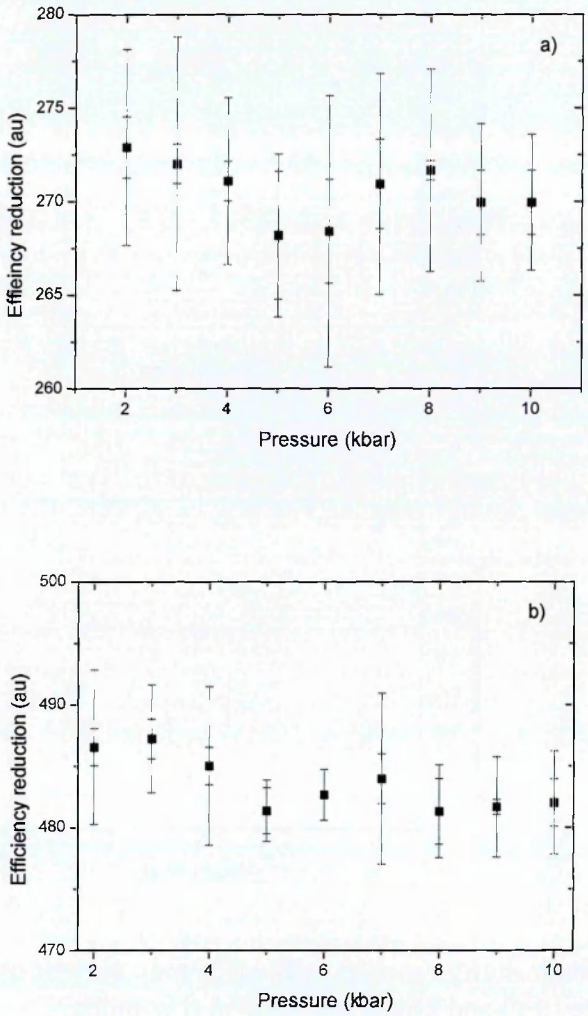

Figure 8-6- The reduction in efficiency from the peak efficiency value to the efficiency at the highest current as a function of pressure for a) a blue LED and b) a green LED

The results show that there is not a significant change in the reduction of the efficiency with increasing pressure and suggests that the loss mechanism responsible for efficiency droop is likely to be pressure-insensitive. This shows that the reduction of the efficiency over the entire current range reduces at the same rate and is consistent with the similar reduction of the light output power with increasing pressure at low and high currents as shown in Figure 8-2.The following sections explore which mechanisms are consistent in explaining the weak pressure dependence of efficiency droop.

8.4 Calculation of the electron and hole wavefunction overlap as a function of piezoelectric field strength

Nextnano software was used to simulate the effects of an increasing piezoelectric field on the electron and hole wavefunction overlap for a blue LED of 0.16 indium content including GaN barriers and an AlGaN EBL of 0.2 aluminium content. Figure 8-7 shows that the square of the electron and hole wavefunction overlap will reduce from ~9% as the piezoelectric field is increased from 2.46MVcm^{-1} to 2.56MVcm^{-1}. This increase in piezoelectric field was calculated to occur as pressure is applied from 2kbar to 10kbar (see Section 7.5).

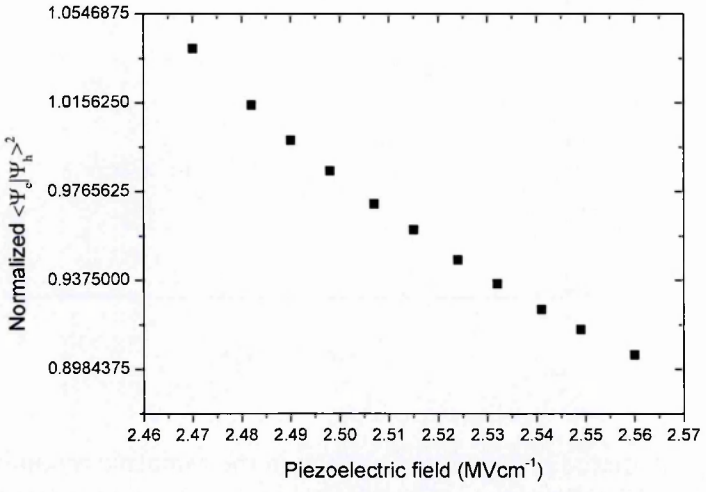

Figure 8-7- The square of the electron and hole wavefunction overlap as a function of piezoelectric field calculated using nextnano software for a blue LED with an indium content of 0.16. The y-axis in the right shows the normalized reduction of the overlap intensity.

The reduction of the overlap between the electron and hole wavefunction overlap is expected to be the cause of the reducing light output power with increasing pressure as shown in Figure 8-2. The influence of the increasing piezoelectric field as pressure is applied on the recombination processes will be described in the following sections.

8.5 The dependence of the radiative recombination coefficient on pressure

In addition to the reduction of the electron and hole wavefunction overlap with increasing pressure the radiative recombination rate is expected to increase at a rate which is proportional

to the square of the increasing band gap energy [121, 122] . The black line in Figure 8-8 shows the expected proportional increase of the radiative recombination rate due to an increasing band gap energy if it is assume that the band gap will increase at a rate of 3.75meV/kbar (see Section 7.6). The reduction of the radiative recombination rate with increasing pressure is calculated if both the effects of an increasing piezoelectric field strength and an increasing band gap energy are considered as shown by the red line in the diagram.

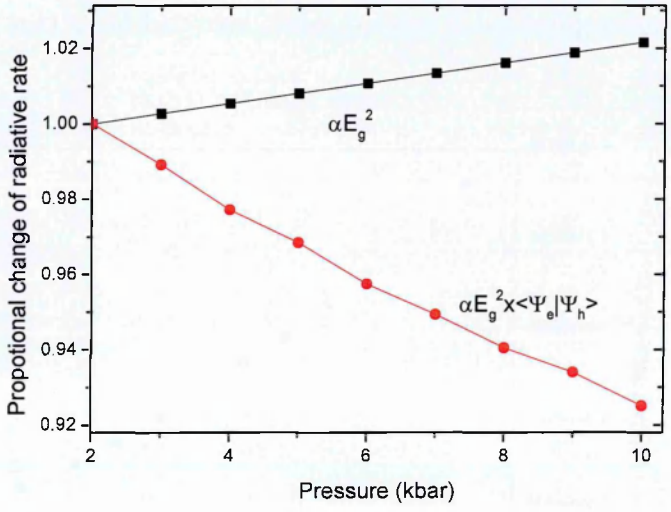

Figure 8-8- The calculated proportional change in the radiative recombination rate as a function of pressure. The black squared line represents the change in the radiative recombination rate that is due to the increasing band gap energy, the red circled line also includes the influence of an increasing field with increasing pressure.

The resultant change in the radiative recombination rate as pressure is applied is found to be approximately a 7% reduction as pressure is increased from 2kbar to 10kbar. This indicates the dominant effect on the radiative rate with increasing pressure is the increasing internal field strength. The 7% reduction is in line with the 4% of light output reduction observed in Figure 8-2. The reduction of the radiative recombination rate is expected to increase the carrier concentration for at a given current. The combined effect of a reduced radiative recombination coefficient and an increasing carrier concentration is expected to increase the relative non-radiative recombination rate with increasing pressure. The following sections will consider the effect of pressure on the candidate droop-causing mechanisms.

8.6 The dependence of carrier leakage on pressure

The increase in the bandgap energy with increasing pressure is mainly due to the upwards movement of the conduction band compared where it is considered that the change in the valence band will be small [123]. Figure 8-9 shows that the effect of pressure in the absence of internal field would be to increase the confinement energy due to the larger pressure coefficient of the GaN barrier (3.9meV/kbar) compared with the InGaN quantum well (3.75me/kbar- extrapolated value for a blue LED with 0.14 indium content).

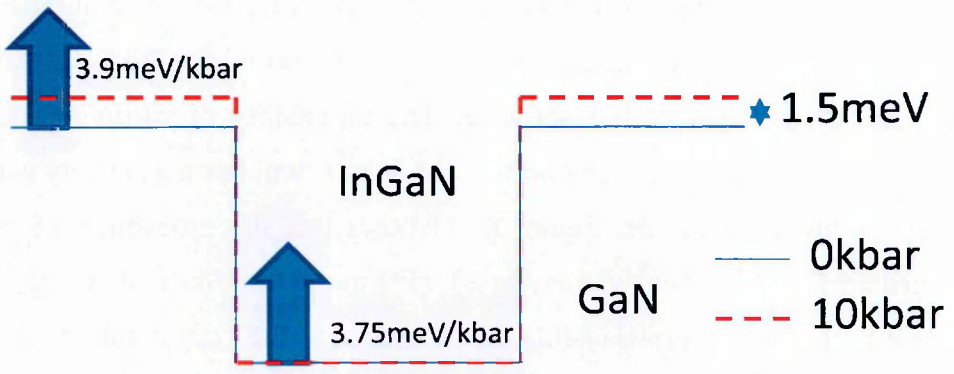

Figure 8-9- Schematic showing the influence of pressure on the conduction band of a blue InGaN quantum well of indium content 0.16 if the influence of the internal field strength is neglected.

The increase in the confinement energy will be countered by the increasing internal polarization field strength that occurs with increasing pressure. The reduction of the GaN barrier is calculated to be 26.8meV as there is an increase in the piezoelectric field as pressure is applied from 0kbar to 10kbar. The overall change in confinement energy of the conduction band as pressure is applied to 10kbar is therefore expected to reduce by ~25meV as schematically shown in Figure 8-10.

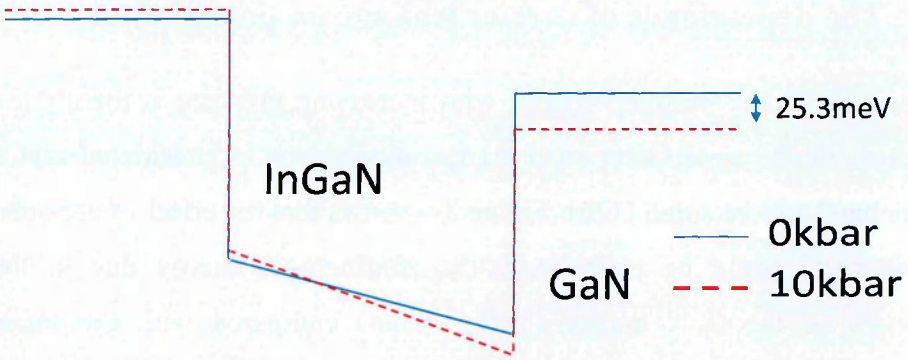

Figure 8-10- Schematic showing the effect of pressure on the conduction band of an InGaN blue LED with 0.16 indium content as pressure is applied to 10kbar.

The probability of carrier leakage may be calculated by consideration of the Fermi function. In the calculation it is assumed that at 0kbar the Fermi level is equal to the ground energy state as calculated using the nextnano software. The probability of carrier leakage may then be calculated by considering the probability that carriers will reach an energy which is larger than the top of the GaN barrier. Figure 8-11 shows that the probability of carrier leakage is expected to increase from ~0.60% to ~1.15% as the confinement energy is reduced from 134meV to 109meV (corresponding to the energy of the GaN being at ~2.74eV at 0kbar to 2.71eV at 10kbar).

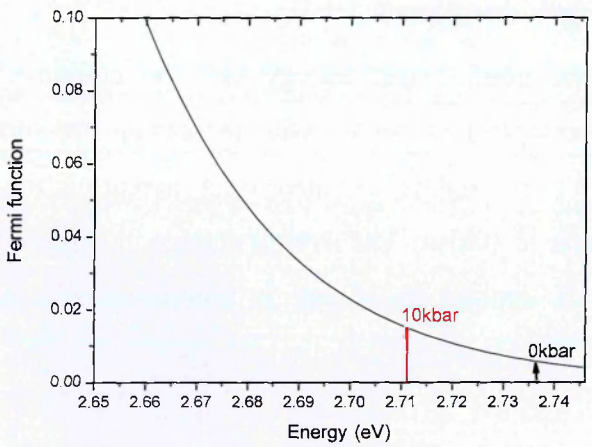

Figure 8-11- The Fermi function dependence on energy with a Fermi energy of 2.6eV where the black arrow represents the energy difference between the ground state energy level and the top of the GaN conduction band at 0kbar and the red line represents the energy difference at 10kbar.

The carrier leakage rate would therefore be expected to increase by a factor of 2 as pressure is applied to 10kbar. As there is a lower dependence of the efficiency on pressure observed in the

experiment carrier leakage is unlikely to explain the observations of Figure 8-4. The carrier leakage rate is also likely to be further increased with increasing pressure due to the increase in carrier concentration that results from the reduction of the radiative recombination rate.

The observations of this section are in line with the findings of Lee *et al.* [124] and Li *et al.* [125] where it was found that the efficiency droop effect was not significantly different for devices grown on the m-plane (which are free of the strong internal fields) compared with devices grown on the c-plane (which consist of strong internal fields). However, it must be noted that contrary to the findings (and the observations of this chapter), other studies have shown that there is a reduced efficiency droop effect for devices of reduced internal fields which may be due to an increasing proportion of defect-related recombination as described in further detail in Section 3.4.4 [48, 126].

8.7 The dependence of Auger recombination on pressure

Auger recombination is another loss mechanism which has widely been speculated as the dominant cause of efficiency droop. Previous high pressure studies on other material systems (such as InGaAs/ GaInNAs) have found that the Auger recombination rate reduces with increasing pressure [127, 128]. An additional reduction to the Auger recombination coefficient will be caused by the reducing electron and hole wavefunction overlap with increasing piezoelectric field as shown in Figure 8-7. Whilst the dependence of the Auger coefficient on the overlap will be different from that of radiative recombination, it is also expected to reduce with increasing internal polarization field [92]. The reduced efficiency with increasing pressure is therefore not consistent with Auger recombination being the dominant recombination process.

The effect of pressure on inter-conduction band Auger recombination will depend on the band gap energy of the device. Figure 8-12 shows pressure will cause the band gap energy of the blue LED to move away from the Auger recombination resonance whilst the band gap of the green LED will move towards the resonance.

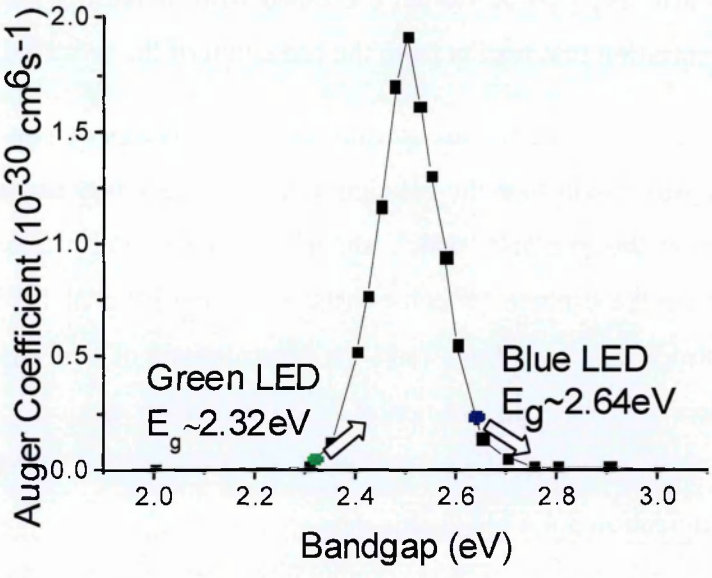

Figure 8-12-The theoretically calculated Auger coefficient dependence on band gap energy due to interband Auger recombination showing that the effect of pressure on the band gap energy is expected to move the band gap of the green LED towards a predicted Auger recombination resonance and blue LEDs will move away from the resonance.

The efficiency of the LEDs is therefore expected to have opposite dependence on pressure if inter-conduction band Auger recombination is the dominant cause of efficiency droop. Inter-conduction band Auger recombination is therefore not expected to be the dominant cause of efficiency droop as the efficiency is observed to decrease as pressure is applied to both the blue and green LEDs as shown in Figure 8-4.

8.8 Fitting the pressure dependence of droop using a defect-related cause of efficiency droop

There is expected to be a lower influence of the internal field strength on the monomolecular defect-related recombination coefficient, A_0, compared with the radiative recombination coefficient, B_0, as described in section 5.8.3. Despite this, the proportion of defect-related recombination compared with the total recombination is expected to increase with increasing field strength due to the reduced radiative recombination rate.

In Sections 8.6 and 8.7 it was shown that carrier leakage and Auger recombination are unlikely to explain the pressure dependence of efficiency droop. A defect-related recombination mechanism as the cause of droop is therefore considered to explain the pressure

dependence of efficiency droop. In Chapter 5 a simple model was presented whereby there was an increase in the defect-related recombination coefficient as a function of carrier concentration due to the increasing probability that carriers will recombine with defect sites at high energies. A good fit with the experimental observations (Figure 8-13) is found if the defect-related recombination model is used to model the data. Figure 8-13 shows the fitted efficiency behaviour as a function of current density when the following relationship, which is the same as equation 3-9 where Auger recombination is assumed to be negligible, is employed to convert the carrier concentration (which is used in the model) to the current density (which was measured in the experiment).

$$J = eL(An + Bn^2) \qquad 8\text{-}1$$

where e is the electronic charge, L is the combined quantum well thickness, A is the defect-related recombination coefficient, B is the radiative recombination coefficient and n is the carrier concentration.

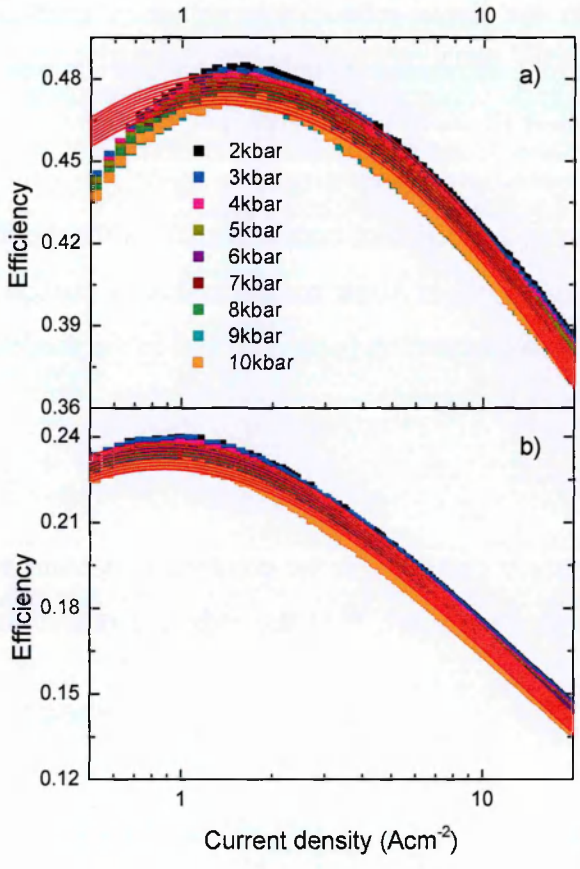

Figure 8-13- Fitting to the efficiency as a function of current with a defect-related recombination model for efficiency droop is used for (a) a blue LED and (b) a green LED. The parameters used are A_0=5.7x10^{7}s^{-1}, n_p=8x10^{17}cm^{-3} and D= 6.0x10^{-19}cm^{3}s^{-1} for the blue LED, A_0=5x10^{7}s^{-1}, n_p=6x10^{17}cm^{-3} and D=7.5x10^{-19}cm^{3}s^{-1} for the green LED and n_0=5x10^{18}cm^{-3} which are assumed to be constant as a function of pressure. B_0=7.0x10^{-11}cm^{-3}s^{-1} at 2kbar and reduces by 3.75x10^{-13}cm^{-3}s^{-1}kbar-1 for the blue LED. B_0=2.0x10^{-11}cm^{-3}s^{-1} at 2kbar and reduces by 1.25x10^{-13}cm-3s^{-1}kbar^{-1} for the green LED.

The A_0 parameter is the defect-related recombination coefficient at low currents where it is assumed that only active region bandgap defect sites contribute to the defect-related recombination. This is considered to be 5.7x10^{7}s^{-1} for the blue LED and 5x10^{7}s^{-1} for the green LED. These values are comparable to the monomolecular coefficient of previous studies [31] where a slightly reduced value for the green LED takes into account the increased carrier localization [94]. The higher carrier localization effect in the green LED is also assumed to be the cause of the lower D (6.0x10^{-19}cm^{3}s^{-1}) compared with that of the blue LED (7.5x10^{-19} cm^{3}s^{-1}). n_p, is comparable with the carrier concentration required for density-activated defect related recombination to take place that is used in Piprek *et al.* with 8x10^{17}cm^{-3} (blue LED)

and $6x10^{17}cm^{-3}$ (green LED) [43]. The lower carrier density for the green LED is also assumed to be due to its higher defect-density.

The parameters relating to the defect-related recombination are assumed to be constant as a function of piezoelectric field (and hence applied pressure), as described in Section 5.8.3, due to a lower dependence on the electron wavefunction overlap of the defect states compared with radiative recombination [90].

The fitting of the pressure dependence of the efficiency is achieved by the reducing the B_0 values in the model. The B_0 value at 2kbar is obtained from the literature [27, 31] and a higher value used for the blue LED takes into account (a) a reduced internal field strength that results from the reduced polarization mismatch between the active and cladding regions and (b) the relatively larger band gap [33]. The fitted model found that B_0 reduces from $7.0x10^{-11}cm^{-3}s^{-1}$ at a rate of $3.75x10^{-13}cm^{-3}s^{-1}kbar^{-1}$ in the case of the blue LED. For the green LED, B_0 = $2.0x10^{-11}cm^{-3}s^{-1}$ at 2kbar and reduces at a rate of $1.25x10^{-13}cm^{-3}s^{-1}kbar^{-1}$. Whilst there is only a small reduction in the B_0 coefficient as pressure is increased from 2kbar to 10kbar (5%), there will be an impact on the radiative efficiency as the reduction in the radiative recombination rate will also cause an increase to the carrier concentration for a fixed current. The combined effect of the reduced radiative recombination coefficient, in addition to an increased carrier concentration will cause there to be a proportion increase in the defect-related recombination. The n_0 parameter that is due to the saturation of the radiative coefficient is assumed to be $5x10^{18}cm^{-3}$ as determined in previous studies [23, 43] for both LEDs. As was the case in fitting the temperature dependence of efficiency droop, the parameters A_0, B_0, and n_0 were obtain from the literature values and the n_p and D values were determined by fitting the data.

An earlier onset of efficiency droop with increasing pressure is expected to be the result of a larger carrier concentration at a fixed current that is the result of a reduced radiative recombination rate [40]. This causes the filling of potential minima and an onset of the increasing defect-related recombination coefficient to occur at a reduced current with increasing pressure. The relatively pressure-insensitive efficiency droop may be explained by a similar rate of non-radiative recombination at high injection currents where there is less influence of the potential minima at all pressures.

8.9 Chapter Summary

This chapter builds on the pressure investigation of InGaN blue-green LEDs from chapter 7. It was shown that the light output power will reduce with increasing pressure for both the blue and the green LEDs. This reduction is expected to be the result of a reducing radiative recombination rate with increasing quantum confined Stark effect as pressure is applied. The proportional reduction of the light output power with increasing pressure is found to be similar at low and high currents. This result suggests that the reduction of the light output power with increasing pressure is due to the reduction in the radiative recombination that subsequently results in the relative increase of defect-related recombination.

The results show that the efficiency reduces almost equally over the entire current range with increasing pressure. Carrier leakage or Auger recombination arguments as the cause of efficiency droop are unlikely to explain these observations. This is because there is expected to be an increase in the droop effect due to the expected increase of the carrier leakage rate by a factor of 2 as pressure is applied to 10kbar. In contrast, Auger recombination is expected to reduce as a function of pressure and is therefore unlikely to explain the observed efficiency reduction with increasing pressure. The results are also inconsistent with interconduction band Auger recombination as opposite dependencies of the efficiency on pressure for the blue and green LEDs are not observed.

An efficiency model which uses an increasing defect-related recombination coefficient with increasing current (as described in Chapter 5) was shown to fit the measured efficiency dependence on current density at low and high pressures. This suggests that the reduced efficiency over the entire current range with increasing pressure is the result of an increasing proportion of defect-related recombination that results from the reducing radiative recombination rate. The reduced radiative recombination rate will lead to an increased carrier concentration which will cause the filling of the potential minima to occur at an earlier current and there will subsequently be an earlier onset of efficiency droop with increasing pressure.

9 InGaN: Future Applications

9.1 Chapter aim

The aim of this chapter is to investigate the recombination processes which take place in InGaN-based LEDs grown on silicon substrates and InGaN-based laser diodes (LDs). This chapter investigates whether the loss mechanisms which limit the efficiency of InGaN-based LEDs on sapphire are the same as those which limit the efficiencies of InGaN-based LEDs grown on silicon substrates. The second part of this chapter will investigate the non-radiative recombination processes which limit the efficiency of InGaN-based LDs. The technology used to produce InGaN-based LDs has advanced rapidly in recent years leading to many commercially-available applications such as blu-ray players and HD-DVD storage. The threshold currents of InGaN-based LDs, particularly those with emission in the green part of the spectra, are required to be reduced in order to meet the increasing demand for applications.

The results of this chapter will be used as an extension of the findings in Chapters 6, 7 and 8 where the loss processes which affect InGaN-based LEDs were investigated. The determination of the efficiency limitations of the LEDs grown on silicon substrates and LDs may be used to understand how to achieve more efficient performance in devices which are expected to have a strong commercial impact over the next few years.

9.2 InGaN Based LEDs Grown on silicon substrate

There is a strong need for high intensity visible LEDs to be used in lighting applications as a replacement of incandescent light bulbs. Silicon may be used as an alternative substrate material to sapphire in InGaN-based devices in order to reduce production costs by up to 90% [129]. The reduced costs can be attributed to the abundance of silicon in addition to the ability to produce six inch and larger wafers. In comparison, sapphire is currently only able to produce two inch wafers at a similar production cost. Not only will the larger wafers produce a larger number of LEDs, but there will be a reduced proportion of poor quality LEDs that are produced near the edge of the wafers. Researchers have also demonstrated that 8 and 12 inch silicon wafers may be produced [130, 131] that will further reduce production costs. However, InGaN-based LEDs grown on silicon substrates currently have light output powers which are

40% lower compared with InGaN-based LEDs grown on sapphire substrates [132]. A strong need to increase the efficiency of the LEDs grown on silicon is therefore required in order to enable commercialization.

9.3 Device Structure

A schematic of the InGaN-based LED grown on a silicon substrate which is studied in this chapter is shown in Figure 9-1.

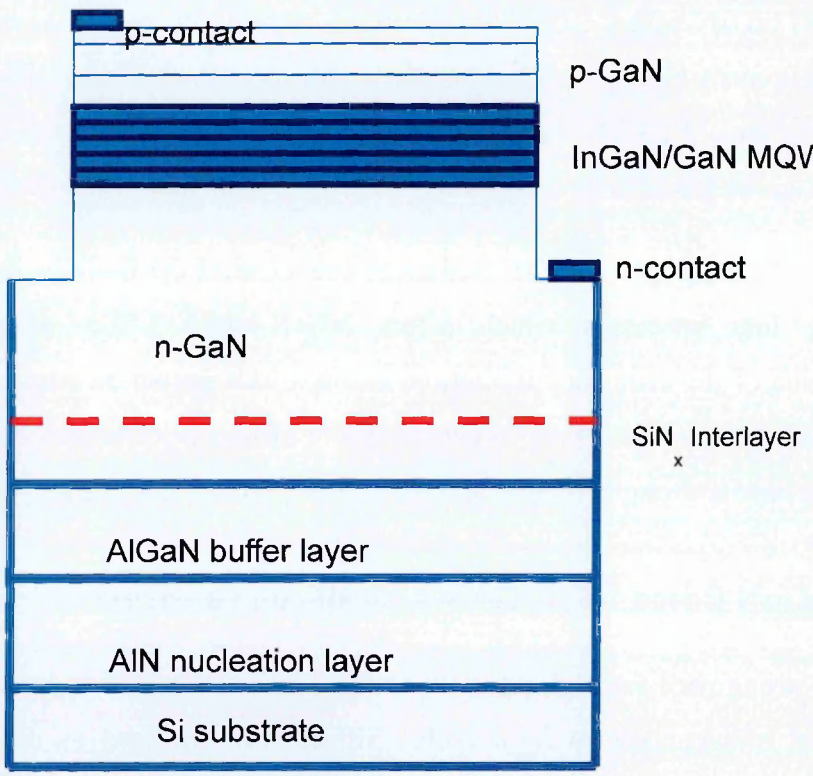

Figure 9-1- A schematic showing the device structure including the silicon substrate, nucleation layers, an silicon nitride interlayer, nGaN layer, InGaN/GaN MQW, pGaN layer and the p and n contacts [133].

The buffer and nucleation layers are required in order to prevent a high threading dislocation density from penetrating the active layers. More details on the device structure may be obtained from [133]. The high dislocation density results from the large lattice mismatch between the (17%) GaN and Si [132] which is larger than the lattice mismatch between GaN

and sapphire (14%) [134]. Previous TEM studies have shown that the threading dislocation density is larger in GaN-based devices grown on silicon ($2x10^9$ cm^{-2}) [132] compared with those grown on sapphire substrates ($5x10^8 cm^{-2}$) [30].

The influence of a larger defect density results in a reduced efficiency over the entire current range for LEDs grown on silicon substrates in comparison with blue LEDs grown on a sapphire substrates as can be seen in comparing blue LEDs in Figure 9-2.

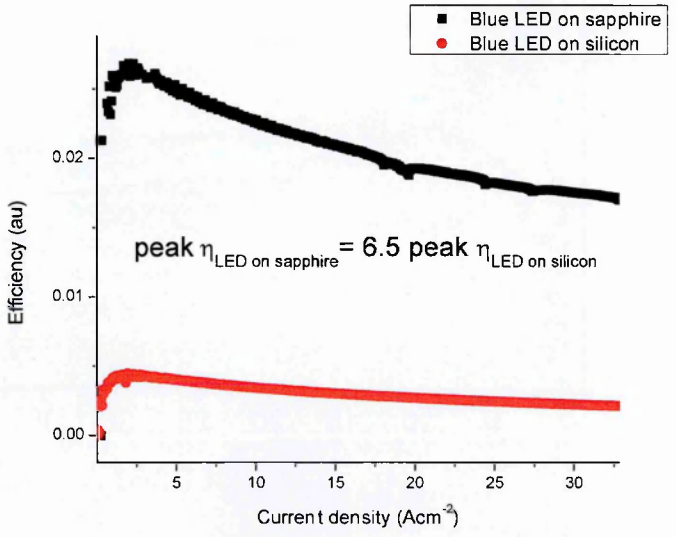

Figure 9-2- The electroluminescence efficiency dependence on current density for a blue LED grown on sapphire substrates (Nichia blue LED-black line) and blue LEDs grown on a silicon substrate (red line) in pulsed mode with a pulse width of 2μs and a frequency of 10kHz

Whilst the peak efficiency is observed to be lower for the LED grown on silicon, there is also a reduced effect of efficiency droop. This is expected to be caused by the strong influence of defect-related recombination at on the peak efficiency compared with the efficiency at high currents.

9.4 The temperature dependence of InGaN-based LEDs grown on silicon substrates

The investigation into the temperature dependence of InGaN-based LEDs which are grown on sapphire substrates in chapter 6 is extended here to include the temperature dependence of

LEDs grown on silicon substrates. Figure 9-3 shows the temperature dependence of efficiency droop in LEDs grown on silicon substrates for temperatures between 80K and 240K.

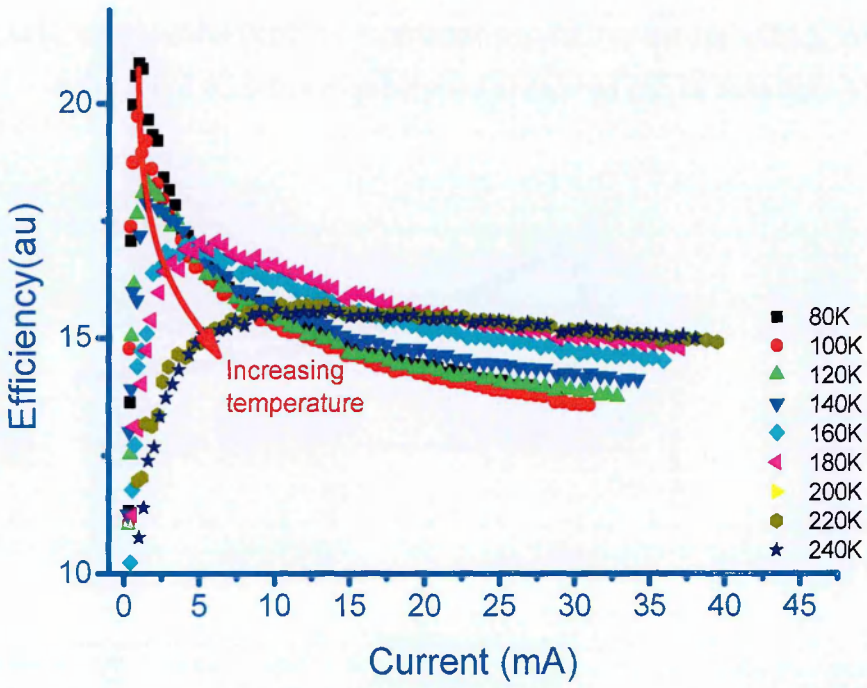

Figure 9-3- The electroluminescence efficiency dependence on current for different temperatures between 80K and 240K for a blue LED grown on a silicon substrate in pulsed mode with a pulse width of 2μs and a frequency of 10kHz

In agreement with the results of Figure 6-12 for an InGaN-based LED which is grown on sapphire with no EBL, the LEDs that are grown on silicon substrates (also with no EBL) have a peak efficiency which is the highest at the lowest temperatures. These results are in agreement with the poor performance of the blue and green LEDs grown on sapphire in Chapter 6 (see Figure 6-4) being due to the inclusion of EBLs. This shows that there is an enhanced non-radiative recombination process for devices which include EBLs due to the low injection of holes into the active region. The reduced rate at which the voltage for a fixed current increases with decreasing temperature for the devices on either silicon or sapphire substrates which do not include EBLs is due to less issues relating to hole injection. Figure 9-3 shows that the efficiency at a fixed current of 30mA increases with increasing temperature. Interestingly, the temperature-dependence of all the LEDs investigated in this study shows that the efficiency droop effect reduces with increasing temperature. This observation is likely to be attributed to an increase of the hole injection efficiency resulting in a reduction of field-

induced carrier leakage with increasing temperature. The reduction of the efficiency droop effect is found to continue as temperature is further increased above 240K as shown in Figure 9-4.

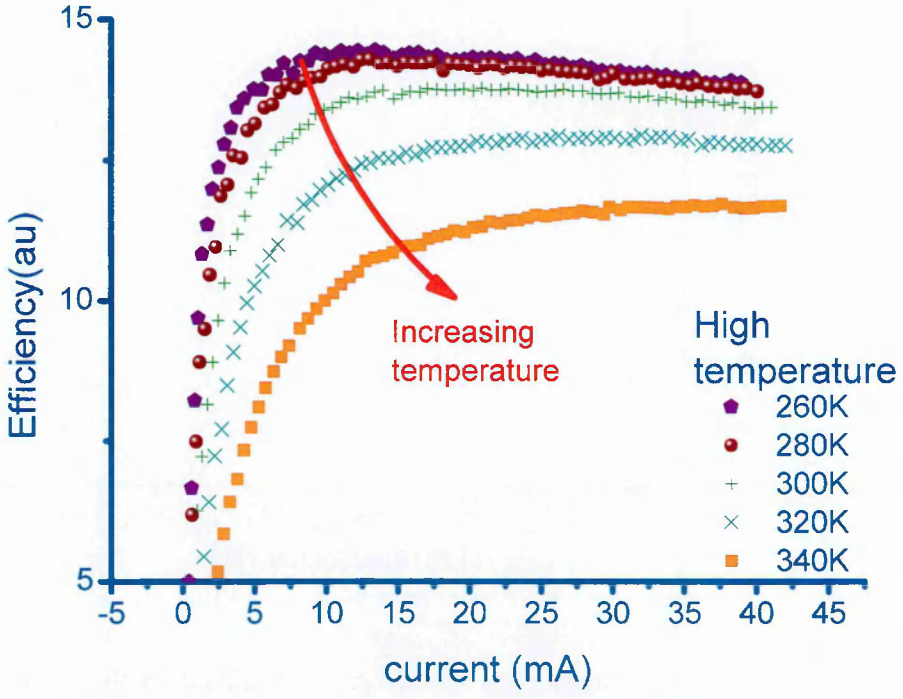

Figure 9-4- The electroluminescence efficiency dependence on current for a blue LED grown on silicon for temperatures above 260K in pulsed mode with a pulse width of 2μs and a frequency of 10kHz

The results are consistent with the results of Section 6.9 where the efficiency droop effect was also observed to be highly influenced by defect-related recombination at temperatures where there are expected to be no hole injection issues. In agreement with those results, it was found that the reduction in the peak efficiency with reducing temperature occurs at a larger rate that compared with the reducing rate of the efficiency at high currents. This is likely to be explained by the larger influence of the defect-related recombination at low currents. The increase of defect-related recombination with increasing temperature causes a reduction of efficiency at a fixed low current of 0.5mA as shown in Figure 9-5.

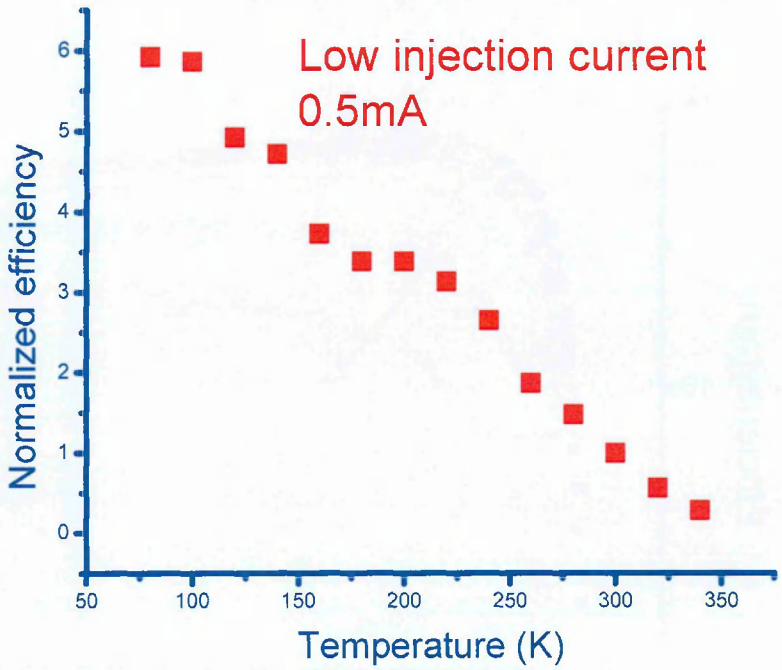

Figure 9-5- The electroluminescence efficiency normalized to the efficiency at 300K as a function of temperature for a blue LED grown on a silicon substrate in pulsed mode with a pulse width of 2μs and a frequency of 10kHz at a fixed current of 0.5mA.

The efficiency at a fixed current of 30mA, where there is a lower influence of active region band gap defect-related recombination, is observed to increase with increasing temperature from 80K to 240K before reducing with a further increase in temperature as shown in Figure 9-6.

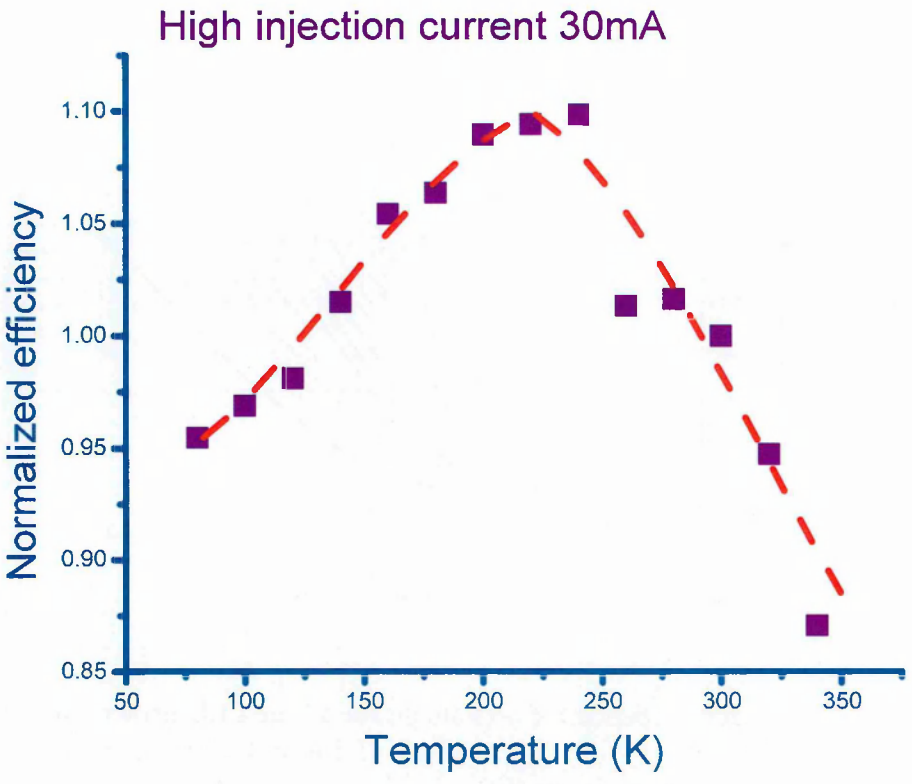

Figure 9-6- The electroluminescence efficiency normalized to the efficiency at 300K in pulsed mode with a pulse width of 2μs and a frequency of 10kHz at a fixed current 30mA at different temperatures.

The improvement of efficiency as temperature is increased from 80K to 240K may be explained by an improvement of hole injection. It is expected that the stronger influence of defect-related recombination as temperature is further increased above 240K causes the reduction in efficiency.

Figure 9-7 provides evidence that there are hole injection issues at low current due to a larger voltage required to achieve a fixed current with reducing temperature.

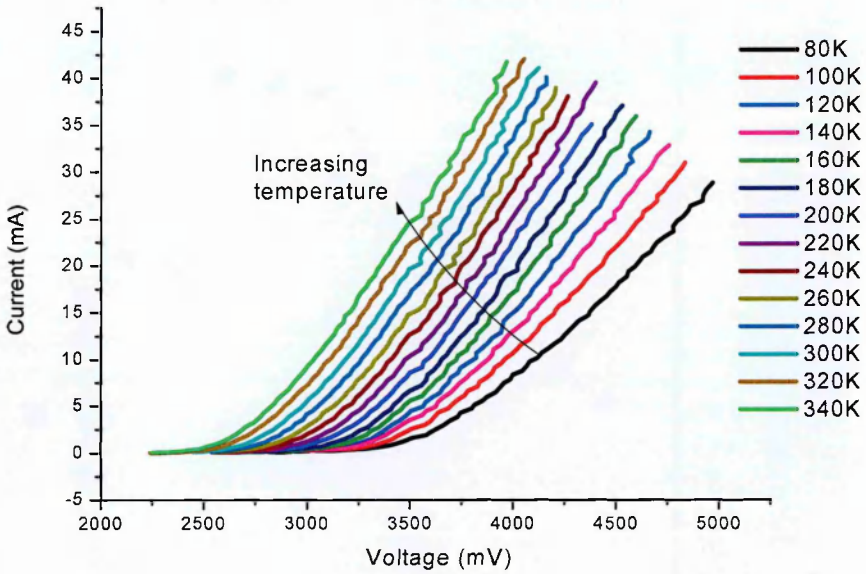

Figure 9-7- The current dependence on voltage for a blue LED grown on a silicon substrate in pulsed mode with a pulse width of 2μs and a frequency of 10kHz with no EBL at different temperatures

The larger rate at which the current increases with increasing voltage at higher temperatures may be explained by the improvement of the hole transport. This results in holes obtaining enough energy to overcome potential barriers leading to an improved distribution of holes among the quantum wells.

9.5 The pressure dependence of efficiency droop in devices grown on silicon substrates

Figure 9-8 shows that the application of pressure on the LEDs grown on silicon substrates has a similar impact as that for the devices grown on sapphire substrates (Figure 8-4) where the efficiency reduces over the entire current range with increasing pressure.

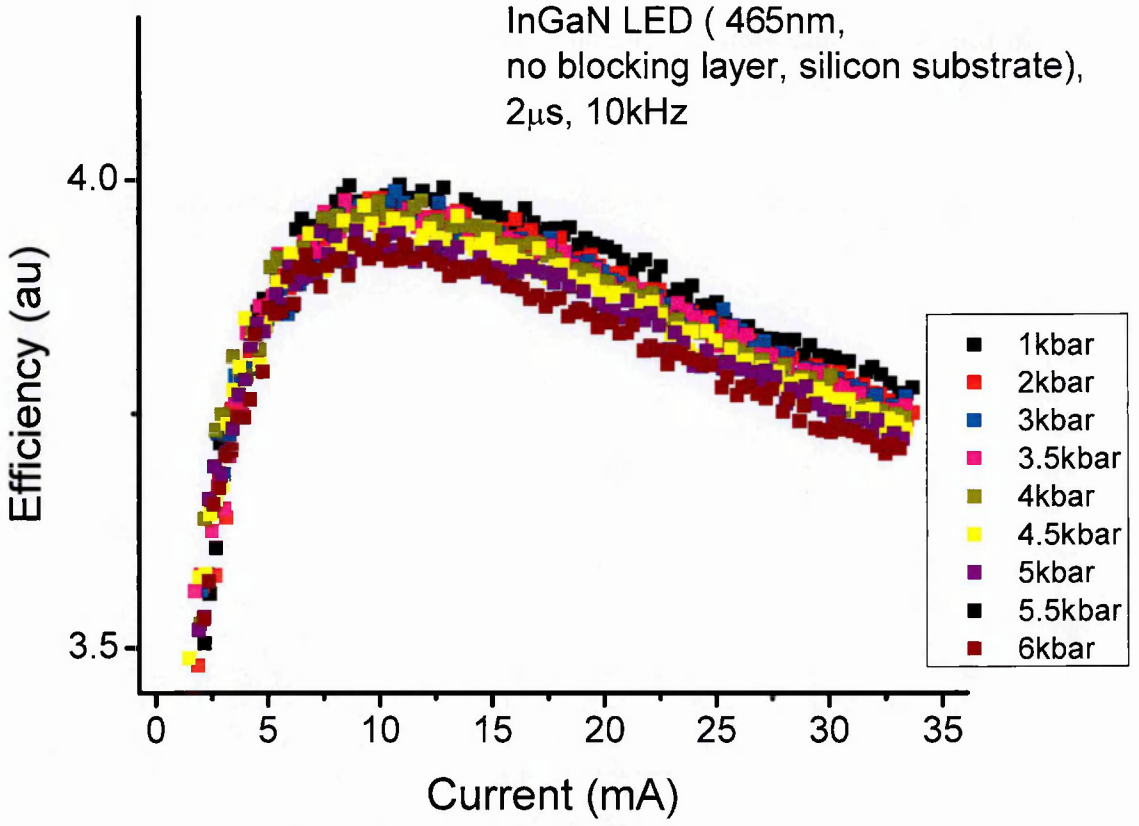

Figure 9-8- The electroluminescence efficiency dependence on current at different pressures for a blue LED which was grown on silicon in pulsed mode with a pulse width of 2μs and a frequency of 10kHz

As described in detail in Section 8.5, the reduction of efficiency is expected to be caused by the enhancement of the internal fields with increasing pressure that results in a reduction in the radiative recombination rate. The earlier current at which efficiency peaks is likely to be explained by an increased carrier concentration causing the filling of potential minima to occur at an earlier current as described in section 8.8. Subsequently, there will be an earlier onset current at which the defect-related recombination coefficient increases and hence an earlier current at which the efficiency droops. These results are also unlikely to be explained by carrier leakage as there would be a stronger reduction of efficiency with increasing pressure. The Auger recombination rate is also unlikely to explain this observation as there its rate is expected to reduce with increasing pressure.

9.6 InGaN Based Laser Diodes

In this section the temperature and pressure dependence of the optoelectronic properties in InGaN-based LDs will be presented. The LDs studies in this chapter are from a commercial source and therefore limited structural information was provided. Figure 9-9 shows the light output dependence on current at different temperatures for a violet LD.

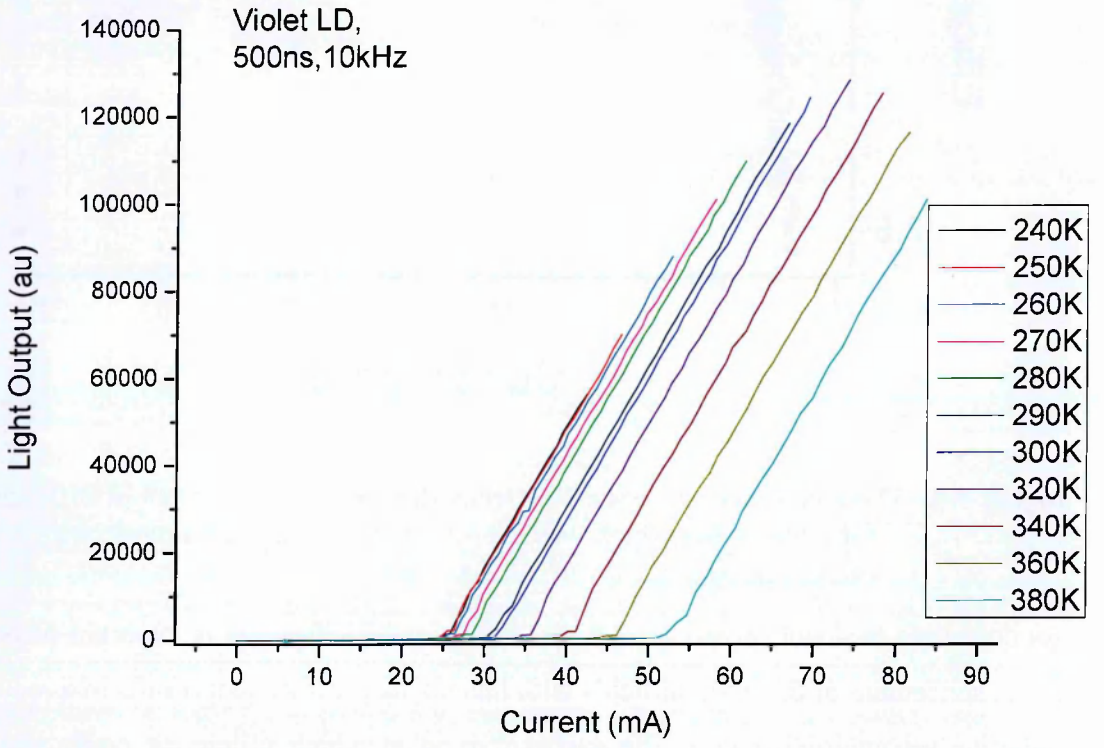

Figure 9-9- The electroluminescence light output dependence on current at different temperatures for a violet LD in pulsed mode with a pulse width of 500ns and a frequency of 10kHz

It is also important to note that the LDs did not lase at temperatures below 200K. This is expected to be consistent with the LED data whereby hole injection results in a low radiative recombination rate. The performance of the devices will therefore be limited at low temperatures if there is the inclusion of an EBL in the device structure. The poor hole injection is likely to cause the voltage at threshold current to increase with reducing temperature below 250K as shown in Figure 9-10.

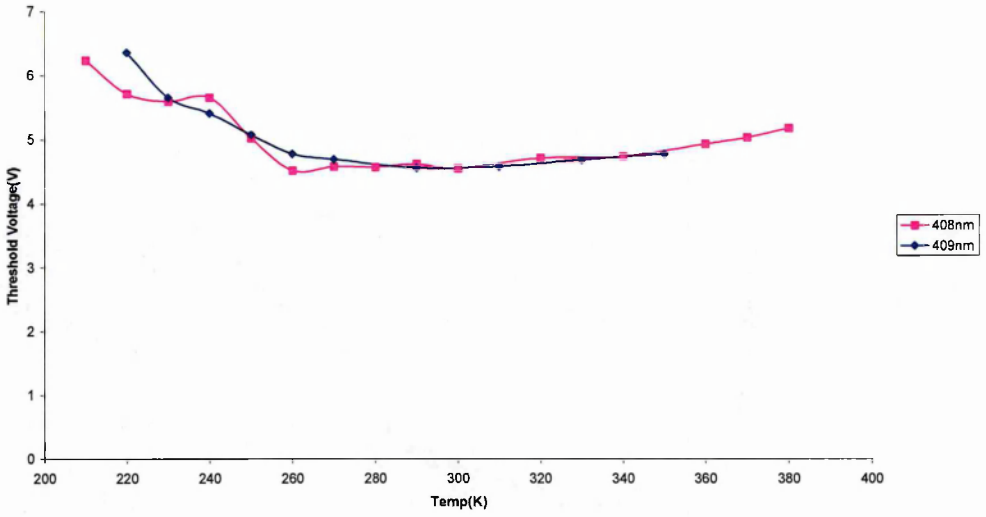

Figure 9-10- The voltage at threshold current as a function of temperature for a violet LD in pulsed mode with a pulse width of 500ns and a frequency of 10kHz

The diodes achieved lasing at temperatures above 200K. The threshold current was observed to increase with increasing temperature for a violet, blue and green LD as shown in Figure 9-11, Figure 9-12 , and Figure 9-13, respectively.

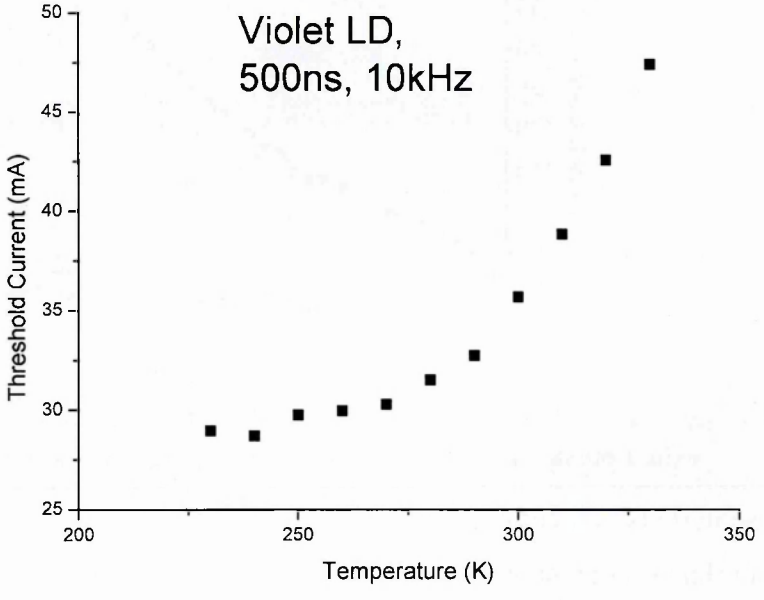

Figure 9-11- The threshold current dependence on temperature for a violet LD in pulsed mode with a pulse width of 500ns and a frequency of 10kHz

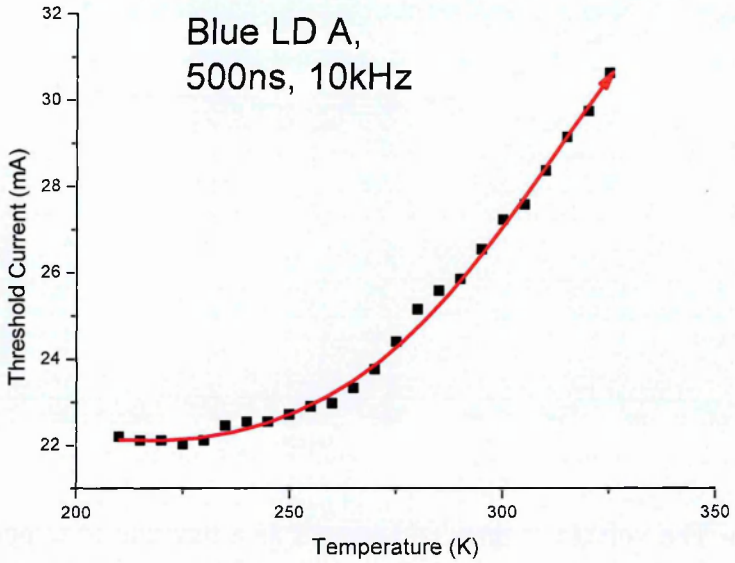

Figure 9-12- The threshold current dependence on temperature for a blue LD in pulsed mode with a pulse width of 500ns and a frequency of 10kHz

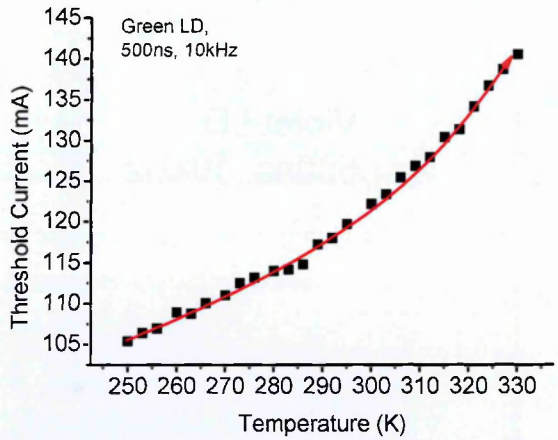

Figure 9-13-The threshold current dependence on temperature for a green LD in pulsed mode with a pulse width of 500ns and a frequency of 10kHz

The increase in threshold current with increasing temperature may be due to increasing defect-related recombination as shown in for InGaN LEDs in section 6.9. However, the effects of Auger recombination and carrier leakage may also cause this threshold current dependence. This is because the carrier concentration is much higher in LDs compared with LEDs and therefore these two higher order loss mechanisms may have a significantly stronger effect.

The external differential efficiency may be used to investigate the proportion of carriers injected into the well if the losses are assumed to be temperature insensitive as described in section 2.12.3 (equation 2-16). The differential external efficiency is determined by,

$$\eta_{ede} = \eta_i \left(\frac{\alpha_m}{\alpha_m + \alpha_i}\right) \qquad 9\text{-}1$$

where η_i is the injection efficiency, α_m is the mirror loss and α_i is the internal loss.

Figure 9-14 show that there is an approximately temperature insensitive external differential efficiency for violet, blue and green LDs, respectively.

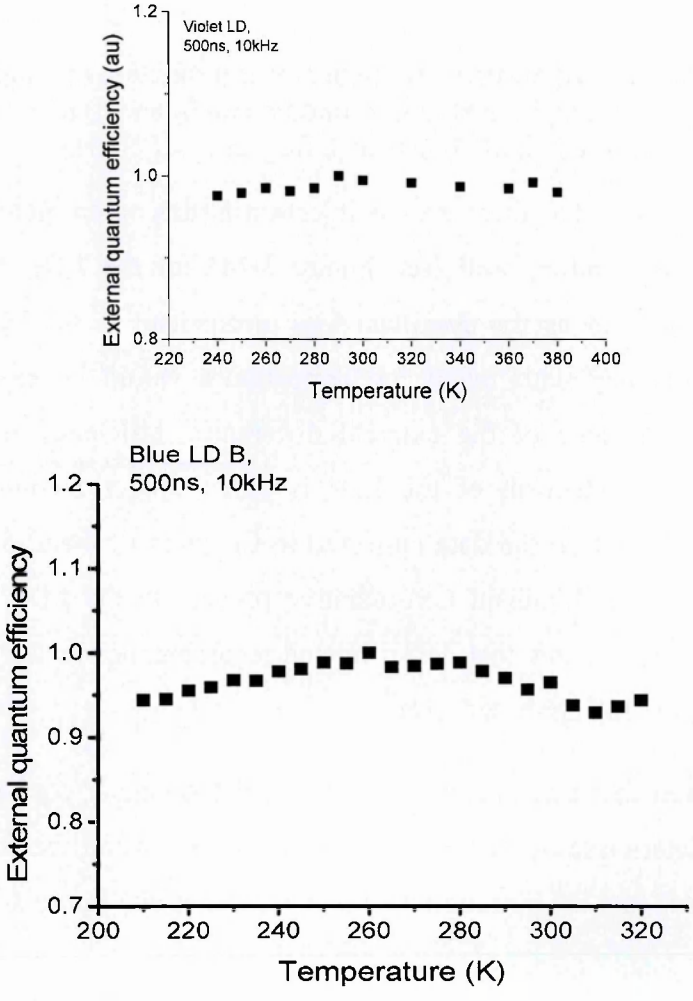

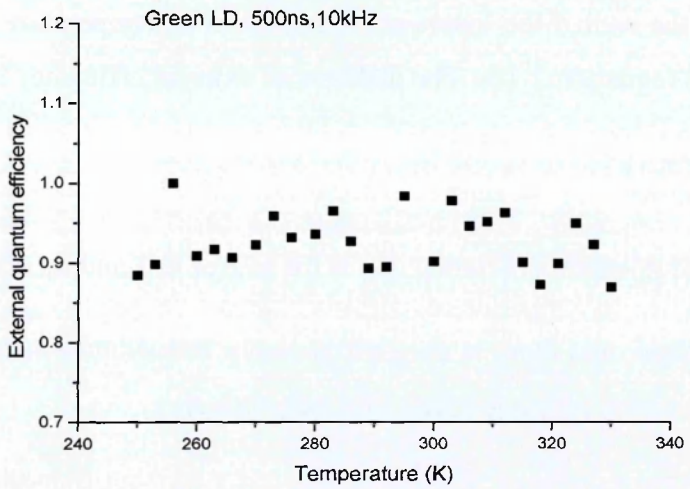

Figure 9-14-The external differential efficiency as a function of temperature for a violet LD (upper graph), a blue LD (middle graph) and c) a green LD in pulsed mode with a pulse width of 500ns and a frequency of 10kHz

These findings show that there are no injection issues or problems associated with carriers overshooting the quantum well (see Figure 3-14) for the LDs. It also shows that carrier leakage is unlikely to be the dominant loss mechanism in the LDs as a reducing external differential efficiency with increasing temperature would be expected to occur. A weak temperature dependence of the external differential efficiency is likely to show that the dominating loss mechanism of the LDs is either Auger recombination or defect-related recombination. Based on the data collected in Chapters 6, 7 and 8, it is unlikely that Auger recombination is the dominant non-radiative process in the LDs. The weak dependence is therefore expected to show that defect-related recombination is the dominant loss mechanism taking place in the InGaN-based LDs.

It must be noted that this analysis assumes that the carrier concentration pins at threshold current. The determination of whether this occurs is beyond the scope of this project, but a method to investigate the pinning effect is discussed in the future studies section of this thesis (Chapter 11).

9.7 Pressure dependence of InGaN-based LDs

The pressure coefficients of the LDs were calculated in a similar manner to those of the LEDs which are presented in Chapter 7. However, the pressure coefficient in the case of the LDs is

measured from the lasing emission energy which occurs above the threshold current where there is a large carrier concentration. Figure 9-15, Figure 9-16, and Figure 9-17 show the pressure coefficients for violet, blue and green LDs, respectively, are larger than those measured for the InGaN-based LEDs.

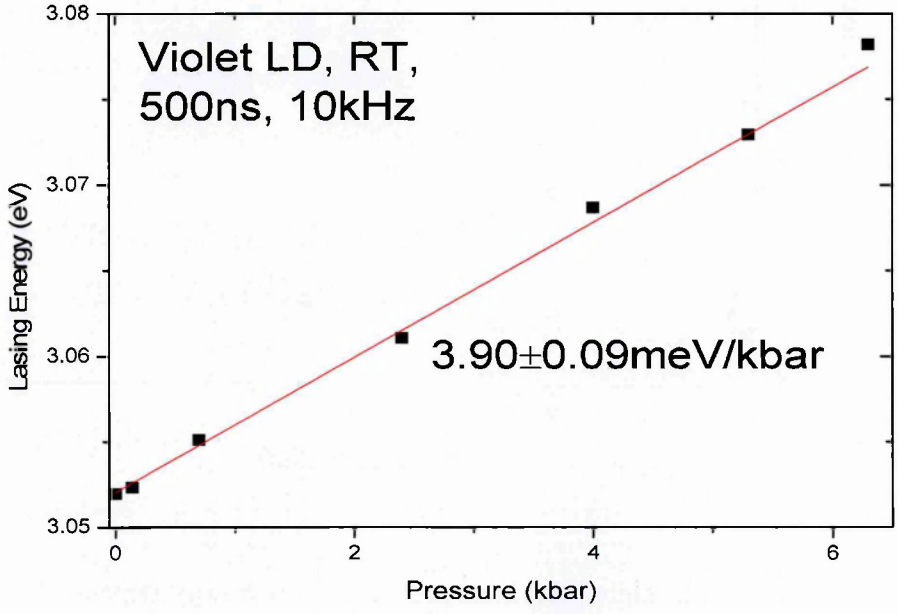

Figure 9-15- The lasing electroluminescence emission energy dependence on pressure for a violet LD in pulsed mode with a pulse width of 500ns and a frequency of 10kHz

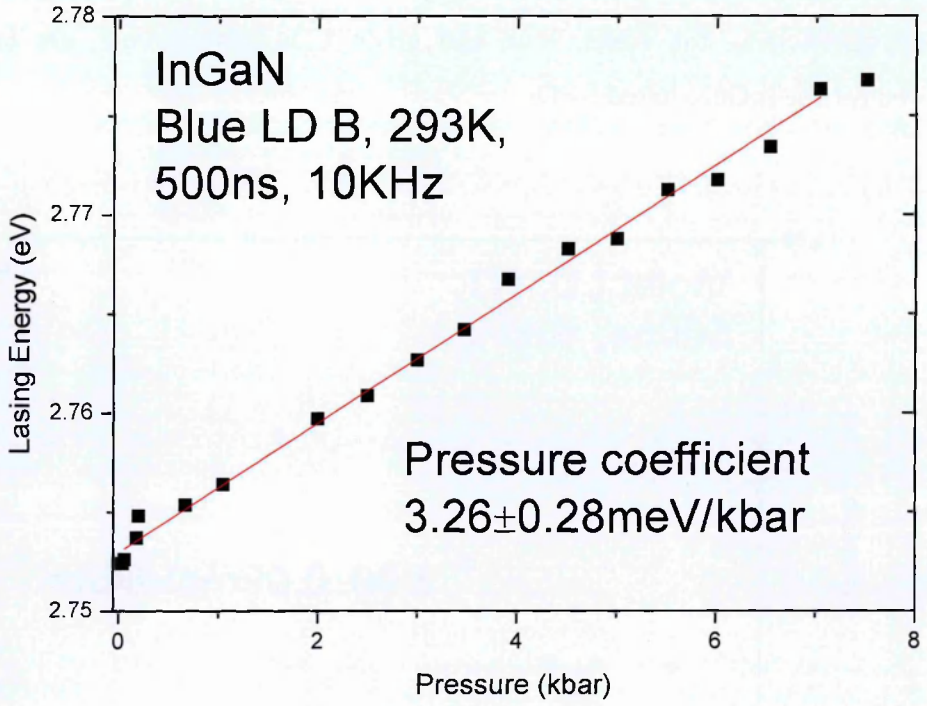

Figure 9-16- The lasing electroluminescence emission energy dependence on pressure for a blue LD in pulsed mode with a pulse width of 500ns and a frequency of 10kHz

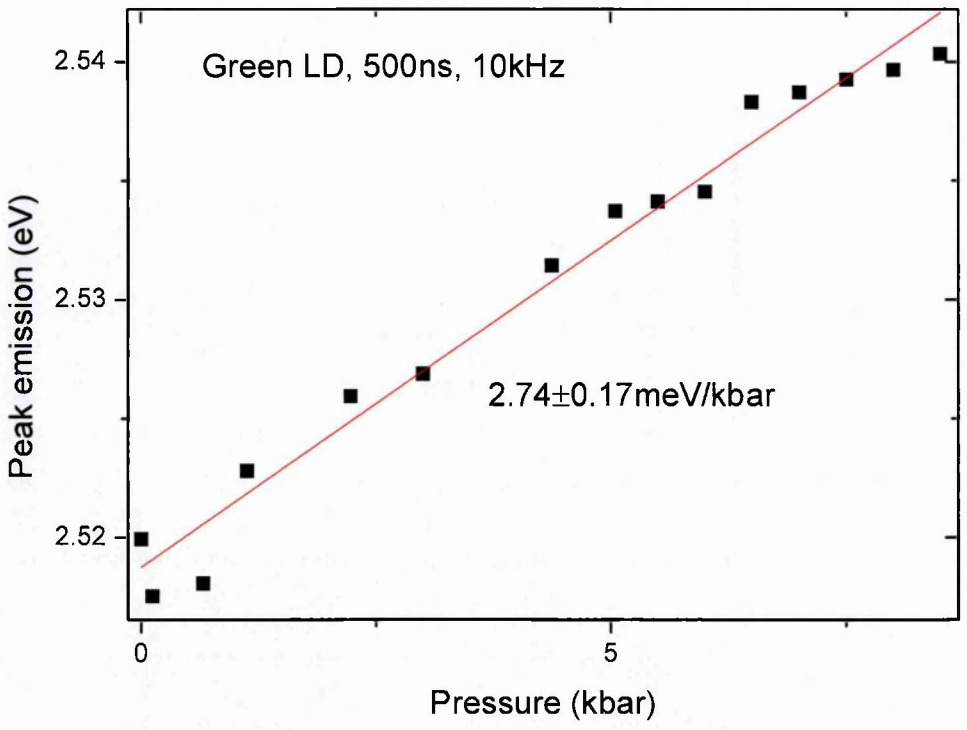

Figure 9-17- The electroluminescence lasing emission energy as a function of pressure for a green LD in pulsed mode with a pulse width of 500ns and a frequency of 10kHz

The stronger pressure coefficients indicate that there is efficient carrier screening of the internal polarization fields at threshold current.

9.8 Dependence of the threshold current on pressure

The threshold current is found to increase with increasing pressure in violet, blue and green LDs as shown in Figure 9-18, Figure 9-19 and Figure 9-20, respectively.

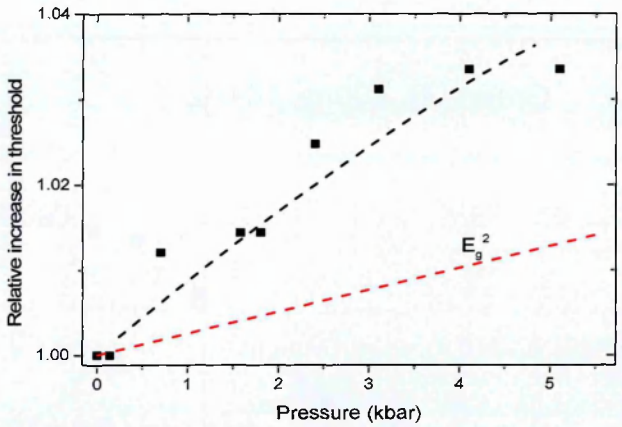

Figure 9-18- The threshold current dependence on pressure for a violet LD in pulsed mode with a pulse width of 500ns and a frequency of 10kHz where the red line represents the square of the band gap energy as a function of pressure

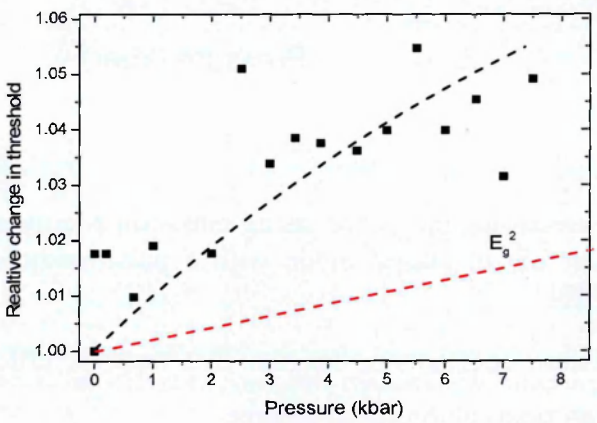

Figure 9-19- The threshold current dependence on pressure for a blue LD in pulsed mode with a pulse width of 500ns and a frequency of 10kHz where the red line represents the square of the band gap energy as a function of pressure

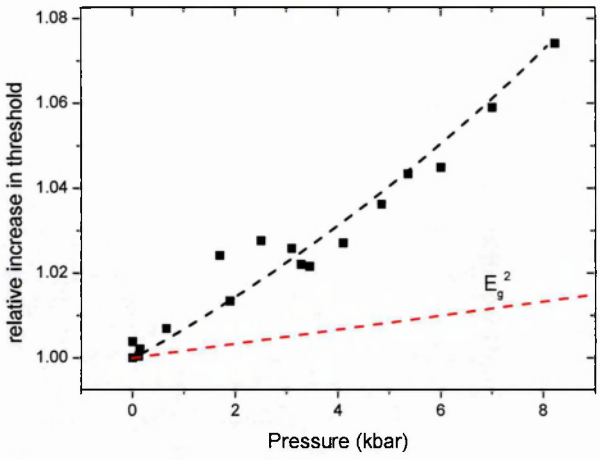

Figure 9-20- The threshold current dependence on pressure for a green LD in pulsed mode with a pulse width of 500ns and a frequency of 10kHz where the red line represents the square of the band gap energy as a function of pressure

The radiative recombination is expected to increase with pressure at a rate proportional to E_g^2. The threshold current would also be expected to increase at a rate that is proportional to the square of the band gap if radiative recombination was the dominant recombination mechanism (as shown by the red line in the graphs). The threshold current is observed to increase at a rate which is larger than this and therefore signifies that there is a loss process which is enhanced with increasing pressure. The result shows that Auger recombination is unlikely to be the dominant recombination process in the InGaN LDs as this loss process is expected to reduce with increasing pressure (see Section 8.7) and would therefore also cause the threshold current to have a weaker dependence on pressure than the radiative recombination.

The threshold current dependence is also not consistent with inter-conduction band Auger recombination as the blue LD moves away from the Auger resonance with increasing pressure and therefore the threshold current would be expected to be less than that of the radiative recombination. Similarly the application of pressure will also move the band gap energy of the green LD (~2.52eV at ambient conditions) away from the resonance causing a strong reduction of the inter-conduction band Auger recombination rate as shown in Figure 9-21.

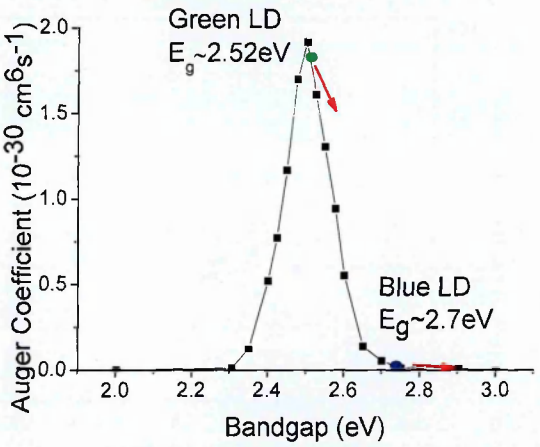

Figure 9-21- The theoretically calculated Auger coefficient as a function of bandgap energy due to interband Auger recombination where the arrows represent the effect of pressure on the band gap energies of the blue and green LDs.

The results are therefore not consistent with interconduction band Auger recombination. Consistent with the findings shown earlier in this thesis, the increase in the threshold current with increasing pressure is expected to be due to an increase in the defect-related recombination rate. This is due to the fact that the defect sites in the GaN barrier are expected to have a weak dependence on pressure and therefore the application of pressure causes the Fermi level within the quantum well to move towards the defect level. Such an effect will lead to the enhancement of the defect-related recombination rate and an increase of the threshold current.

9.9 Chapter summary

The aim of this chapter was to explore the recombination mechanisms of devices which are expected to have a big impact in the future nitride-based device industry. The first section of the chapter investigates InGaN-based LEDs grown on silicon substrates which have reduced production costs in comparison with InGaN-based LEDs grown on sapphire substrates. It is observed that whilst there is a reduced efficiency droop effect in the LEDs grown on silicon substrates in comparison with that of LEDs grown on sapphire, there is also a lower efficiency over the entire current range. The relatively poor efficiency of the LEDs grown on silicon is expected to be the result of a high threading dislocation density which is caused by a large lattice constant mismatch between the GaN layer and the silicon substrate. It is shown that there is a high influence of defect-related recombination on the light output performance of

these LEDs as the peak efficiency reduces with increasing temperature. This is expected to be due to the localization of carriers away from defect sites at low temperatures. In agreement with the results of chapter 6 the efficiency droop effect becomes more severe with reducing temperature. This is expected to be due to hole injection issues leading to a strong electron leakage rate for all of the LEDs investigated in this thesis. It is also found that there is an increase in the influence of defect-related recombination with increasing temperature at temperatures where hole injection is not expected to be problematic for the LEDs grown on either silicon or sapphire substrates. Similar findings are found for the pressure dependence of the LEDs which are grown on silicon as those grown on sapphire as the efficiency reduces almost equally over the entire current range with increasing pressure. The results are expected to be explained by a reduction in the radiative recombination rate due to the enhancement of the piezoelectric fields with increasing pressure. This will subsequently result in an increasing proportion of defect-related recombination for a given current as discussed in further in Chapters 7 and 8.

In the final section of this chapter the findings on the temperature and pressure dependence of the optoelectronic properties in violet, blue and green InGaN-based LDs are presented. Hole injection issues are also found to occur in the LDs at low temperature as all the LDs did not lase. It was found that all the LDs exhibit an increasing threshold current with increasing temperature above 200K. Such behaviour is expected to be the result of an increasing rate of defect-related recombination with increasing temperature. The external differential efficiency, which represents the efficiency of the laser above threshold current, was observed to have weak temperature dependence for the LDs and provides further support that the dominant recombination process is defect-related in the LDs.

The stronger pressure coefficients in InGaN LDs compared with those of the InGaN LEDs indicates that there is efficient carrier screening of the internal polarization field effects in the LDs. It was also observed that there is an increase in the threshold current with increasing pressure for all the LDs and is in agreement with the temperature dependent data that defect-related recombination is the dominant non-radiative process in InGaN.

The findings of this chapter indicate that defect-related recombination and the internal polarization field strength have a strong impact on the light output power of LEDs grown on silicon substrates and InGaN-based LDs. The enhancement of the efficiency of LEDs grown

on silicon substrates and the reduction of the threshold current in LDs will therefore be achieved by reducing the proportion of defect-related recombination through improvements of device growth. Efforts should also be made to reduce the internal polarization field that will enhance the radiative recombination rate in InGaN-based light emitters.

10 Conclusions

The beginning of this thesis introduced relevant semiconductor theory that may be used to describe the operation of the devices investigated in this study. It was shown that the density of available states in the conduction and valence bands are multiplied by the Fermi function in order to obtain the carrier concentrations of the bands. Doping is shown to be a necessary process in order to achieve efficient devices. The inclusion of a material with a relative reduced band gap energy is found to achieve efficient carrier and light confinement. Other methods are also presented to enhance the efficiency of such devices such as the inclusion of the epoxy encapsulates which increases the extraction efficiency by 50%.

The next chapter introduced the efficiency droop effect which occurs in nitride-based devices. It was shown that there is a relative reduction in efficiency as a function of current following a low current peak in an effect is shown to be stronger for green LEDs compared with blue LEDs. The main arguments which have been presented as the cause of efficiency droop including Auger recombination, carrier leakage and a defect-related recombination process are described. Many studies show that the measured efficiency dependence on current may be modelled using an ABC model whereby the only recombination processes are defect-related, radiative and Auger recombination. Whilst there is good agreement with this model and the experimentally measured droop effect, the physical reason for an Auger recombination coefficient which is orders of magnitude higher than expected remains unknown. Groups have suggested that the high Auger coefficient may be attributed to a phonon-assisted process, where there is an increase in the phonon-assisted Auger recombination rate due to the relaxation of energy and momentum laws. However, other studies have calculated that even including the phonon-assisted contributions the Auger recombination coefficient will be negligible at the low currents at which efficiency droop begins. Previous studies have also shown that devices which include an electron blocking layer to prevent electron leakage will have a larger efficiency at high currents compared with devices which do not consist of electron blocking layers. However, other studies have found that the efficiency droop effect is stronger in devices which contain electron blocking layers that may be attributed to poor hole injection that leads to an enhanced droop effect.

The temperature and pressure dependence of InGaN-based devices is presented in this thesis. Observations suggest that the performance of the devices at low temperature is limited by poor

hole injection which subsequently leads to strong electron leakage at low temperature. Poor hole injection is expected to cause an increasing in the required voltage to achieve a set current with decreasing temperature. A stronger blueshift in the emission peak for a fixed current range below where the efficiency peaks with reducing temperature is presented. This is expected to be due to an increasing internal field with reducing temperature. This effect is found to be stronger for the green LED compared with the blue LED. The existence of an additional emission peak in the spectra of the green LED at low temperature is also consistent with a stronger leakage effect in the green LED. The reducing electron leakage rate with increasing temperature is expected to be the result of improving hole injection efficiency due to the higher thermal energy of the holes facilitating hole transportation. At temperatures where the improved hole injection efficiency saturates, a strong influence of an increasing defect-related recombination rate on the performance of the LEDs occurs as the efficiency is observed to reduce with increasing temperature over the entire current range.

The peak emission is found to have an "s-shape" dependence on temperature which is consistent with carrier localization taking place in the InGaN-based LEDs in an effect with is stronger for the green LED. The carrier localization is expected to result from well width fluctuations and indium fluctuations due to being a random alloy which result in a fluctuating band gap. Such effects are expected to be enhanced in InGaN due to the high internal strain and piezoelectric fields which exist. Further evidence of indium fluctuations in InGaN is found in the relatively weak pressure dependence of the peak emission in electroluminescence measurements for both the blue and green LEDs compared with GaN and InN. The weaker pressure coefficient of the green LED compared with the blue LED is expected to also indicate stronger indium clustering effects.

Based on the findings a defect-related cause of efficiency droop is proposed. This is due to the fact that there is expected to be a relative low proportion of defect-related recombination at low currents where there is a strong localization of carriers. As there is carrier delocalization there is an increase in the defect-related recombination rate. This will consequently reduces the efficiency with increasing current density. A model is presented whereby there is an increase in the defect-related recombination coefficient, A, and a reduction in the radiative recombination coefficient, B with increasing current. This model is shown to be fitted to the experimentally measured droop behaviour for the blue and green LEDs. The droop behaviour with increasing temperature may also be fitted using this model for temperatures provided that

there are no hole injection problems. Measurements of efficiency droop at low and high pressures are also described using this model. The enhancement of the piezoelectric field strength with increasing pressure causes an increase to the quantum confined Stark effect that will result in an increasing separation of the electron and hole wavefunction overlap that subsequently reduces the radiative coefficient. The reduced radiative recombination rate with increasing pressure is expected to cause an increase to the carrier concentration at a fixed current that will result in a lower current required in order for potential minima to be filled. This will cause an earlier efficiency droop onset current but the efficiency droop will remain approximately pressure insensitive.

In the final chapter of this thesis the temperature and pressure dependence of InGaN-based LEDs which are grown on silicon substrates and InGaN-based laser diodes are presented. Both of these devices are expected to have a strong impact on the future nitride semiconductor industry. The results are consistent with those of the study of LEDs where defect-related recombination is expected to be the dominant loss mechanism influencing the light output performance of InGaN-based light emitters. Improvements to the growth techniques used to produce the devices, in addition to a reduction of the internal polarization field strength, must therefore be made in order to produce devices of higher efficiency.

11 Future Studies into InGaN-based emitters

This section describes relevant experiments that could be used to build on the findings of this thesis. The temperature dependence of InGaN-based LEDs (Chapter 6) revealed that carrier leakage is likely to be enhanced with decreasing temperature and will result in a strong droop effect. The carrier leakage at low temperature is expected to be caused by poor hole injection. It would therefore be useful to grow a set of devices which could probe the effects of hole transportation at different temperatures. This could be achieved by the growth of a device which consists of quantum wells of different energies as illustrated in Figure 11-1.

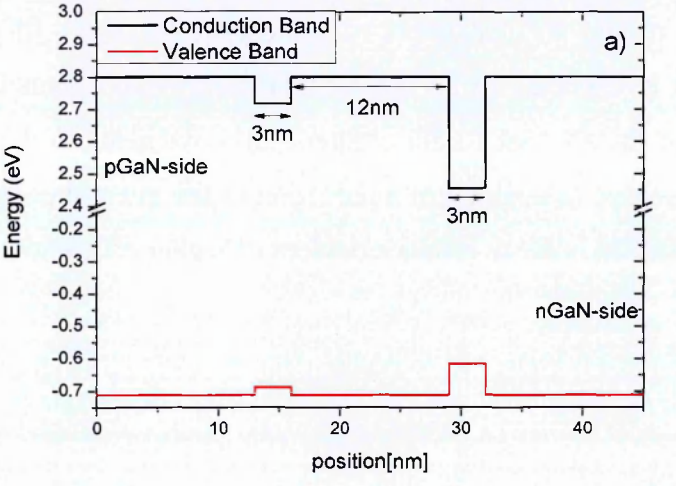

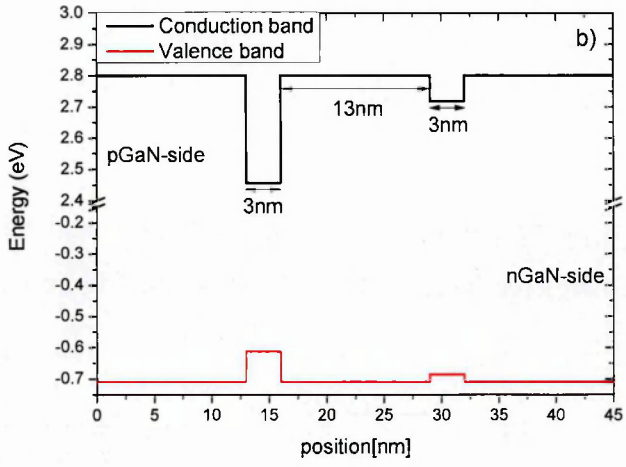

Figure 11-1- Band structure of proposed devices to investigate carrier leakage where device a) consists (a) consisting of 5% indium content (400nm) for quantum well 1 (2nm) and 20% indium content (470nm) in quantum well 2 (3nm) and (b) consisting of consisting of 20% indium content (470nm) quantum well 1 (3nm) and a 5% indium content (400nm) for quantum well 2 (3nm). The barriers in all the structures are 13nm

There are inconsistencies in the literature to whether the radiative recombination occurs across all the quantum wells or only the quantum well closest to the pGaN side of the active region. Spectroscopy measurements on the electroluminescence emission from the structures illustrated in Figure 11-1 could be used to show where the radiative recombination occurs. Most of its recombination is expected to occur in the quantum well on the nGaN side of the device shown in Figure 11-1(a). The spectroscopy measurement will therefore be able to show whether this is the case over the entire temperature range. The structure shown in Figure 11-1(b) is the reverse of that in Figure 11-1(a) and would therefore be expected to have stronger emission from the quantum well on the nGaN side of the quantum well. It would therefore be interesting to observe whether there is emission from the pGaN side quantum well at high temperatures. Photoluminescence measurements could also be employed on the structures with lasing emission energy which corresponds to a slightly higher energy to that of the lowest energy quantum well. This would be able to investigate at which temperatures there will be leakage from the quantum well of lower energy to the higher energy quantum well.

The pressure range that is applied to the InGaN-based commercial blue-green LED (Chapters 7 and 8) may be extended by using a new method that is currently being developed at the University of Surrey. This method uses a sapphire ball system to apply pressures up to 30kbar and would therefore be able to increase the pressure range by three times the amount as the

applied pressure investigated in this thesis. Such measurements would be used to confirm whether the measurements from this study will continue for larger applied pressures. This method of applying pressure would also be ideal to take absorption measurements as a function of pressure which could further measure the effects of the internal fields.

Another extension to the pressure-dependent findings would be the growth of devices with quantum wells of staggered indium content as shown in Figure 11-2.

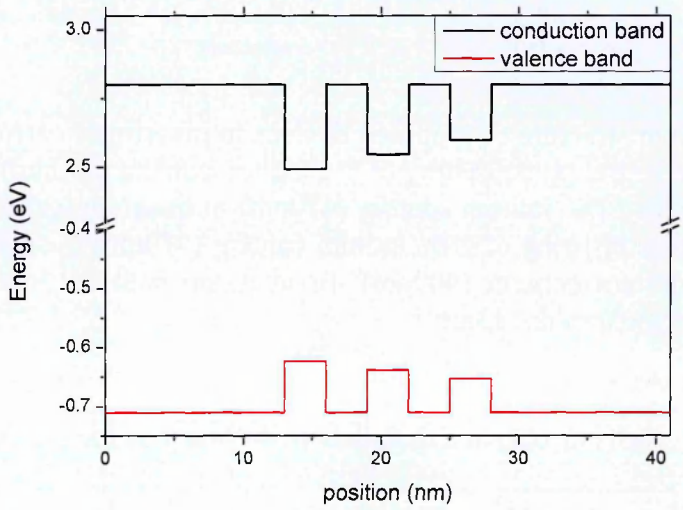

Figure 11-2- The growth of a device with quantum wells which have staggered indium content of 18%, 15%, 12% for 2nm quantum well width with quantum barriers of 3nm.

There is expected to be an increase in the radiative recombination rate with increasing pressure for the structure presented in Figure 11-2. This is due to the weaker pressure coefficient of the quantum well closest to the nGaN in comparison with that of the pGaN side leading to a larger overlap of the electron and hole wavefunction overlap. In this structure there is a small barrier width (3nm) to enhance the coupling between the quantum wells. An additional device could be grown which has the staggered quantum wells in the opposite direction (i.e. the lowest indium quantum well is positioned nearest to the nGaN side of the device). Applying pressure would have the opposite effect where the electron and hole wavefunction overlap will reduce leading to a reduced radiative recombination rate. These measurements could be used to determine whether the growth of staggered quantum wells is a viable method to produce high efficient InGaN-based devices.

The investigations into the temperature and pressure dependence of the InGaN-based laser diodes (LDs) could also be further investigated. As the LDs investigated in Chapter 9 were produced in their experimental stage, further investigations may be made on LDs which are now currently commercially-available and expected to have higher efficiencies. Photoluminescence measurements as a function of temperature could also be used to determine whether indium inhomogeneities play a role in the lasing emission. This could be achieved by measuring the peak emission energy for a relatively high beam intensity to observe whether there is "s-shape" or Varshni dependence with increasing temperature. Similarly, the peak emission energy in electroluminescence measurements at low and high currents could be used to investigate the influence of indium inhomogeneities in the spontaneous and stimulated emission, respectively. Investigating the pressure coefficient below and above threshold current could also provide additional information about the effects of indium clustering on the lasing emission. The simultaneous measurements of spontaneous ad stimulated emission over different temperature and pressure conditions would also provide further information about the recombination dynamics of InGaN LDs. The spontaneous emission of LDs may be measured by collecting emission through the GaN substrate (if less than 7μm as GaN will be transparent for a device consisting of top contacts) or by measuring the emission through a window that is fabricated by the use of a FIB technique which was developed at the University of Surrey. These experiments would also be able to investigate the efficiency droop effect in InGaN LDs under various conditions.

12 References

[1] S. Nakamura, in *The blue laser diode: The complete story*, ed New York: Springer, 2000, p. 16.

[2] U. Lafont, H. v. Zeijl, and S. v. d. Zwaag, "Increasing the reliability of solid state lighting systems via self-healing approaches: A review," *Microelectronics Reliability*, vol. 52, pp. 71-89, 2012.

[3] http://www.semiconductor-today.com/news_items/2010/APRIL/YOLE_140410.htm, April 2010.

[4] R. Haitz and J. Y. Tsao, "Solid-state lighting," *Optik & Photonik*, vol. 6, pp. 26-30, 2011.

[5] http://www.digikey.co.uk/product-detail/en/XPGWHT-L1-0000-00F53/XPGWHT-L1-0000-00F53TR-ND/2171902?cur=GBP, October 2012.

[6] J. K. Kim and E. F. Schubert, "Transcending the replacement paradigm of solid-state lighting," *Opt. Express*, vol. 16, pp. 21835-21842, 2008.

[7] http://www.amazon.com/Philips-409904-Dimmable-AmbientLED-12-5-Watt/dp/B004IUMGV4/, October 2012.

[8] http://www.amazon.com/97490-60-Watt-870-Lumen-Crystal-2-Pack/dp/B00006IBEH/ref=sr_1_13?s=hi&ie=UTF8&qid=1349601603&sr=1-13&keywords=60+watt+incandescent, October 2012.

[9] http://www.amazon.com/74198-13-Watt-Energy-60-Watt-Output/dp/B002GK0O3A/, October 2012.

[10] M. H. Crawford, "LEDs for Solid-State Lighting: Performance Challenges and Recent Advances," *Selected Topics in Quantum Electronics, IEEE Journal of*, vol. 15, pp. 1028-1040, 2009.

[11] http://www.guardian.co.uk/environment/2012/aug/31/lightbulbs-incandescent-europe, August 2012.

[12] http://gigaom.com/cleantech/ikea-to-sell-only-leds-by-2016/, October 2012.

[13] www.colorkinetics.com/support/whitepapers/LEDLifetime.pdf, October 2012.

[14] I. Eliashevich, Y. Li, A. Osinsky, C. A. Tran, M. G. Brown, and J. R. F. Karlicek, "InGaN blue light-emitting diodes with optimized n-GaN layer," pp. 28-36, 1999.

[15] J. Piprek, in *Semiconductor Optoelectronic devices: Introduction to Physics and Simulation*, ed San Diego: Academic Press, 2003, p. 133.

[16] J. W. Raring, E. M. Hall, M. C. Schmidt, C. Poblenz, B. Li, N. Pfister, D. F. Feezell, R. Craig, J. S. Speck, S. P. DenBaars, and S. Nakamura, "High-power high-efficiency continuous-wave InGaN laser diodes in the violet, blue, and green wavelength regimes," San Francisco, California, USA, 2010, pp. 760218-10.

[17] E. F. Schubert, "Light-Emitting Diodes," ed New York: Cambridge Univeristy Press, 2003, p. 94.

[18] J. Piprek, in *Semiconductor Optoelectronic devices: Introduction to Physics and Simulation*, ed San Diego: Academic Press, 2003, p. 94.

[19] J.-K. Sheu, Y. S. Lu, M.-L. Lee, W. C. Lai, C. H. Kuo, and C.-J. Tun, "Enhanced efficiency of GaN-based light-emitting diodes with periodic textured Ga-doped ZnO transparent contact layer," *Applied Physics Letters*, vol. 90, p. 263511, 2007.

[20] P. M. Smowton and P. Blood, "The differential efficiency of quantum-well lasers," *Selected Topics in Quantum Electronics, IEEE Journal of*, vol. 3, pp. 491-498, 1997.

[21] P. M. Smowton and P. Blood, "Fermi level pinning and differential efficiency in GaInP quantum well laser diodes," *Applied Physics Letters*, vol. 70, pp. 1073-1075, 1997.

[22] E. F. Schubert, "Light-Emitting Diodes," ed New York: Cambridge Univeristy Press, 2003, pp. 48-51.

[23] P. G. Eliseev, M. Osinski, H. Li, and I. V. Akimova, "Recombination balance in green-light-emitting GaN/InGaN/AlGaN quantum wells," *Applied Physics Letters,* vol. 75, pp. 3838-3840, 1999.

[24] J. Hader, J. V. Moloney, and S. W. Koch, "Beyond the ABC: carrier recombination in semiconductor lasers," San Jose, CA, USA, 2006, pp. 61151T-7.

[25] R. Olshansky, C. Su, J. Manning, and W. Powazinik, "Measurement of radiative and nonradiative recombination rates in InGaAsP and AlGaAs light sources," *Quantum Electronics, IEEE Journal of,* vol. 20, pp. 838-854, 1984.

[26] J. Hader, J. V. Moloney, and S. W. Koch, "Density-activated defect recombination as a possible explanation for the efficiency droop in GaN-based diodes," *Applied Physics Letters,* vol. 96, p. 221106, 2010.

[27] A. David and M. J. Grundmann, "Droop in InGaN light-emitting diodes: A differential carrier lifetime analysis," *Applied Physics Letters,* vol. 96, pp. 103504-3, 2010.

[28] J. Piprek, "Efficiency droop in nitride-based light-emitting diodes," *physica status solidi (a),* vol. 207, pp. 2217-2225, 2010.

[29] R. Fehse, S. Tomic, A. R. Adams, S. J. Sweeney, E. P. O'Reilly, A. Andreev, and H. Riechert, "A quantitative study of radiative, Auger, and defect related recombination processes in 1.3-μm GaInNAs-based quantum-well lasers," *Selected Topics in Quantum Electronics, IEEE Journal of,* vol. 8, pp. 801-810, 2002.

[30] M. F. Schubert, S. Chhajed, J. K. Kim, E. F. Schubert, D. D. Koleske, M. H. Crawford, S. R. Lee, A. J. Fischer, G. Thaler, and M. A. Banas, "Effect of dislocation density on efficiency droop in GaInN/GaN light-emitting diodes," *Applied Physics Letters,* vol. 91, p. 231114, 2007.

[31] Y. C. Shen, G. O. Mueller, S. Watanabe, N. F. Gardner, A. Munkholm, and M. R. Krames, "Auger recombination in InGaN measured by photoluminescence," *Applied Physics Letters,* vol. 91, pp. 141101-3, 2007.

[32] B. Pasenow, S. W. Koch, J. Hader, J. V. Moloney, M. Sabathil, N. Linder, and S. Lutgen, "Auger losses in GaN-based quantum wells: Microscopic theory," *physica status solidi (c),* vol. 6, pp. S864-S868, 2009.

[33] E. Kioupakis, P. Rinke, K. T. Delaney, and C. G. V. d. Walle, "Indirect Auger recombination as a cause of efficiency droop in nitride light-emitting diodes," *Applied Physics Letters,* vol. 98, p. 161107, 2011.

[34] A. Laubsch, M. Sabathil, J. Baur, M. Peter, and B. Hahn, "High-Power and High-Efficiency InGaN-Based Light Emitters," *Electron Devices, IEEE Transactions on,* vol. 57, pp. 79-87, 2010.

[35] M. Brendel, A. Kruse, H. Jonen, L. Hoffmann, H. Bremers, U. Rossow, and A. Hangleiter, "Auger recombination in GaInN/GaN quantum well laser structures," *Applied Physics Letters,* vol. 99, pp. 031106-3, 2011.

[36] K. T. Delaney, P. Rinke, and C. G. V. d. Walle, "Auger recombination rates in nitrides from first principles," *Applied Physics Letters,* vol. 94, p. 191109, 2009.

[37] F. Bertazzi, M. Goano, and E. Bellotti, "A numerical study of Auger recombination in bulk InGaN," *Applied Physics Letters,* vol. 97, pp. 231118-231118-3, 2010.

[38] T. Uenoyama, "Excitonic enhancement of optical gain in quantum wells," *Physical Review B,* vol. 51, pp. 10228-10231, 1995.

[39] E. Kioupakis, P. Rinke, A. Schleife, F. Bechstedt, and C. G. Van de Walle, "Free-carrier absorption in nitrides from first principles," *Physical Review B,* vol. 81, p. 241201, 2010.

[40] M. Zhang, P. Bhattacharya, J. Singh, and J. Hinckley, "Direct measurement of auger recombination in In[sub 0.1]Ga[sub 0.9]N/GaN quantum wells and its impact on the efficiency of In[sub 0.1]Ga[sub 0.9]N/GaN multiple quantum well light emitting diodes," *Applied Physics Letters,* vol. 95, p. 201108, 2009.

[41] M. Meneghini, N. Trivellin, G. Meneghesso, E. Zanoni, U. Zehnder, and B. Hahn, "A combined electro-optical method for the determination of the recombination parameters in InGaN-based light-emitting diodes," *Journal of Applied Physics,* vol. 106, pp. 114508-114508-4, 2009.

[42] W. G. Scheibenzuber, U. T. Schwarz, L. Sulmoni, J. Dorsaz, J. F. Carlin, and N. Grandjean, "Recombination coefficients of GaN-based laser diodes," *Journal of Applied Physics,* vol. 109, pp. 093106-093106-6, 2011.

[43] J. Piprek, "Unified model for the GaN LED efficiency droop," 2011, p. 793916.

[44] J. Hader, J. V. Moloney, and S. W. Koch, "Temperature-dependence of the internal efficiency droop in GaN-based diodes," *Applied Physics Letters,* vol. 99, p. 181127, 2011.

[45] W. Shan, W. Walukiewicz, J. W. Ager, III, E. E. Haller, J. F. Geisz, D. J. Friedman, J. M. Olson, and S. R. Kurtz, "Band Anticrossing in GaInNAs Alloys," *Physical Review Letters,* vol. 82, pp. 1221-1224, 1999.

[46] http://www.ioffe.rssi.ru/SVA/NSM/Semicond/GaN/figs/cbnd_ganwtz.gif, October 2012.

[47] M.-H. Kim, M. F. Schubert, Q. Dai, J. K. Kim, E. F. Schubert, J. Piprek, and Y. Park, "Origin of efficiency droop in GaN-based light-emitting diodes," *Applied Physics Letters,* vol. 91, p. 183507, 2007.

[48] M. F. Schubert, J. Xu, J. K. Kim, E. F. Schubert, M. H. Kim, S. Yoon, S. M. Lee, C. Sone, T. Sakong, and Y. Park, "Polarization-matched GaInN/AlGaInN multi-quantum-well light-emitting diodes with reduced efficiency droop," *Applied Physics Letters,* vol. 93, pp. 041102-3, 2008.

[49] J. Xie, X. Ni, Q. Fan, R. Shimada, U. Ozgur, and H. Morkoc, "On the efficiency droop in InGaN multiple quantum well blue light emitting diodes and its reduction with p-doped quantum well barriers," *Applied Physics Letters,* vol. 93, p. 121107, 2008.

[50] X. Ni, Q. Fan, R. Shimada, U. Ozgur, and H. Morkoc, "Reduction of efficiency droop in InGaN light emitting diodes by coupled quantum wells," *Applied Physics Letters,* vol. 93, p. 171113, 2008.

[51] K. J. Vampola, M. Iza, S. Keller, S. P. DenBaars, and S. Nakamura, "Measurement of electron overflow in 450 nm InGaN light-emitting diode structures," *Applied Physics Letters,* vol. 94, p. 061116, 2009.

[52] A. David, M. J. Grundmann, J. F. Kaeding, N. F. Gardner, T. G. Mihopoulos, and M. R. Krames, "Carrier distribution in (0001)InGaN/GaN multiple quantum well light-emitting diodes," *Applied Physics Letters,* vol. 92, pp. 053502-3, 2008.

[53] B. Galler, A. Laubsch, A. Wojcik, H. Lugauer, A. Gomez-Iglesias, M. Sabathil, and B. Hahn, "Investigation of the carrier distribution in InGaN-based multi-quantum-well structures," *physica status solidi (c),* vol. 8, pp. 2372-2374, 2011.

[54] P. Kozodoy, H. Xing, S. P. DenBaars, U. K. Mishra, A. Saxler, R. Perrin, S. Elhamri, and W. C. Mitchel, "Heavy doping effects in Mg-doped GaN," *Journal of Applied Physics,* vol. 87, pp. 1832-1835, 2000.

[55] J. Piprek and S. Li, "Electron leakage effects on GaN-based light-emitting diodes," *Optical and Quantum Electronics,* vol. 42, pp. 89-95, 2010.

[56] C. H. Wang, S. P. Chang, P. H. Ku, J. C. Li, Y. P. Lan, C. C. Lin, H. C. Yang, H. C. Kuo, T. C. Lu, S. C. Wang, and C. Y. Chang, "Hole transport improvement in InGaN/GaN light-emitting diodes by graded-composition multiple quantum barriers," *Applied Physics Letters,* vol. 99, pp. 171106-3, 2011.

[57] Y.-K. Kuo, J.-Y. Chang, M.-C. Tsai, and S.-H. Yen, "Advantages of blue InGaN multiple-quantum well light-emitting diodes with InGaN barriers," *Applied Physics Letters,* vol. 95, p. 011116, 2009.

[58] E. F. Schubert, "Light-Emitting Diodes," ed New York: Cambridge Univeristy Press, 2003, pp. 75-77.

[59] S. Grzanka, G. Franssen, G. Targowski, K. Krowicki, T. Suski, R. Czernecki, P. Perlin, and M. Leszczynski, "Role of the electron blocking layer in the low-temperature collapse of electroluminescence in nitride light-emitting diodes," *Applied Physics Letters,* vol. 90, p. 103507, 2007.

[60] S.-H. Han, D.-Y. Lee, S.-J. Lee, C.-Y. Cho, M.-K. Kwon, S. P. Lee, D. Y. Noh, D.-J. Kim, Y. C. Kim, and S.-J. Park, "Effect of electron blocking layer on efficiency droop in InGaN/GaN multiple quantum well light-emitting diodes," *Applied Physics Letters,* vol. 94, p. 231123, 2009.

[61] F. Bernardini and V. Fiorentini, "Spontaneous versus Piezoelectric Polarization in III–V Nitrides: Conceptual Aspects and Practical Consequences," *physica status solidi (b),* vol. 216, pp. 391-398, 1999.

[62] V. Fiorentini, F. Bernardini, F. Della Sala, A. Di Carlo, and P. Lugli, "Effects of macroscopic polarization in III-V nitride multiple quantum wells," *Physical Review B,* vol. 60, pp. 8849-8858, 1999.

[63] P. Waltereit, O. Brandt, A. Trampert, H. T. Grahn, J. Menniger, M. Ramsteiner, M. Reiche, and K. H. Ploog, "Nitride semiconductors free of electrostatic fields for efficient white light-emitting diodes," *Nature,* vol. 406, pp. 865-868, 2000.

[64] D. N. Zakharov, Z. Liliental-Weber, B. Wagner, Z. J. Reitmeier, E. A. Preble, and R. F. Davis, "Structural TEM study of nonpolar a-plane gallium nitride grown on (112[over ¯]0)4H-SiC by organometallic vapor phase epitaxy," *Physical Review B,* vol. 71, p. 235334, 2005.

[65] R. Aleksiejūnas, L. Lubys, M. Vengris, K. Jarašiūnas, T. Wernicke, V. Hoffmann, C. Netzel, A. Knauer, M. Weyers, and M. Kneissl, "Study of excess carrier dynamics in polar, semi-polar, and non-polar (In,Ga)N epilayers and QWs," *physica status solidi (c),* vol. 8, pp. 2154-2156, 2011.

[66] S.-C. Ling, T.-C. Lu, S.-P. Chang, J.-R. Chen, H.-C. Kuo, and S.-C. Wang, "Low efficiency droop in blue-green m-plane InGaN/GaN light emitting diodes," *Applied Physics Letters,* vol. 96, pp. 231101-3, 2010.

[67] C. J. Humphreys, "Does In form In-rich clusters in InGaN quantum wells?," *Philosophical Magazine,* vol. 87, pp. 1971-1982, 2007/05/01 2007.

[68] Y. Narukawa, Y. Kawakami, M. Funato, S. Fujita, S. Fujita, and S. Nakamura, "Role of self-formed InGaN quantum dots for exciton localization in the purple laser diode emitting at 420 nm," *Applied Physics Letters,* vol. 70, pp. 981-983, 1997.

[69] T. M. Smeeton, M. J. Kappers, J. S. Barnard, M. E. Vickers, and C. J. Humphreys, "Electron-beam-induced strain within InGaN quantum wells: False indium ``cluster'' detection in the transmission electron microscope," *Applied Physics Letters,* vol. 83, pp. 5419-5421, 2003.

[70] M. J. Galtrey, R. A. Oliver, M. J. Kappers, C. J. Humphreys, D. J. Stokes, P. H. Clifton, and A. Cerezo, "Three-dimensional atom probe studies of an In[sub x]Ga[sub 1 - x]N/GaN multiple quantum well structure: Assessment of possible indium clustering," *Applied Physics Letters,* vol. 90, pp. 061903-3, 2007.

[71] J. W. Orton, P. F. Fewster, J. P. Gowers, P. Dawson, K. J. Moore, P. J. Dobson, C. J. Curling, C. T. Foxon, K. Woodbridge, G. Duggan, and H. I. Ralph, "Measurement of 'material' parameters in multi-quantum-well structures," *Semiconductor Science and Technology,* vol. 2, p. 597, 1987.

[72] D. M. Graham, A. Soltani-Vala, P. Dawson, M. J. Godfrey, T. M. Smeeton, J. S. Barnard, M. J. Kappers, C. J. Humphreys, and E. J. Thrush, "Optical and microstructural studies of

InGaN/GaN single-quantum-well structures," *Journal of Applied Physics,* vol. 97, pp. 103508-5, 2005.

[73] S. Nakamura, M. Senoh, S.-i. Nagahama, N. Iwasa, T. Yamada, T. Matsushita, H. Kiyoku, Y. Sugimoto, T. Kozaki, H. Umemoto, M. Sano, and K. Chocho, "InGaN/GaN/AlGaN-based laser diodes with modulation-doped strained-layer superlattices grown on an epitaxially laterally overgrown GaN substrate," *Applied Physics Letters,* vol. 72, pp. 211-213, 1998.

[74] C. Kim, I. K. Robinson, J. Myoung, K. Shim, M. Yoo, x, Cheol, and K. Kim, "Critical thickness of GaN thin films on sapphire (0001)," *Applied Physics Letters,* vol. 69, pp. 2358-2360, 1996.

[75] Q. Dai, M. F. Schubert, M. H. Kim, J. K. Kim, E. F. Schubert, D. D. Koleske, M. H. Crawford, S. R. Lee, A. J. Fischer, G. Thaler, and M. A. Banas, "Internal quantum efficiency and nonradiative recombination coefficient of GaInN/GaN multiple quantum wells with different dislocation densities," *Applied Physics Letters,* vol. 94, p. 111109, 2009.

[76] http://www.oceanoptics.com/Products/hr4000.asp, Ocotber 2012.

[77] http://www.chemicool.com/definition/monochromators.html, Ocotber 2012.

[78] http://www.apptechy.com/OpticalMeasure/Silicon_Responsivity.jpg, Ocotber 2012.

[79] http://www.arscryo.com/Images/DrawingImages/LaboratoryCryogenicSystemBlockDiagramwidth760px.jpg, October 2012.

[80] http://www.oxford-instruments.com/products/low-temperature/opticaland-spectroscopy/optistatdn-v/Pages/optistatdn-v.aspx, January 2010.

[81] B. Ikyo, "Physical Properties of Interband and Interband Cascade Edge- and Surface-Emitting Mid-Infrared Lasers," PhD thesis, Faculty of Physical Science and Egineering, University of Surrey, 2012.

[82] S. R. Jin, S. J. Sweeney, S. Tomic, A. R. Adams, and H. Riechert, "High-pressure studies of recombination mechanisms in 1.3-μm GaInNAs quantum-well lasers," *Selected Topics in Quantum Electronics, IEEE Journal of,* vol. 9, pp. 1196-1201, 2003.

[83] N. Hossain, I. P. Marko, S. R. Jin, K. Hild, S. J. Sweeney, R. B. Lewis, D. A. Beaton, and T. Tiedje, "Recombination mechanisms and band alignment of GaAs[sub 1 - x]Bi[sub x]/GaAs light emitting diodes," *Applied Physics Letters,* vol. 100, p. 051105, 2012.

[84] T. Takeuchi, S. Sota, M. Katsuragawa, M. Komori, H. Takeuchi, H. Amano, and I. Akasaki, "Quantum-Confined Stark Effect due to Piezoelectric Fields in GaInN Strained Quantum Wells," *Japanese Journal of Applied Physics,* vol. 36, 1997.

[85] A. Neogi, C.-W. Lee, H. O. Everitt, T. Kuroda, A. Tackeuchi, and E. Yablonovitch, "Enhancement of spontaneous recombination rate in a quantum well by resonant surface plasmon coupling," *Physical Review B,* vol. 66, p. 153305, 2002.

[86] R. A. Arif, Y.-K. Ee, and N. Tansu, "Polarization engineering via staggered InGaN quantum wells for radiative efficiency enhancement of light emitting diodes," *Applied Physics Letters,* vol. 91, p. 091110, 2007.

[87] M. B. Nardelli, K. Rapcewicz, and J. Bernholc, "Polarization field effects on the electron-hole recombination dynamics in In[sub 0.2]Ga[sub 0.8]N/In[sub 1 - x]Ga[sub x]N multiple quantum wells," *Applied Physics Letters,* vol. 71, pp. 3135-3137, 1997.

[88] E. Berkowicz, D. Gershoni, G. Bahir, A. C. Abare, S. P. DenBaars, and L. A. Coldren, "Optical Spectroscopy of InGaN/GaN Quantum Wells," *physica status solidi (b),* vol. 216, pp. 291-300, 1999.

[89] J. Bai, T. Wang, and S. Sakai, "Influence of the quantum-well thickness on the radiative recombination of InGaN/GaN quantum well structures," *Journal of Applied Physics,* vol. 88, pp. 4729-4733, 2000.

[90] Y.-L. Li, Y.-R. Huang, and Y.-H. Lai, "Efficiency droop behaviors of InGaN/GaN multiple-quantum-well light-emitting diodes with varying quantum well thickness," *Applied Physics Letters,* vol. 91, p. 181113, 2007.

[91] J. Piprek, R. Farrell, S. DenBaars, and S. Nakamura, "Effects of built-in polarization on InGaN-GaN vertical-cavity surface-emitting lasers," *Photonics Technology Letters, IEEE,* vol. 18, pp. 7-9, 2006.

[92] A. David and M. J. Grundmann, "Influence of polarization fields on carrier lifetime and recombination rates in InGaN-based light-emitting diodes," *Applied Physics Letters,* vol. 97, pp. 033501-3, 2010.

[93] J. Hader, J. V. Moloney, and S. W. Koch, "Supression of carrier recombination in semiconductor lasers by phase-space filling," *Applied Physics Letters,* vol. 87, pp. 201112-3, 2005.

[94] S. Nakamura, "The Roles of Structural Imperfections in InGaN-Based Blue Light-Emitting Diodes and Laser Diodes," *Science,* vol. 281, pp. 956-961, August 14, 1998 1998.

[95] N. K. Dutta and R. J. Nelson, "The case for Auger recombination in In[sub 1 - x]Ga[sub x]As[sub y]P[sub 1 - y]," *Journal of Applied Physics,* vol. 53, pp. 74-92, 1982.

[96] S. R. Bank, L. L. Goddard, M. A. Wistey, H. B. Yuen, and J. S. Harris, Jr., "On the temperature sensitivity of 1.5-μm GaInNAsSb lasers," *Selected Topics in Quantum Electronics, IEEE Journal of,* vol. 11, pp. 1089-1098, 2005.

[97] T. R. Chen, B. Chang, L. C. Chiu, K. L. Yu, S. Margalit, and A. Yariv, "Carrier leakage and temperature dependence of InGaAsP lasers," *Applied Physics Letters,* vol. 43, pp. 217-218, 1983.

[98] U. T. Schwarz, H. Braun, K. Kojima, Y. Kawakami, S. Nagahama, and T. Mukai, "Interplay of built-in potential and piezoelectric field on carrier recombination in green light emitting InGaN quantum wells," *Applied Physics Letters,* vol. 91, p. 123503, 2007.

[99] M. F. Schubert, Q. Dai, J. Xu, J. K. Kim, and E. F. Schubert, "Electroluminescence induced by photoluminescence excitation in GaInN/GaN light-emitting diodes," *Applied Physics Letters,* vol. 95, p. 191105, 2009.

[100] http://www.ioffe.rssi.ru/SVA/NSM/Semicond/GaN/bandstr.html#Donors, October 2012.

[101] D.-S. Shin, D.-P. Han, J.-Y. Oh, and J.-I. Shim, "Study of droop phenomena in InGaN-based blue and green light-emitting diodes by temperature-dependent electroluminescence," *Applied Physics Letters,* vol. 100, pp. 153506-4, 2012.

[102] W. Shan, B. D. Little, J. J. Song, Z. C. Feng, M. Schurman, and R. A. Stall, "Optical transitions in In[sub x]Ga[sub 1 - x]N alloys grown by metalorganic chemical vapor deposition," *Applied Physics Letters,* vol. 69, pp. 3315-3317, 1996.

[103] J.-C. Lee, Y.-F. Wu, Y.-P. Wang, and T.-E. Nee, "Temperature and current dependences of electroluminescence from InGaN/GaN multiple quantum wells," *Journal of Crystal Growth,* vol. 310, pp. 5143-5146, 2008.

[104] N. E. Christensen and I. Gorczyca, "Optical and structural properties of III-V nitrides under pressure," *Physical Review B,* vol. 50, pp. 4397-4415, 1994.

[105] http://www.ioffe.ru/SVA/NSM/Semicond/GaN/mechanic.html, October 2012.

[106] http://www.ioffe.ru/SVA/NSM/Semicond/InN/mechanic.html, October 2012.

[107] I. Vurgaftman, J. R. Meyer, and L. R. Ram-Mohan, "Band parameters for III--V compound semiconductors and their alloys," *Journal of Applied Physics,* vol. 89, pp. 5815-5875, 2001.

[108] P. Perlin, V. Iota, B. A. Weinstein, P. Wisniewski, T. Suski, P. G. Eliseev, and M. Osinski, "Influence of pressure on photoluminescence and electroluminescence in GaN/InGaN/AlGaN quantum wells," *Applied Physics Letters,* vol. 70, pp. 2993-2995, 1997.

[109] S. X. Li, J. Wu, E. E. Haller, W. Walukiewicz, W. Shan, H. Lu, and W. J. Schaff, "Hydrostatic pressure dependence of the fundamental bandgap of InN and In-rich group III nitride alloys," *Applied Physics Letters,* vol. 83, pp. 4963-4965, 2003.

[110] P. Perlin, I. Gorczyca, T. Suski, P. Wisniewski, S. Lepkowski, N. E. Christensen, A. Svane, M. Hansen, S. P. DenBaars, B. Damilano, N. Grandjean, and J. Massies, "Influence of pressure on the optical properties of In_{x}Ga_{1-x}N epilayers and quantum structures," *Physical Review B,* vol. 64, p. 115319, 2001.

[111] J. A. Tuchman and I. P. Herman, "General trends in changing epilayer strains through the application of hydrostatic pressure," *Physical Review B,* vol. 45, pp. 11929-11935, 1992.

[112] D. Bertho, J.-M. Jancu, and C. Jouanin, "Equations of state and a tight-binding model for strained layers: Application to a ZnSe-GaAs epilayer," *Physical Review B,* vol. 48, pp. 2452-2459, 1993.

[113] T. Suski, P. Perlin, H. Teisseyre, M. Leszczynski, I. Grzegory, J. Jun, M. Bockowski, S. Porowski, and T. D. Moustakas, "Mechanism of yellow luminescence in GaN," *Applied Physics Letters,* vol. 67, pp. 2188-2190, 1995.

[114] K. Shimada, T. Sota, K. Suzuki, and H. Okumura, "First-Principles Study on Piezoelectric Constants in Strained BN, AlN, and GaN," *Japanese Journal of Applied Physics,* vol. 37, 1998.

[115] J. Pal, G. Tse, V. Haxha, M. A. Migliorato, and S. Tomić, "Second-order piezoelectricity in wurtzite III-N semiconductors," *Physical Review B,* vol. 84, p. 085211, 2011.

[116] S. M. C, K. I. M. Kwang-Choong, S. Hitoshi, F. Natalie, M. Hisashi, N. Shuji, D. S. P, and S. J. S, "High Power and High External Efficiency m-Plane InGaN Light Emitting Diodes," *Japanese journal of applied physics. Pt. 2, Letters & express letters,* vol. 46, p. 126, 2007/02/25 2007.

[117] G. Staszczak, T. Suski, A. Khachapuridze, P. Perlin, M. Funato, and Y. Kawakami, "Different behavior of semipolar and polar InGaN/GaN quantum wells: Pressure studies of photoluminescence," *physica status solidi (a),* vol. 208, pp. 1526-1528, 2011.

[118] I. Gorczyca, T. Suski, A. Kamińska, G. Staszczak, H. P. D. Schenk, N. E. Christensen, and A. Svane, "In-clustering effects in InAlN and InGaN revealed by high pressure studies," *physica status solidi (a),* vol. 207, pp. 1369-1371, 2010.

[119] I. Gorczyca, S. P. Łepkowski, T. Suski, N. E. Christensen, and A. Svane, "Influence of indium clustering on the band structure of semiconducting ternary and quaternary nitride alloys," *Physical Review B,* vol. 80, p. 075202, 2009.

[120] M. D. McCluskey, C. G. V. d. Walle, C. P. Master, L. T. Romano, and N. M. Johnson, "Large band gap bowing of In[sub x]Ga[sub 1 - x]N alloys," *Applied Physics Letters,* vol. 72, pp. 2725-2726, 1998.

[121] A. R. Adams, M.Silver, and J. Allam, *High Pressure in Semiconductor Physics II, pp 310-311,* 1998.

[122] J. Piprek, in *Semiconductor Optoelectronic devices: Introduction to Physics and Simulation*, ed San Diego: Academic Press, 2003, pp. 136-138.

[123] M. Hadis, *Handbook of Nitirde Semiconductors and Devices, Materials Properties, Physics and Growth,* 2009.

[124] J. Lee, X. Li, X. Ni, U. Ozgur, H. Morkoc, T. Paskova, G. Mulholland, and K. R. Evans, "On carrier spillover in c- and m-plane InGaN light emitting diodes," *Applied Physics Letters,* vol. 95, pp. 201113-3, 2009.

[125] X. Li, X. Ni, H. Y. Liu, F. Zhang, S. Liu, J. Lee, V. Avrutin, Ü. Özgür, T. Paskova, G. Mulholland, K. R. Evans, and H. Morkoç, "On the reduction of efficiency loss in polar c -plane and non-polar m -plane InGaN light emitting diodes," *physica status solidi (c),* vol. 8, pp. 1560-1563, 2011.

[126] C. Ching-Hsueh, L. Da-Wei, L. Chien-Chung, L. Zhen-Yu, K. Hao-chung, L. Tien-Chang, W. Shing-chung, L. Wei-Tsai, T. Tomoyuki, H. Yoshio, Y. Masahito, and S. Nobuhiko,

"Reduction of Efficiency Droop in Semipolar (1-101) InGaN/GaN Light Emitting Diodes Grown on Patterned Silicon Substrates," 2011, p. JWA94.

[127] S. R. Jin, S. J. Sweeney, C. N. Ahmad, A. R. Adams, and B. N. Murdin, "Radiative and Auger recombination in 1.3 mu m InGaAsP and 1.5 mu m InGaAs quantum-well lasers measured under high pressure at low and room temperatures," *Applied Physics Letters,* vol. 85, pp. 357-359, 2004.

[128] R. Fehse, S. J. Sweeney, A. R. Adams, E. P. O'Reilly, A. Y. Egorov, H. Riechert, and S. Illek, "Insights into carrier recombination processes in 1.3 μm GaInNAs-based semiconductor lasers attained using high pressure," *Electronics Letters,* vol. 37, pp. 92-93, 2001.

[129] http://www.rsc.org/chemistryworld/News/2009/January/30010901.asp, January 2009.

[130] http://www.i-micronews.com/upload/iLED/AC_iLED_avril2012.pdf, April 2012.

[131] http://www2.ensc.sfu.ca/~glennc/e495/e495l2j.pdf, October 2012.

[132] D. Zhu, C. McAleese, M. Haberlen, C. Salcianu, T. Thrush, M. Kappers, A. Phillips, P. Lane, M. Kane, D. Wallis, T. Martin, M. Astles, N. Hylton, P. Dawson, and C. Humphreys, "Efficiency measurement of GaN-based quantum well and light-emitting diode structures grown on silicon substrates," *Journal of Applied Physics,* vol. 109, p. 014502, 2011.

[133] D. Zhu, C. McAleese, M. Häberlen, C. Salcianu, T. Thrush, M. Kappers, A. Phillips, P. Lane, M. Kane, D. Wallis, T. Martin, M. Astles, and C. Humphreys, "InGaN/GaN LEDs grown on Si(111): dependence of device performance on threading dislocation density and emission wavelength," *physica status solidi (c),* vol. 7, pp. 2168-2170, 2010.

[134] H. Amano, N. Sawaki, I. Akasaki, and Y. Toyoda, "Metalorganic vapor phase epitaxial growth of a high quality GaN film using an AlN buffer layer," *Applied Physics Letters,* vol. 48, pp. 353-355, 1986.